# Enhanced Stratified Preclinical Simulation of the Natural Knee

Philip Alan Straw

Submitted in accordance with the requirements for the degree of
Doctor of Philosophy

The University of Leeds

School of Mechanical Engineering

January 2023

The candidate confirms that the work submitted is his/her own and that appropriate credit has been given where reference has been made to the work of others.

# Acknowledgements

I would like to thank my supervisors Prof Louise Jennings, Dr Hazel Fermor and Dr Raelene Cowie for their guidance and support throughout the project. I would like to thank the EPSRC for funding the project. Thank you to all the other academics and postdoctoral researchers who provided me with advice.

I would like to thank Nicola Conway for sectioning and staining the histological samples, Camille Hammersley for assistance with scanning silicone replicas onto the Alicona and Dr Raelene Cowie for assistance grading the wear, damage and deformation of cartilage and meniscal surfaces.

A special thanks to Rae for all of your help throughout the PhD and for providing motivational oranges.

Thank you to all the technical staff for your advice, support and providing some comic relief.

Thank you to all the other PhD students who experienced this journey with me, it wouldn’t have been the same without you.

Thank you to all my friends and family for providing a non-PhD related escape.

And finally, to my favourite person, thank you for all the love, laughs and support and for helping to drag me across the finish line. I couldn’t have done it without you.

# Abstract

There is a lack of *in vitro* experimental evidence demonstrating the mechanical and tribological performance of early-stage knee interventions before clinical use. An *in vitro* experimental porcine knee joint simulation model was previously developed at the University of Leeds to enable the assessment of early-stage knee interventions. The aim of the current work was to improve the simulation capabilities of this system to enable more clinically relevant results to be generated. This aim was achieved by determining a suitable lubricant for tribological investigations of articular cartilage, extending simulation duration, validating the use of AccuTrans silicone to replicate articulating surfaces after longer simulations and simulating activities of daily living. Knowledge from these studies was then combined to enable the performance of a novel decellularised porcine osteochondral allograft to be compared with the existing gold standard allograft under enhanced simulation conditions.

Tribological investigation of reciprocating cartilage-on-cartilage contacts revealed the lubricant had a significant influence on the maintenance of the structural integrity of the articulating surfaces during pin-on-plate experiments. Isotonic bovine serum lubricants demonstrated the ability to maintain cartilage surfaces for up to 96-hours whereas extensive damage was observed to articulating surfaces after 72-hours when using Ringer's Solution as a lubricant. Extending porcine knee joint simulation duration from 2 hours to 48 hours did not result in non-physiological motion, fracture or dislocation of the joint. Analysis of articulating surfaces using a clinical grading system showed minimal changes after 48 hours. This demonstrated the potential to simulate natural tissue for an extended duration. AccuTrans silicone was validated as an appropriate method for replicating articular cartilage surfaces after extended duration simulations. It was not possible to simulate stair ascent and deep squat motions consistently when using physical spring constraints to replicate ligament function; this was possible using displacement control.

After 48-hour simulations of activities of daily living (47 hours walking gait + 1 hour stair ascent), decellularised allografts showed similar wear and damage behaviour to articular cartilage surfaces of porcine allografts based on the clinical grading and histological evidence. Analysis of silicone surface replicas using an optical profiler highlighted decellularised allografts were less stable than allografts, based on relative height difference between graft and femoral condyle surfaces at different timepoints; this difference was significant after the stair ascent simulation. This works demonstrates the importance of simulating a range of *in vivo* activities to identify differences between interventions.

# Table of Contents

# List of Tables

# List of Figures

# Abbreviations

| | |
|---|---|
| AA | adduction-abduction |
| ACI | autologous chondrocyte implantation |
| ACL | anterior cruciate ligament |
| AF | axial force |
| AP | anterior-posterior |
| CoF | coefficient of friction |
| CoR | centre of rotation |
| CI | confidence interval |
| DoF | degrees of freedom |
| ECM | extracellular matrix |
| FE | flexion-extension |
| HA | hyaluronic acid |
| IE | internal-external (tibial rotation) |
| MCL | medial cruciate ligament |
| ML | medial-lateral |
| MPa | Mega Pascals |
| EDTA | ethylenediaminetetraacetic acid |
| GAG | glycosaminoglycan |
| Hz | Hertz |
| ICRS | International Cartilage Regeneration and Joint Preservation Society |
| ISO | International Standards Organisation |
| k | stiffness |
| LCL | lateral cruciate ligament |
| mm | millimetres |
| μ | dynamic coefficient of friction |
| μm | micrometres |
| NBCS | new-born calf serum |
| N | Newtons |

| | |
|---|---|
| OA | Osteoarthritis |
| OARSI | Osteoarthritis Research Society International |
| PBS | phosphate buffered saline |
| PCL | posterior cruciate ligament |
| PMMA | poly(methyl methacrylate) |
| RCT | randomised control trial |
| ROM | range of motion |
| TJR | total joint replacement |
| TKR | total knee replacement |
| TR | tibial rotation |
| SI | superior-inferior |
| SD | standard deviation |
| UHMWPE | ultra-high-molecular-weight-polyethylene |

# Chapter 1

# Introduction and Literature Review

## 1.1 Introduction

In 2013/2014 treatment of musculoskeletal conditions contributed to £4.7 billion of NHS spending and predictions anticipate this figure to increase due to rising obesity (Agha and Agha, 2017), reduced physical activity (British Heart Foundation, 2015) and an aging population (Office for National Statistics, 2018). In 2019 this had increased to £5 billion per year (gov.uk, 2019). Osteoarthritis (OA) of the knee accounts for a significant proportion of this spending, affecting more than 5 million people over the age of 45 in England Scotland and Wales (Versus Arthritis, 2021). OA is a debilitating condition, the most common symptoms being pain and reduced functional capacity (Creamer and Hochberg, 1997a), consequently, OA is the primary reason cited for total knee replacement (TKR) (NJR, 2022).

Cartilage damage acquired through trauma, osteoarthritis or otherwise has a limited ability to repair itself. TKR is an effective end-stage treatment for alleviating pain and improving functional capability in the elderly (Carr et al., 2012), however younger and more active patients have greater functional demands, making TKR less effective. Alternative early-stage knee interventions for repair of cartilage injury have been developed to cater to younger or active patients. Some interventions, such as osteochondral grafting have demonstrated good results in some situations (Keszég et al., 2022) (Torrie et al., 2015) but remain a suboptimal solution; however alternative solutions, such as decellularised osteochondral grafts, have shown limited success or clinical failure (Farr et al., 2016). Often there has been limited preclinical *in vitro* evidence demonstrating their mechanical and tribological performance before clinical use (Bowland et al., 2015) (Patel et al., 2019).

Preclinical assessment of joint replacement enables predictions about *in vivo* performance of these devices to be made; one aspect of preclinical assessment involves wear testing in joint simulators. By replicating physiological loads and motions, simulators subject joint replacements to similar operating conditions experienced within the human body. The ability to replicate *in vivo* conditions is crucial for ensuring preclinical simulations generate clinically translatable results.

To enable preclinical assessment of early-stage knee interventions, an experimental natural knee joint simulation model incorporating a porcine knee was developed at the University of Leeds (Liu et al., 2015). This system has been used to assess the mechanical and tribological performance of osteochondral allograft interventions (P. Bowland et al., 2018) and undergone subsequent optimisation to improve the physiological relevance (Liu et al., 2019). Whilst a significant step forward, this system is still limited to recreate the *in vivo* environment an early-stage knee intervention is likely to experience and clinical evidence suggests robust preclinical assessment may be necessary to prevent poor outcomes.

## 1.2 Structure and Function of the Knee Joint

### 1.2.1 The Knee

The knee is a diarthrodial joint and the largest synovial joint within the human body. The major structures involved are four bones: femur, tibia, fibula and patella; four ligaments: anterior and posterior cruciate ligaments (ACL, PCL) and medial and lateral collateral ligaments (MCL, LCL); and the medial and lateral menisci (Figure 1.1). These structures are arranged into three distinct articulating compartments, the medial and lateral aspects of the tibiofemoral joint (TFJ) and the patellofemoral joint. In the TFJ, the femoral condyles of the distal femur articulate with the superior surfaces of the menisci and proximal tibia. In the patellofemoral joint, the posterior patella surface articulates against the trochlea groove on the anterior surface of the distal femur. Bones confer mechanical strength and support, ligaments constrain allowable motion and the menisci improve congruence between the femur and tibia to transfer loads across the joint space and facilitate smooth articulation.

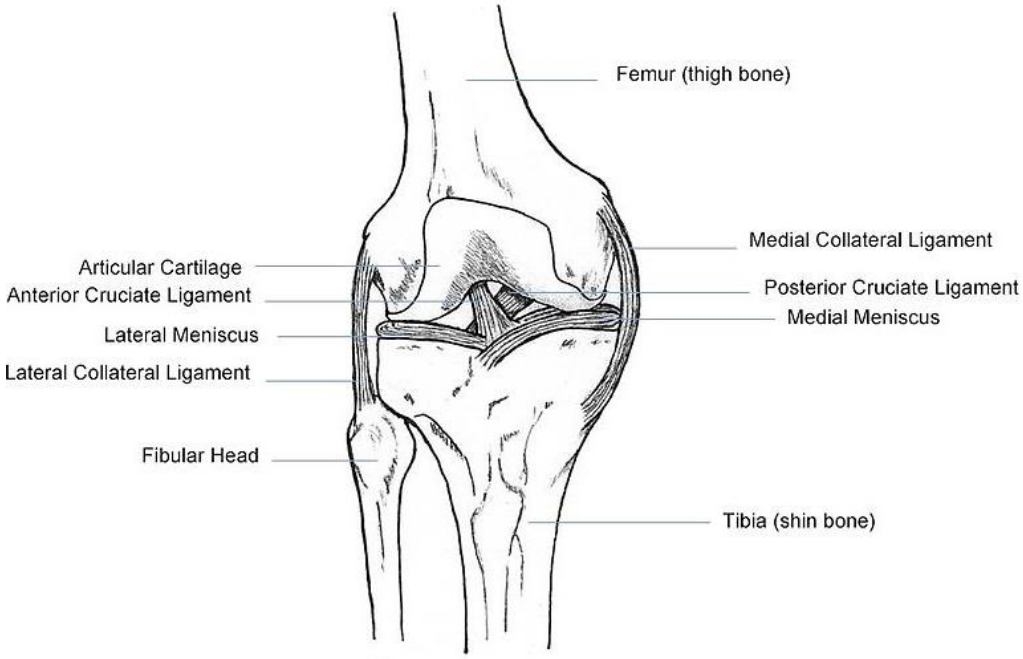


**Figure 1.1: Important structures within the human knee joint: bones, ligaments, menisci and articular cartilage. The patella is not shown in the image as its anterior position would obscure the view of the structures within the tibiofemoral joint.**

### 1.2.2 Biomechanics of the Knee

The design and geometry of the knee ensures both stability and mobility; this enables it to withstand significant loading whilst allowing a considerable range of motion (ROM). Due to incongruence of articulating surfaces in the tibiofemoral joint motion in six degrees of freedom (DoF) is possible: anterior-posterior (AP), medial-lateral (ML) and superior-inferior (SI) translation and flexion-extension (FE), internal-external (IE) and adduction-abduction (AA) rotation (Figure 1.2). The range of motion and magnitude of forces transmitted through the joint have been observed to vary considerably during activities of daily living (Stewart and Hall, 2006). In the knee, the ACL prevents excessive anterior translation of the tibia during flexion and assists tibial rotation during extension and the PCL prevents excessive posterior translation of the tibia during flexion and prevents abduction-adduction in full extension (Flandry and Hommel, 2011).

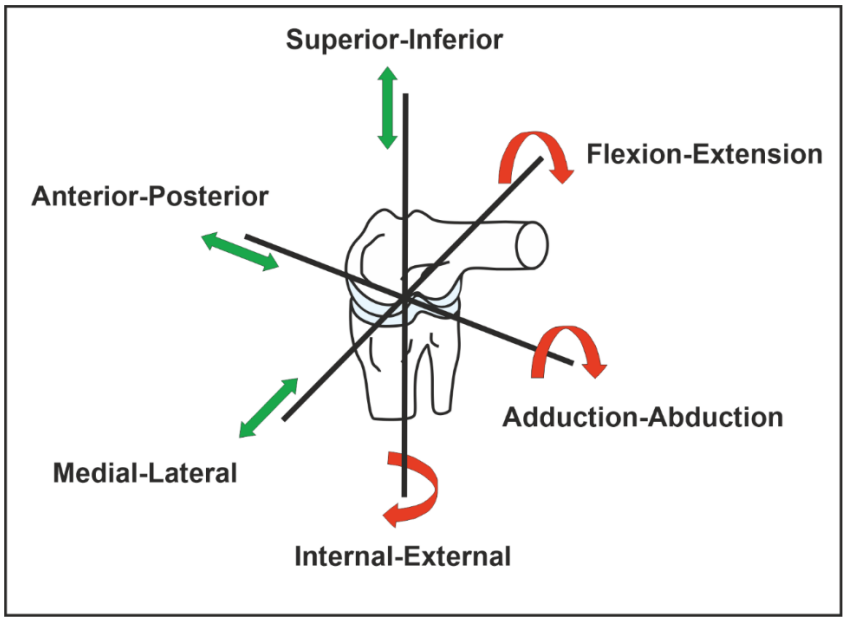


**Figure 1.2: The anatomical axes of motion within the tibiofemoral joint. Allowable motions, three translations (green arrows) and three rotations (red arrows) enable motion in six degrees of freedom within the joint.**

The majority of motion occurs around the flexion-extension axis; flexion and extension of the tibiofemoral joint are controlled by contraction of the hamstrings and quadriceps muscles respectively. As the joint travels through its range of flexion-extension motion, internal-external rotations are also generated. During the gait cycle the knee flexes up to 70° during swing phase, as the knee extends in preparation for heel strike the tibia rotates externally up to 30° ('screw-home' mechanism), following contact with the ground the knee flexes and internally rotates the tibia to absorb shock during the stance phase. At toe-off the knee once again flexes to lift the foot off the floor and back into the swing phase. Different tribological behaviours are theorised to occur during motion of the knee. During early flexion posterior rolling of the femur on the tibia is generated, as the flexion angle increases and the point of contact moves posteriorly, anterior sliding of the femur is also initiated. With increasing flexion the sliding mechanism starts to predominate over the rolling mechanism, until deep flexion where posterior translation of the femur is restrained by the ACL (Masouros et al., 2010).

### 1.2.3 Anatomy of the Knee

The knee incorporates various specialised connective tissues of the musculoskeletal system. These work in combination to allow the joint to perform its intended functions (Flandry and Hommel, 2011).

### 1.2.4 Bone

The primary function of the human skeleton is to provide a strong rigid frame upon which muscular contractions can occur to allow locomotion. Bone consists of both organic (30-40% of dry weight) and inorganic (40-60% of dry weight) components. The organic components contribute to the tensile strength and fracture toughness whilst the inorganic component provides the compressive strength (Standring, 2016). Within long bones such as the femur and tibia two distinct structural arrangements are typically observed. Layers of dense plates known as lamellae form a shell of cortical bone on the exterior surface, whilst the interior is comprised of a honeycomb network of trabecular structures. Cortical bone provides mechanical strength and trabecular bone provides support whilst minimising weight. Bones are constantly remodelled to adapt to the forces exerted upon them. Muscular contraction induces mechanical strain within bone, these mechanical stimuli are then converted into a biochemical response with initiates remodelling. This process is known as mechanotransduction and is thought to be mediated by osteocytes (Rosa et al., 2015). Bone and cartilage meet at a region known as the bone-cartilage interface; this region enables transmission of loads from the zone of calcified cartilage to the subchondral bone. The individual components of this structure interact to maintain proper joint function; changes to either component is thought to affect the properties of the other (Goldring, 2012).

### 1.2.5 Tendon and Ligament

The principle components of both tendons and ligaments are collagen, proteoglycans, glycoproteins and water. The majority of collagen content being large, crimped fibres of collagen type I; tendons 95% (Wang, 2006), ligaments 85% (Frank, 2004). Both tissues have a hierarchical structure, with small diameter collagen fibrils grouped to form larger diameter collagen fibres which are bundled together into fascicles. Although very similar in composition, tendons and ligaments have been shown to differ in function due to the orientation and diameter of the fibrils and the functional environment in which they operate (Rumian et al., 2007).

Tendons attach muscles to the bones via a junction known as the enthesis. The collagen fibres are orientated parallel to line of action of the associated muscle and this gives tendons considerable tensile strength. Their primary function is to transmit mechanical force generated by muscular contraction to the bones and enable movement. In the knee for example, contraction of the quadriceps femoris muscles applies a tensile force to the quadriceps/patella tendon causing extension of the joint. Like muscle and bone, tendons

adapt their structural properties to the mechanical forces exerted upon them (Wang, 2006).

Ligaments attach bone to bone, fibres are orientated more obliquely allowing them to resist tension in multiple directions (Standring, 2016); they function to maintain stability within a joint by limiting the distance adjacent bones can move from one another. The MCL and LCL are located on the medial and lateral sides of the knee joint respectively, they function to resist excessive tibial abduction-adduction forces. Ligament laxity is thought be a contributing factor to the progression of OA in the knee joint.

Both tendons and ligaments exhibit non-linear elastic behaviour due to crimping of the collagen fibres. Stress-strain curves have an initial toe-region which can be explained as a straightening or re-orientation of these fibres during extension; the linear region represents a stretching or sliding of adjacent fibres and failure occurs as fibres begin to tear (Screen et al., 2004). The biphasic nature of these tissues means they also exhibit viscoelastic properties (stress relaxation and creep). Different extension rates result in different responses due to fluid movement within the tissue. At fast extension rates fluid has less time to flow resulting in a higher Young's Modulus (Sanctuary et al., 2005).

### 1.2.6 Menisci

The menisci are crescent-shaped fibrocartilage structures located between the femoral condyles and tibial plateau within the medial and lateral compartments of the TFJ. The principle constituents of meniscal tissue are water (72%) and collagen (22%) with the remainder made up of proteoglycans, non-collagenous proteins and glycoproteins. Meniscal ECM is composed mainly of highly cross-linked fibres of collagen type I and has three layer structural arrangement. Fibres in the superficial and lamellar layer are orientated randomly and the fibres in the deepest layer are orientated circumferentially. This structural arrangement gives each layer different mechanical properties and allows the menisci to convert axial forces into hoop stresses and effectively transfer loads across the joint (Fox et al., 2012). In addition, the menisci also facilitate smooth articulation by increasing congruency between the opposing sliding surfaces and are thought to contribute other functions, such as: providing nutrients to the articular hyaline cartilage, proprioception, lubrication and shock absorption (Fox et al., 2012).

### 1.2.7 Cartilage

Cartilage is a specialised connective tissue found throughout the body, three distinct types exist: fibrocartilage, elastic cartilage and hyaline cartilage. The type and exact structural and chemical composition vary depending on the functional environment in which the tissues operate. Each type of cartilage consists of the same basic constituents: cartilage cells, extracellular matrix (ECM) and a ground substance. Cartilage cells are known as chondroblasts when young and still capable of dividing and chondrocytes when older and less metabolically active. These cells are responsible for the synthesis, secretion and maintenance of ECM constituents. The ECM is composed mostly of a network of fine collagen type II fibrils suspended in a ground substance of proteoglycans and water. The solid and fluid phases combine to impart cartilage with its unique mechanical properties (Fox et al., 2009). Proteoglycan molecules join collagen fibrils to one another creating a porous scaffold (Figure 1.3) capable of resisting tensile loading as it expands. Highly negatively charged and hence hydrophilic glycosaminoglycan (GAG) side chains are incorporated into the larger proteoglycan molecules. The presence of these GAGs draws water into the porous scaffold causing the tissue to swell and become turgid. The osmotic pressure generated is what gives cartilage its ability to resist large compressive loads (Standring, 2016).

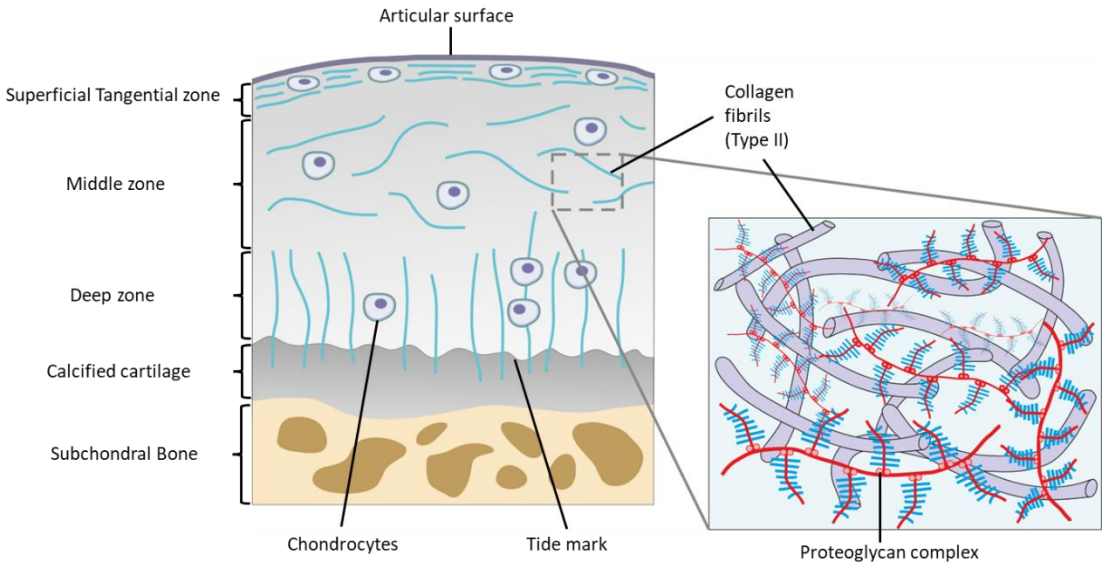


**Figure 1.3: The structure of articular hyaline cartilage. Visualisation of how the orientation of collagen fibrils and chondrocyte size and morphology alters throughout the depth of the tissue creating distinct zones which contribute specific mechanical properties (left). Detailed view of the network of collagen fibrils and proteoglycans complexes which make up the ECM scaffold structure of articular hyaline cartilage (right).** (Adapted from: Standring, 2016)**.**

Articular cartilage is a specialised form of hyaline cartilage found on the end of bones in synovial joints, it functions to allow the transmission of loads through joints. Its presence is designed to maximise contact area and minimise contact stresses by increasing congruency between opposing articulating surfaces. This ensures smooth low friction motion can occur during movement. Structurally, articular cartilage is organised into distinct zones (Figure 1.3), with each zone adapted to confer a particular function to the tissue. This specialisation occurs due to variation in size, density and orientation of both collagen fibrils and chondrocytes within the different zones. In the superficial/tangential zone (10%-20% of cartilage thickness) close to the site of articulation, fine collagen fibrils and small elongated chondrocytes are orientated parallel to the surface to prevent shearing. A higher density of thicker collagen fibrils is found deeper into the tangential zone. Large, rounded chondrocytes and collagen fibrils adopting various orientations are typically observed in the tangential/intermediate zone (40%-60%). Below this, in the deep/radial zone (30%-40%), both the chondrocytes and collagen fibrils are arranged vertically and additional varieties of collagen (type IX & XI) are present. The deepest layer of articular cartilage is the calcified zone. This anchors the cartilage to the underlying subchondral bone and prevents sliding between the two (Standring, 2016).

Articular cartilage thickness varies between joints. Less congruent surfaces, such as those within the knee, have been shown to have significantly thicker cartilage than the hip or ankle in human cadavers (Shepherd and Seedhom, 1999). In addition, differences between cartilage thickness of the femoral condyle, patella, tibial plateau contacting the femur and tibial plateau covered by menisci were also observed. More recent work has shown histological and mechanical properties of porcine cartilage vary between the regions covered by menisci and the uncovered regions (Iijima et al., 2014). Previously, total meniscectomy was indicated as the treatment of choice for damaged menisci, however partially resected menisci were shown to retain a significant amount of load carrying capacity (Seedhom, 1979). Due to this load carrying capacity and to prevent exposure of the articular cartilage beneath, minimising removal of meniscal tissue is preferable. Hence, partial meniscectomy is the current gold standard treatment. Bone (Huiskes et al., 2000), muscle (Campos et al., 2002) and tendon (Wang, 2006) adapt to increases in mechanical loading, however unlike these tissues, articular cartilage thickness does not appear to depend upon increased loading conditions (Eckstein et al., 2006). Although moderate exercise was shown to improve GAG content in a randomised control trial (Roos and Dahlberg, 2005). Conversely, inactivity appears to negatively influence cartilage health as periods of reduced mechanical loading have been linked to cartilage atrophy within the knee joint (Vanwanseele et al., 2003), (Hinterwimmer et al., 2004).

### 1.2.8 Synovial fluid

Synovial fluid is a dialysate of blood plasma with an added muccopolysaccharide, hyaluronic acid (HA), it is produced by the synovial membrane of synovial joints. In addition, to hyaluronic acid, synovial fluid contains many other molecules including proteins, the most abundant being albumin and globulin, proteoglycan 4 (PRG4) also known as superficial zone protein or lubricin and surface-active phospholipids (SAPLs) (Schmidt et al., 2007). It behaviours as a non-Newtonian fluid, exhibiting shear thinning characteristics (Cooke et al., 1978) and has a variable viscosity which is dependent on the hyaluronic acid content (Davies, 1966). Synovial fluid has three recognised functions: lubrication of the articulating surfaces of synovial joints, supply of nutrients to the avascular articular cartilage and removal of metabolic waste products. The synovial fluid provides lubrication via a fluid film mechanism whereas its constituents have shown to be involved in the boundary lubrication mechanism within synovial joints (Schmidt and Sah, 2007) (Schmidt et al., 2007).

### 1.2.9 Cartilage Lubrication Theory

Wear is a commonly observed phenomenon; relative motion between contacting surfaces under load can result in mechanical and/or chemical degradation of these surfaces over time. In certain situations wear is a considerable problem as damage to surfaces may compromise not only function but also safety (Gallo et al., 2013) (Drummond et al., 2015). To reduce the chance of wear and subsequent degeneration occurring, surfaces must be prevented from contacting one another and the coefficient of friction minimised; this is usually achieved using a lubricant.

Prevention of wear is particularly important within the synovial joints of the human body as they are intended to last for a lifetime. *In vitro* coefficient of friction measurements for articular cartilage reciprocating against articular cartilage have shown to range from 0.005 – 0.023 in a whole human knee joint (Charnley, 1960). The coefficient of friction between worn cartilage surfaces is higher than undamaged surfaces and a compromise in biomechanics occurs leaving individuals susceptible to functional impairment, pain, further degeneration and reduced quality of life. During a typical day joints will experience a variety of loading conditions. Fluid film, elastohydrodynamic, boundary, mixed, boosted and biphasic lubrication have all been proposed as explanations for how the human body copes with this variability in mechanical loading. Currently, these lubrication mechanisms are thought to work both individually and in combination to bestow cartilage with its remarkable low friction properties (Ateshian, 2009).

Lubricants function to reduce the coefficient of friction; in fluid film lubrication this is achieved through two strategies. The first simply involves separating articulating surfaces to prevent direct asperity contact, the second is due to differences in mechanical properties. The lubricant has much lower shear strength than the surfaces it separates, so when a force is applied shearing occurs within the lubricant, not the surfaces themselves (Hamrock et al., 2004). The thickness of fluid film (h) must be three times greater than the combined average roughness (Ra) of the surfaces to maintain this lubrication regime; fluid film lubrication is the desired mode of lubrication to prevent wear (Figure 1.4). Synovial fluid is the lubricating medium present within the synovial joints of the human body.

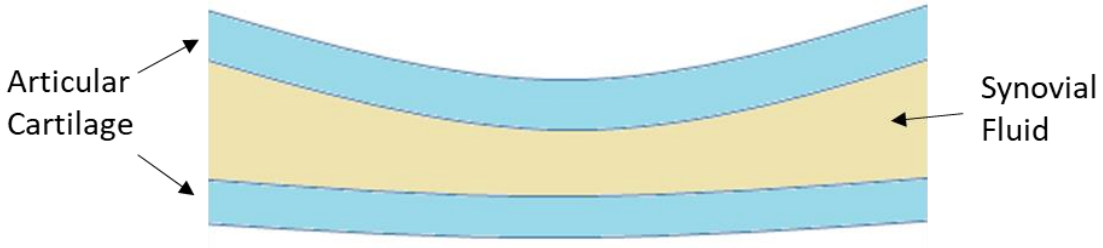


**Figure 1.4: Fluid film lubrication - cartilage surfaces are completely separated and all load is carried by the fluid film.**

Elastohydrodynamic lubrication is an extension of the fluid film lubrication theory in which the articulating surfaces are elastic (Hamrock et al., 2004). During loading a hydrostatic pressure is generated within the fluid film. In synovial joints this pressure elastically deforms articular cartilage reducing contact stresses and encourages movement of synovial fluid into the site of articulation via either an entraining or squeeze film action (Figure 1.5) (Tanner, 1966) (Dowson, 1966). Elastohydrodynamic lubrication is theorised to only occur in the lower limb and thought to predominate in cyclic conditions with high sliding velocities such as walking (Dowson, 1966). However, the presence of this lubrication method has yet to be conclusively proved.

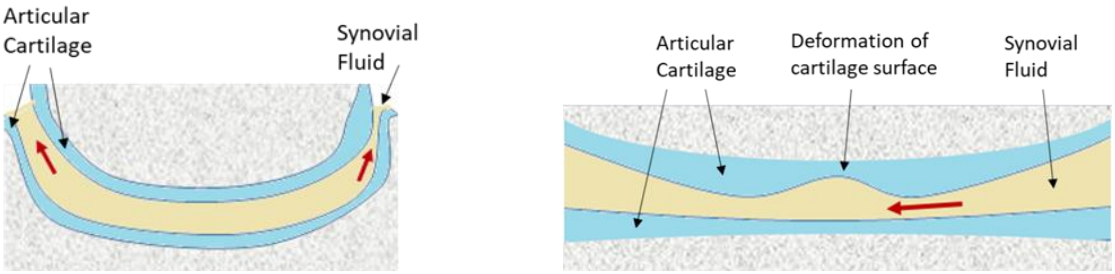


**Figure 1.5 Elastohydrodynamic lubrication mechanisms. Left: Squeeze Film action, deformation hinders lubricant flow from the contact area, this increases pressure and viscosity, maintaining film thickness. Right: Entraining action, sliding motion between surfaces drags lubricant into the contact area. Red arrows represent direction of synovial fluid flow.**

If fluid film thickness reduces below a certain threshold, then direct asperity contact between opposing cartilage surfaces will occur at some locations. In areas with sufficient film thickness the elastohydrodynamic lubrication regime is maintained, whereas in areas of direct asperity contact friction increases and boundary lubrication comes into effect. The condition where load is distributed between synovial fluid and asperity contact is referred to as mixed lubrication (Hamrock et al., 2004) (Figure 1.6).

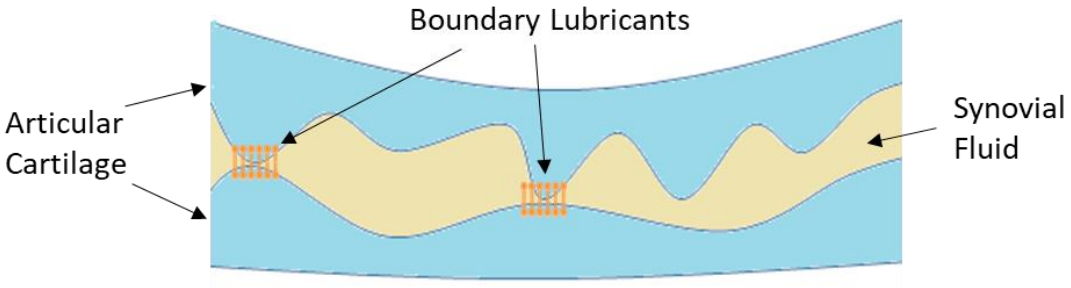


**Figure 1.6: Mixed lubrication - contact between cartilage surfaces occurs in a few regions but surfaces remain separated by the fluid film in other regions.**

Once significant asperity contact compromises the ability of the fluid film to lubricate a joint the coefficient of friction becomes independent of viscosity and boundary lubrication effects start to dominate (Hamrock et al., 2004) Figure 1.7. Within synovial joints boundary lubrication is mediated by the presence of glycoprotein and phospholipid molecules adhered to the articular cartilage (HA, PRG4, SAPLs). During motion molecules on opposing sides of the articulation slide over one another creating a boundary which prevents direct contact of the cartilage surfaces. Glycoprotein concentration is mediated by the synovial fluid. The constituents of synovial fluid have

been shown to contribute individually and in combination to support the boundary lubrication mechanism (Schmidt et al., 2007).

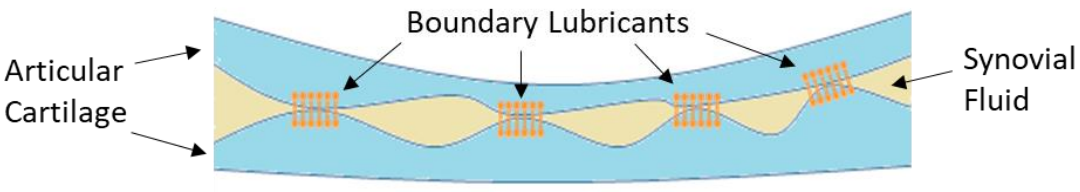


**Figure 1.7: Boundary lubrication – contact of cartilage surfaces occurs in multiple regions increasing the contribution of boundary lubrication mechanisms and reducing the contribution of the fluid film.**

If the fluid film becomes very thin due to high load, water from the synovial fluid will flow into the articular cartilage matrix. This leaves a viscous gel of proteins in the joint space which maintains a continuous fluid film between the surfaces. This theory is known as boosted lubrication (Walker et al., 1968) (Figure 1.8).

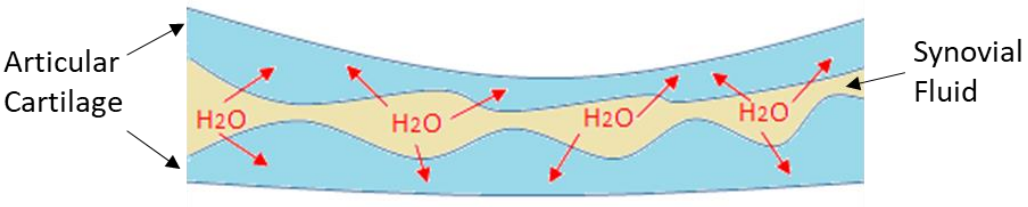


**Figure 1.8: Boosted lubrication – water is squeezed into the articular cartilage leaving a viscous fluid film within the joint space.**

The biphasic lubrication theory (Lewis and McCutchen, 1959) (McCutchen, 1962) (Mow et al., 1980) (Ateshian, 2009) provides an explanation for how articular cartilage maintains effective lubrication under extreme loading conditions; situations with constant loading and little movement i.e. standing for an extended duration. Upon application, a load is initially supported by the fluid phase due to the high water content of articular cartilage. Over time the water is exuded out of the cartilage tissue, the load is gradually transferred to the solid ECM phase of the cartilage and the coefficient of friction increases Figure 1.9. Under these conditions interstitial fluid pressurisation is the primary contributor to load support within the tissue and the influence of synovial fluid is minimal (Forster and Fisher, 1996) (Ramaswamy Krishnan et al., 2004) (Caligaris and Ateshian, 2008).

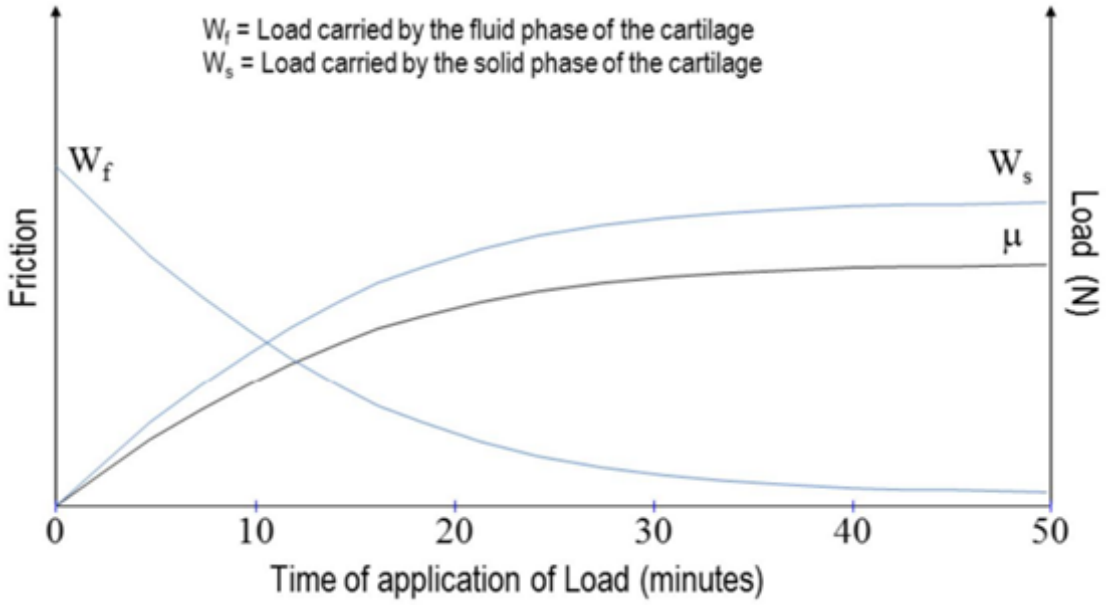


**Figure 1.9: The biphasic lubrication mechanism demonstrates the effect of prolonged loading of articular on the coefficient of friction. Load is initially supported by the fluid phase ($W_f$) and friction (μ) is low, as time increases load is transferred to the solid phase ($W_s$) and the friction increases.**

## 1.3 Cartilage Injury and Assessment

### 1.3.1 Cartilage Injury

There are numerous ways in which articular cartilage can become compromised including: trauma, disease, genetic disorders or as part of the natural aging process (Creamer and Hochberg, 1997a). The resultant damage presents in various forms, most commonly as chondral lesions, osteochondral lesions, OA or osteochondritis dissecans (OCD) lesions (Widuchowski et al., 2007).

Articular cartilage gradually thins as people age and the water content reduces. This presents as a receding of the cartilage from the subchondral bone margin (tidemark) towards the articulating surface as more cartilage becomes calcified (Standring, 2016). Reduced hydration and increased stiffness affect the deformation behaviour of cartilage and may reduce its ability to effectively transfer load to subchondral bone (Sophia Fox et al., 2009). During traumatic injury, commonly acquired through sporting activity (McAdams et al., 2010) (Hambly et al., 2012), excessive stresses and strains generated within the cartilage result in mechanical damage to the tissue (Buckwalter, 1998); this can produce defects in the surface. These influence the lubrication mechanisms within the joint, increasing friction and compromising smooth articulation. Cartilage damage is

particularly prevalent in those with existing knee injuries. Two large scale retrospective studies identified chondral lesions in 63% (Curl et al., 1997) and 60% (Widuchowski et al., 2007) of patients with pre-existing knee issues during arthroscopic evaluation. In a considerable number of cases, chondral lesions were shown to be associated with concomitant injury to other knee structures, most commonly the medial meniscus and ACL (Widuchowski et al., 2007) (Curl et al., 1997). Weakening of subchondral bone caused by avascular necrosis may lead to conditions such as osteochondritis dissecans (OCD). Subchondral bone damage reduces stability from beneath, leaving the articular cartilage surface unsupported which may lead to softening of the cartilage and compromised load transmission (Kocher et al., 2006).

Aging, participation in sporting activities and disease are all risk factors for the subsequent development/progression of pathological OA (Loeser et al., 2012). The degenerative progression of OA is thought to involve mechanical and biochemical factors which combine to produce an imbalance between anabolic and catabolic processes; this results in the abnormal remodelling of tissues within the knee joint (Loeser, 2006). The surface roughness of osteoarthritic cartilage has been shown to be considerably greater than that of healthy cartilage (Walker et al., 1968).

### 1.3.2 Assessment and Classification of Cartilage Injury

Patients usually visit a doctor due to pain; a number of questions will be asked and a physical assessment will be performed. If the doctor suspects chondral damage or OA then the patient may be referred for further investigation to confirm the diagnosis.

The identification of chondral damage or OA can be performed either invasively or non-invasively. Various invasive imaging approaches have been utilised; these are mostly performed arthroscopically. Radiography (x-ray), magnetic resonance imaging (MRI) and computed tomography (CT) are currently the most frequently utilised non-invasive imaging techniques (Novakofski et al., 2016). Despite its inability to directly visualise chondral tissue and inferior resolution compared to other methods, radiographic assessment is the most commonly used method due to ease of access (Braun and Gold, 2012). The Kellgren-Lawrence radiographic assessment of knee OA was developed in 1957 (Kellgren and Lawrence, 1957), this method is specific to the knee and considers joint narrowing and osteophyte formation. Improvements have been made since its initial application and the Kellgren-Lawrence system continues to be used today, although there are several criticisms of this approach (Creamer and Hochberg, 1997b) (Altman and Gold, 2007). A significant weakness of the radiographic approach is that it cannot detect early-stage chondral injury. MRI, CT and several arthroscopic techniques have

the potential for early detection but currently each has inherent drawbacks limiting their widespread application (Novakofski et al., 2016). Further technological improvements may see other modalities increase in popularity.

Two classification systems are commonly used for the visual assessment of chondral damage Table 1.1, the Outerbridge classification (Outerbridge, 1961) and the International Cartilage Regeneration and Joint Preservation Society (ICRS) grading system (Brittberg and Winalski, 2003). In addition to visual inspection, the ICRS approach combines patient reported, clinical evaluation and medical imaging components as well as including a grading system for OCD lesions. It also includes a method for evaluating the quality of cartilage repair after intervention. Research has also validated this approach, showing the ICRS system to be a reliable method for the classification of chondral defects (Dwyer et al., 2017) and chondral repair (van den Borne et al., 2007). Research to develop criteria for the classification of OA has also been conducted (Altman et al., 1986), some methods looking at a more comprehensive approach which assesses multiple structures within the joint (menisci, subchondral bone and synovium) to (Cook et al., 2010).

**Table 1.1: Clinical systems commonly used for the visual assessment of cartilage surfaces which aim to classify the extent of chondral damage within the knee.**

| Classification | Outerbridge | ICRS |
|---|---|---|
| Grade 0 | normal | normal |
| Grade I | cartilage with softening and swelling | nearly normal: Superficial lesions, soft indentations and/or superficial fissure and cracks |
| Grade II | a partial-thickness defect with fissures on the surface that do not reach subchondral bone or exceed 1.5 cm in diameter | abnormal: Lesions <50% of cartilage depth |
| Grade III | fissuring to the level of subchondral bone in an area with a diameter more than 1.5 cm | severely abnormal: defects >50% of cartilage depth but not through subchondral bone, blisters |
| Grade IV | exposed subchondral bone | severely abnormal: defects through subchondral bone |

The prevalence of defect severity has been shown to vary. *Widuchowski et al.* found Grade II defects (42%) to be most common whereas *Curl et al.* found a higher percentage of Grade III defects (41%) when classifying defects using the Outerbridge and a modified Outerbridge system respectively (Widuchowski et al., 2007) (Curl et al., 1997).

### 1.3.3 The Problem with Cartilage Injury

Chondral damage is of particular concern as articular hyaline cartilage has a limited regenerative capacity once damaged. Due to lack of vasculature and immobility of the chondrocytes embedded in the ECM, articular cartilage does not respond to injury through the classical healing pathway for partial thickness defects (Newman, 1998). Defects in the articular surface have been observed to significantly increase the coefficient of friction (Lane et al., 2009). Full-thickness defects have access to the vascular supply of subchondral bone and hence respond in a more classical manner. However, this results in formation of fibrocartilage which is thought to be functionally inferior to articular hyaline cartilage and is likely to contribute to further degradation (Newman, 1998). Another problem associated with chondral injury arises due to the aneural nature of cartilage tissue. Chondral injuries are often asymptomatic; therefore, it is possible for an individual to be unaware of significant damage as they do not experience any pain. Asymptomatic defects appear to be particularly prevalent in professional athletes (Flanigan et al., 2010). A significant undiagnosed cartilage defect may prevent the potential for early intervention.

Due to the limited healing capacity of articular cartilage, clinical intervention is often required if damage occurs. The exact methods employed are dependent on patient related factors and the size of the defect; most ICRS grade III or IV defects require an operation to restore the cartilage surface (Brittberg, 2018). For an intervention to truly restore pre-injury function it must withstand mechanical loading in a similar manner to intact cartilage. Articular cartilage is arranged into structurally distinct zones each of which contributes specialised functions to the tissue. Ideally an intervention must therefore replicate this specialised structural arrangement. A variety of approaches have been investigated for the management of chondral damage thus far.

## 1.4 Current Interventions

### 1.4.1 Conservative Treatment

At the present time OA/chondral damage cannot be reversed, therefore treatment of these conditions is aimed at limiting pain and preventing further degeneration. Initially conservative management strategies are employed. The typical approach encompasses a number of treatments which are usually prescribed sequentially (Creamer and Hochberg, 1997a). These include physical therapy, paracetamol, non-steroidal anti-inflammatory drugs (NSAIDs), intra-articular corticosteroid injections, hyaluronic acid,

and PRP or stem cell injections (Creamer and Hochberg, 1997a) (Brittberg, 2018). If conservative management is unsuccessful, the next step is surgical intervention.

### 1.4.2 Knee Replacement

For significant cartilage defects or persistent pain due to end stage arthritis the only available option is knee replacement; this can be total or partial. The procedure involves resurfacing articulating surfaces of the knee with a combination of metallic, plastic or ceramic components. In the United Kingdom, over 1.5 million procedures have been recorded by the National Joint Registry since 2003 (NJR, 2022). For older patients who suffer traumatic injury or those living with pathological knee conditions such as OA, knee arthroplasty has shown to be an effective procedure, reducing pain and improving quality of life (Choi and Ra, 2016). A systematic review of patient satisfaction found typically 80-100% of patients were satisfied with this procedure (Kahlenberg et al., 2018). Reduced mobility and potentially multiple revision procedures limit the lifespan of the implant in younger and/or active patients. The 18-year revision rate for males receiving a TKR before 55 years of age is over 12%, this is a higher failure rate than other patient groups and early revision increases the chance of subsequent re-revision (NJR, 2022). Therefore, alternative solutions have been developed in an attempt to treat younger more active individuals.

### 1.4.3 Debridement/Microfracture

Arthroscopic debridement is a simple approach in which compromised tissue is removed from the defect site; it can reduce pain and stop the problem spreading. Bone marrow stimulation (BMS) is another frequently employed method. It is most commonly achieved through the use of the microfracture technique. A surgical tool is used to agitate the defect site causing bleeding, this is intended to initiate a repair response and the formation of new cartilage tissue. This method has shown effectiveness in the short term for small defects (Kreuz et al., 2006) but subsequent deterioration is likely. In addition, for microfracture, most commonly the new tissue formed is fibrocartilage and therefore lacks the performance of the desired articular hyaline cartilage (Mithoefer et al., 2009). Microfracture is the most commonly used method for the treatment of small cartilage defects.

### 1.4.4 Cellular Approaches

Cellular approaches, such as autologous chondrocyte implantation (ACI), its matrix-assisted version (MACI) and characterised chondrocyte implantation (CCI) are other viable techniques. A cartilage biopsy is taken from a reduced weight-bearing area of a patient's cartilage from which chondrocytes are cultured; these are subsequently implanted into the cartilage defect site of the patient (Brittberg et al., 1994) or seeded onto a scaffold and implanted. Current National Institute for Health and Care Excellence (NICE) guidelines recommend ACI for treatment of defects > 2 $cm^2$ in symptomatic patients with minimal OA and no previous cartilage surgery as long as treatment is provided at a tertiary referral centre (NICE, 2017).

### 1.4.5 Osteochondral Grafting

Osteochondral grafting involves removal of the cartilage defect and replacement with an osteochondral graft harvested from a suitable donor site; this procedure can be performed with both autologous and allogeneic tissue. To be successful an osteochondral graft must restore smooth low friction articulation and remain stable within the graft site (Bowland et al., 2015). Where multiple osteochondral plugs are utilised to fill a single defect, the technique is known as mosaicplasty. Mosaicplasty provides satisfactory clinical outcomes at 12-year follow-up for small cartilage defects, however an increasing number of plugs was associated with increased degeneration (Filardo et al., 2015). No complications were observed at 10-year follow-up of four patients with large unstable osteochondritis dissecans (OCD) lesions, however one patient was observed to have incomplete osteochondral repair (Ronga et al., 2016). Mosaicplasty provides a good to excellent outcome in 92% of patients treated for femoral condylar defects at 10-year follow-up (Hangody and Fules, 2003). A 55% failure rate for mosaicplasty has been observed at 10-year follow-up for large cartilage defects (Bentley et al., 2012). Analysis of a large US insurance database identified a trend for increased use of osteochondral grafting procedures (autograft/allograft); 4123 procedures were performed in 2011, compared to only 2271 procedures in 2005 (McCormick et al., 2014). There are several issues related to the tissue source when considering osteochondral grafting. Allografts are limited in supply, have the potential to cause an immunogenic response or transmit pathogens and are very expensive. Although, osteochondral allografts have recently demonstrated to be clinically and cost effective as both a primary and revision procedures (Mistry et al., 2019). Autograft supply is also limited and in addition, this technique causes significant donor site morbidity (Andrade et al., 2016).

### 1.4.6 Osteochondral Scaffolds

Due to limited availability of graft tissue and to prevent donor site morbidity, alternative approaches for treatment of osteochondral defects have been sought. Scaffolds are a commonly used method in regenerative medicine applications, they provide mechanical support by replacing damaged structures and are designed to encourage the proliferation of new cells. Upon implantation, host cells migrate into the scaffold and integrate it with surrounding tissue. Alternatively, scaffolds can be seeded with host cells and/or growth factors and cultured prior to implantation. To ensure scaffolds are capable of withstanding forces generated in the *in vivo* environment they are often preconditioned in bioreactors which simulate the expected physiological conditions. This approach may increase the chance of successful integration but requires additional time for culturing. Numerous natural and synthetic osteochondral scaffolds are being investigated (Nooeaid et al., 2012). There are limitations to each approach with natural scaffolds often showing poor mechanical properties and synthetic scaffold having limited cellular interaction due to lack of cell binding motifs/ligands (Davis et al., 2021) (Niu et al., 2023).

### 1.4.7 Decellularised Scaffolds

Another option for overcoming the limitations of existing cartilage restoration approaches is decellularisation. This technique removes cellular components from donor tissues (Figure 1.10) via chemical, enzymatic and mechanical degradation leaving only an extracellular matrix scaffold (Fermor et al., 2015). Due to absence of donor cells, decellularised scaffolds do not elicit an adverse immune response when implanted in the host; this mitigates the chance of rejection, reduces recovery time and eliminates reliance on potentially harmful immunosuppressant drugs. Furthermore, donor site morbidity is eliminated and waiting time can be reduced by making an off-the-shelf product. The decellularisation process has been successfully demonstrated for both xenogeneic and allogeneic tissues. There are several approaches to decellularisation (Benders et al., 2013) and tissues differ in composition, therefore the exact decellularisation protocol may vary depending on which tissue is being processed. The decellularisation process has been shown to affect the mechanical properties of osteochondral grafts (Kheir et al., 2011) (Fermor et al., 2015) and porcine superflexor tendons (Herbert et al., 2015) (Edwards et al., 2019).

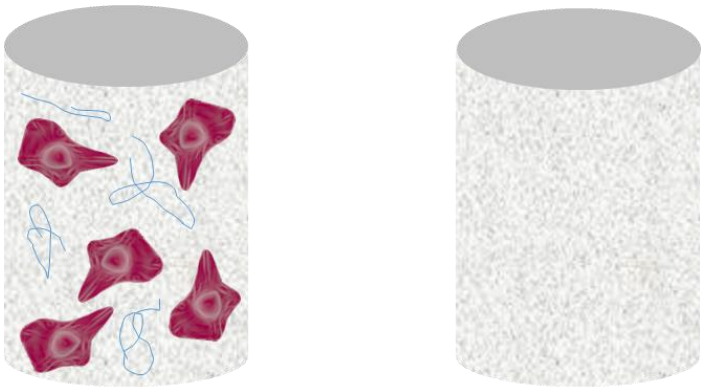

**Figure 1.10: Visualisation of a native untreated osteochondral graft (left), and a decellularised osteochondral graft after removal of cellular components.**

Decellularised tissues are currently available as off-the-shelf products for some healthcare applications. Decellularised dermis has been applied for various treatments (Moore et al., 2015) and has demonstrated success in treating hard to heal wounds (Greaves et al., 2013) (Kimmel and Gittleman, 2017). Decellularised osteochondral scaffolds are also available clinically; all osteochondral studies to date have evaluated outcomes when using Chondrofix (Zimmer Biomet), a commercially available decellularised osteochondral allograft. To create this product osteochondral tissue is procured from the femoral condyles of cadaveric human knee joints. Lipids and bone marrow are removed using a proprietary process, grafts are soaked in methylene blue under light illumination as a viral inactivation process and then gamma irradiated (Gomoll, 2013). An early case report demonstrated both bony and cartilage integration of a Chondrofix plug whilst in a suboptimal healing environment (Reynolds and Bishai, 2014). However, evidence supporting the clinical effectiveness of this product from larger patient groups highlights poor outcomes Table 1.2.

**Table 1.2: Clinically reported failure rates of the Chondrofix decellularised osteochondral scaffold at short-term follow-up.**

| Number of patients | Number of failures | Failures as percentage of total | Study |
|---|---|---|---|
| 58 | 5 | 8% | (Long et al., 2016) |
| 36 | 11 | 31% | (Degen et al., 2016) |
| 34 | 21 | 39% | (Johnson et al., 2017) |
| 32 | 23 | 72% | (Farr et al., 2016) |

It has been shown that the decellularisation process reduces GAG content of osteochondral tissues (Kheir et al., 2011) (Fermor et al., 2015). GAGs are a crucial component in the interstitial fluid pressurisation mechanism of articular cartilage, removal of these molecules has the potential to compromise the mechanical properties of decellularised tissues. Sufficient preclinical evidence to support the clinical use of decellularised osteochondral scaffolds is currently lacking. In vitro functional assessment of a decellularised osteochondral graft under physiologically relevant loading has the potential to mitigate in vivo failure.

### 1.4.8 Comparison of early-stage knee interventions

ACI was found to provide a significant improvement in functional outcome compared to mosaicplasty for large femoral condyle, trochlea and patella defects (1-10.5 $cm^2$ ACI, 1-20 $cm^2$ mosaicplasty) at 10-year follow-up (Bentley et al., 2012). Recently CCI demonstrated to be cost effective and likely to improve quality of life and reduce the chance of subsequent knee replacement in comparison to microfracture (Elvidge et al., 2016). A 2018 study found osteochondral grafting to have a reduced risk of reoperation at 2-year-follow-up compared to microfracture and ACI (Frank et al., 2018). Four randomised control trials (RCTs) compared microfracture vs mosaicplasty at long term follow-up (Gudas et al., 2012) (Lim et al., 2012) (Ulstein et al., 2014) (Solheim, Hegna, Strand, et al., 2018). These were all level of evidence I or II studies, however, the quality of evidence produced by three of the studies was criticised in a 2016 systematic review (Gracitelli et al., 2016). The authors deemed the evidence produced insufficient to draw meaningful conclusions. Mosaicplasty was shown to provide superior clinically relevant outcomes (Lysholm Score) compared to microfracture for femoral condyle or trochlea defects (2-5 $cm^2$) at 15-year follow-up (Solheim, Hegna, Strand, et al., 2018). A 2017 systematic review evaluated RCTs comparing various cartilage repair techniques (Devitt et al., 2017), they concluded no technique could be recommended over others. The authors state only studies at low risk of bias were included, however, two of these were studies considered at high risk of bias by (Gracitelli et al., 2016). Discrepancies in subjective scoring make interpretation of results produced by the reviewed studies difficult. Both research groups recommended further RCTs need to be conducted to identify the best option. The search criteria of Devitt et al. identified no RCTs comparing surgical approaches with conservative therapies (Devitt et al., 2017). However, debridement has shown to offer no additional benefits when compared with physical and medical therapy in a RCT (Kirkley et al., 2008). In addition, a RCT to compare ACI against arthroscopic debridement and physiotherapy is currently in progress (Randsborg et al., 2016) (Clinical Trial: NCT02636881 - expected completion September 2024).

### 1.4.9 Summary

Microfracture and osteochondral autografting (mosaicplasty) can be effective for small defects, whereas ACI/MACI/CCI and osteochondral allografts are comparatively superior for larger defects (Devitt et al., 2017). Even though the effectiveness of microfracture has been shown to be limited (Solheim et al., 2016) and other techniques to potentially provide superior outcomes (Solheim, Hegna, Strand, et al., 2018), microfracture has been the most commonly used non-TKR option due to its simplicity and cost-effectiveness. Which knee cartilage repair intervention provides the best overall outcome remains undecided (Devitt et al., 2017) and there is very limited evidence (Solheim, Hegna, Strand, et al., 2018) demonstrating a statistically significant difference between approaches. This has led some to argue rehabilitation may be responsible for improvements, not the type of procedure (Randsborg et al., 2016). In addition, it has been recently suggested patient specific factors are more likely to influence long term outcomes of cartilage repair surgery than the type of intervention used (Solheim, 2018). From the literature it can be seen there is lack of consensus on the most effective non-TKR cartilage treatments and further research is needed. Following the approach used for total joint replacements (NJR, 2022) the ICRS has setup a registry to monitor outcomes of cartilage repair strategies (Tawy and McNicholas, 2022). This will hopefully allow more definitive conclusions about the performance of these interventions to be made.

## 1.5 Functional Assessment of Knee Repair Technologies

Competent authorities such as the Medicines and Healthcare products Regulatory Agency (MHRA) in the United Kingdom and Food and Drug Administration (FDA) in the United States are responsible for ensuring the safety of medical devices. These entities oversee notified bodies e.g. British Standards Institute (BSI) in the UK, which are responsible for performing conformity assessments on medical devices to check they are fit for purpose. Manufacturers must provide notified bodies sufficient evidence to demonstrate the efficacy of a product before it will be allowed onto market.

### 1.5.1 Functional assessment in living animal models

To enable functional assessment of new medical technologies and to assess safety, interventions are implanted into living animal models before clinical use. For the assessment of osteochondral interventions various approaches have been utilised, ranging from small animals such as mice, rats or rabbits to larger animals such as dogs,

sheep, goats, pigs, horses and primates (Maglio et al., 2019) (Meng et al., 2020) (Oláh et al., 2021) (Wang et al., 2022).

Small animal studies are cheaper compared to larger animal studies due to the reduced cost associated with rearing, housing and looking after the animals and reduced healing time minimising study durations; this also enables larger sample sizes to be investigated. In addition, the surgical procedures for the implantation of osteochondral grafts into the knees of larger animals can be more technically demanding, requiring experienced surgeons (Oláh et al., 2021). Small animals are considered effective for early assessment of biocompatibility or degradation of biomaterials (Meng et al., 2020) but lack the physiological relevance of larger animal models. Therefore, despite the increased cost, large animal models are required prior to clinical translation of osteochondral interventions. Being more similar in size, weight and cartilage thickness, large animal models provide an environment which more accurately simulates *in vivo* loading conditions.

Whilst more similar to humans, the ranges of motion in animal knee joints are not a perfect match and one limitation common of all animal models is they are quadrupedal, whereas humas are bipedal. These factors influence the percentage of mechanical loading transmitted through the joint potentially resulting in variable performance between species (Maglio et al., 2019) (Wang et al., 2022).

Animal testing provides valuable insight during the development of medical technologies, however it's use has been questioned and there has been a shift towards more ethical treatment of animals. The 3R's principle: replacement, reduction and refinement was introduced to try and minimise the unnecessary suffering of animals. The approach is supported by both legislation and the MHRA. According to the current legislation, animal models should only be used where no validated alternative exists for the assessment of factors crucial to clinical safety and performance of a medical device (MHRA, 2018). Whilst biocompatibility or integration of grafts with host tissue can only currently be investigated using a living animal model, there has been a push to develop *in vitro* experimental methods to investigate other relevant factors or alternative approaches.

### 1.5.2 *In vitro* assessment of total joint replacements vs early-stage knee interventions

*In vitro* assessment of total joint replacements (TJRs) is used to try and predict *in vivo* wear performance and mitigate the chance of subsequent, potentially dangerous failure occurring. Serious issues affecting patient safety have previously been encountered after implantation of some joint replacements including catastrophic osteolysis of total knee replacements (Robinson et al., 1995) and pseudotumors associated with metal-on-metal

hips (Pandit et al., 2008). This has led to the recall of these devices and the effects of some of these issues have been long-lasting (Matharu et al., 2018). Current *in vitro* test conditions for the wear testing of total knee replacements (TKRs) are prescribed by international standards (BS ISO, 14243-1:2009+A1:2020) (BS ISO, 14243-1:2014+A1:2020) a minimum of five million cycles is recommend for simulation of TKRs in the ISO standards. Additional guidance is also available (ASTM, 2017.).

Early knee interventions have been introduced to delay or potentially prevent the need for TKR, however, there is limited preclinical evidence demonstrating their mechanical and tribological function (Bowland et al., 2015) (Patel et al., 2019). Despite the problems experienced with total joint replacements, clinical failure of some early-stage knee interventions (Farr et al., 2016) and potential issues being identified more than 20 years ago (Wu et al., 2002), standards for *in vitro* assessment of non-TKR interventions have yet to be developed. The FDA and ICRS recommend mechanical testing for tissue engineered cartilage products, however these guidelines are suggested to be outdated and no ISO standards currently exist (Marchiori et al., 2019); in addition, there are no guidelines for the assessment of tribological properties (Link et al., 2020). There is an existing standard for assessing the biocompatibility of medical devices (ISO, 10993-1:2018).

### 1.5.3 Simple Frictional Assessment of Chondral/Osteochondral Interventions

One factor limiting the *in vitro* assessment of early-stage knee interventions is a suitable preclinical experimental model in which to assess them. A common approach to the assessment of cartilage mechanical and tribological properties has been pin-on-plate or pin-on-disc methodologies (Link et al., 2020). These approaches involve sliding a chondral/osteochondral sample or tissue engineered scaffold under load against a counter surface in a lubricant; glass, metal and articular cartilage are commonly used counter surfaces. These simple geometry configurations enable assessment of individual parameters such as applied load (Krishnan et al., 2005), type of motion (Northwood and Fisher, 2007) or lubricant (Forster and Fisher, 1996) (Shi et al., 2011); the influences of these factors have often been measured as changes in the coefficient of friction. More recent approaches (Lizhang et al., 2011) (Oungoulian et al., 2015) (Cilingir, 2015) (Bowland et al., 2018) (Durney et al., 2020) have started to focus on the assessment of wear, damage or deformation as outcome measures as this cannot necessarily be inferred by low coefficient of friction (Krishnan et al., 2004) (Greene et al.,

2011). The pin-on-plate/disc approaches have two inherent limitations which affect their ability to replicate the *in vivo* scenario:

- They do not replicate the complex geometries of the natural knee joint which will influence how the samples articulate against each other

- Chondral/osteochondral samples are removed from larger sections of tissue; therefore, fluid can escape from the extracellular matrix via the cut edges. This may compromise the interstitial fluid load support leaving samples susceptible to the initiation of wear, damage and deformation

Alternative configurations have been utilised to try and improve the physiological relevance by incorporating sections of opposing tibial and femoral osteochondral from the same joint (Caligaris and Ateshian, 2008) (Caligaris et al., 2009). Whilst an improvement, these approaches were restricted to sliding and limited to recreate the loads and motions experienced by the natural knee *in vivo*. Due to the limitations associated with the pin-on-plate/disc approach, assessment of osteochondral interventions has progressed into whole natural knee joints.

### 1.5.4 Advancing the clinical relevance of *in vitro* assessment of early stage knee interventions

### 1.5.5 Introduction to Knee Simulation

Knee simulators (Figure 1.11) are machines which have been designed to replicate physiological loads and motions of the natural knee. They were initially created to enable the wear of knee replacements to be assessed and have gone through several stages of development to improve the physiological relevance (Maag et al., 2021). Knee simulators have been used to investigate clinically relevant factors which may influence knee replacement performance including implant materials, application of different activities and variations in surgical alignment (Abdelgaied et al., 2022). More recently, research has progressed to include the simulation of natural knee joints, this has provided the opportunity to assess knee early-stage knee interventions (and TKRs) in a more physiologically relevant environment.

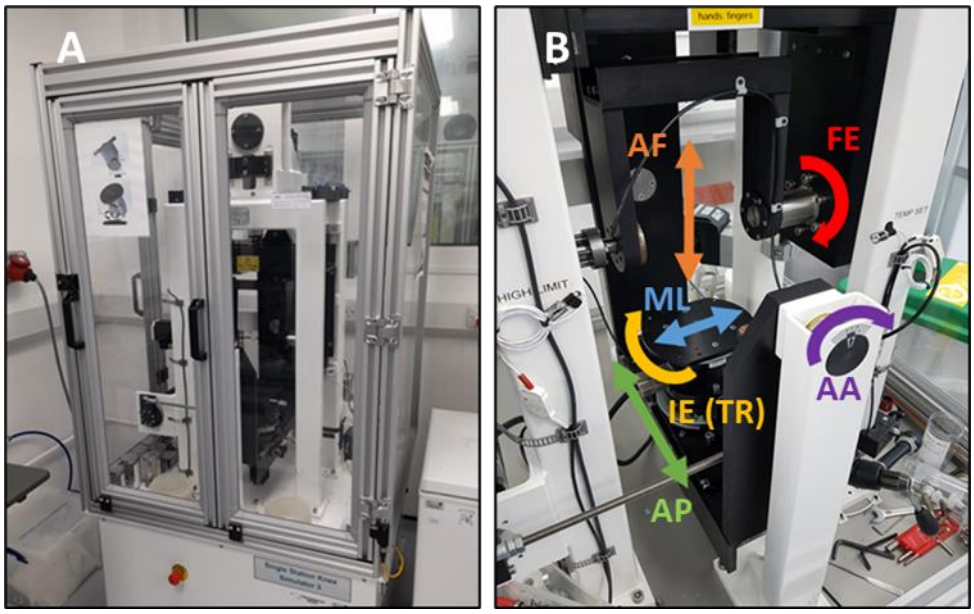


**Figure 1.11: ProSim Electrotechnical Single Station Knee Simulator used throughout the current thesis (A). Axes of motion within the simulator enabling the three translations and three rotations possible within the tibiofemoral joint (B).**

Knee simulators usually operate in one of two ways: displacement control or force control (Table 1.3); these refer to the methods for applying kinetic and kinematic input profiles to generate physiological motions. There are corresponding internationally recognised standards for both approaches (BS ISO, 14243-3:2014+A1:2020) and (BS ISO, 14243-1:2009+A1:2020); these prescribe the forces and displacements to be applied to the test specimen by each axis during walking gait simulations. Axial force and flexion extension profiles are equivalent for both control modes and applied in the same way: axial force is driven in force control and flexion-extension is driven in displacement control. The input profiles for the anterior-posterior and internal-external (tibial rotation) axes differ for each control mode and are driven in displacement control or force control respectively. ISO force and torque inputs are based on forces calculated from gait analysis of healthy subjects whereas ISO anterior-posterior displacement and internal-external (tibial rotation) inputs are derived from the outputs of TKR simulation studies which applied the ISO force and torque inputs (Abdelgaied et al., 2022). The ISO standards do not prescribe values for the adduction-abduction or medial-lateral axes. Another standard for wear testing of TKRs under force control has been developed which prescribes inputs for a range of activities of daily living (ASTM, 2017).

**Table 1.3: Control modes specified for each of the simulator axes in ISO standards. AF = axial force, FE = flexion-extension, AP = anterior-posterior, IE = internal-external, AA = adduction-abduction, ML = medial-lateral.**

| Standard | Driven axes and control mode<br>Red = displacement control<br>Green = force control<br>- = not prescribed | | | | | |
|---|---|---|---|---|---|---|
| | AF | FE | AP | IE (TR) | AA | ML |
| Force (ISO 14243-1:2009+A1:2020) | | | | | - | - |
| Displacement (ISO 14243-3:2014+A1:2020) | | | | | - | - |

Each control mode has associated advantages and disadvantages. When using displacement control, motion of the test sample is generated by inputting a specific displacement value, enabling precise control. When using force control, motion of the test sample is generated by the interaction of the applied forces and torques with the constraint mechanism designed to replicate ligament function (see section 1.5.6) and the geometry of the articulating surfaces. This creates more physiological motion but makes the experimental test setup more complex and increases the potential for dislocation. An inherent weakness of both approaches is the loads and displacements are based on an average patient. There is significant variation within the population in terms of BMI, age, geometry etc. which may influence kinematics *in vivo*; prescribed values may under constrain or over constrain motion and not necessarily produce results representative of the patient population. For wear assessment of TKRs it has been suggested the different control modes should be used to assess different factors (e.g. displacement control for materials and force control for design features) and results using different control modes should not be compared (Abdelgaied et al., 2022).

### 1.5.6 Soft tissue replication in knee simulation

In the natural knee, relative motion between articulating structures occurs during normal movement. To maintain correct alignment and stability, the soft tissues of the joint, particularly the ligaments, exert reactionary forces upon these structures to restrain excessive motion and prevent injury. In cadaveric knees, ACL removal has been shown to double anterior displacement and PCL removal to triple posterior displacement, whilst removal of either ligament resulted in a complete loss of tibial rotation (Fukubayashi et al., 1982). Therefore, any force controlled or unconstrained TKR, or natural joint

simulation model with soft tissues removed must include a means to represent the contribution of these missing structures to keep motion within physiological limits. Recommendations for how this should be achieved are given in the standard (BS ISO, 14243-1:2009+A1:2020); typically approaches have included the application of a spring constraint mechanism.

### 1.5.7 Development of spring constraints for soft tissue replication

Based on ligament stiffness's from Fukubayashi *et al.*, soft tissue constraints were applied through anterior and posterior silicone rubber bumpers in a hydraulic knee simulator (Walker et al., 1997). The authors acknowledged the stiffness of the silicone bumpers was independent of flexion angle and hence did not represent true soft tissue behaviour. To determine appropriate spring stiffness's and spring gaps to replicate natural ligament function in a knee simulator, a mathematical model applying an anterior-posterior or internal-external (tibial rotation) force was developed and compared to the results of Fukubayashi *et al*. (Haider and Walker, 2002). Spring settings for use in TKR simulations (k=7.24N/mm, k=33.8N/mm and ±2.5mm gap) were recommended based on these results. Another study experimentally validated these recommended spring values by comparing anterior-posterior and internal-external (tibial rotation) displacements produced by cadaveric knees (joint capsule intact) subjected to the ISO walking gait profile (van Houtem et al., 2006). One spring combination reproduced anterior-posterior motion but not internal-external (tibial rotation) motion. The authors concluded linear springs work differently to ligaments and suggested springs of intermediate stiffness may more accurately reproduce natural knee motion. Currently, application of an elastic spring element for both anterior-posterior force and internal-external (tibial rotation) torque restraining systems is recommended in the ISO standard+, as is a spring gap around the zero position (±2.5mm anterior-posterior, ±6° internal-external (tibial rotation) to account for ligament laxity (BS ISO, 14243-1:2009+A1:2020). The recommended values for spring stiffness and spring gap represent an average patient with a correctly aligned knee.

An electromechanical simulator was used to evaluate anterior-posterior shear force in the porcine tibiofemoral joint (Liu et al., 2015). Axial force, flexion-extension displacement and internal-external (tibial rotation) displacement inputs from the high kinematic Leeds knee walking gait profile for TKRs (McEwen et al., 2005) were scaled to porcine dimensions and applied to the porcine knees. During simulations three levels of anterior-posterior constraint (constrained, unconstrained and spring constraint) were used to mimic the rolling, sliding and combined rolling/sliding motions theorised to exist

in the knee. The constraint system consisted of physical springs (k=2.69N/mm with no gap). Results showed the approach could differentiate between the three conditions and hence have the potential to evaluate clinical interventions (Liu et al., 2015). The same porcine knee model and spring constraint setup, replicating the combined rolling/sliding motion of the knee, were subsequently used to evaluate tribological performance of osteochondral allografts against controls (P. Bowland et al., 2018). To further optimise the porcine knee model to more accurately mimic physiological motion, effects of varying spring stiffness and incorporating different sized spring gaps into the constraint system were investigated. Anterior-posterior displacement and anterior-posterior shear force for various combinations of spring stiffness and spring gap were compared to an intact knee joint. Two of these combinations, 20N/mm spring with 5mm gap and 9N/mm spring with 4 mm gap, were considered capable of replicating the intact condition (Liu et al., 2019).

### 1.5.8 Virtual spring constraints for soft tissue replication

It has been previously mentioned that linear physical springs do not behave exactly like the ligaments they are meant to represent (Walker et al., 1997) (van Houtem et al., 2006). In addition, inaccurate setup of physical spring constraints, due to user error or simply motion of the specimen during testing, has the potential to limit the validity of simulation results (Haider and Walker, 2002). As an alternative to physical springs, it is possible to apply constraints virtually (Figure 1.12); this approach has several advantages. The stiffness of physical springs is fixed, whereas the stiffness of a virtual spring can change based upon the demands of the system. Information from the previous time point can be used to calculate the necessary restraining force applied in the subsequent time point; this allows the system to constantly update itself (Johnston et al., 2018). In addition, virtual springs can considerably reduce setup time, changeover time and cost, as springs of different stiffness do not have to be purchased or manufactured; the required stiffness can simply be specified when creating the input profile.

A ProSim electromechanical simulator incorporating a virtual spring setup for both anterior-posterior and internal-external (tibial rotation) axes was used to assess how differences in laxity and stiffness influence wear rate for TKR insert designs (Johnston et al., 2018). Altering soft tissue constraints was found to significantly affect kinematics and wear and the authors concluded that variability in the patient population needs to be considered when designing and testing TKRs. A method to apply anterior-posterior and internal-external (tibial rotation) virtual spring constraints to human cadaver knees was developed using a ProSim single station knee simulator (Liu et al., 2020). It was shown each knee required specimen specific spring forces/torques and spring gaps to replicate

soft tissue function. It would seem reasonable to assume spring constrains may exist for early knee interventions. Based on these findings of these studies it would seem reasonable to assume variations in spring constraints may influence the wear damage and deformation behaviour of early-stage knee interventions within natural knee joints.

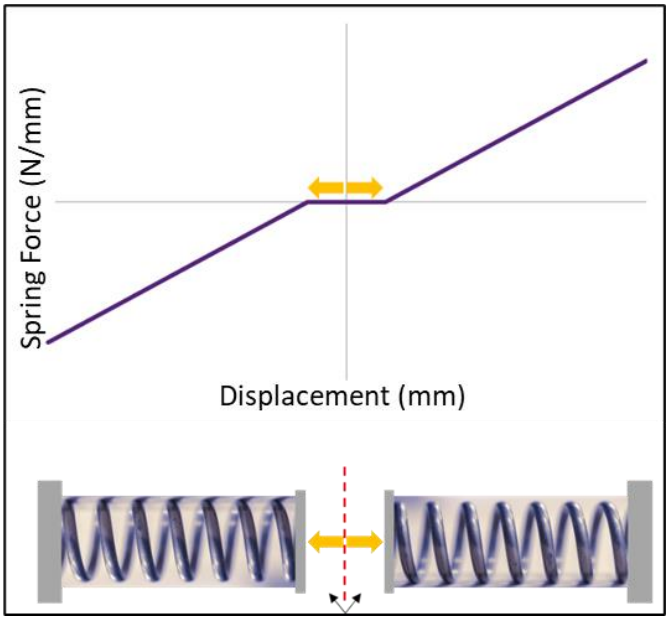


**Figure 1.12: Visualisation of the spring constraint mechanisms which could be applied to the axes of a knee simulator to replicate ligament function during simulations. The spring gap (yellow arrows) is a specified distance from the neutral position (grey line/red dotted line). Inside this region unrestricted movement is allowed to take place to take into account ligament laxity. Outside of this range, forces are applied by either a virtual spring (top) or physical spring (bottom) to prevent excessive displacements and maintain physiological kinematic outputs.**

A 6-DoF commercially available simulator AMTI VIVO™ (Advance Mechanical Technology, Inc.) is capable of testing both TKRs and natural joints. This system incorporates either a multi-fibre ligament model or heuristic model to represent soft tissue function and has been used to assess the function of TKRs in cadaveric knees (Willing et al., 2019) (Sarpong et al., 2020), however published evidence of its use for the assessment of early-stage knee interventions in a natural knee joint could not be found.

### 1.5.9 *In vitro* investigation of knee interventions within natural knee joints

A variety of animal tissue sources (Table 1.4) including caprine, ovine, porcine, bovine and human knee joints (

Table **1.5**) have been utilised during *in vitro* studies of natural knee joints in knee simulators. These approaches have investigated, biomechanics, joint injury and functional assessment of knee interventions . Investigations incorporating natural joint have also been used to optimise simulation performance by improving soft tissue constraints and to assess suitability of existing loading profiles to deliver physiological motion. Approaches range in complexity from single axis motion in materials testing machines to 6 degree-of-freedom (DoF) robot arms and knee simulators.

A single axis approach is easier to control and allows the contribution of individual motions to be assessed but is limited in clinical relevance. Robot arms provide good repeatability and precision measurement and enable joints to be assessed without removal of soft tissues. Dynamic simulation enables physiological loads and motions to be applied to replicate the *in vivo* environment. All three approaches can be used to assess friction parameters within the joint. Due to the difference in the size of the medial and lateral condyles and the multiple radii of curvature, the flexion-extension axis of the natural knee has no single fixed centre of rotation. However, some knee simulators only have a single centre of rotation along the flexion-extension axis, therefore when using a natural joint a centre of rotation must be specified. This may affect natural physiological motion during simulations and influence wear, damage and deformation behaviour in the joint.

**Table 1.4: Knee simulator studies incorporating natural knee joints using animal tissue. AF= axial force, FE = flexion-extension, AP = anterior-posterior, IE = internal-external, AA = adduction-abduction, ML = medial-lateral. *SI = superior-inferior with respect to patellofemoral joint, but driven via AP axis.**

| Paper | Tissue | What was assessed? (Intervention, injury model, simulator performance) | Simulation method | Driven axes and control mode<br>Red = displacement control<br>Green = force Control<br>Purple = semi-constrained<br>Blue = unconstrained<br>Orange = fixed<br>N/A = not applicable<br>NS = not specified | | | | | |
|---|---|---|---|---|---|---|---|---|---|
| | | | | AF | FE | AP | IE | AA | ML |
| (McCann et al., 2009) | Bovine | Effect of meniscectomy on cartilage wear | Simsol Pendulum friction simulator | | | NS | NS | NS | NS |
| (Lane et al., 2009) | Caprine | Osteochondral grafts | Materials testing machine (Instron) | | | N/A | N/A | N/A | N/A |
| (Walter et al., 2013) | Ovine | Cartilage defects | Materials testing machine (MTS 858 Mini Bionix) | | N/A | N/A | | N/A | N/A |
| (Lorenz et al., 2013) | Ovine | Cartilage defects | 6 DoF robot arm (KUKA KR 60-3) | | | | | | |
| (Bobrowitsch et al., 2014) | Ovine | Osteochondral grafts | Materials testing machine (MTS 858 Mini Bionix) | | N/A | N/A | | N/A | N/A |
| (Bobrowitsch et al., 2014) | Ovine | Simulation algorithm | 6 DoF robot arm (KUKA KR 60-3) | | | | | | |
| (Liu et al., 2015) | Porcine | Soft tissue constraints | 6 DoF Prosim Single Station Knee Simulator | | | | | | |
| (van de Bunt et al., 2017) | Caprine | ACL injury | 5 DoF Custom knee simulator | | | | | | |
| (Bowland et al., 2018) | Porcine | Osteochondral grafts | 6 DoF Prosim Single Station Knee Simulator | | | | | | |
| (Liu et al., 2019) | Porcine | Soft tissue constraints | 6 DoF Prosim Single Station Knee Simulator | | | | | | |
| (Walter et al., 2020) | Ovine | Osteochondral grafts | 6 DoF robot arm (KUKA KR 60-3) | | | NS | NS | NS | NS |
| (Cowie et al., 2021) | Porcine | Osteochondral grafts in patella | 6 DoF Prosim Single Station Knee Simulator | | | SI* | | | |

**Table 1.5: Knee simulator studies incorporating natural human knee joints. AF= axial force, FE = flexion-extension, AP = anterior-posterior, IE = internal-external, AA = adduction-abduction, ML = medial-lateral.**

| Paper | Tissue | What was assessed? (Intervention, injury model, simulator performance) | Simulation method | Driven axes and control mode<br>Red = displacement control<br>Green = force Control<br>Blue = unconstrained<br>Orange = fixed<br>NS = not specified | | | | | |
|---|---|---|---|---|---|---|---|---|---|
| | | | | AF | FE | AP | IE | AA | ML |
| (van Houtem et al., 2006) | Human | Soft tissue constraints | 6 DoF Stanmore Knee simulator | | | | | NS | NS |
| (Bedi et al., 2010) | Human | Meniscal repair | 6 DoF Stanmore knee simulator | | | | | NS | NS |
| (Sutton et al., 2010) | Human | Simulator loading profile | 6 DoF Simulator + materials testing machine (MTS) | | | NS | NS | | |
| (Maher et al., 2011) | Human | Meniscal scaffold | Instron-Stanmore KCI knee simulator | | | | | NS | NS |
| (Shimizu et al., 2018) | Human | TKR | Oxford type knee simulator | Quadricep forces, axes not specified | | | | | |
| (Panzica et al., 2015) | Human | Posterolateral complex repair | 6 DoF robot arm (KUKA) + 6 DoF fixation system | | | | | | NS |
| (Borque et al., 2015) | Human | TKR | 6 DoF custom knee simulator | Quadricep and hamstring forces, axes not specified | | | | | |
| (Lorenz et al., 2015) | Human | Patella stability | Custom knee simulator + 6 DoF robot arm (KUKA KR 60-3) | Quadricep and hamstring forces, axes not specified, KUKA robot applied patella motion/forces | | | | | |
| (Boguszewski et al., 2014) | Human | ACL repair | 6 DoF KUKA robot arm | | | | | | |
| (Lorenz et al., 2016) | Human | ACL repair | 6-DoF robot arm (KUKA KR 60-3) | | | | | | |
| (Willing et al., 2019) | Human | TKR | 6 DoF AMTI VIVO™ | | | | | | |
| (Sarpong et al., 2020) | Human | Soft tissue constraints | 6 DoF AMTI VIVO™ | | | | | | |
| (Liu et al., 2020) | Human | Soft tissue constraints | 6 DoF Prosim Single Station Knee Simulator | | | | | | |

### 1.5.10 Issues with cadaveric testing

The most representative *in vitro* environment in which to assess early knee interventions is the cadaveric human knee joint. However, there are several difficulties inherent to working with cadaveric tissue:

- Ethical approval must be granted and the process to obtain it may be lengthy
- Conducting a large-scale study is usually not feasible as tissue availability is limited
- It may be difficult to secure samples which are adequate to answer the research question, as there is high variability of donor tissue in terms of age, size and BMI. It has been shown resistance to fatigue failure of articular cartilage varies considerably between donors and decreases with age (Weightman, 1976).

These issues can be largely overcome with the use of animal tissue. Ethical approval is not required as they can be easily accessed through the food chain and there is a plentiful supply of young healthy samples, enabling larger sample numbers to be investigated. Animal models provide a convenient pathway via which experimental methodologies can be developed. Evidence generated from an animal model can demonstrate proof of concept and ensure only the most promising ideas are translated to human tissue to generate more clinically relevant data.

### 1.5.11 Natural Knee Joint Simulation of Osteochondral Interventions

Of the previously mentioned natural joint studies, five assessed osteochondral grafts (Lane et al., 2009) (Bobrowitsch et al., 2014) (Bowland et al., 2018) (Walter et al., 2020) (Cowie et al., 2021); each of these works analysed the effects of osteochondral graft positioning.

When inserting osteochondral grafts into the medial femoral condyles of caprine knees, all five experimental groups (intact cartilage, defect, osteochondral graft positioned proud, flush or depressed) were found to significantly increase coefficient of friction compared to healthy cartilage when subjected to simulated physiological loading; the proud group had the greatest influence on CoF (Lane et al., 2009). A similar pattern was observed when measuring dissipated energy in an ovine knee (Bobrowitsch et al., 2014), although surprisingly, there were no differences between the proud and healthy cartilage groups. The dissipated energy method was developed to enable frictional measurements

in whole knee joints by calculating the area within a rotation angle vs toque hysteresis curve (Walter et al., 2013). Both methodologies were restricted to analysis of motion along a single axis and lacked a quantified assessment of wear. In addition, these approaches had a very short experimental duration (9 cycles) (Bobrowitsch et al., 2014) or were assessed at a low speed (10mm/min) (Lane et al., 2009).

To overcome limitations of the *Lane et al.,* and *Bobrowitsch et al.,* studies, the biomechanical, tribological and wear, damage and deformation performance of porcine osteochondral allografts were assessed during porcine knee joint simulations (Bowland et al., 2018). This approach enabled assessment of osteochondral grafts implanted in the medial femoral condyles of porcine knees simulated under physiologically relevant conditions (walking gait) in a natural knee joint for the first time. Anterior-posterior shear force, the chosen outcome measure for inferring friction, was unable to detect differences between any of the experimental groups and healthy cartilage. However, optical profilometry measurements showed differences in volume between pre- and post-simulation silicone replicas of medial tibial surfaces (medial meniscus and tibial articular cartilage) to enable wear, damage and deformation to be quantified. Minimal changes were observed for native, flush and defects and proud graft positioning was shown to result in the greatest volume difference. Whilst effective for identifying volume changes, this method was unable to determine the mechanisms responsible for wear, damage and deformation.

The influence of graft position on dissipated energy was measured in an ovine knee under physiological conditions relevant to a sheep (cyclical flexion-extension under static 400N axial compressive load) (Walter et al., 2020); grafts were implanted into the loaded region of the medial femoral condyle. A small significant increase in friction was observed between native and 1mm high (proud) groups and a large increase in friction between the native and even (level with surrounding cartilage surface) and defect (cartilage removed from subchondral bone and subchondral bone implanted level with surrounding cartilage) groups. This study used short experimental duration (20 cycles) and was limited to applying motion in the flexion-extension axis under static loading.

A study assessing osteochondral graft positioning in the patella of a walking gait porcine patellofemoral joint simulation (Cowie et al., 2021) found similar results when using the same optical profiler methodology as Bowland *et al.* (Bowland et al., 2018); proud graft positioning resulted in increased wear, damage and deformation of the opposing cartilage surface. Wear, damage and deformation was also scored using the ICRS clinical grading system; cartilage lesions were observed for proud allografts (ICRS Grade 2) and positive controls (Grade 4). In addition, all grafts in this study had subsided from the initially implanted position into the graft site by the end of the simulation. Only walking

gait was simulated and the simulation duration, whilst the longest of any of the whole joint osteochondral models to date at 3 hours, only enables limited information about graft behaviour over time to be determined.

## 1.6 Enhanced simulation of natural knee joints

### 1.6.1 Introduction

Progression of osteochondral intervention assessment into natural knee joints and under physiological load and motion represented significant steps forward in the clinical relevance of *in vitro* experimental methods. Whilst an improvement, these approaches have still been limited in their ability to replicate the *in vivo* scenario. The development of more clinically relevant simulations will reduce reliance on live animal models and generate more clinically meaningful data. The following sections explore three aspects of preclinical simulation which could be developed to enhance natural knee joint simulation capabilities. The three areas for development discussed are:

- Applying a wider range of simulated activities
- Increasing simulation duration
- Suitable lubricants to use for tribological investigations of natural tissue

### 1.6.2 Increasing the number of simulated activities

Simulation studies have typically applied walking gait when assessing wear performance of knee replacements, however it has been suggested this may be insufficient to replicate loads and motions likely to be experienced by a significant segment of the potential patient population (Jennings et al., 2012) (Abdelgaied et al., 2017) (Abdelgaied et al., 2022). Throughout an average day the human knee experiences various movements during activities of daily living such as sitting, walking, stair ascending, squatting etc. The load and range of motion experienced within the tibiofemoral joint varies depending upon the activity (Lafortune et al., 1992) (Rowe et al., 2000) (Stewart and Hall, 2006) (Mündermann et al., 2008) (D'Lima et al., 2008).

Several common activities of daily living have shown to produce more challenging kinetic and kinematic conditions than those experienced during walking gait. Consequently, more recent wear simulation studies of knee replacements have progressed to apply activities of daily living (Schwiesau et al., 2013) (Schwiesau et al., 2013) (Abdel-Jaber et al., 2015) (Abdel-Jaber et al., 2016) (Abdelgaied et al., 2018) or more severe walking gait kinematics (Brockett et al., 2016). These studies have demonstrated higher

polyethylene wear rates can occur compared to standard walking gait for knee replacements for some activities, which demonstrates the limitations of assessing walking gait alone.

Due to the differences observed when assessing wear performance of knee implants, it would be reasonable to assume application of activities of daily living could also influence the behaviour of an osteochondral intervention within the natural knee. The success of osteochondral grafting relies on restoration of the congruent articulating surfaces and stability of the graft within the graft site to maintain low fiction articulation. Increasing the range of simulated activities may help to differentiate between similar interventions and highlight potential issues prior to implantation.

Recent *in vitro* cadaveric knee joint simulation studies have applied activities of daily living to assess the kinematics of the natural knee (Sarpong et al., 2020) and total knee replacement designs (Borque et al., 2015) (Shimizu et al., 2018) (Willing et al., 2019), however none of these studies looked at the influence of activities of daily living on the mechanical and tribological behaviour of articular cartilage or meniscal surfaces. There is evidence from pin-on-plate experiments showing multi-directional motion (Northwood and Fisher, 2007) or increased loading (Katta et al., 2009) increase wear, damage and deformation when applied to articular cartilage. However, as mentioned in the previous section, the range of kinetic/kinematic conditions used for *in vitro* assessment of osteochondral interventions in whole natural joint models has been limited to uniaxial (Lane et al., 2009) (Bobrowitsch et al., 2014) and walking gait (Bowland et al., 2018).

One goal of early-stage knee interventions is to enable individuals to return to their pre-injury level of activity, these patients are often young and active people who are often involved in sports (Mithoefer et al., 2009) (Harris et al., 2010) (Nielsen et al., 2017). An intervention implanted into this type of individual will likely experience more challenging loading and ranges of motion than one implanted into a less active individual, therefore functional performance may vary between groups and the activities of daily living may still be insufficient to replicate the *in vivo* situation. Therefore it is important to replicate conditions of the patient population who are likely to receive the interventions.

Research has been conducted to preclinically simulate athletic motions. A jump-landing motion has been successfully replicated and shown to be capable of causing non-contact ACL rupture in cadaveric knees using a dynamic knee injury simulator (Hashemi et al., 2007). A method for simulating drop vertical jumps and sidestep cutting tasks was developed using a six DoF robot arm (Bates et al., 2015); this approach was subsequently utilised to assess biomechanical differences in contralateral cadaveric knees (Bates et al., 2017). Preclinical simulation of motions commonly performed during sporting activities, such as: twisting, pivoting side-stepping and jumping and landing,

would provide a more representative assessment of the patient population into which osteochondral interventions are likely to be implanted. In addition, it would also be beneficial to apply input profiles which represent alternative loading experienced within the patient population, e.g. increased loading for patients with a high BMI.

### 1.6.3 Increasing simulation duration when using natural tissue

To date, simulation of osteochondral grafts in an animal joint model has been limited to 2-hours in the tibiofemoral joint (Bowland et al., 2018) and 3-hours in the patellofemoral joint (Cowie et al., 2021). To generate more useful information about early-stage knee intervention behaviour it would be beneficial to increase current simulation durations. Total knee replacements are simulated for millions of cycles; however, this is currently not a feasible strategy for early-stage knee interventions as no suitable experimental model exists in which to assess them. Without proper hydration, nutrition and mechanical stimulation natural tissue will degrade over time; thus the time available to conduct *in vitro* experiments is limited. Assessment of the mechanical properties of cartilage, wear and friction have been investigated for durations exceeding the current longest simulation of an osteochondral graft in a natural knee joint under physiological loading (3 hours). A variety of configurations, including tensile testing, compression testing and reciprocal sliding have been utilised during these extended duration experiments (Table 1.6).

**Table 1.6: Comparing the experimental approaches of *in vitro* studies which assessed chondral or osteochondral tissue for >3 hours duration.**

| Paper | Number of Cycles | Experimental approach |
|---|---|---|
| (Weightman, 1973) | 90,000 | Cyclic compression using Perspex-on-human cartilage (femoral head) |
| (Weightman, 1976) | Up to 100,000 | Tensile testing of human femoral head cartilage |
| (Weightman et al., 1978) | Up to 100,000 | Tensile testing of human femoral head cartilage |
| (Mccormack and Mansour, 1998) | 97,200 | Cyclic compression with indenter, Plexiglas-on-bovine cartilage, then tensile test to failure |
| (Lizhang et al., 2011) | 86,4000 (24 hours) | Bovine cartilage-on-metal (pin-on-plate) |
| (Taylor 2012) | 115,200 (4 x 28,800) | Porcine cartilage-on-metal (acetabulum in pendulum fiction simulator) |
| (Cilingir, 2015) | 150,000 | Bovine cartilage-on-cartilage (pin-on-plate) |
| (Kaplan et al., 2017) | 36,000 (3 x 12,000) | Cyclic compression, metal-on-human cartilage |
| (Vazquez et al., 2019) | 50,000 | Compression, porcine cartilage-on-cartilage (3-month-old) |
| (Durney et al., 2020) | 8,640 (24 hours) 17,280 (48 hours) | Bovine cartilage-on-cartilage (2/3-month-old bovine ankle-on-tibia) |

Several of these studies indicate loading for tens of thousands of cycles *in vitro* may cause fatigue failure of articular cartilage. Damage identical to fibrillation of osteoarthritic cartilage was observed in cadaveric human cartilage after 90,000 cycles at 2 MPa during cyclic compression (Weightman, 1973). Tensile fatigue testing of cadaveric human articular cartilage demonstrated fatigue properties are donor dependent and decrease with age during cycle to failure experiments (Weightman, 1976) (Weightman et al., 1978). A reduction in cartilage tensile strength was observed after cyclic compression with a maximum load of 65N for 97,200 cycles, this was not present at 64,800 cycles (Mccormack and Mansour, 1998). Discolouration, scratching and bone exposure occurred on cartilage when articulating a porcine acetabulum for 115,200 cycles in a pendulum friction simulator with a dynamic load (25 N - 800 N) and flexion-extension motion (±15°) (Taylor, 2012). Increase wear of bovine cartilage was observed with increased static loading (0.5 MPa – 8 MPa) during 24 hours of reciprocal sliding (Lizhang et al., 2011). Cartilage wear occurred during 150,000 cycle reciprocal sliding and rotation

experiments when applying a 60N (1.8 MPa) load to mature bovine cartilage (Cilingir, 2015). For the sliding motion use of bovine serum reduced wear factor compared to phosphate buffered saline throughout the test, this effect was also initially observed for the rotational motion but wear factor increased with an increasing number of cycles. Disruption of the collagen network due to mechanical fatigue was observed when applying loads to simulate walking (20 N/2.83 MPa), extreme weightlifting (120 N/17 MPa) and injury (200 N/28.3 MPa) during 36,000 cyclic compression testing of cadaveric human cartilage (Kaplan et al., 2017); increased number of cycles and increased loading were shown to cause fatigue. Increasing number of cycles resulted in tissue softening and structural damage (surface fibrillation) when applying 10,000 and 50,000 cycles of compression to porcine cartilage at loads between 6 MPa and 10.3 MPa (Vazquez et al., 2019). Delamination of immature bovine cartilage occurred during 8,640 cycle (24-hour) and 17,280 cycle (48-hour) reciprocal sliding experiments when applying a load of 111.2 N (2.2 MPa) (Durney et al., 2020).

Whilst fatigue failure and cartilage damage were observed, these studies also indicate the potential to increase the current simulation duration of a whole natural knee joint. The experimental conditions used during these studies: unconfined compression, cadaveric tissue, non-cartilage counter faces (metal/plastic), direct application of tensile stress instead of compression, could potentially have accelerated fatigue failure. During shorter experiments within the study by Durney *et al*., it was shown delamination occurred sooner when articulating cartilage against glass compared to cartilage against cartilage (Durney et al., 2020). Initiation of fatigue failure in a whole joint may require a greater number of cycles; therefore a whole joint could potentially provide a suitable *in vitro* simulation model for the assessment of early-stage knee interventions of a longer period. In addition, the authors suggested a much larger number of cycles may be required to initiate delamination failure in mature human cartilage *in vivo* than was required for the immature bovine tissue used during their study. This idea is supported by the work of and McCormack and Mansour and *Weightman et al*., which showed some cartilage specimens did not fail after 64,800 (Mccormack and Mansour, 1998) and 100,000 cycles tensile testing (Weightman, 1976) (Weightman et al., 1978). Although these studies did show significant variability in the number of cycles to failure for different donors, some failed immediately upon load application whilst others had not failed after 1000,000 cycles.

In two studies, a reduction in tensile strength (Mccormack and Mansour, 1998) and subsurface delamination (Durney et al., 2020) occurred with no evidence of changes in the articular surfaces. Therefore visual assessment of wear, damage or deformation alone may be insufficient to highlight structural changes during longer experiments.

Only one approach (Taylor, 2012) attempted to assess an intervention in a natural joint under clinically relevant loading. A metal femoral head was articulated against a porcine acetabulum in a hemiarthroplasty setup for hip replacement for 115,200 cycles. As far as the author is aware the longest duration tribological study of osteochondral knee interventions in a natural knee joint are 2-hours in the tibiofemoral joint (Bowland et al., 2018) and 3-hours in the patellofemoral joint (Cowie et al., 2021). Evidence from the studies in this section demonstrates the potential to progress natural knee joint simulation durations from a few hours to a few days.

### 1.6.4 Replicating articulating surfaces during longer simulations

Before, during and after tribological experiments with articular cartilage, changes to the articulating surfaces need to be assessed. Unless cartilage can be measured within an appropriate time window, the articulating surfaces may experience changes due to dehydration or damage from freeze-thawing (if stored frozen), these factors could affect measurements of wear, damage and deformation. Metrological methods which directly contact cartilage surfaces may also introduce changes during measurements. To solve these problems silicone has been used for creating replicas of cartilage surfaces.

Several studies have previously utilised silicone replicas (McCann et al., 2009) (Russell, 2010) (Taylor, 2013) (Bowland et al., 2018) (Cowie et al., 2021). Silicone replicas have been shown to have similar surface roughness to the original surface of both native and damaged cartilage (McCann et al., 2009). The use of an optical profiler (Alicona Infinite Focus) to calculate comparable volume loss to gravimetric wear when analysing scans of AccuTrans silicone replica samples has also been validated (Bowland, 2016). AccuTrans silicone is recommended for imaging curved surfaces using the Alicona as it is less reflective than other silicone compounds. This has enabled its use for the assessment of wear, damage, deformation and graft stability during whole joint simulation studies of the tibiofemoral (Bowland et al., 2018) and patellofemoral joint (Cowie et al., 2021). The studies were only assessed for two and three hour respectively. Prolonged simulation durations may result in more advanced stages of damage which could contraindicate the use of AccuTrans silicone. Whether it remains a viable option for replicating surfaces over a longer time period is currently not known.

In addition to enabling measurement of surfaces, silicone replicas are advantageous in situations where it is impractical to continually pause experiments and wait whilst samples are analysed, or the immediate post-test condition needs to be captured. This can reduce experimental duration and increase efficiency by allowing concurrent analysis of the replicas as experiments are running.

### 1.6.5 Lubricants for *in vitro* wear studies of natural tissue

One important component which will influence tribology and therefore potentially simulation duration is the lubricant. In the natural knee joint synovial fluid contributes to both lubrication and delivery of nutrients to the articular cartilage (Schmidt and Sah, 2007) (Schmidt et al., 2007). Whilst the ideal choice to ensure proper function and hence physiological relevance, synovial fluid only exists in small volumes reportedly between 0.2 ml (Binette and Schmid, 1965) and 2.5ml (Goldring and Goldring, 2017) within the joint space. This makes it impractical for use during *in vitro* simulations of TKR's or natural joints where the joint capsule has been removed, as these may require much higher volumes of lubricant. Therefore, due to limited availability and other practical issues, a suitable alternative is required.

During *in vitro* wear assessment of TKR's, standards recommend bovine calf serum diluted to 20 g/l with deionized water as a synovial fluid substitute (BS ISO, 14243-1:2009+A1:2020) (BS ISO, 14243-3:2014+A1:2020). This produces a lubricant which replicates the protein concentration in human synovial fluid (Decker et al., 1959) (Binette and Schmid, 1965) (Saari et al., 1993) and enables simulations to generate wear behaviour similar to that observed on *ex vivo* implant retrievals. However, this approach does have limitations. Protein degradation and precipitation formation influencing wear processes (Harsha and Joyce, 2011), difficulty comparing lab results due to differences in protein concentration and composition of serum batches (Bortel et al., 2015) and not effectively replicating the synovial fluid of the patient population (Galandáková et al., 2017) have all been highlighted as potential issues.

Simple isotonic lubricants consisting of water and ions, such as Ringer's Solution or PBS, are employed during *in vitro* experimental methods to maintain tissue hydration and provide lubrication. When assessing cartilage contacts, it has been shown Ringer's Solution and PBS provide inferior tribological performance compared to synovial fluid (Forster and Fisher, 1996) (Schmidt and Sah, 2007) (Caligaris and Ateshian, 2008) (Caligaris et al., 2009) or other lubricants which more accurately mimic synovial fluid (Cilingir, 2015) (Veselack et al., 2018) (Furmann et al., 2020). Once interstitial fluid pressure has subsided these simple lubricants as less effective at preventing cartilage damage due to a lack of boundary lubricating molecules which are present in other lubricants.

Used alone, or in combination, evidence in the literature suggests hyaluronic acid, proteins and phospholipids are fundamental to the tribological performance of articular cartilage (Murakami et al., 2013) (Furmann et al., 2020). Hyaluronic acid has shown to be responsible for the viscosity of synovial fluid (Mazzucco et al., 2004) (Zhang et al., 2014) (Rebenda et al., 2020). The viscosity gives synovial fluid shear thinning behaviour;

this protects articular cartilage from excessive shear stresses as shearing occurs in the fluid and not the articulating surfaces (Hamrock et al., 2004). Albumin and immunoglobulin G are the most abundant proteins in synovial fluid and are involved in boundary lubrication mechanisms. Phospholipids have been shown to contribute to boundary lubrication of cartilage (Schmidt et al., 2007) (Forsey et al., 2006).

Two studies have assessed the influence of lubricants on the tribology of cartilage-on-cartilage contacts over an extended duration. Greater wear factor was found when using PBS compared to bovine serum during 150,000 cycle experiments (Cilingir, 2015). It was shown the lubricant did not influence the onset of damage or CoF when comparing phosphate buffered saline and synovial fluid for 8,640 cycles (24 hour) and 17, 280 (48 hour experiments) (Durney et al., 2020). Both these approaches had limitations. In the first study, samples were weighed to measure volume loss, this is not necessarily the most useful approach for assessing chondral changes as it only assesses wear, not damage or deformation. Surface fibrillation may occur but damaged cartilage may not detach from surface, non-visible subsurface damage may be present or the articulating surfaces may be permanently deformed. These issues could compromise function and are important to identify. Measurements of volume loss do not take this type of damage into account, as functionally inept tissue still partially attached to the surface would be included during volume calculations. The second study provided a more comprehensive wear and damage assessment; however the 24-hour and 48-hour experiments were conducted at a frequency of 0.1Hz and therefore completed far fewer cycles overall.

A natural knee experimental tribological simulation model developed at the University of Leeds (Liu et al., 2015) (Liu et al., 2019) (Bowland et al., 2018) aimed to enable the assessment of early-stage interventions within the tibiofemoral joint. Two of the studies were short (300 cycle) method development studies to assess kinematic spring constraints and used 25% NBCS (Liu et al., 2015) and Ringer's Solution (Liu et al., 2019) respectively. In the latter study, Ringer's Solution was used due to its simplicity and reduced cost compared to 25% NBCS in PBS and was more physiologically relevant than PBS or water due to having a more similar ion concentration to synovial fluid. The third study utilised 25% NBCS in PBS during walking gait simulations assessing the tribological performance of osteochondral grafts (Bowland et al., 2018) this was chosen due to its availability and history of use within TKR simulation. This study did not assess influence of the 25% NBCS in PBS lubricant on graft performance.

### 1.6.6 Summary

Use of early stage knee interventions is increasing, to enable predictions about the *in vivo* performance of these interventions *in vitro* experimental methods need to be developed. Natural knee joint simulation models provide a physiologically relevant environment in which to explore the mechanical and tribological behaviour of these interventions. Development of *in vitro* methods has the potential to provide the evidence needed to support clinical use of early-stage knee interventions and reduce reliance on preclinical live-animal models.

Thus far, *in vitro* investigation of osteochondral interventions has been restricted to walking gait. Evidence from simulation of total knee replacements and cartilage-on-cartilage pin-on-plate studies demonstrate alternative motions may increase the wear, damage and deformation of cartilage surfaces. The influence of alternative loading and motion on the functional performance of osteochondral grafts in natural knee joints is unknown.

Potential experimental durations for *in vitro* investigations of osteochondral interventions in natural knee joints are limited due to degradation of the non-living tissue used. Existing study durations have been limited to only a few hours; therefore little is known about long-term performance. Evidence from the few studies which have assessed mechanical and tribological performance of cartilage for longer suggests the potential to increase experimental simulation durations from hours to days. Extending simulation duration has the potential to invalidate silicone replicas as a viable method for assessing wear, damage and deformation due changes in the cartilage surface. This method needs to be assessed on cartilage samples which have been simulated for an extended duration.

The use of bovine serum in saline solution for replicating synovial fluid in total joint replacement simulations has been questioned and existing lubricants are not necessarily representative of the early-stage knee intervention patient population. There is currently no consensus on the most appropriate lubricant to use when simulating natural knee joints.

## 1.7 Aims and Objectives

### 1.7.1 Aims:

- The first aim of the research in this thesis was to advance an experimental porcine knee joint simulation model used to study the wear of early knee interventions, by investigating suitable lubricants, activities of daily living and the maximum study duration

- The second aim was to assess the tribological performance of a novel decellularised porcine osteochondral allograft under these enhanced simulation conditions for the first time

### 1.7.2 Objectives:

- To determine an appropriate lubricant to use for extending the duration of tribological investigations of non-living porcine cartilage. A simple geometrical pin-on-plate configuration will be used to systematically study different lubricants.

- To determine the feasibility of extending simulation duration for porcine knee joints during walking gait simulations in a six-axis knee simulator by assessing the physical and biological degradation of the knee joint and lubricant

- To validate the use of Accutrans AB silicone for replicating articular cartilage surfaces

- To assess the feasibility of simulating other activities of daily living, which may involve movements with more challenging loading and complex motion, using the porcine knee joint model. Assess the influence of different activities on the functional performance of osteochondral interventions

- To compare the tribological performance of a novel decellularised porcine osteochondral intervention to osteochondral allografts in a porcine knee joint for the first time

# Chapter 2

# Materials and Methods

## 2.1 Materials

### 2.1.1 PBS

Phosphate buffered saline (PBS) (Oxoid) is a buffer solution used to maintain constant pH and has a history of use during *in vitro* research. PBS is isotonic with bodily fluids and was used throughout this study to keep tissue samples hydrated during dissection and storage. In addition, PBS was used for diluting new-born calf serum to a specific protein concentration to create a lubricant. The solution was prepared by dissolving 10 PBS tablets in 1l of deionised water and stored at room temperature. The PBS had a pH of 7.3 and the exact composition used throughout this study can be found in (Table 2.1).

**Table 2.1: Composition of PBS tablets (Oxoid BR0014).**

| Formula | Grams/litre |
|---|---|
| Sodium chloride | 8.0 |
| Potassium chloride | 0.2 |
| Disodium hydrogen phosphate | 1.15 |
| Potassium dihydrogen phosphate | 0.2 |

### 2.1.2 Ringer's Solution

Ringers Solution (Sigma Aldrich) is a combination of several salts dissolved in water. During this project Ringer's Solution was used as a lubricant for pin-on-plate and knee simulator experiments articulating cartilage surfaces against one another. Ringer's Solution is isotonic with body fluids, this prevents diffusion of solutes between the lubricant and interstitial fluid within the cartilage samples and keeps tissue samples hydrated. Ringer's Solution was prepared by dissolving eight ¼ strength Ringer's Solution tablets in 1l of deionised water and stored at room temperature. The exact composition of the Ringer's Solution used throughout this study can be found in (Table 2.2).

**Table 2.2: Composition of Ringer's Solution tablets (Sigma 96724).**

| Formula | Grams/litre |
|---|---|
| Sodium Chloride | 2.25 |
| Potassium Chloride | 0.105 |
| Calcium Chloride | 0.12 |
| Sodium Bicarbonate | 0.05 |

### 2.1.3 New-Born Calf Serum

New-born calf serum (NBCS) (Gibco®) is sourced from the blood of calves <20 days old. It contains various nutrients, proteins, phospholipids and growth factors which maintain cellular function. During this project NBCS was diluted with PBS or Ringer's Solution to create a 25% NBCS in PBS or Ringer's Solution lubricant for tribological investigations of articulating cartilage surfaces; this lubricant had total protein content of 15.75 g/L. Lubricants were used immediately or stored frozen at -20°C until required. The composition of NBCS used throughout can be seen in (Table 2.3).

**Table 2.3: Typical Biochemical and Hormone Profile for Serum (ThermoFisher 16010159).**

| Constituents | Concentration mean(range) |
|---|---|
| Total protein | 6.9 (6.1 – 7.5) g/dl |
| Albumin | 3.6 (3.4 – 3.8) g/dl |
| Globulin (total) | 3.3 (2.6 – 3.7) g/dl |
| Glucose | 105 (90 - 118) mg/dl |
| Cholesterol | 78.3 (95 - 121) mg/dl |
| Triglycerides | 16.3 (15 – 17) mg/dl |
| Sodium | 137 (134 – 142) meq/L |
| Potassium | 5.5 (4.9 – 6.0) meq/L |
| Calcium (total) | 9.9 (9.7 – 10.0) mg/dl |
| Chloride | 106.7 (99 – 112) meq/L |
| Phosphorus (inorganic) | 7.6 (6.8 – 8.4) mg/dl |
| Iron (total) | 74 (53 – 93) µg/dl |
| pH | 7.6 (7.3 - 8.1) |

### 2.1.4 Sodium Azide

Sodium azide is an inorganic salt commonly used as an antibacterial and antimicrobial agent as it inhibits the growth of gram-negative bacteria. During this project 0.04% sodium azide was added to 25% NBCS in Ringer's Solution lubricants to retard bacterial growth during knee simulation studies.

### 2.1.5 Soya Lecithin

Phospholipids are found within human synovial fluid and have been shown to contribute to tribological behaviour. Soya lecithin is composed of a mixture of various phospholipids which are found within synovial fluid. During this project powdered soya lecithin (BioServ) was used when making physiological synovial fluid substitutes.

### 2.1.6 Bovine Serum Albumin

Albumin is a water-soluble globular protein and the most abundant protein found within human synovial fluid and has been shown to contribute to tribological behaviour. During this project powdered bovine serum albumin (Sigma A7030) was used when making physiological synovial fluid substitutes.

### 2.1.7 Bovine Immunoglobulin G

Immunoglobulin G is an antibody present within the immune system which protects against viral and bacterial infection. Immunoglobulin G is one of the main proteins found within human synovial fluid and has been shown contribute to tribological behaviour. During this project powdered bovine immunoglobulin G (MP Biomedicals) was used when making physiological synovial fluid substitutes.

### 2.1.8 Hyaluronic Acid

Hyaluronic acid is a non-sulphated glycosaminoglycan responsible for the non-Newtonian shear thinning properties of synovial fluid. During this project powdered hyaluronic acid (Sigma 53747) (1.5 MDa -1.8 MDa) was used when making physiological synovial fluid substitutes.

### 2.1.9 Natural tissue samples

Porcine tissue (Large White Pigs, ~6 months) was used for all studies during this project and bovine tissue (~18 months) was used for the pin-on-plate study only; all tissue was sourced from the local food chain (John Penny and Sons). Porcine legs were delivered whole and required dissection of soft tissue to access the relevant tissues for a particular study. Bovine femurs were delivered with the soft tissues already removed, except the patella which was retained to maintain hydration and protect the cartilage surface of the trochlea groove during transport. Throughout the project efforts were made to donate unused tissue (ankle joints, patellae, femoral heads etc.) to other research projects to minimise cost and tissue waste.

### 2.1.10 Polymethylmethacrylate Cement

Polymethylmethacrylate (PMMA) cement was created by mixing a powder component and liquid component in a 2:1 ratio. PMMA was poured into femoral and tibial pots and left to set for a minimum of 30 minutes to fix porcine knee joints in the desired alignment and enable them to be mounted into the knee simulator.

### 2.1.11 AccuTrans AB Silicone

AccuTrans AB casting silicone (Coltène/Whaledent AG) consists of a base and catalyst component which are combined using a mixing tip to form a silicone that sets in four minutes at 20°C. During this study AccuTrans was used to create replicas of articular cartilage surfaces for the visual and quantitative assessment of wear, damage and deformation.

### 2.1.12 Thioglycollate Medium USP

Thiogylcollate (Oxoid) (Table 2.4) is a medium used to cultivate aerobic and anaerobic organisms. During this project Thioglcollate broths were used to assess bacterial growth on cartilage surfaces.

**Table 2.4: Composition of Thioglycollate powder (Oxoid CM0173)**

| Formula | Grams/litre |
|---|---|
| Yeast extract | 5 |
| Tryptone | 15 |
| Glucose | 5.5 |
| Sodium thioglycollate | 0.5 |
| Sodium chloride | 2.5 |
| L-cystine | 0.5 |
| Resazurin | 0.001 |
| Agar | 0.75 |
| pH 7.1 ± 0.2 at 25°C | |

### 2.1.13 Tryptone Soya Broth

Tryptone Soya (Oxoid) Table 2.5 is a medium used to cultivate aerobic and anaerobic organisms. During this project Tryptone Soya broths were used to assess bacterial growth on cartilage surfaces.

**Table 2.5: Composition of Tryptone Soya powder (ThermoFisher CM0129b).**

| Typical Formula* | Grams/litre |
|---|---|
| Pancreatic digest of casein | 17.0 |
| Enzymatic** digest of soya bean | 3.0 |
| Sodium chloride | 5.0 |
| Di-potassium hydrogen phosphate | 2.5 |
| Glucose | 2.5 |
| pH 7.3 ± 0.2 at 25°C | |
| ** contains papain | |
| * adjusted as required to meet performance standards | |

## 2.2 Methods

### 2.2.1 Uniaxial Reciprocating Pin-on-Plate Friction and Wear Rig

During this study two reciprocating pin-on-plate friction rigs were used to study the tribology (wear and friction) of articular cartilage, Friction Rig A (Figure 2.1) and Friction Rig B; the setup and operation was identical for each rig. A stationary pin sample held in a plain bearing was articulated under constant load against a plate sample attached to a translating stage. The load was applied via a mass positioned on a cantilevered loading arm above the plain bearing. As the stage translated, frictional forces generated at the pin and plate interface caused the pin-holder to apply pressure to the plain bearing resulting in movement of the bridge component the plain bearing was situated within. Movement of the bridge was transferred to a piezoelectric sensor via a Tourin washer, this compressed a crystal within the piezoelectric sensor generating an output voltage; this signal was then sent to a charge amplifier and LabView data acquisition unit (National Instruments) connected to a computer where it could be processed to calculate the CoF.

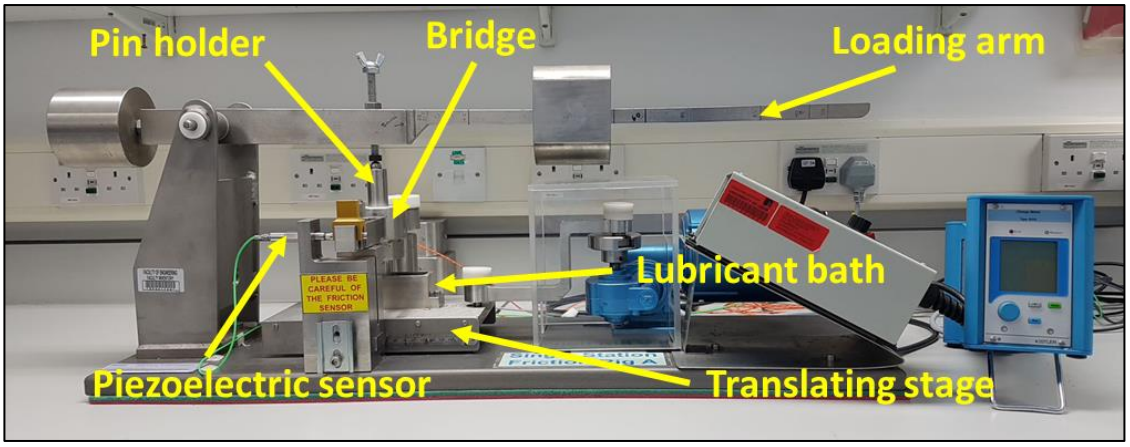


**Figure 2.1: Reciprocating friction rig A.**

The following describes, how the friction rigs were calibrated, how pin-on-plate experiments were setup and how data were recorded and processed. Differences between polymer-on-metal (control) and cartilage-on-cartilage setup will be highlighted where necessary.

### 2.2.2 Calibration of the Reciprocating Friction Rig

To ensure friction data generated from pin-on-plate experiments was reliable both friction rigs were calibrated prior to studies. There were two stages to the calibration process, calibration of the piezoelectric sensor and calibration of the loading arm, the procedure was identical for each rig. Before calibration began the stroke length and sliding speed of the translating stage were set. The stroke length was adjusted by changing the position of the arm in the slot of a scotch yoke mechanism the verified using callipers. To set the sliding speed the motor was switched on and the number of revolutions in 30 seconds was counted. The motor speed was then adjusted until the correct number of revolutions occurred during the 30 second window for a given stroke length (for this study 15 revolutions in 30 seconds = 10mm/s sliding speed for a stroke length of 20mm).

### 2.2.3 Calibration of Piezoelectric Force Sensor

To calibrate the piezoelectric sensor the rig was positioned at the edge of the workbench and a pulley wheel was clamped to the rig and workbench at this end (Figure 2.2). The loading arm was raised and the pin-holder was then placed through the plain bearing and secured in place with a grub screw so it was suspended above the reciprocating stage but did not contact it. Next, a string was wrapped around the bottom end of the pin holder at one end and fed through a hole in the rig beneath the loading arm and over the

wheel at the other. The string was allowed to dangle freely but pulled taught so it did not contact the edges of the hole.

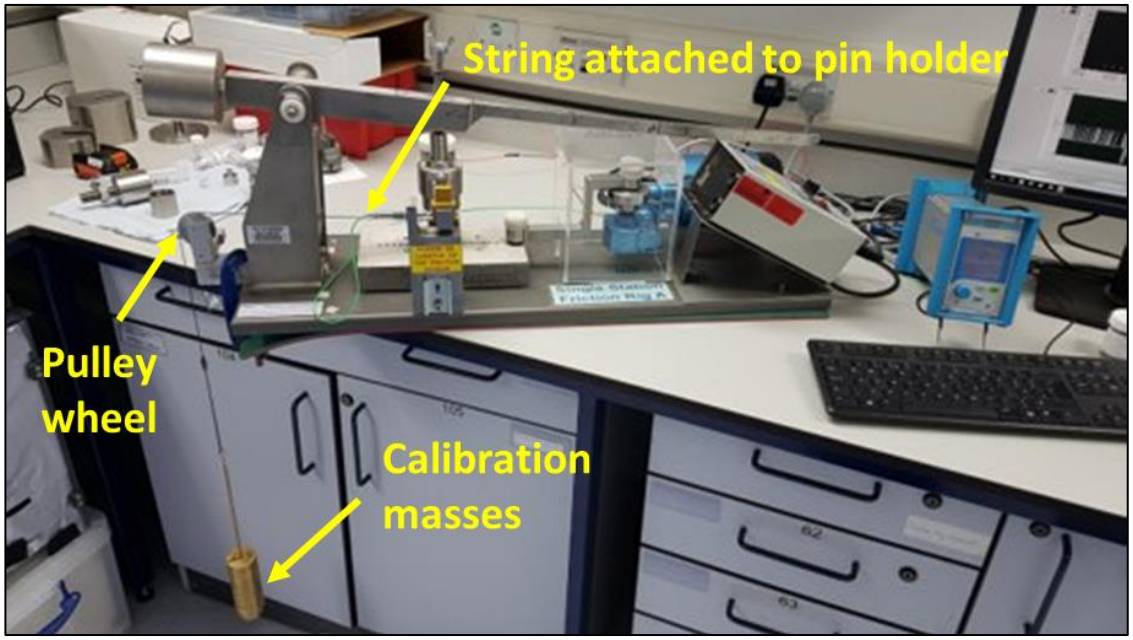


**Figure 2.2: Calibration of the piezoelectric sensor on Friction Rig A.**

A LabVIEW (National Instruments) program recorded the output voltage generated with zero load applied, three measurements were taken with data logged for 10 seconds every 20 seconds. Next, a 200g hanger was added to the string and an additional three measurements were taken, this process was repeated by adding 200g masses until a total of 2200g had been applied. Voltages generated are based on the applied load, the 2200g total was chosen to ensure the piezoelectric sensor would be accurate within the range of voltages produced during future experiments. The process was then reversed, with the sequential removal of the 200g masses until only the string was left and zero load applied. This was done to determine the influence of hysteresis to check the piezoelectric sensor functioned the same during loading and unloading. The loading and unloading procedure was repeated three times to check for drift and ensure repeatability (Figure 2.3). The calibration process produced a calibration curve for each rig from which calibration constants were obtained (Figure 2.4). During calibration, it was only possible to set up the pulley wheel at one end of the rig. Therefore, the force applied to the sensor by the hanging masses was only applied in one direction and this is what the calibration constants are based on. To confirm the sensor was also working correctly in the opposite direction, control tests were run prior to experiments (see Setting up a Pin-on-Plate Test section on p.8).

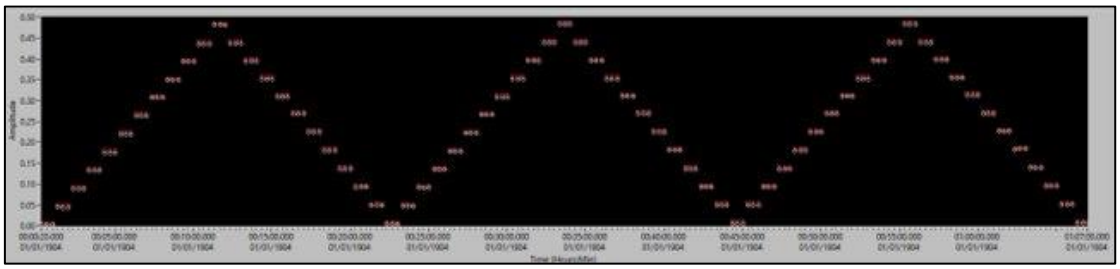

**Figure 2.3: Charge amplifier readings for three consecutive periods of loading and unloading during calibration of the piezoelectric sensor on Friction Rig A.**

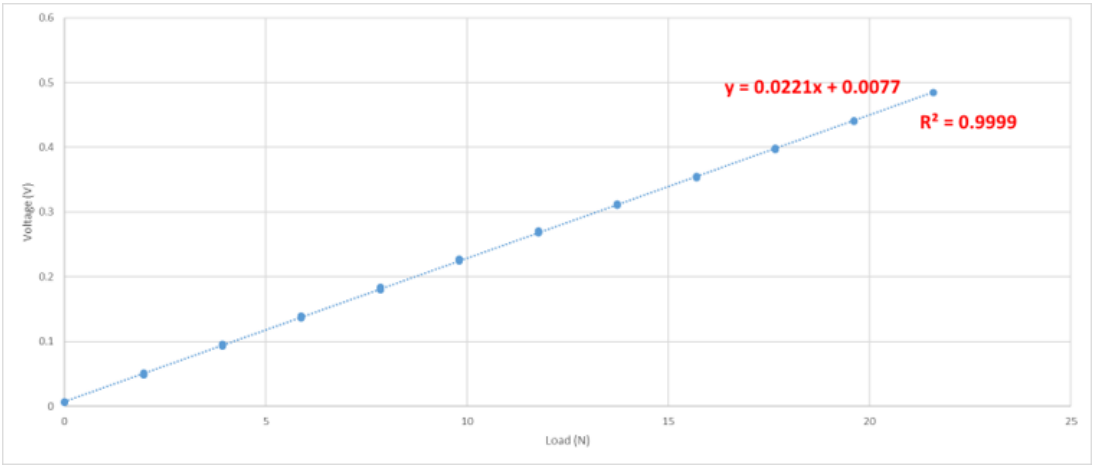


**Figure 2.4: Calibration curve generated for Friction Rig A.**

### 2.2.4 Calibration of Loading Arm

The second phase of the calibration process was to ensure the mass on the loading arm was in the correct position to apply the desired load. A 500N load cell was plugged in and allowed to warm up for 30 minutes before use. The load cell was placed above the plain bearing and held in place using a screw inserted through the loading arm. A spirit level was used to check the loading arm was parallel. The mass was placed onto the loading arm and the applied load read from the load cell display; the position of the mass was adjusted until the load cell displayed the desired value (120N) and this point was then marked onto the loading arm.

### 2.2.5 Calculating CoF

To calculate the dynamic CoF (μ) the calibration constants obtained from the calibration curve, average voltages and applied load were substituted into *Equation (1)* using Microsoft Excel (Microsoft Corporation).

$$\mu = \frac{\left(\frac{\left(\frac{maximium\ average\ voltage - minimum\ average\ voltage}{2}\right) - y\ intercept}{gradient\ of\ calibration}\right)}{load} \quad (1)$$

Due to the reciprocating nature of the pin-on-plate rig there are periods when pin and plate surfaces are in motion and periods when they are stationary. The voltage has the greatest magnitude when the plate stops and changes direction, the maximum and minimum values (Figure 2.5) are measures of static friction at this point. The minimum average (MinAV) and maximum average (MaxAV) voltages (Figure 2.5) are dependent on the number of peaks and troughs in the waveform, if n is large then the output is representative of the flat part of the waveform as the plate is moving and MinAV and MaxAV can be used as a measure of dynamic friction.

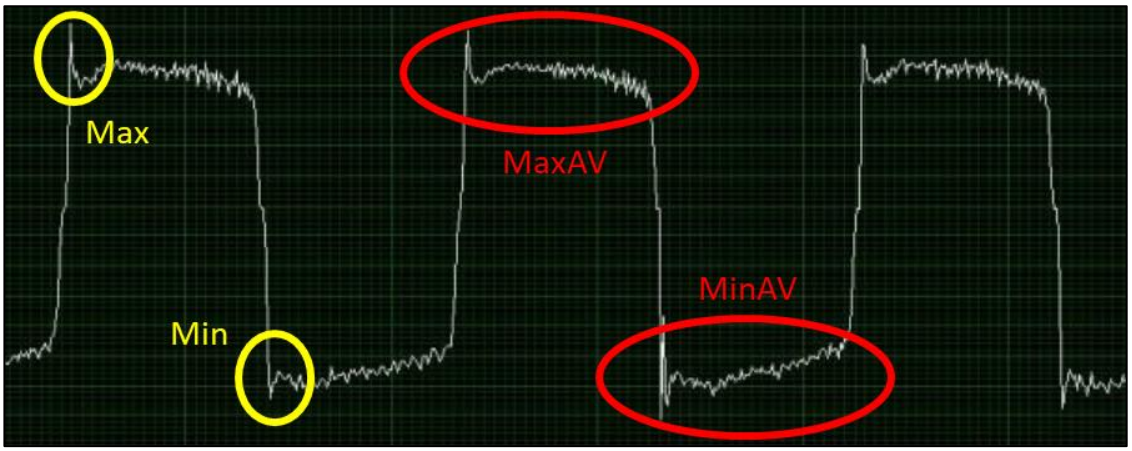


**Figure 2.5: 5 An output voltage trace from the pin-on-plate rig highlighting regions where voltage measurements were taken, maximum and minimum voltages (yellow circles), maximum average and minimum average voltage (red ovals).**

### *2.2.6* Setting up a Pin-on-Plate Test

To check the function of the rig, ensure charge meter outputs were within a range appropriate for the materials and prevent natural tissue samples being wasted, a verification with materials of known CoF was performed. A UHMWPE pin against stainless-steel plate control was run prior to each natural tissue experimental group. Previous work within the institute running control tests on the pin-on-plate rig has produced a CoF values of 0.042 – 0.1 (Bowland, 2016). The UHMWPE pin was inserted into a metal collet and secured in the pin-holder using a grub screw and the stainless-steel plate was secured in the lubricant bath using screws.

The setup for cartilage samples was slightly different. Osteochondral pins were secured in the pin-holder using a grub screw as before, however a custom-made plate clamp with a window cut into it was used to secure the plate into the lubricant bath (Figure 2.6). Preliminary work identified damage to articular cartilage surfaces could result in a considerable reduction in the clearance between the pin-holder/collet and the plate clamp and could result in metal-on-metal contact. Therefore, spacers were added beneath osteochondral pin samples to provide additional clearance and ensure no metal-on-metal contact occurred during testing.

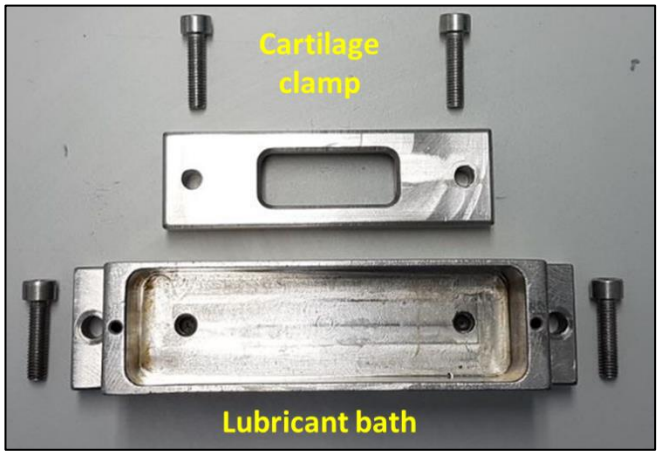


**Figure 2.6: Lubricant bath and cartilage clamp.**

The lubricant bath was attached to the translating stage and lubricant added until it almost filled the bath. The pin-holder was fed through the plain bearing in the arm/bridge so that it contacted the plate surface. A ball bearing assembly was placed on top of the pin holder and held in place by a screw inserted through the loading arm. The screw height was adjusted until the loading arm was parallel with the bench, this was checked using a spirit level. The ball bearing was then centred to ensure the load being transferred from the pin to the plate was evenly distributed. For the UHMWPE-on-stainless-steel verification the mass was added to the loading arm and the motor switched on. For the cartilage-on-cartilage experimental tests the motor was switched on allowed and the samples were allowed to reciprocate several times before the mass was positioned on the loading arm.

### 2.2.7 Harvesting Natural Tissue Samples for Pin-on-Plate Experiments

The current work aimed to enhance an existing experimental natural knee joint simulation model (Liu et al., 2015) (Bowland et al., 2018) (Liu et al., 2019), this model incorporated a porcine knee joint, therefore the pins used during the pin-on-plate studies were porcine. Ideally a porcine plate would be used, however the porcine knee is too small to obtain plates of suitable dimensions, therefore plates were dissected from the trochlea groove of bovine knee joints instead. This porcine on bovine pin-on-plate configuration has been used previously for method development of the existing whole knee joint simulation model (Bowland et al., 2018).

### 2.2.8 Porcine osteochondral pins

Osteochondral pins were harvested from the femoral condyles of right hind porcine legs (Large White Pigs, ~6 months); these were sourced from the local food chain (John Penny and Sons). Legs arrived whole, therefore all soft tissues had to be dissected away from the femur using a scalpel to expose the tibiofemoral joint. The LCL, MCL, ACL, PCL and meniscal attachments were then cut to separate the femur from the tibia. Once the joint capsule had been perforated and articular cartilage surfaces exposed to the environment, tissue hydration was maintained by regularly spraying with PBS or wrapping with PBS-soaked paper towels until completion of the dissection process.

Osteochondral pins (Ø12mm) were obtained using a drill-ended corer attached to either a hand drill or pillar drill. When using the hand drill, the femur was clamped into a table-mounted vice and orientated with the condyles facing upward using a custom fixture. A 12mm biopsy punch was placed onto the surface and pressed down to the subchondral bone; this was done to provide a guide for the hand drill and mitigate the potential for drill slippage when it contacted the cartilage surface. The hand drill was lined up with the biopsy punch mark by eye and a hole was drilled to a depth of ~20mm.

When using the pillar drill, the femoral condyles had to be mounted into a custom jig, condyles were removed by clamping the femur into a table-mounted vice and cutting with a hacksaw. The condyles were then secured into the jig which was attached to the table beneath the pillar drill (Figure 2.7). The drill was lowered to line up the corer with a suitable region of the condyle and the jig adjusted to optimise the orientation. The cutting depth was set at 20mm and the hole drilled; PBS was sprayed onto the cartilage surface during drilling.

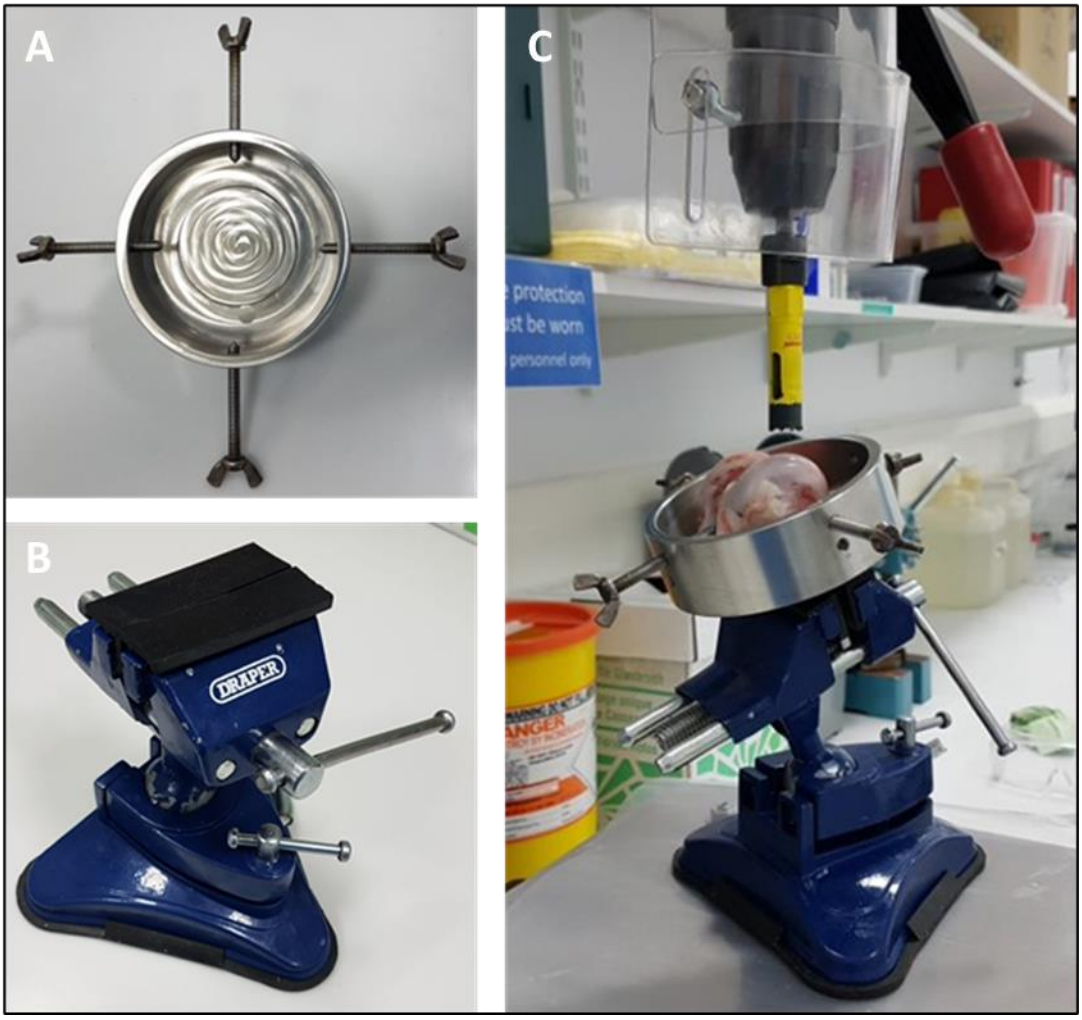


**Figure 2.7: Fixtures used to remove osteochondral pins with pillar drill. Custom fixture for holding femoral condyles in place (A), universal jig used to orientate samples (B), fixture setup on pillar drill before sample removal (C).**

In both cases samples were removed from the anterior, central or posterior regions of both the medial and lateral condyles depending on the size and curvature of the condyles; drilling was done slowly to minimise potential cartilage damage. Once the drill was removed the biopsy punch was placed over the osteochondral sample and wiggled back and forth to snap the sample from the subchondral bone; a tamp was then inserted to push samples out of the biopsy punch. Paper towels were stuffed into the biopsy punch before the tamp was inserted to protect the cartilage surface. Samples were rinsed in PBS and inspected for quality; if the articular surfaces had an excessive slope or any wear, damage and deformation was present, either pre-existing or as a consequence of the dissection process samples were rejected. Suitable samples (Figure 2.8) were then wrapped in PBS-soaked paper towels, sealed in plastic bags and frozen at -20°C until required. Pin samples were adjusted to a length of ~15mm either prior to freezing or once defrosted using bone nibbling pliers and a file and checked to ensure they had a flat

bottom and there was sufficient clearance between the cartilage surface and the pin holder. For some samples spacers were placed beneath the sample to increase the clearance.

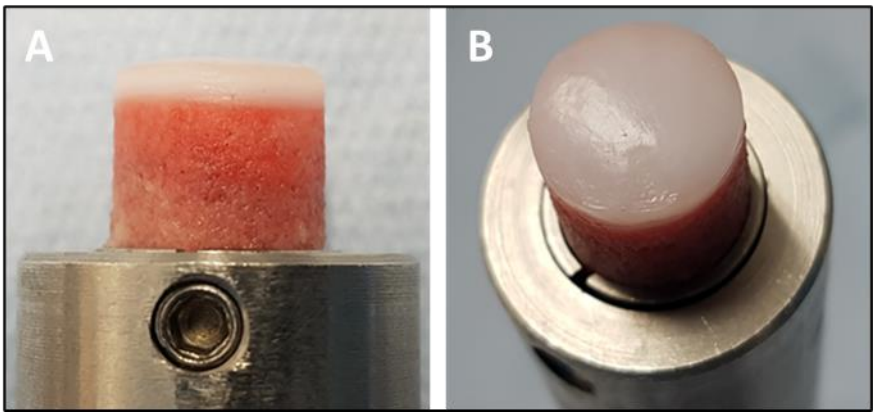


**Figure 2.8: Osteochondral pin sample in pin holder. View highlighting cartilage thickness and clearance from pin holder (A), condition of the articulating surface (B).**

### 2.2.9 Bovine Osteochondral Plates

Osteochondral plates were harvested from the trochlea groove of bovine femurs (~18 months); these were sourced from the local food chain (John Penny and Sons). Bovine femurs arrived with all soft tissue removed but the patella still attached to protect the cartilage during transport. A scalpel was used to remove the patella and expose the trochlea groove, tissue hydration was maintained by regularly spraying with PBS or wrapping with PBS-soaked paper towels until completion of the dissection process.

Femurs were clamped into a table-mounted vice and orientated with the trochlea groove facing upwards using a custom fixture (Figure 2.9). Using a hacksaw, the medial and lateral edges of the trochlea groove were removed and a cut made down the centre; proximal and distal cuts were then made across the width of the trochlea groove. The orientation of the femur was changed so the outer edge of the femoral condyles were parallel with the floor. The hacksaw blade was placed against the cartilage surface to determine the flattest region of the trochlea groove and a cut was made from the outer edge into the centre; this detached a portion of cartilage from which an osteochondral plate could be formed. The femur was then turned over and the process repeated for the other side of the trochlea groove.

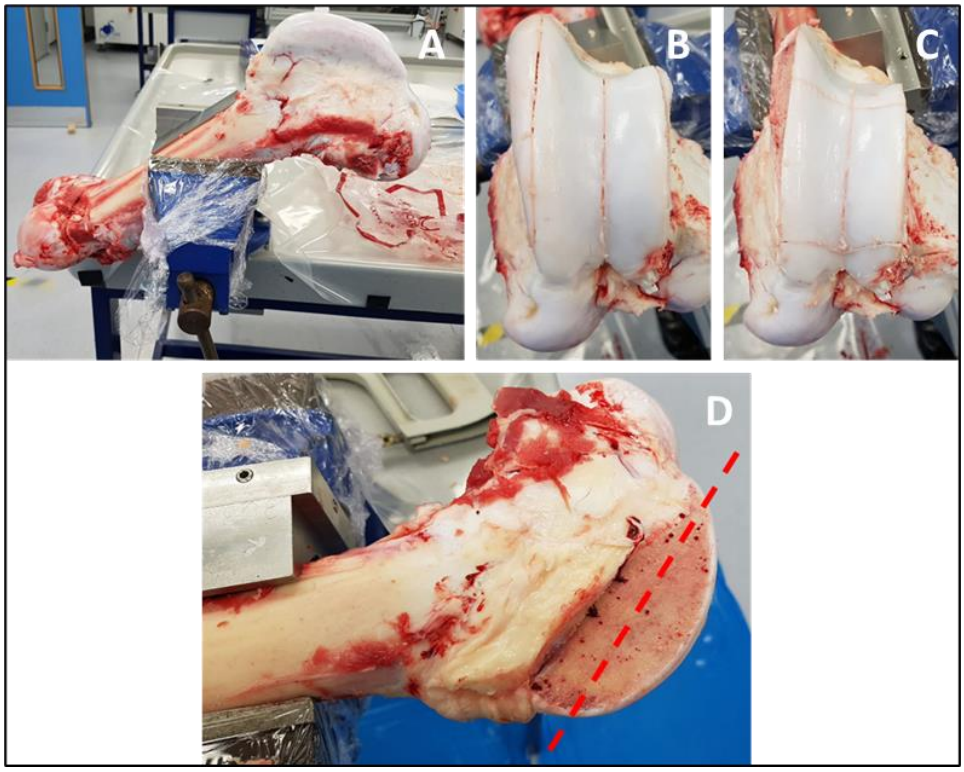


**Figure 2.9: Process for removing osteochondral plates from bovine femurs. Femur in custom fixture positioned in table mounted vice (A), cuts made to remove edges of medial and lateral trochlea groove and central cut to approximate width of bovine plate samples (B), proximal and distal medial-lateral cuts made so removed section will fit into custom thickness jig (C), reorientation of femur in vice to allow removal of section to be cut to appropriate thickness (D).**

The detached portions were secured in a custom-made jig and cut to a height of 7mm (Figure 2.10). These were then adjusted to the necessary dimensions required to fit into the plate clamps (47mm x 18mm x 7mm) using a hacksaw, bone nibbling pliers and a file.

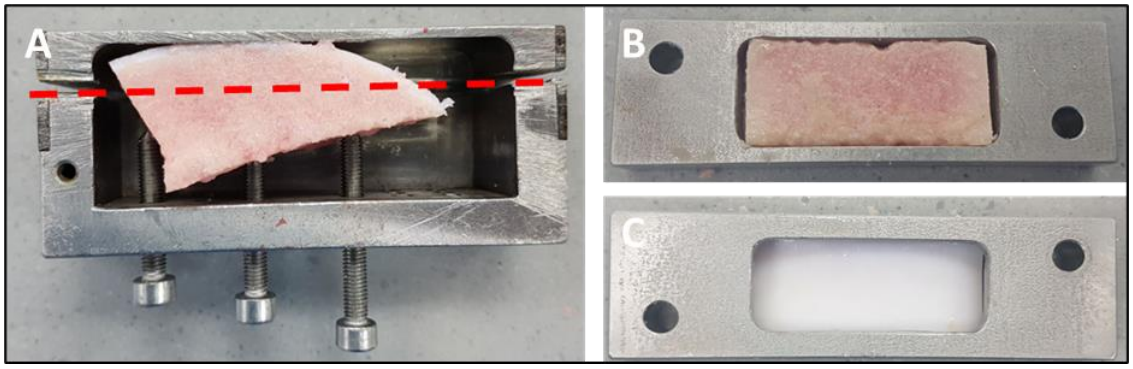

**Figure 2.10: Process for adjusting osteochondral plate samples to the correct dimensions. Section of trochlea grove removed from femur positioned in custom thickness jig (left), posterior view of bovine plate in cartilage clamp (top right), anterior view of cartilage plate through window in cartilage clamp 9bottom right).**

### 2.2.10 Physiological Lubricants for Pin-on-Plate Studies

Two lubricants were developed to act as substitute synovial fluids during the pin-on-plate study in Chapter 3. Both consisted of the same constituents in different concentrations (Table 2.6). To make the lubricants, Ringer's solution was poured into a 250ml pot. The other substances were then added sequentially, from highest molecular weight to lowest molecular weight. HA was added first and the pot shaken until a viscous gel-like consistency was obtained. The IgG was added next and shaken until no solid particles were visible, this process was then repeated for the BSA and lecithin. At each stage, if the substances had not fully dissolved, the pot was placed into a sonic bath for a few minutes until solid particles were no longer visible in the solution. Lubricants were stored frozen at -20°C until required.

**Table 2.6: Composition of physiological synovial fluid substitutes.**

| | **Quantities** | |
|---|---|---|
| **Constituents** | **Healthy Physiological Lubricant** | **Traumatic Physiological Lubricant** |
| Hyaluronic acid (HA) | 0.48g | 0.32g |
| Bovine immunoglobulin G (IgG) | 2.016g | 4.66g |
| Bovine Serum Albumin (BSA) | 1.184g | 1.63g |
| Soy Lecithin | 0.024g | 0.048g |
| Ringer's Solution (RS) | 160ml | 160ml |

The recipe for these synovial fluid substitutes was based on a lubricant previously developed for use during TKR simulations (Bortel et al., 2015). The concentrations were then adjusted to mimic concentrations of healthy and traumatic synovial fluid based on

values found in the literature. Traumatic, in this case, is defined as a patient undergoing arthroscopic evaluation with no history of joint disease.

### 2.2.11 Single Station Knee Simulator

The machine used to run simulations for all studies in the project (SSKS3) was an electromechanically operated ProSim Single Station Knee Simulator (Simulation Solutions Ltd). This machine enables motion in six degrees of freedom (DoF) with five controlled axes and one uncontrolled axis (Figure 2.11) ; the five controlled axes may be driven via force or displacement control (Table 2.7).

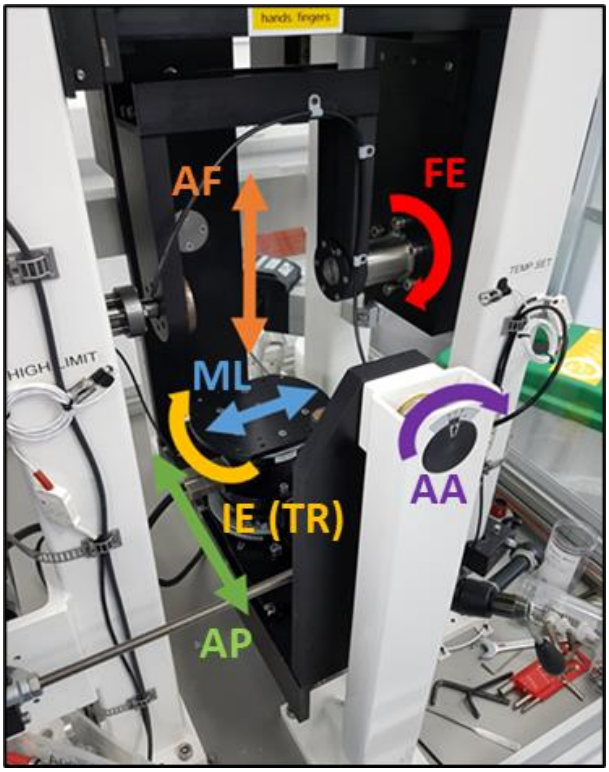


**Figure 2.11: Axes of motion in SSKS3: axial force (superior-inferior) (orange), anterior-posterior displacement (green), internal-external (tibial) rotation (yellow), flexion-extension rotation (red), abduction-adduction rotation (purple), medial-lateral displacement (blue).**

**Table 2.7: Functional capabilities of SSKS3.**

| Axis | Control Mode | Range | Accuracy |
|---|---|---|---|
| Axial Force (AF) (superior-inferior) | Force | 0N - 5000N | - |
| Anterior-Posterior (AP) | Force or Displacement | ± 1000N, ± 25mm | ± 0.1mm |
| Internal-External (Tibial) Rotation (IE) | Torque or Displacement | ± 20Nm, ± 25° | 0.09° |
| Flexion-Extension (FE) | Torque or Displacement | ±30Nm, ± 90° from vertical | 0.03° |
| Abduction-Adduction (AA) | Torque or Displacement | ±30Nm, ± 10° | 0.03° |
| Medial-Lateral (ML) | Uncontrolled (may be locked to give specific displacement) | ± 10mm | ± 0.1mm |
| Anterior-Posterior 2 Force (AP2 Force) | Force | ± 500N | - |

Forces and torques were measured via a 6-axis tension-compression load cell situated beneath the tibial component mounting plate; except the anterior-posterior 2 force (AP2 Force), which was measured via a separate load cell mounted onto the tibial rotation component. FE, TR and AA displacement were measured via optical encoders in the motors and AP and ML displacements measured via magneto inductive position sensors.

### 2.2.12 Calibration

The accuracy of the sensors in the simulator may drift over time, therefore the sensors required calibration to confirm they were outputting accurate values prior to a series of experiments. Sensors were individually calibrated for each axis and this was done in a predefined order. For each axis loads/displacements were applied and sensor outputs recorded, these were then compared an existing standard to determine sensor accuracy. Calibration of the single station simulator was carried out by an engineer from Simulation Solution.

### 2.2.13 Verification Checking

Before each experiment, verification checks were performed to ensure axis zero positions were accurate. Periodic readings were assessed and the zero position of the AP axis confirmed by placing slip gauges between the AP carriage and AA carriage. A

standard control test was then conducted to ensure the simulator was delivering the correct output waveforms from the inputs and that these were within the acceptable tolerance levels. A curved stainless steel femoral dummy and a flat UHMWPE tibial dummy were used to perform standard control tests. These were mounted into the simulator and Vaseline applied to the articulating surface of both components to provide lubrication. The dummies were run in the simulator using the 'Complex Porcine' walking gait profile and the AP shear force and AP displacement outputs compared to previous results.

### 2.2.14 Creating Simulator Input Profiles

To run simulations within SSKS3 which mimic physiological motion, it was necessary to create input profiles to supply the desired kinetic and kinematic conditions. Input profiles were created using Microsoft Excel (Microsoft Corporation) then converted into 128-point Text (Tab delimited) (*.txt) format so they could be uploaded into a simulation test file as specified by the ProSim simulator software user manual (Simulation Solutions).

### 2.2.15 Profile tuning

Due to hardware/software limitations the output profile generated by the simulator did not always match the demanded input profile; especially when applied to natural tissue. SSKS3 operates using a proportional plus integral plus derivative (PID) controller, this continually calculates the error value between the demand and the output and applies a correction to minimise discrepancies. Due to anatomical variation between samples the output profile often required turning to match the demand when running a simulation with natural tissue. This was achieved through PID tuning; the (P), (I) and (D) gain values represent the current, past and future error signal respectively and could be altered so the output waveform more closely matched the input waveform. If this was insufficient to correct the error then the position of individual or multiple points which comprise the profile were moved to further reduce the difference. The ISO standards require profile following to be ±5% of the demanded value for wear testing of TKRs.

## 2.2.16 Porcine Knee Sample Preparation

### 2.2.16.1 Porcine Knee Joint Model

The aim of this project was to develop an *in vitro* simulation model with the potential to produce clinically translatable results; an ideal simulation model would incorporate a human cadaver knee joint. Use of cadaver tissue was unfeasible during method development due to ethical considerations and limited availability of suitable tissue; therefore an appropriate animal model was utilised. The porcine knee is similar in size and cartilage thickness to the human knee and its efficacy for the development of preclinical simulation methods has been previously demonstrated (Liu et al., 2015) (Bowland et al., 2018) (Liu et al., 2019). In addition, porcine tissue could be easily sourced from the food chain with a high level of consistency in geometry and cartilage quality between animals. Therefore, throughout this project, simulations were conducted using porcine knee joints.

### 2.2.16.2 Specimen Preparation

In order to run simulations on porcine knee joints in SSKS3, each sample (Figure 2.12) was prepared by following a previously developed protocol (Liu et al., 2015).

### 2.2.16.3 Dissection

During dissection, removal of soft tissue may alter the alignment of the joint; to ensure natural alignment was maintained after dissection, the joint was fixed in position. Using a scalpel, a small rectangular window was created to expose the lateral knee joint. Metal braces were placed across the tibiofemoral joint and bent to sit flush against the bony surfaces. Holes were drilled into the proximal tibia and distal femur and the plates secured in place with metal screws. This process was then repeated for the medial aspect of the joint. Once the joint was fixed in position, all remaining soft tissues, except the menisci and their attachments, were dissected away from the knee joint in a step-by-step process.

Phosphate buffered saline solution was sprayed onto knee joints at regular intervals to maintain tissue hydration during dissection.

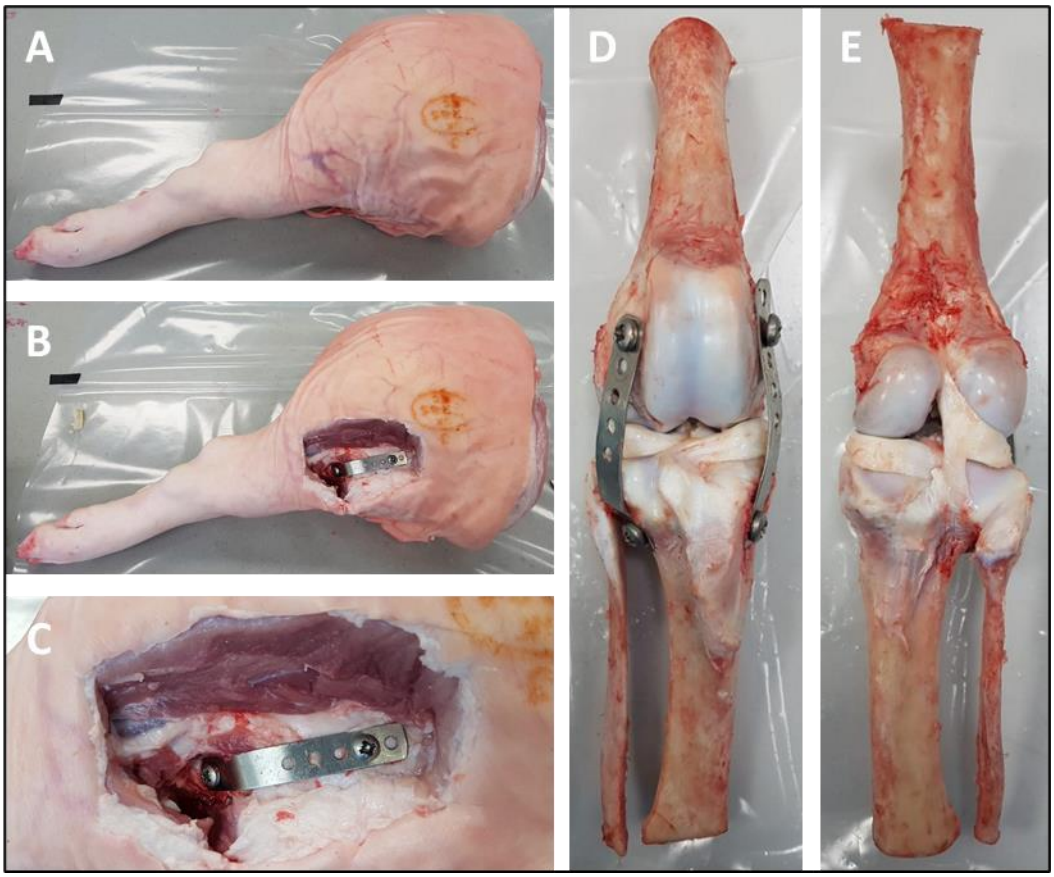


**Figure 2.12: Stages of the dissection process for a porcine knee to be mounted into the knee simulator. Whole leg prior to dissection (A), lateral window cut to expose tibiofemoral joint (B), metal braces attached to maintain joint alignment (C), anterior view of porcine tibiofemoral joint after dissection (D), posterior view of porcine tibiofemoral joint after dissection (E).**

#### 2.2.16.4 Alignment

To allow knee joints to be mounted into the simulator and ensure they maintain correct alignment during simulations a customised jig was used (Figure 2.13). The femur, tibia and fibula were cut to the necessary length to enable alignment within the jig. The femoral centre of rotation (CoR) along the flexion-extension axis was defined using a template method (McCann et al., 2008). Circles of known diameter were matched to the curvature of the femoral condyles then holes drilled at the centre of these circles to mark the CoR. During the gait cycle the medial compartment of the tibiofemoral joint experiences a greater proportion of the loading. Therefore each sample was aligned with a medial-lateral offset of 0.07 x tibial width from the line of action of the axial force, as recommended by the ISO standards (BS ISO, 14243-1:2009+A1:2020) (ISO, 14243-1:2014+A1:2020). To simulate the point at which heel strike occurs during the porcine gait cycle a femoral offset of 24° flexion was applied.

### 2.2.16.5 Cementing

Once the desired alignment had been achieved using the jig, the femur was positioned within a Delrin pot and permanently fixed in place using PMMA cement (Figure 2.13). PBS-soaked paper towels were wrapped around the joint to maintain hydration whilst the cement cured. Once the cement had cured the joint was inverted and the tibia and fibula cemented in place. After the cement in the tibial pot had cured the metal braces were removed.

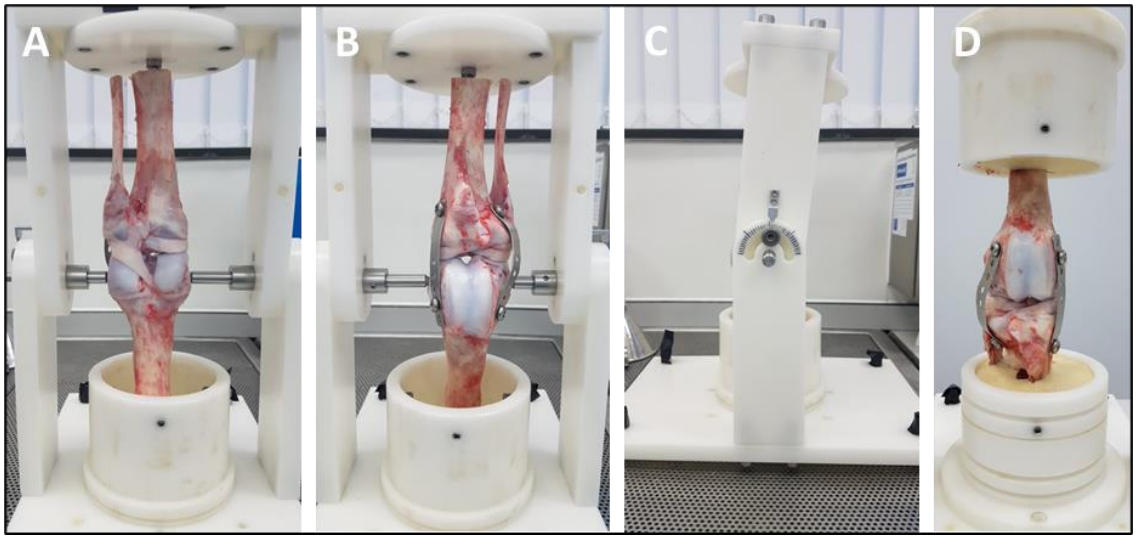


**Figure 2.13: Stages of the alignment and cementing process for a porcine knee to be mounted into the knee simulator. Posterior view of knee joint before femoral cementing (left), anterior view of knee joint before femoral cementing (middle left), angle of cementing jig to achieve 24° femoral offset (middle right), porcine knee after femoral and tibial cementing (right).**

### 2.2.16.6 Storage

Knee joints were then wrapped in PBS-soaked paper towels, sealed in plastic bags and stored frozen at -20°C until required.

## 2.2.17 Minimising Microbial Contamination

Efforts were made to minimise microbial contamination of the knee joint environment before beginning simulations, as this had the potential to interfere with the tribological performance of the knee joint. The femoral and tibial pots, anti-rotation screws, gaiters and lubricant sample pots were all autoclaved at 121.5°C for 15 minutes then sprayed

with ethanol prior to use. To make the serum-based lubricants Ringer's Solution was mixed with NBCS. A plastic jugs was sprayed with ethanol and the lubricants poured into the jug, a sterile syringe was then used to take a pre-test lubricant sample from the jug and transferred to the autoclaved sample pot. Where used, sodium azide was added to the Ringer's Solution prior to being poured into the jug. Whilst these measures were implemented the dissection and cementing processes were carried out on a dissection table and downdraft table and hence the knee joint itself was exposed to the environment.

### 2.2.18 Mounting

A gaiter was attached via a groove in the tibial pot then taped and secured with a jubilee clip to create a tight seal. Specimens were then mounted into the simulator and the gaiter attached to the femoral pot groove. The desired lubricant was then poured through a funnel placed between the gaiter and femoral pot until the articulating surfaces were completely submerged. A second jubilee clip was then placed around the femoral pot to seal the gaiter at the top. At this stage samples were ready for simulation. For non-simulated controls the above process was repeated, however these knees were instead mounted into the cementing jig. The jig placed into the rear of the simulator, leaving clearance between the jig and travel path of the simulator axes. This was done so that both simulated and control knees would experience the same environmental conditions during experiments.

Post-test samples were removed from the contact region of both simulated knee joints and non-simulated controls using a hacksaw and scalpel. Osteochondral samples of medial tibial plateau and medial femoral condyle and medial meniscus sample were used for histology and a cartilage sample was removed from the lateral femoral condyle for sterility testing. All samples were wrapped in PBS-soaked paper towels and stored frozen at -20°C until required.

### 2.2.19 Histology

Histological staining was used through this project to enable visualisation of wear, damage, deformation and microbial growth on osteochondral and meniscal samples. In all chapters histological samples were fixed in neutral buffered formalin for 48 hours, processed for 21 hours (Table 2.8) in a tissue processor (Leica Biosystems) then embedded in paraffin wax. Once cooled, wax blocks were sectioned with a microtome,

placed onto glass coverslips and stained with Haematoxylin and Eosin (H&E), 1% Safranin-O (Saf-O) + 0.01% Fast Green and 0.1% Picrosirius Red.

**Table 2.8: Tissue processor protocol used for dehydrating and clearing porcine osteochondral tissue samples.**

| Station Number | Contents | Time (hours & minutes) |
|---|---|---|
| 1 | 70% alcohol (ethanol) | 1 h |
| 2 | 90% alcohol (ethanol) | 1 h |
| 3 | 100% alcohol (ethanol) | 1 h 10 m |
| 4 | 100% alcohol (ethanol) | 1 h 10 m |
| 5 | 100% alcohol (ethanol) | 3 h 20 m |
| 6 | 100% alcohol (ethanol) | 4 h 20 m |
| 7 | Xylene | 1 h |
| 8 | Xylene | 1 h 30 m |
| 9 | Xylene | 2 h |
| 10 | Molten wax | 2 h 30 m |
| 11 | Molten wax | 2 h |
| | | Total 21 hours |

### 2.2.20 Microscopy

For the histological images in Chapter 4 stained histological samples were imaged at 2.5x magnification using a light microscope (Zeiss), H&E and Saf-O slides were imaged using normal light and SR slides using polarised light. Histological images in Chapter 5 and Chapter 7 were imaged at 20x magnification using a slide-scanner (Axioscan Z1, Zeiss). All images were compared using microscopy imaging software (Zeiss Zen Lite).

### 2.2.21 Assessment of Bacterial Growth during Simulations

#### 2.2.21.1 Broths

Cartilage samples from the lateral femoral condyle of simulated knees and non-simulated controls were removed post-test. These were then bisected and cultured in thioglycolate and tryptone soya broths in an incubator at 37°C for 14 days to assess bacterial growth. Negative controls were broths with nothing added and positive control contained concentrations of staphylococcus aureus and bacillus fragilis. Visual assessment of bacterial growth was made after 2, 7 and 14 days and photographed.

#### 2.2.21.2 Lubricant Filtering

Pre- and post-test lubricant samples from simulated knees and non-simulated controls were filtered to separate any microorganisms present from the bulk fluid. Aseptic filters were placed over a valved manifold connected to a vacuum pump and an aseptic plastic cup placed over the manifold to secure the filter in place. Lubricant samples were poured into the cup and the vacuum was switched on to suck the fluid through the filter leaving any remaining microorganisms on the filter paper. The filters were then transferred to blood agar plates using sterile forceps and cultured in an incubator for 14 days. Visual assessment of bacterial growth was made every day and photographed.

### 2.2.22 Alicona Infinite Focus

The Alicona Infinite Focus G5 (Figure 2.14) is optical profiler which was used for the 3D measurement and analysis of silicone replicas of cartilage surfaces. It functions based on focus variation (Danzl et al., 2011). The optical system has a small depth of field which can only focus on a shallow segment of the sample surface at any given time. Therefore, the system moves vertically during the scanning process to build up a 3D image of the entire surface. A comprehensive explanation of the function and operation of the Alicona Infinite Focus has been described previously (Bowland, 2016).


**Figure 2.14: Alicona Infinite Focus.**

For the studies in this project the Alicona Infinite Focus was used to scan AccuTrans silicone replicas of the articulating surfaces (cartilage/meniscus) of natural tissue to create 3D datasets which could be analysed. The Alicona Infinite Focus analysis software was then to visualise and quantify the presence of wear, damage, deformation and graft stability. The Alicona Infinite Focus has previously been validated for the measurement of AccuTrans silicone replicas; it was shown that the Alicona can produce comparable results to gravimetric weighing when measuring wear volume (Bowland, 2016). This Alicona has been used for the measurement of silicone replicas of the articulating surfaces within porcine knee joints (Bowland et al., 2018) (Cowie et al., 2021).

# Chapter 3

# Investigation of an appropriate lubricant for long-term tribological investigations of natural knee joints

## 3.1 Introduction

Thus far, before clinical use, early-stage knee interventions have not been subjected to the same rigorous preclinical assessment as total knee replacements and little is known about their tribological and mechanical performance in the long-term. One contributing factor is the lack of a suitable preclinical experimental model in which to assess them. Degradation of natural tissue currently limits potential simulation durations. The longest tribological cartilage investigations thus far have typically lasted only a few hours.

An important component for a successful natural knee experimental tribological simulation is the lubricant. To increase investigation duration from hours to days, the structural integrity and function of articulating surfaces must be maintained to ensure any observed changes (wear, damage, deformation) are a result of the intervention or experimental conditions, and not inability of the lubricating fluid to replicate a suitable tribological environment. An ideal lubricant would mimic the tribological properties/performance of synovial fluid by enabling low friction, low wear articulation whilst also being cost effective. Various lubricants have been used as synovial fluid substitutes, however, there is currently no consensus on the most appropriate lubricant for preclinical evaluation of natural tissue.

A natural knee experimental simulation model to assess knee interventions (Chapter 2) was developed at the university of Leeds (Liu et al., 2015) (Liu et al., 2019) (Bowland et al., 2018). This approach incorporates non-living natural knee joints; therefore, tissue will naturally degrade over time compromising its efficacy as a suitable environment for tribological investigations. Over an extended duration, a suboptimal lubricant may result in premature degradation of natural tissue and limit potential test durations. The current work aims to enhance the simulation capabilities of this system to improve its physiological relevance. One potential direction for this development is the mimicking of disease states which would be more representative of the patient population.

A pin-on-plate study was designed to assess the appropriateness of five lubricants for longer-term tribological investigations using natural tissue.

## 3.2 Aims and Objectives

### 3.2.1 Aim

- The aim of this study was to identify suitable lubricants for use during tribological investigations of whole natural knee joints

### 3.2.2 Objectives

- To assess the ability of five different lubricants to maintain the structural integrity of non-living cartilage-on-cartilage contacts subject to uniaxial sliding and clinically relevant contact pressure for up to 96 hours using a pin-on-plate configuration

- To provide a qualitative and quantitative assessment of wear, damage and deformation of cartilage surfaces

- To assess if low coefficient of friction can be maintained for up to 96 hours

- To assess whether changes in coefficient of friction result in/lead to wear, damage or deformation occur

## 3.3 Experimental Design

### 3.3.1 Experimental Groups

To determine the influence of different lubricants on wear, damage and deformation of cartilage surfaces, during reciprocating pin-on-plate experiments five experimental groups were assessed:

- Ringer's Solution (n=4)
- 25% NBCS in PBS (n=4)
- 25% NBCS in Ringer's Solution (n=3)
- Healthy Physiological Lubricant (n=4)
- Traumatic Physiological Lubricant (n=4)

The constituents used in each lubricant, physiological properties they were intended to replicate and rationale for their inclusion can be seen in (Table 3.1). Details relating to the exact composition of each lubricant, the constituents used and how they were prepared and stored can be found in (Chapter 2).

### 3.3.2 Physiological Lubricants

The two physiological were based on a previously developed lubricant consisting of hyaluronic acid, proteins and phospholipids dissolved in Ringer's Solution, which has been used to assess UHMWPE pins sliding against CoCr discs (Bortel et al., 2015) (Heuberger et al., 2020). To create lubricants representative of the synovial fluid in healthy knees (Healthy Physiological Lubricant) and knees which had experienced trauma (Traumatic Physiological Lubricant) some adjustment of the lubricant constituent concentrations used by Bortel *et al.,* were necessary as the levels used were intended to create a lubricant for use during total knee replacement simulations. For the healthy version, total protein concentration was reduced from 30 g/L (osteoarthritic) to 20 g/L (healthy). For the traumatic version total protein concentration was increased to 39.3 g/L (traumatic), in addition the healthy concentration of phospholipids (lecithin) was increased and the concentration of hyaluronic acid decreased; these adjustments were based on values found in the literature (Galandáková et al., 2017).

**Table 3.1: Lubricants included during the pin-on-plate experiments. PBS = phosphate buffered saline, NBCS = new-born calf serum.**

| Experimental group | Synovial fluid constituents included | Physiological properties replicated | Rationale for Inclusion |
|---|---|---|---|
| **Ringer's Solution** | Water, ions | Maintains cartilage hydration as Ringer's Solution is isotonic with body fluids. | Cheap, quick to produce, easy to store, previous use during short-term (300 cycle) simulation of natural knee joints (Liu et al., 2019). |
| **25% NBCS + PBS** | Water, ions, proteins, phospholipids | Cartilage hydration (PBS isotonic). Serum diluted to similar protein concentration as healthy synovial fluid. Proteins and phospholipids protect cartilage surfaces via boundary lubrication mechanisms (Forsey et al., 2006) (Schmidt et al., 2007). | Serum in deionized water is recommended for artificial joint simulation by ISO standards. Similar protein content to healthy synovial fluid produces similar wear mechanisms to explants. Previous use of 25% NBCS in PBS during natural knee joint simulation for 2 hours (Bowland et al., 2018) and 3 hours (Cowie et al., 2021). |
| **25% NBCS + Ringer's Solution** | Water, ions, proteins, phospholipids | Cartilage hydration (Ringer's Solution isotonic). Serum diluted to similar protein concentration as synovial fluid. Proteins and phospholipids protect cartilage surfaces via boundary lubrication mechanisms. | Ringer's Solution is more physiologically relevant than PBS. Ion concentration is more similar to synovial fluid, preventing cartilage swelling. Ringer's Solution without bicarbonate inhibits cartilage metabolism less than Normal Saline (NaCl) hence is considered more physiological (Bulstra et al., 1994). Ionic concentration of solutions affects Donnan osmotic pressure, this influences interstitial fluid pressurisation which can change the mechanical and friction response of cartilage (Ateshian et al., 2003). |

**Table 3.1: continued…**

| Experimental group | Synovial fluid constituents included | Synovial fluid properties replicated | Rationale for Inclusion |
|---|---|---|---|
| **Healthy Physiological Lubricant** | Water, ions, Hyaluronic acid, albumin, globulin, lecithin (phospholipids) | Cartilage Hydration (Ringer's Solution isotonic). Hyaluronic acid responsible for viscosity of synovial fluid (Mazzucco et al., 2004) (Zhang et al., 2014) (Rebenda et al., 2020), viscosity gives synovial fluid shear thinning properties that protect cartilage (Hamrock et al., 2004). Hyaluronic acid contributes to boundary lubrication (Schmidt et al., 2007) (Greene et al., 2011) (Bonnevie et al., 2015). Proteins (albumin and globulin) and phospholipids (lecithin) protect cartilage surfaces via boundary lubrication mechanisms. | A synovial fluid substitute that matched (as closely as possible with the available resources) the concentrations of albumin, globulin, molecular weight of hyaluronic acid etc. of molecules found in healthy synovial fluid would, in theory, be the most appropriate substance to prevent cartilage damage during simulations. |
| **Traumatic Physiological Lubricant** | Water, ions, Hyaluronic acid, albumin, globulin, lecithin (phospholipids) | Cartilage Hydration (Ringer's Solution isotonic). Hyaluronic acid responsible for viscosity of synovial fluid, viscosity gives synovial fluid shear thinning properties, which protect cartilage surfaces. Proteins (albumin and globulin) and phospholipids (lecithin) protect cartilage surfaces via boundary lubrication mechanisms. | Patients who experienced knee trauma have different synovial fluid to healthy knees (Galandáková et al., 2017). A traumatic lubricant is more representative of the early-stage knee intervention patient group. Lubricants imitating synovial fluid of patient populations (osteoarthritis) have been used during investigation of biomaterials (Bortel et al., 2015). |

### 3.3.3 Experimental Protocol

Porcine osteochondral pins (Ø=12mm, length=~15mm) were reciprocated against bovine osteochondral plates (45mm x 17mm x 7mm) using a pin-on-plate friction rig (Figure 3.1); detailed description of the dissection procedures and operation of the rig have been described previously (Chapter 2). This simple geometry approach allowed individual variables to be assessed, in this case, the lubricant composition. Two rigs were available, so two samples could be run simultaneously and the small baths minimised the volume of lubricant required, thus reducing cost. Prior to each experiment, pin, plate and lubricant samples were defrosted in a warm water bath whilst still sealed in bags/containers. Plate samples were fixed into the lubricant bath using a custom-made cartilage clamp, the bath was attached to the translating stage of the friction rig and 40ml of the chosen lubricant added. Pin samples were secured into the pin holder and positioned within the bearing in the bridge to allow pin and plate surfaces to contact. Finally, the ball bearing was placed between the top of the pin holder and a screw in the loading arm; the screw was adjusted until the loading arm was parallel with the bench and checked using a spirit level. Once everything was set up, the motor was switched on and the stage was allowed to translate back and forth several times before the mass was added to the loading arm.

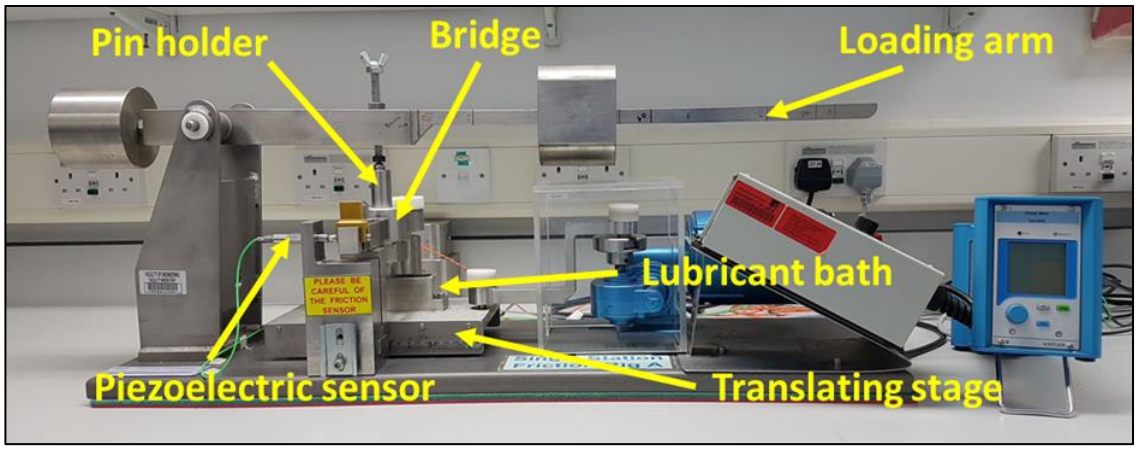


**Figure 3.1: Reciprocating pin-on-plate friction rig.**

Experiments were run for 24 hours, paused to allow samples to be assessed for wear, damage and deformation, then returned to the rig for another 24 hours. This process was repeated for up to 96 hours or until samples had sustained extensive damage to the articulating surfaces causing the experiment to be terminated. Upon completion of each experiment, pin and plate samples were wrapped in PBS-soaked paper towels, sealed in plastic and stored in a freezer at -20°C.

### 3.3.4 Experimental Conditions

The plate was reciprocated with a stroke length of 20mm and sliding velocity of 10mm/s (0.5Hz) whilst a 120N load (1.06MPa contact pressure) was applied to the pin. The contact pressure was chosen as it has previously shown to result in no observable damage to cartilage surfaces during three-hours of articulation in 25% NBCS in PBS (Bowland, 2016) and it was within the range of physiologically relevant contact pressures observed to occur in the knee during activities of daily living (Park et al., 2008). The stroke length and sliding velocity were chosen to be representative of a physiological knee joint (Bowland et al., 2018) and ensure a migrating contact area (Bell et al., 2006) (Caligaris and Ateshian, 2008). In addition, a sliding velocity of 10mm/s has shown the potential to maintain cartilage hydration by delivering fluid/solutes to the centre of cartilage pins (Graham et al., 2017).

### 3.3.5 Wear, Damage, Deformation Analysis

For analysis of wear, damage and deformation, photographs of pin and plate samples were taken and AccuTrans AB silicone replicas of the articulating surfaces were created. Replicas were created once samples had been secured in the pin holder and lubricant bath. Each pin and plate sample were assigned a grade for the severity of wear, damage and deformation based on the ICRS articular cartilage injury classification system (Chapter 1). Values reported are the mean with standard deviation. Both creation of replicas and ICRS grading was carried out pre-experiment at t=0 and then every 24 hours up to a maximum 96 hours, at which point experiments were terminated.

### 3.3.6 Depth Analysis using Alicona

Pin and plate replicas were scanned onto the Alicona Infinite Focus optical profiler (Chapter 2). Plate samples were cut to size with the cropping tool leaving an area of cartilage around the contact region of the pin to use as a reference point for unworn cartilage. To measure wear depth, a trace was drawn from the top of the long edge of each plate to the bottom edge. The green crosshair was placed at the top of the long edge of the plate in the ‘unworn’ region and the red crosshair was placed in the centre of the plate. The relative distance between the two points was then calculated by the software to indicate the wear depth.

### 3.3.7 Data Logging

The output voltage measurements from the piezoelectric force sensor were recorded every 20 seconds for the first 60 minutes, then every 300 seconds for the remainder of the experiment using a LabView (National Instruments) program. The dynamic CoF for each pair of pin and plate samples was calculated from this data as previously described in Chapter 2. Dynamic CoF values reported were the mean for each experimental groups with 95% confidence limits during each 24-hour period.

### 3.3.8 Statistical Analysis

ICRS/OARSI data were not normally distributed. A non-parametric test, a Kruskal-Wallis* test with a post-hoc Dunn's test with Bonferroni correction was performed to assess statistical significance. *Minimum sample size for Kruskal-Wallis is meant to be n=5, each experimental group in this study only had n=3/4 samples. ICRS/OARSI data are reported as the mean grade for each experimental group with standard deviation.

Mean dynamic coefficient of friction for each experiment and relative height data for cartilage plates were normally distributed. A parametric test, a one-way ANOVA with a post-hoc Tukey HSD was used to assess statistical significance in both cases. Mean dynamic CoF between experimental groups at each time point and mean relative height change for the cartilage plates between experimental groups from pre-test to 96 hours were compared. Mean dynamic coefficient of friction and relative height data for the plates are reported as the mean value for each experimental group with 95% confidence limits.

A Shapiro-Wilk test was performed to assess if data were normally distributed, $\alpha$ was set at 0.05 and statistical significance was set at $p<0.05$ in all cases. All data analysis was carried out using IBM SPSS Statistics 26 for Windows.

### 3.3.9 Hypothesis

Protein containing lubricants will result in less wear, damage and deformation of cartilage surfaces compared to non-protein containing lubricants and maintain a lower coefficient of friction during extended duration (96 hour) pin-on-plate experiments

## 3.4 Results

### 3.4.1 Experimental issue affecting sample numbers

Due to unforeseen circumstances one of the Ringer's Solution experiments and one of the 25% NBCS in PBS experiments had to be terminated after 48 hours, hence, for these experimental groups there were n=4 samples form 0-48 hours and n=3 samples from 72-96 hours.

### 3.4.2 Qualitative description of wear, damage and deformation

**Overview:** Distinct differences in the timing, presentation and extent of wear, damage and deformation to pin and plate articular cartilage surfaces were observed for the different experimental groups. The following describes the condition of pin and plate samples pre-experiment and at the end of each 24-hour period.

**0 hours:** Pre-experiment, at t=0 the typical condition of pin and plate samples was smooth and shiny with no obvious wear, damage or deformation on the cartilage surfaces (Figure 3.2).

**Figure 3.2: Typical condition of pre-experiment (t=0) condition of porcine osteochondral pin and bovine osteochondral plate samples.**

**24-hour summary:** Changes were observed for all experimental group samples after 24 hours.

**Pins (**Figure 3.3**):** Reddening in the centre of the pin indicated cartilage thinning for all experimental samples; except the 25% NBCS in PBS group and advanced thinning was observed for one sample in the Ringer's Solution group. For two pins, one Ringer's Solution sample and one 25% NBCS in Ringer's Solution sample, deformation of the surface was observed, the central region was raised with a noticeable ring formed around the circumference about 1mm in from the edge. One sample from the 25% NBCS in PBS group had a flap of cartilage at the edge and one 25% NBCS in Ringer's Solution sample showed evidence of scratching.

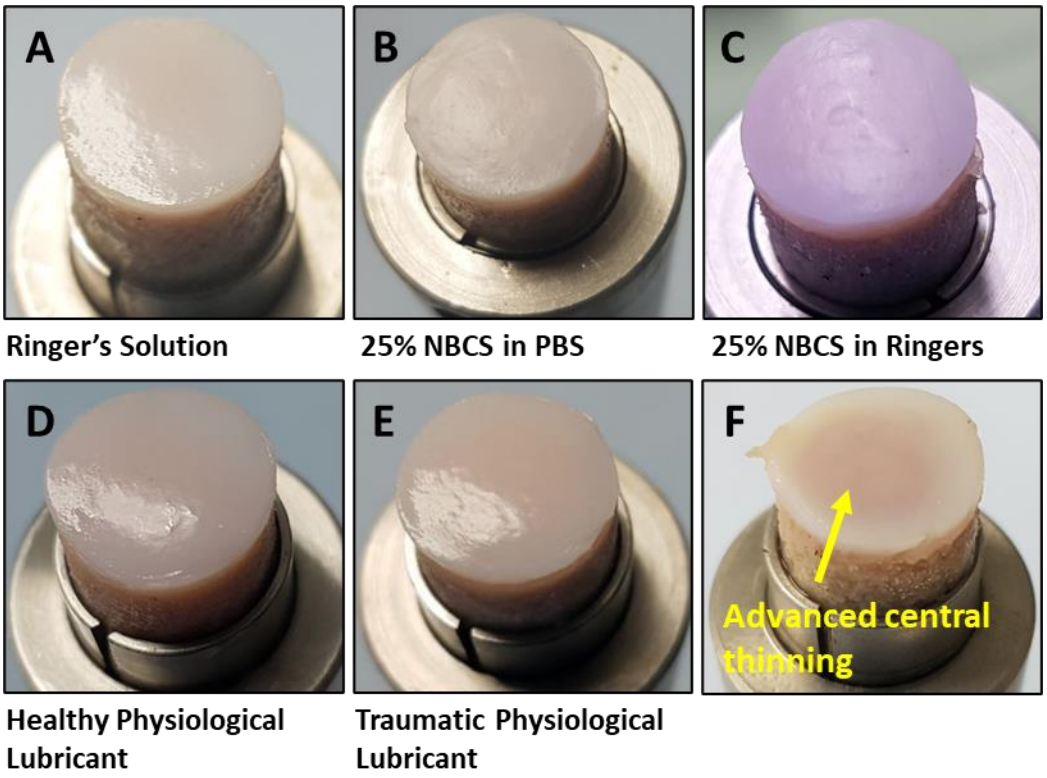


**Figure 3.3: Representative images for the condition of each experimental lubricant group after 24 hours (A–E). Advanced central thinning observed for one sample in the Ringer's Solution group (F). *Note* - the pin in image C may appear duller and rougher than other samples; this is due to some samples being photographed in different locations and hence under different lighting conditions.**

**Plates (**Figure 3.4**):** Plate appearance was consistent across all experimental groups. Shallow deformations were observed in the surface; the deformation length corresponded to the sliding distance of the pin. Three samples showed additional damage, two, one from the 25% NBCS in PBS group and one from Healthy Physiological Lubricant group, had small deep indentations within the larger deformation and another, from the 25% NBCS in Ringer's Solution group, had some scratches.

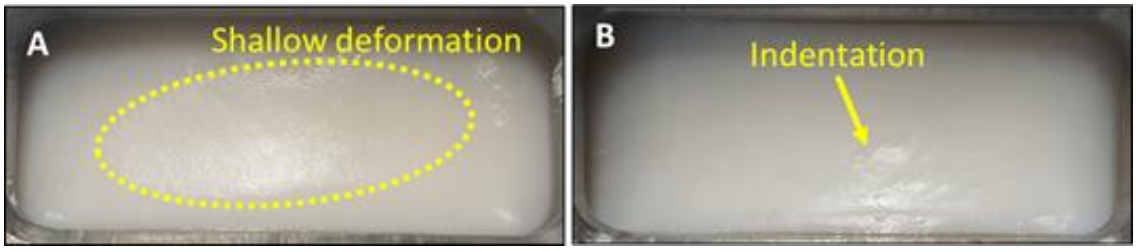


**Figure 3.4: Representative image of typical plate condition of all experimental group after 24 hours (A), representative image of the indentations observed in the surface of two plate samples (B).**

**48-hour summary:** Progression of wear, damage and deformation; the extent varied considerably between samples.

**Pins (**Figure 3.5**):** For all Ringer's Solution samples surfaces were rougher and redder in the centre indicating further cartilage thinning, on one sample cartilage was displaced to the edge of the pin and a wedge-shaped deformation had appeared in another. All healthy and traumatic lubricant samples were slightly rougher but showed little change from the 24-hour condition, except one traumatic sample where delamination of the upper layers had occurred. Serum in PBS samples had become rougher, with some thinning of one sample and another having a raised central region about 1mm in from the edge of the pin. For the serum in Ringer's group one sample changed little from the 24-hour condition; scratches were observed on the other two samples.

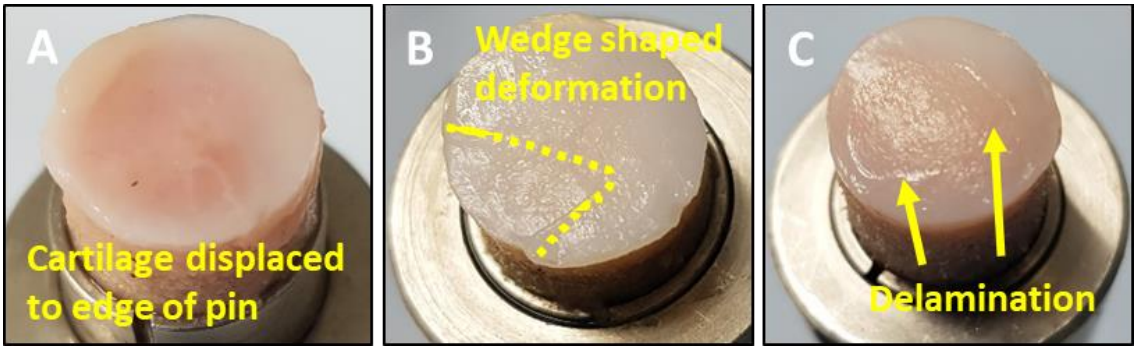


**Figure 3.5: Presentation of pin wear, damage and deformation after 48-hours. Displacement of cartilage towards to edge of the pin for one Ringer's Solution sample (A), wedge shaped deformation for another Ringer's Solution sample (B) and chondral delamination of the upper layers for one traumatic physiological lubricant sample (C).**

**Plates (**Figure 3.6**):** Plate condition varied considerably after 48-hours. Within the deformation observed 24 hours previously, all Ringer's Solution plates had a wear scar due to chondral delamination, and a gel-like substance had formed on the surface. For 11 of the 15 plates in the other experimental groups, the deformation had become deeper and the surface was rougher. Of the four remaining samples, three (one from the serum in PBS group and two from the healthy physiological) had varying degrees of chondral delamination but no gel formation whilst the remaining sample had several scratches parallel to direction of sliding.

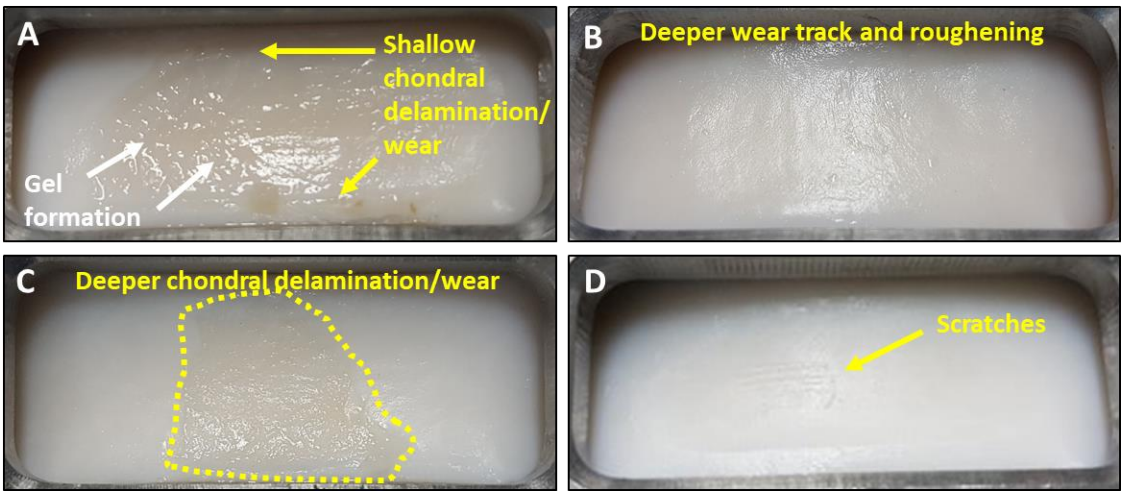


**Figure 3.6: Presentation of plate wear, damage and deformation after 48-hours. Typical condition of Ringer's Solution group (A) with delamination of upper layers appearing to initiate from the edges of the wear track (A - yellow arrows) and a gel-like substance formed on the surface (A - white arrows). Typical condition of most plate samples (B). Deeper chondral delamination seen in 25% NBCS in PBS and healthy physiological lubricant groups (C). Scratches aligned with sliding direction for one sample in 25% NBCS in Ringer's Solution group (D).**

**72-hour summary:** Further progression of wear, damage and deformation. Ringer's Solution group experiments terminated due to excessive damage.

**Pins (**Figure 3.7**):** Ringer's Solution samples showed considerable deterioration from 48 hours. Two samples had lesions penetrating to subchondral bone (ICRS grade 4) and cartilage displaced beyond the edge of the pin but still attached. The third had completely lost structural integrity; the surface was soft and a ring of cartilage had detached. For both serum-based groups some samples showed little change from the 48-hour condition whilst others were rougher with scratching or potential superficial cracking.. Healthy Physiological Lubricant samples experienced thinning and were considerably rougher. One showed chondral delamination in some regions, another had cartilage displaced beyond the edge of the pin and another was scratched. In the Traumatic Physiological Lubricant group, all samples were rougher, this was minimal for two samples, two samples had scratches and two samples showed cartilage thinning.

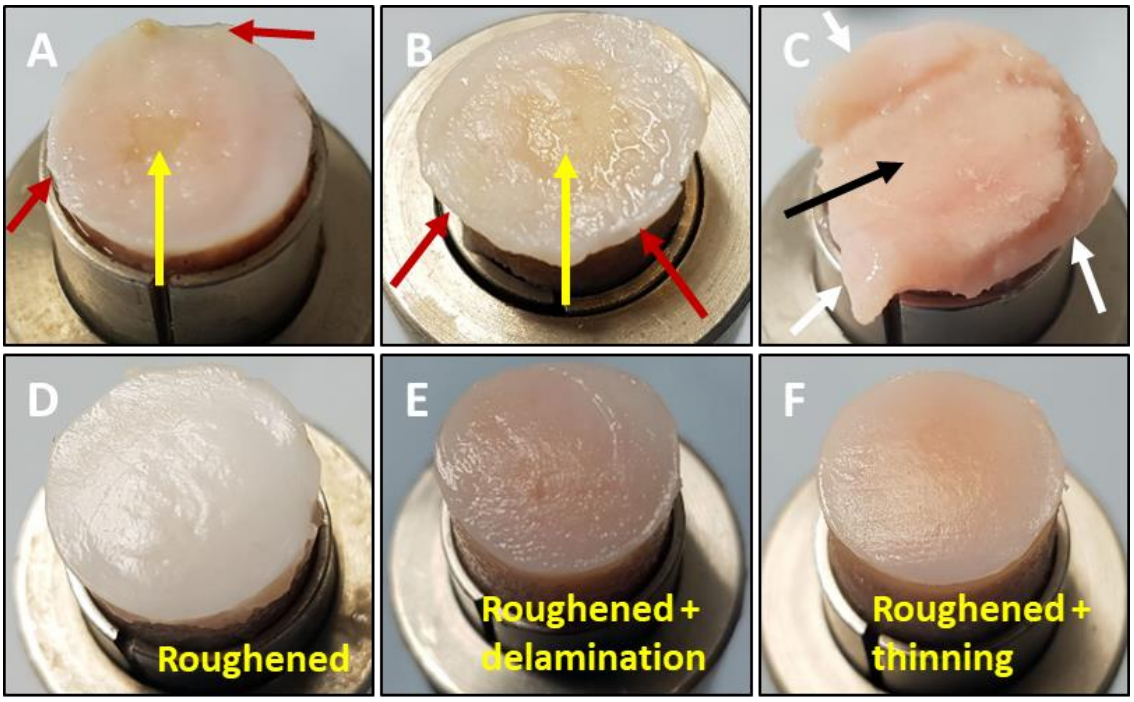


**Figure 3.7: Presentation of pin wear, damage and deformation after 72-hours. Ringer's Solution samples (A-C) showing lesions penetrating to subchondral bone (yellow arrows), cartilage displacement beyond the edge of the pin (red arrows), detached ring of cartilage (white arrows) and softening of pin surface (black arrow). Representative images for the typical condition of both serum-based groups (D), the healthy physiological lubricant group (E) and traumatic physiological lubricant group (F).**

**Plates (**Figure 3.8**):** Wear scars penetrating to subchondral bone were observed in the Ringer's Solution group, this occurred centrally for one sample and across the entire surface for the other two leaving a large volume of gel-like substance loosely attached to the plates. For one serum in PBS sample the condition was similar to at 48 hours, for another indentations and delamination were present in and around the deformed region and for the other existing damage covered a larger area. For the serum in Ringer's group, two samples were similar to the 48-hour condition; a small scratch/indentation was present in one. The remaining sample had a deeper deformation with a large indentation within and a scratch running the length of the plate. Healthy Physiological Lubricant samples experienced deepening of the deformation and chondral delamination across the plate that roughened surfaces and produced a gel-like substance. Three Traumatic Physiological Lubricant samples experienced similar changes to the Healthy group, but delamination was isolated to small regions around the edges of the deformed region and no gel-like substance was produced; no changes were observed for the other sample.

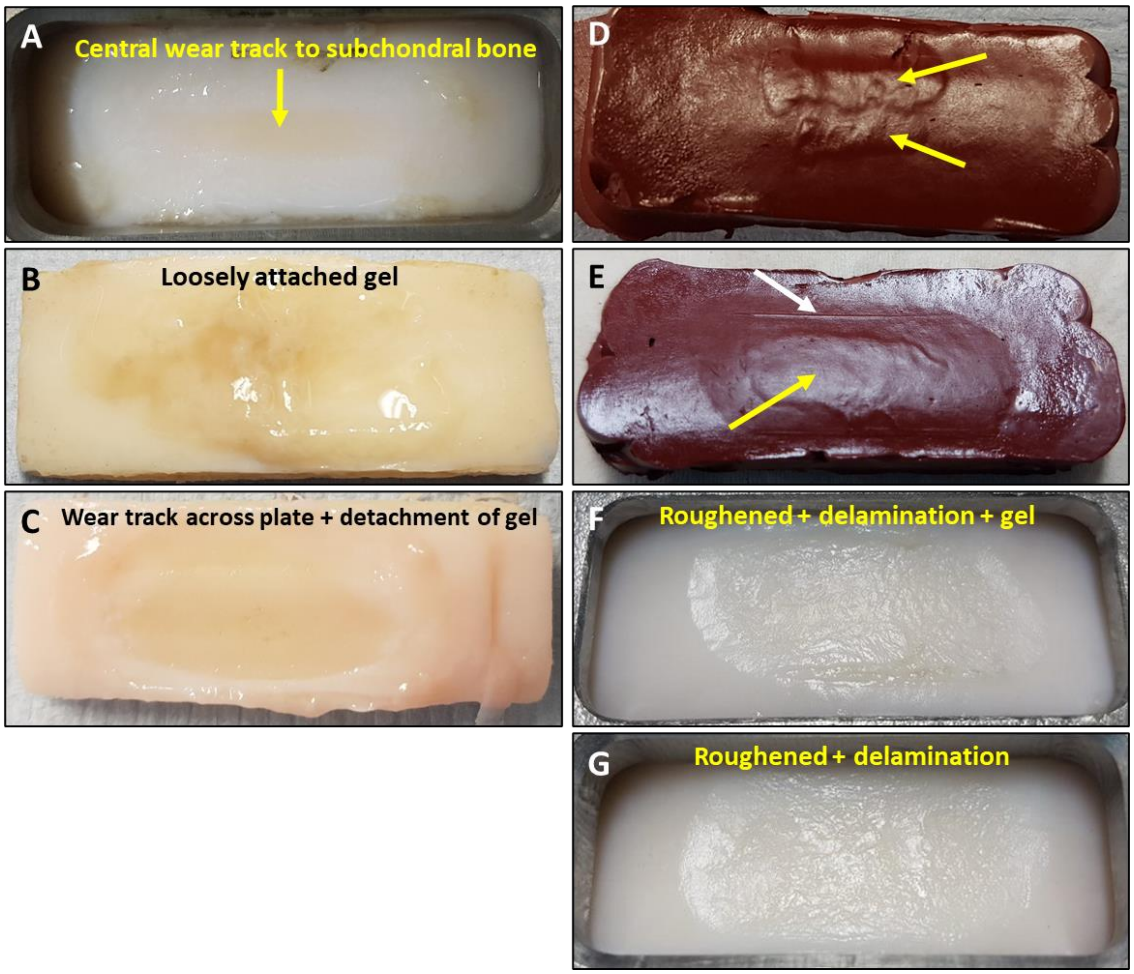


**Figure 3.8: Presentation of plate wear, damage and deformation after 72-hours. Ringer's Solution group (A-C). Silicone replicas of serum in PBS (D) and serum in Ringer's (E) groups highlighting indentations (yellow arrows) and scratch (white arrow); replica photographs were included as the changes could not be easily seen from the photographs of the cartilage surfaces. Typical condition of healthy (F) and traumatic (G) physiological lubricant groups.**

**96-hour summary:** Further progression of wear, damage and deformation, more extensive for some samples than others.

**Pins (**Figure 3.9**):** For two serum in PBS samples there was little difference from the 72-hour condition, the third was rougher with a raised central region; the typical condition at t=96 was roughened. For two serum in Ringer's samples, there was little difference from the 72-hour condition except some scratches; the remaining sample was considerably rougher with scratches across the entire surface and a deep indentation on one side of the pin. The typical condition at t=96 hours was roughened with some scratches. Three Healthy Physiological Lubricant pins had lesions penetrating to subchondral bone; the remaining sample showed thinning and roughening with scratches running across the

pin. Further thinning and roughening had occurred for all Traumatic Physiological Lubricant pins. Two samples experienced scratching with evidence of blistering of the surface of one, another had lesions approaching subchondral bone and the remaining sample showed little change from the 72-hour condition. The typical condition was roughened and thinning.

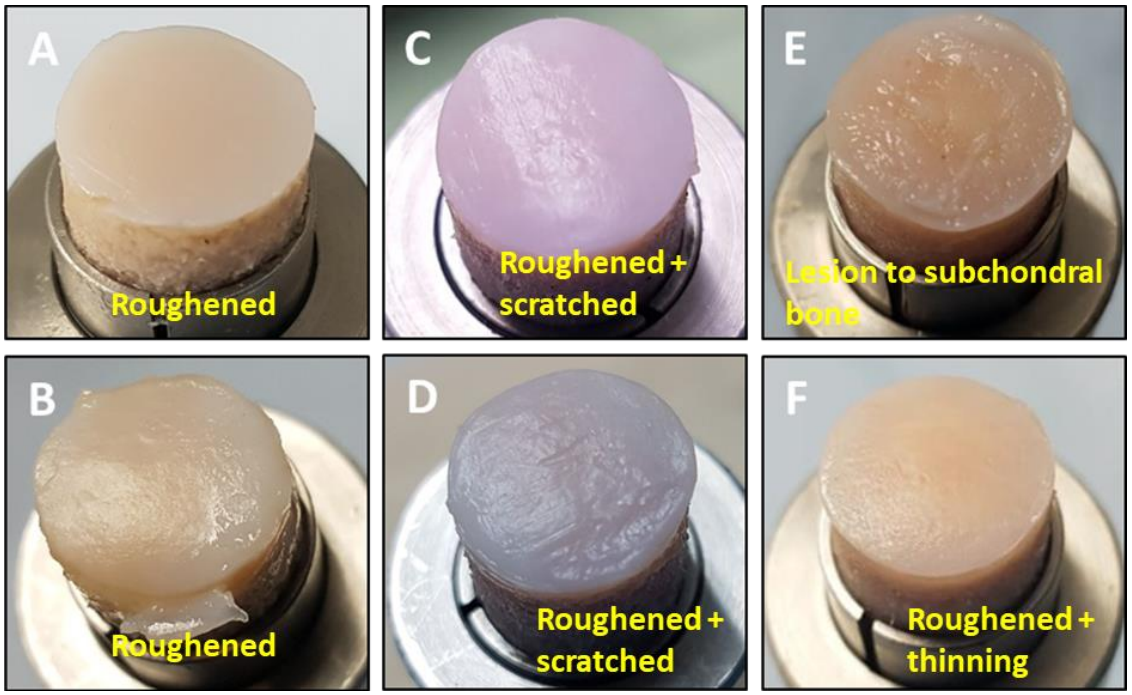


**Figure 3.9: Presentation of pin wear, damage and deformation after 96-hours. Typical condition of serum in PBS pins (A & B), serum in Ringer's Solution pins (C & D), Healthy Physiological Lubricant pins (E) and Traumatic Physiological Lubricant pins (F). Pins A and C articulating against plates showing minimal damage and pins B and D articulating against plates with significant delamination.**

**Plates (**Figure 3.10**):** For one serum in PBS sample the surface was slightly rougher, for another chondral delamination left a shallow wear scar across the width of the plate where indentations had been, for the remaining sample previous damage had increased in depth and area. A long scratch and small but deep indentation formed in one serum in Ringer's sample. For the other two samples chondral delamination occurred leaving wear scars across the width of the plates; one of these penetrated close, if not through, to subchondral bone. Both minimal damage and significant delamination/wear were observed in the serum-based groups. Healthy Physiological Lubricant samples experienced further chondral delamination, deepening of wear scars and increased volume of gel-like substance; one sample had several scratches along the length of the

plate. For all Traumatic Physiological Lubricant samples, the deformed region was slightly deeper and rougher but little change was observed from the 72-hours condition, except for a scratch along the length of the plate of one sample and chondral delamination in more locations around the edge of the deformed region in another.

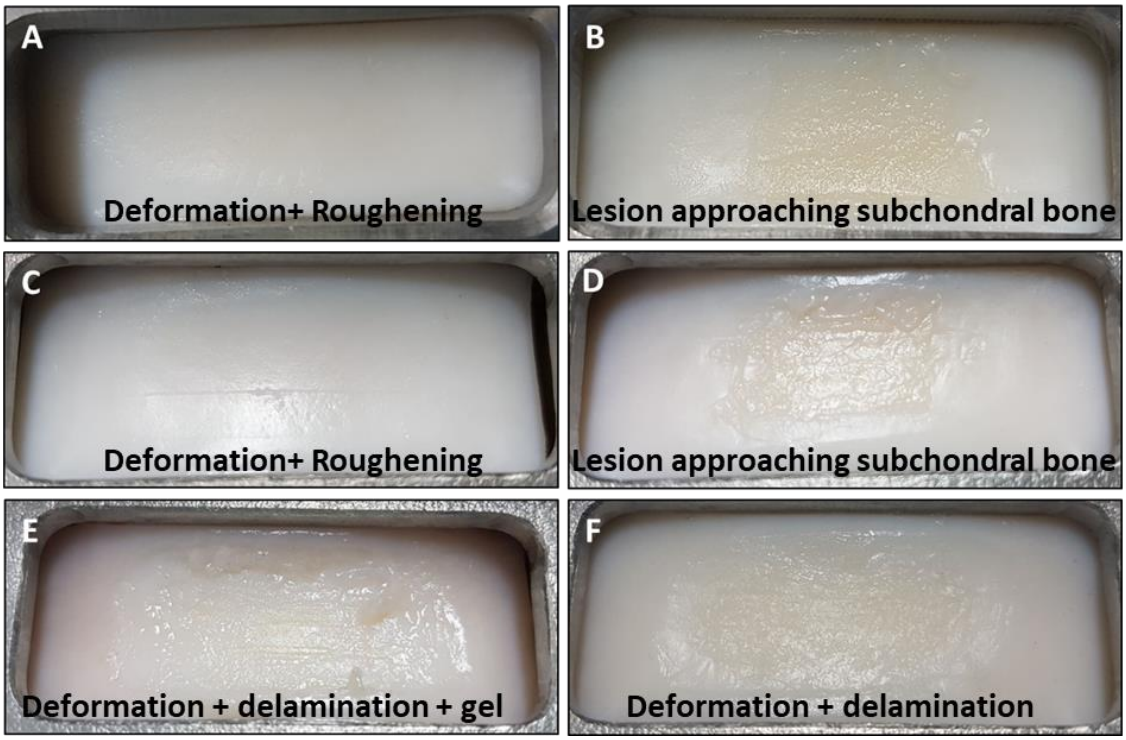


**Figure 3.10: Presentation of wear, damage and deformation after 96-hours. Typical condition of serum in PBS plates (A & B), serum in Ringer's Solution plates (C & D), Healthy Physiological Lubricant plates (E) and Traumatic Physiological Lubricant plates (F).**

### 3.4.3 ICRS grading

Grading for wear, damage and deformation based on ICRS guidelines was completed at each time point (Figure 3.11), values shown are the mean with standard deviation. There was a statistically significant difference between Ringer's Solution and 25% NBCS in Ringer's Solution for pins ($p=0.02$) and plates ($p=0.008$) at 72-hours and between Ringer's Solution and Healthy Physiological Lubricant pins at 48-hours ($p=0.026$). There was an increase in mean ICRS grade (from 0 to 1) for all experimental samples after 24 hours. For the two serum-based groups and the Traumatic Physiological Lubricant group there was a slow increase in mean ICRS grade from 24 hours to 96 hours (from 1 to 2); a similar trend was observed for the Healthy Physiological Lubricant group plates, however, there was a faster increase in mean ICRS grade for the pins at both 72 hours (from 1 to 2) and 96 hours (from 2 to 3/4). For the Ringer's Solution group increases in mean ICRS grade were faster between 24 hours and 48 hours (from 1 to 2) and 48 hour and 72 hours (from 2 to 4) than the other experimental groups.

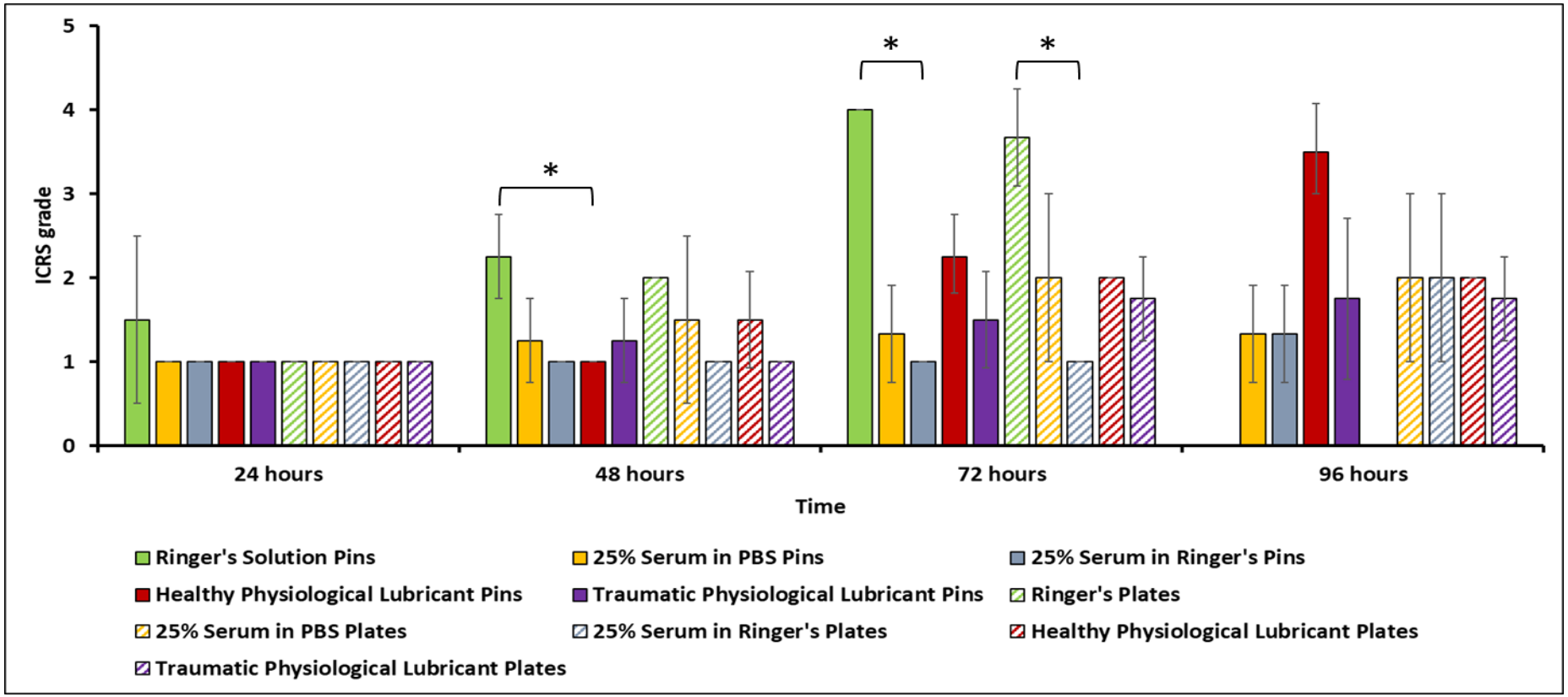


**Figure 3.11: Mean ICRS grade for cartilage pin and plate samples in each experimental group at each time point with standard deviation. Samples scored 0 to 4 using ICRS grading system (0 = normal, 4 = severely abnormal). Ringer's Solution: n=4 for 0-48 hours, n=3 for 72 hours; 25% NBCS in PBS: n=4 for 0-48 hours, n=3 for 72-96 hours; 25% NBCS in Ringer's Solution: n=3 for all time points; Healthy & Traumatic Physiological Lubricants: n=4 for all time points. Statistical analysis performed using Kruskal-Wallis test with post hoc Dunn-Bonferroni correction (* indicates statistical significance between Ringer's Solution and 25% NBCS in Ringer's Solution for pins (p=0.02) and plates (p=0.008) at 72-hours and Ringer's Solution and Healthy Physiological Lubricant pins at 48-hours (p=0.026)). No bars for Ringer's Solution at 96-hours, experiments terminated after 72-hours due to extensive damage to the samples (ICRS grade 4).**

### 3.4.4 Coefficient of Friction

All lubricants could maintain low dynamic coefficient of friction (0.02 – 0.05) throughout the experiment (Figure 3.12). For all experimental groups (except Ringer's Solution) friction was lower at 96 hours than at 24 hours. Mean friction at each 24-hour interval was highest for the Traumatic Physiological Lubricant at 24 and 48 hours, the Ringer's Solution at 72 hours and the Healthy Physiological Lubricant at 96 hours. Serum-based lubricants had lower friction compared to other experimental groups at every time point, however no statistically significant differences in dynamic coefficient of friction were observed between any of the experimental groups at any time point (one-way ANOVA, $p>0.05$).

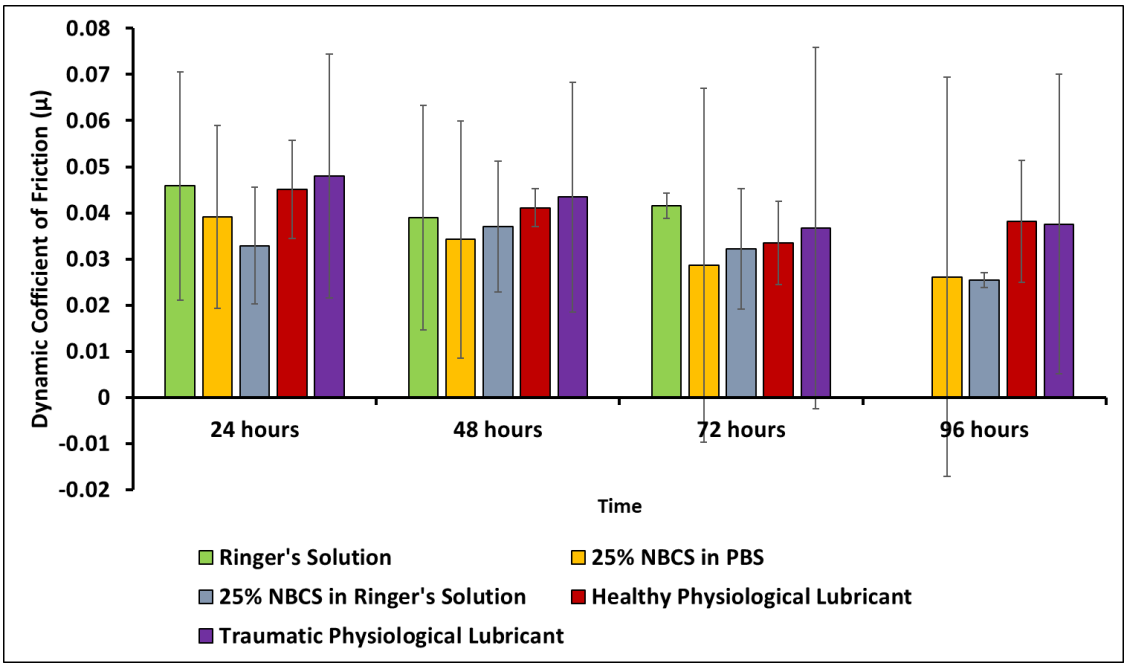


**Figure 3.12: Dynamic coefficient of friction for the pin-on-plate study experimental groups. Values stated are the mean with 95% confidence limits. Ringer's Solution: n=4 for 0-48 hours, n=3 for 72 hours; Serum in PBS: n=4 for 0-48 hours, n=3 at 48-96 hours; Serum in Ringer's Solution and Healthy Physiological Lubricant: n=3 at all time points; Traumatic Physiological Lubricant: n=4 at all time points.**

For 16 of the 17 studies, changes were observed in the dynamic coefficient of friction at some point during the test (Figure 3.13), these could be gradual or sudden; alterations to articulating surfaces were almost always observed during an inspection period if a change in friction had occurred during the previous 24 hours. For the only experiment which experienced no obvious change in friction throughout the experiment, 25% NBCS in PBS 1, the cartilage samples showed the least change from the original condition.

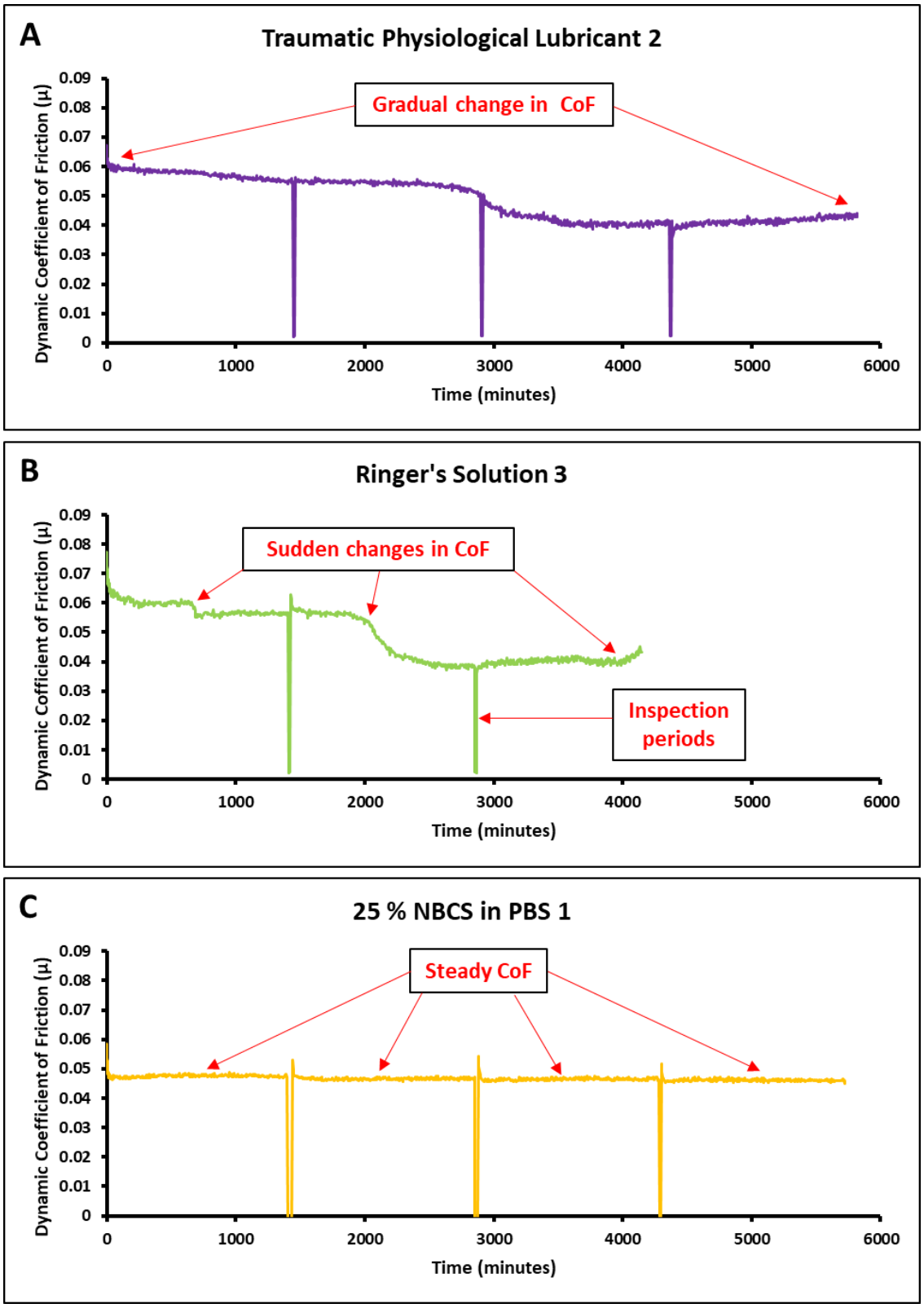


**Figure 3.13: Variation in dynamic coefficient of friction for different samples during pin-on-late experiments. Gradual change in CoF (A), sudden change in CoF (B), little to no change in CoF (C). Spikes extending down to the x-axis represent periods when samples were removed for inspection but the data acquisition unit was still active.**

### 3.4.5 Measurement of wear depth (Alicona)

Difference in relative height of the edge of the plate and the centre of the plate was calculated. There was a trend for an increase in wear depth for all experimental groups over 48 (Ringer's Solution only) or 96 hours (all other groups) of testing. The smallest change in wear depth was observed in the 25% NBCS in PBS group and largest change in wear depth was observed for the healthy physiological lubricant group, although Ringer's Solution group measurements are at the 48-hour stage not 96 hours (Figure 3.14). No statistically significant differences in mean relative height difference were observed between any of the experimental groups (one-way ANOVA, $p>0.05$).

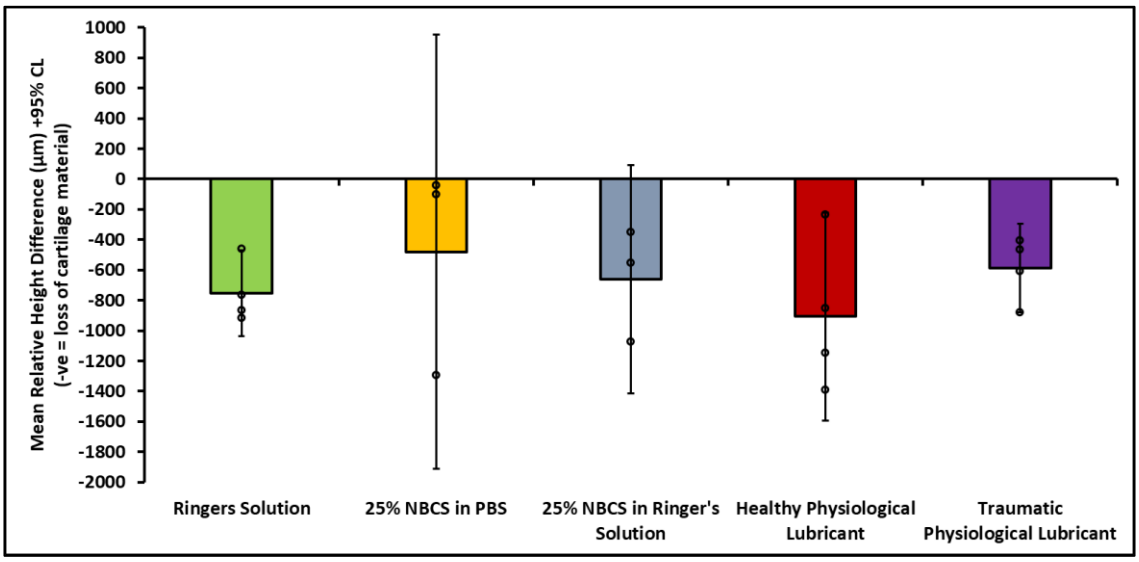


**Figure 3.14: Mean change in plate cartilage height with 95% confidence limits for each experimental group after 96-hours (48-hours for Ringer's Solution). Ringer's solution (n=4), Healthy Physiological Lubricant (n=4), Traumatic Physiological Lubricant (n=4), 25% NBCS in PBS (n=3) and 25% NBCS in Ringer's Solution (n=3). The negative values indicate a decrease in the height of the cartilage plate surface and therefore an increase in wear, damage and deformation depth.**

The following pseudo-colour images and traces (Figure 3.15) (Figure 3.16) (Figure 3.17) (Figure 3.18) (Figure 3.19) highlight the various plate geometries and how they altered from the initial condition to the final condition. For all the pseudo-colour images, orange indicates the highest point on the sample and pink represents the lowest point, however, the scales are not equal between timepoints or between samples, therefore the colours should not be used to compare between timepoints or samples.

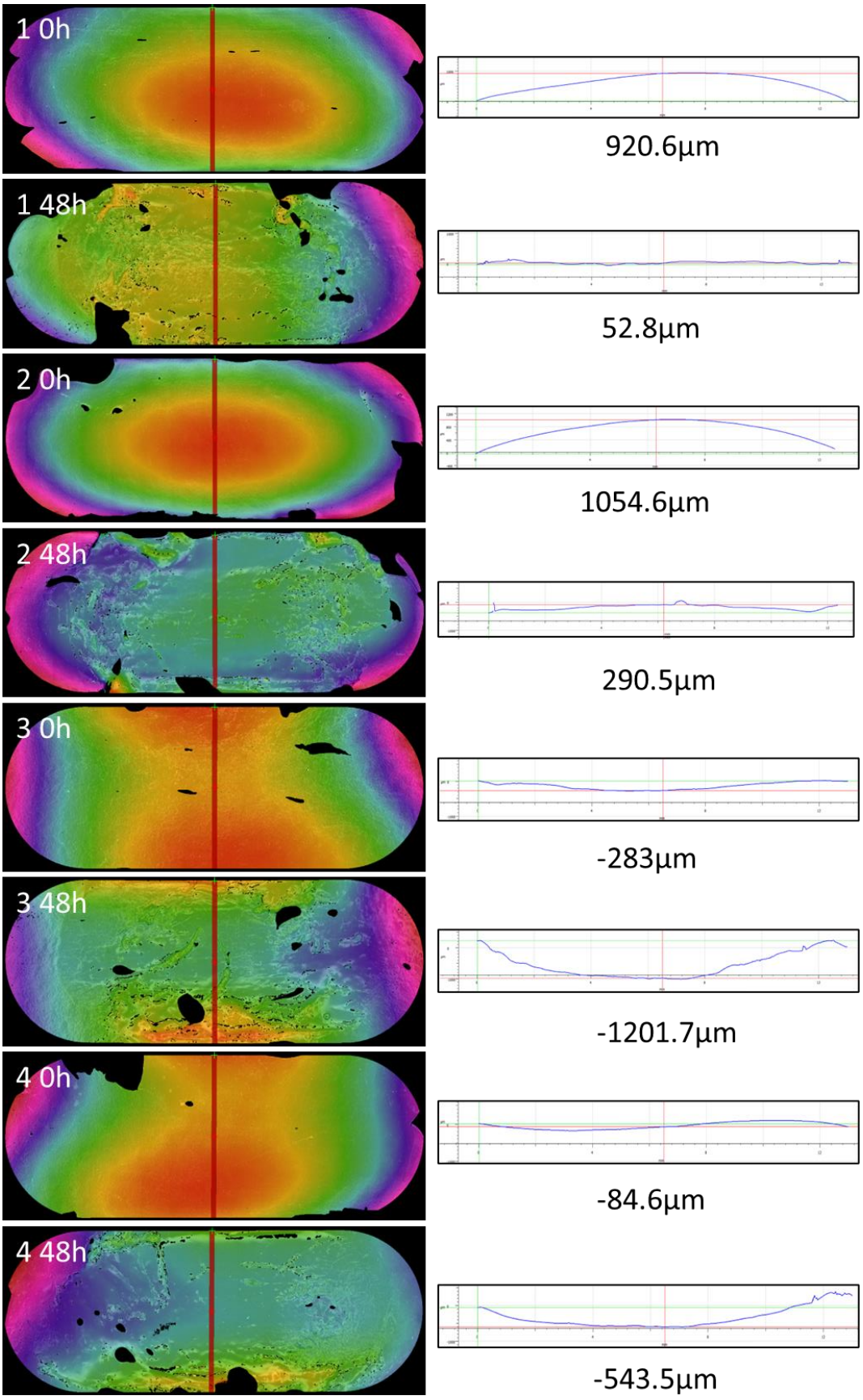


**Figure 3.15: Relative height difference between top edge of plate (green crosshairs) and centre of plate (red crosshair) at 0 hours and 48 hours for the Ringer's Solution group.**

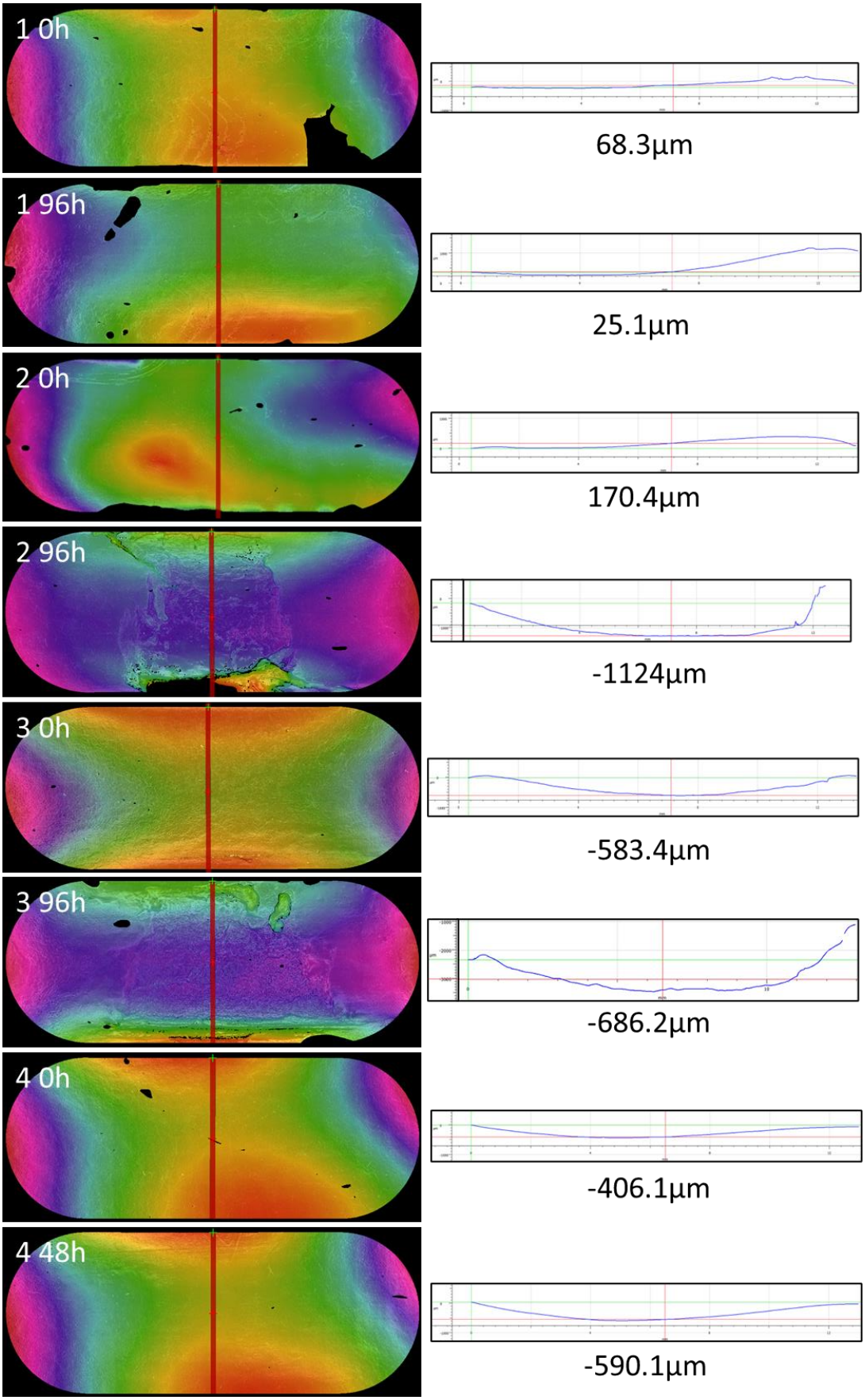


**Figure 3.16: Relative height difference between top edge of plate (green crosshairs) and centre of plate (red crosshair) at 0 hours and 96* hours for the 25% NBCS in PBS group. *48 hours for sample 4.**

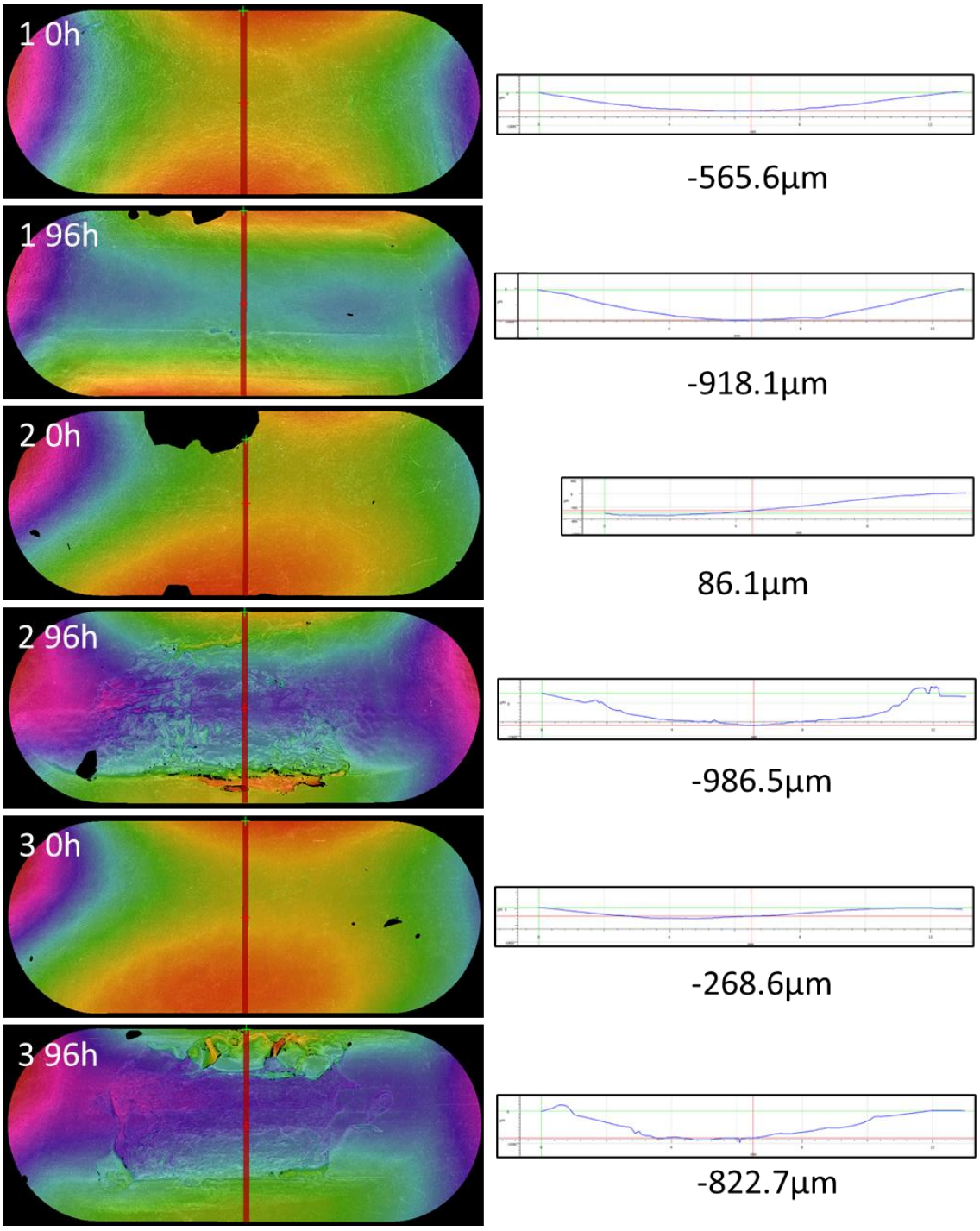


**Figure 3.17: Relative height difference between top edge of plate (green crosshairs) and centre of plate (red crosshair) at 0 hours and 96 hours for the 25% NBCS in Ringer's Solution group.**

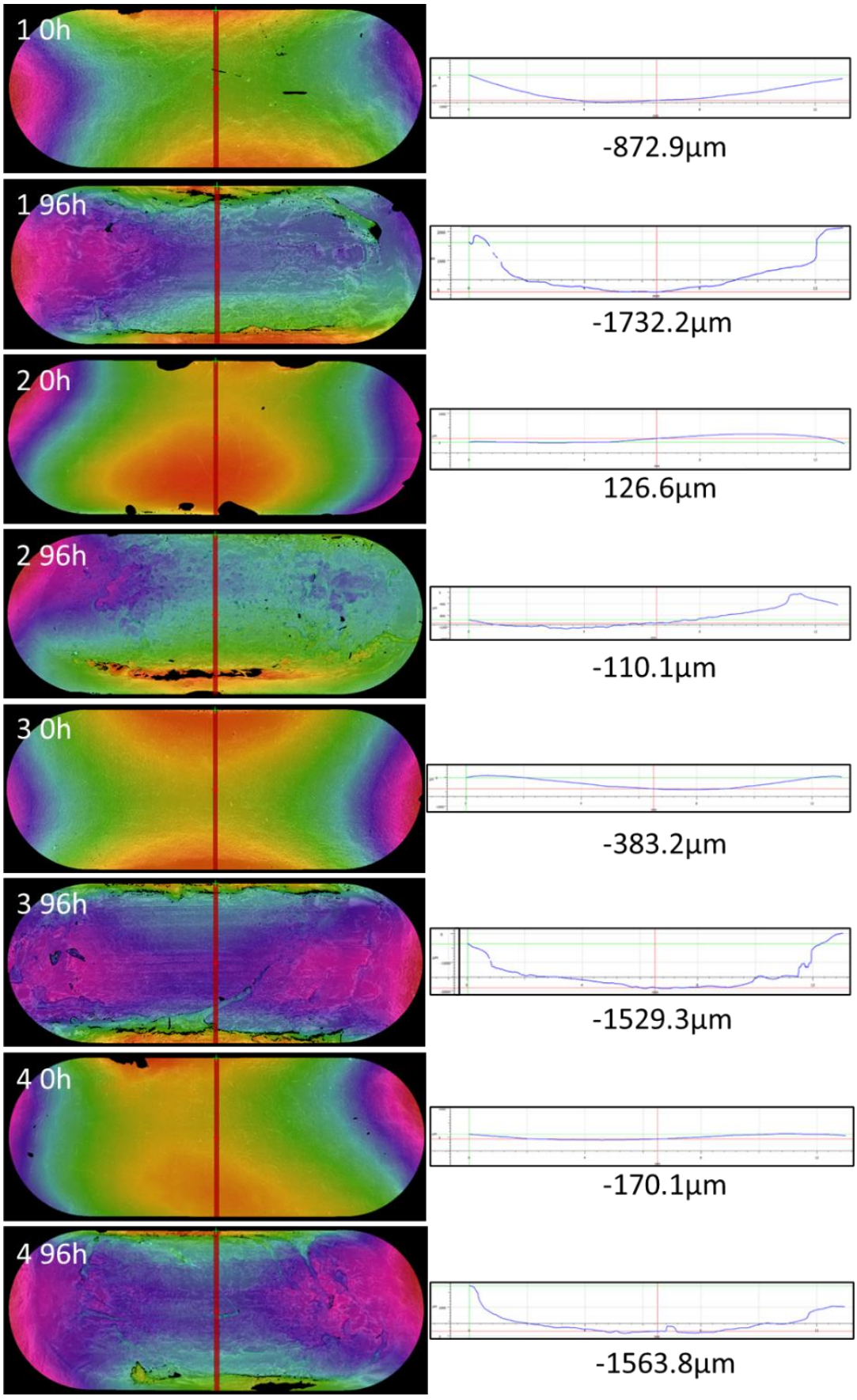


**Figure 3.18: Relative height difference between top edge of plate (green crosshairs) and centre of plate (red crosshair) at 0 hours and 96 hours for the Healthy Physiological Lubricant group.**

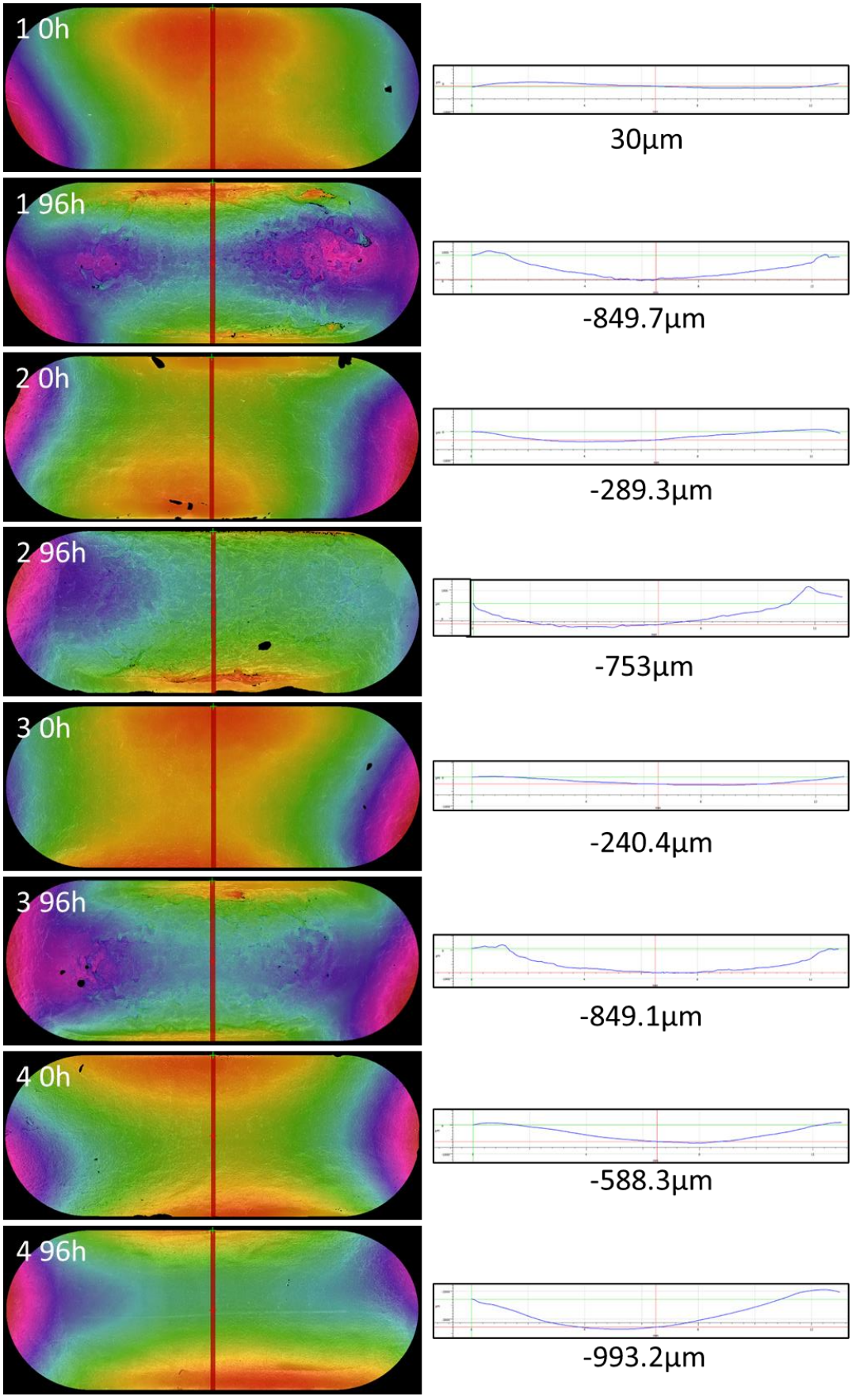


**Figure 3.19: Relative height difference between top edge of plate (green crosshairs) and centre of plate (red crosshair) at 0 hours and 96 hours for the Traumatic Physiological Lubricant group.**

## 3.5 Discussion

### 3.5.1 Summary

The aim of this study was to assess different lubricants to determine their appropriateness for long-term tribological investigations of natural knee joints. One experiment from each of the serum-based groups and one from the Traumatic Physiological Lubricant Group demonstrated minimal damage to cartilage surfaces after 96-hours indicating the potential of these lubricants for this application. However, there was considerable variability within these groups. Further investigation with a larger sample size is necessary to develop more robust conclusions. In the current study, sliding conditions were chosen to maintain favourable tribological conditions (fluid film lubrication), a sliding velocity of 10mm/s, has shown to effectively rehydrate cartilage pins (Graham et al., 2017), however, during most experiments, lubricants were unable to maintain cartilage surfaces for 96 hours. During the current study, changes in mechanical properties may have compromised interstitial fluid load support leaving cartilage surfaces vulnerable to the initiation of wear, damage and deformation. All lubricant groups experienced roughening and reddening of pin cartilage indicating thinning of samples.

### 3.5.2 Influence of lubricants on wear damage and deformation

Whilst all samples experienced some form of wear, damage and deformation, distinct differences in mechanisms and severity were observed between groups; this demonstrates lubricants influenced outcomes. The four protein-containing lubricants resulted in less wear, damage and deformation than the non-protein containing lubricant (Ringer's Solution). This agrees with findings from a previous long-term (150,000 cycles) pin-on-plate study, which showed uniaxial sliding of bovine cartilage in serum reduced wear factor compared to PBS (Cilingir, 2015).

When Ringer's Solution alone was used as a lubricant, consistent wear, damage and deformation occurred, resulting in complete loss of structural integrity of cartilage surfaces; a similar trend also occurred for the Healthy Physiological Lubricant Group but the progression of the damage was slower than when Ringer's solution alone was used as a lubricant. An absence of proteins in the Ringers solution likely influenced the boundary lubrication regime. Proteins, phospholipids and hyaluronic acid have all been shown to contribute to the protection of cartilage surfaces (Forsey et al., 2006) (Schmidt et al., 2007) (Greene et al., 2011) (Bonnevie et al., 2015). Absence of these substances left cartilage surfaces vulnerable, especially once interstitial fluid pressurisation had

subsided as the load was transferred from the fluid phase to the solid phase. The concentrations of hyaluronic acid, albumin, globulin, and phospholipids used in the Healthy Physiological Lubricant were intended to represent healthy synovial fluid. *In vivo* these concentrations, in combination with metabolic activity, maintain the structure and function of articular cartilage. In the current study, the concentrations used along with absence of metabolic activity may have been insufficient to provide effective boundary lubrication to the non-living cartilage tissue and provide an explanation for the similar damage mechanisms as observed in the Ringer's Solution group.

Within Ringer's Solution and Healthy Physiological Lubricant groups, cartilage damage resulted in formation of a gel along the edges of wear scars on plate surfaces. The amount of gel increased as cartilage material was removed from plate surfaces at later time points and clung to the pin during articulation. Gel formation has previously been described for polyethylene and thermoset polyurethane pins articulating against cartilage plates when using PBS as a lubricant (Russell, 2010); however, this was not observed during a 3-hour cartilage-on-cartilage control during the same study. This was explained as shearing of surface proteins in the gel-forming groups and the control maintaining a mixed lubrication regime. In the current study, all experimental groups were cartilage-on-cartilage contacts, but the gel only formed for the Ringer's Solution and Healthy Physiological Lubricant samples even though damage occurred for all experimental groups. *Russell et al.* suggested the gel was a combination of the surface amorphous layer and superficial cartilage layer and mentioned histological analysis of the gel would be beneficial to determine its constituents (Russell, 2010). The gel formation may be due to denaturing of the collagen into gelatine (Stoop et al., 1999). In the current study, pin surfaces seemed to wear, whereas plate surfaces delaminated and turned to gel, this could potentially be due to differences in the contacts as the pin was constantly under load whilst the plate was periodically unloaded. Or alternatively, differences in damage may be related to material properties as the pin was porcine tissue whereas the plate was bovine tissue.

Displacement of cartilage towards and extrusion beyond the edge of the pin occurred for the Ringer's Solution group and one sample from the Healthy Physiological Lubricant group; this has been previously observed in two separate studies assessing cartilage against orthopaedic hemiarthroplasty materials. This failure mechanism has been described as 'mushrooming' (Lizhang et al., 2011) or 'swelling' (Oungoulian et al., 2015). The *Lizhang et al.* study aimed to define the conditions at which unrecoverable cartilage wear occurred when articulating bovine pins against cobalt chrome plates; catastrophic pin failure was observed after 1 hour at 12MPa (Lizhang et al., 2011). During the current study, catastrophic failure was observed in Ringer's Solution group but at a much lower

contact pressure (1.06MPa) over a much longer duration (48-72 hours). During the *Lizhang et al.* study, a contact pressure of 8MPa also resulted in severe damage to cartilage pins, whereas lower contact pressures (0.5-4MPa) typically resulted in a central thinning of pin cartilage with material displaced toward the periphery after 24 hours (Lizhang et al., 2011). A central thinning of cartilage pins was observed after 6 hours at 7.5MPa in Ringer's Solution (Taylor, 2013). This pattern was observed in the current work at the 48-hour mark for Ringer's Solution and 72-hour mark for one Healthy Physiological Lubricant group sample.

Presentation, severity and timing of wear, damage and deformation was consistent within the Ringer's Solution and Healthy Physiological Lubricants groups. There was inconsistency within the serum-based and Traumatic Physiological Lubricant groups, some experienced minimal damage and others extensive damage; this could potentially have been influenced by a number of factors. These include: the lubricants, inherent differences between samples from different donors, congruence of the contact between samples and orientation of the pin during sliding (see limitations).

Hyaluronic acid was added to physiological lubricants; this was intended to give them a viscosity more similar to natural synovial fluid, enable shear-thinning during fluid film lubrication (Hamrock et al., 2004) and contribute to boundary lubrication mechanisms. The Healthy Physiological Lubricant had a higher hyaluronic acid content than the Traumatic Physiological Lubricant and therefore it may be expected this group would experience reduced wear, damage and deformation; however, the opposite was true. Elevated levels of albumin, globulin and phospholipids present within the Traumatic Physiological Lubricant may have provided a protective effect that outweighed the negative impact of reduced hyaluronic acid concentration. Alterations to synovial fluid in the traumatic knee *in vivo* may serve to mitigate subsequent articular cartilage damage after sustaining a knee injury. Conducting further parameterised pin-on-plate testing would be beneficial to verify the contribution of each constituent over an extended duration. In addition, evidence in the literature demonstrates hyaluronic acid and lubricin (SZP/PRG4) act synergistically to reduce friction and minimise wear (Greene et al., 2011) (Das et al., 2013) (Bonnevie et al., 2015). Absence of lubricin may have limited the intended boundary lubricating effects of the hyaluronic acid in the physiological lubricants. This may also provide an explanation for why both physiological lubricants provided inferior performance compared to serum-based lubricants. Rheological analysis of lubricants was not performed during the current study therefore the exact viscosity of the healthy or traumatic physiological lubricants was not known.

Addition of bovine serum albumin and gamma globulin and Ringer's Solution to physiological lubricants may have resulted in excessive ion concentration due to

presence of additional salts in these substances (Bortel et al., 2015). This may have reduced the viscosity and compromised the effectiveness of shear-thinning in the lubricants, leaving cartilage surfaces susceptible to the initiation of wear, damage and deformation. In future, measuring salt content or using deionised water in place of Ringer's solution may produce a more optimal lubricant, as previously suggested (Bortel et al., 2015).

### 3.5.3 Quantitative Analysis using Aliocna

Post-experimental analysis of pin and plate samples using the Alicona was intended to provide quantification of wear damage and deformation of the cartilage surfaces. It was presumed cartilage surfaces would remain intact due to maintenance of preferential tribological conditions (maintenance of fluid film); however, extensive damage occurred to several samples so only a limited analysis was possible. A previous study measured wear, deformation and damage volume from silicone replicas of cartilage surfaces using an optical profiler (Bowland et al., 2018). In these short-term experiments (2 hours), minimal damage had occurred to pin cartilage at the conclusion of the study so the unworn surface could be used as a suitable reference from which to measure. In the current study, due to the extended duration of the study (48 or 96 hours), extensive cartilage damage occurred over the entire pin surface leaving no suitable reference from which to measure so a quantitative analysis of the pins could not be made. In future, a reference surface external to the pin could be incorporated into replicas to enable measurement.

Plate samples included an unworn region suitable for use as a reference surface to enable measurement of wear depth, however for some samples, extensive damage occurred in the reference region (Figure 3.20). Once damaged, cartilage delaminated, leaving strings of extracellular matrix loosely attached to plate surfaces; in certain instances, this interfered with the quality of the replicas that could be produced, and hence, what it was possible to measure using the Alicona.


**Figure 3.20: Plate sample showing a suitable area outside of the contact region (yellow arrow) to use a reference (left). Plate sample with extensive damage leaving no suitable reference region dur to removal (red arrow) or displacement of cartilage (right).**

The strings could have been removed from the surface, however, were left in situ, as they could have influenced the wear, damage and deformation at future time points. A reference frame had to be selected for each plate, variation in the accuracy of the reference frame placement at each time point may have limited the accuracy of the results.

In addition, variation in plate geometry made it impossible to use the volume calculation method, as the value calculated was not representative of the actual volume loss (Figure 3.21). Volume loss of a domed plate would be underestimated as the reference mesh applied to a worn sample would not account for the position of the original cartilage surface. The volume under the mesh of an unworn concave plate could be larger than the volume of a flat plate which had actually experienced material loss. As with the pins, inclusion of a reference frame within the replica may enable volume to be calculated.

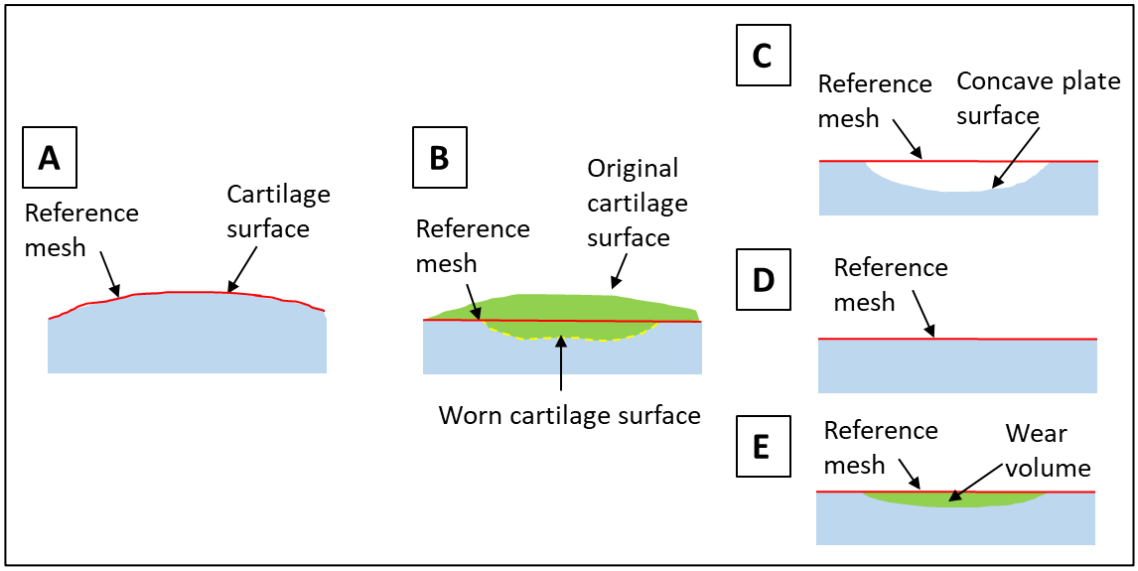


**Figure 3.21: Influence of plate geometry on Alicona volume calculation. Domed plate with mesh hugging the surface (A). Underestimation of volume loss on a domed plate - total volume loss (whole green region) vs calculated volume loss (green region between red line and yellow dotted line) (B). Unworn concave plate (C). Unworn flat plate (D). Worn flat plate (E). Software may calculate a larger "volume loss" for an unworn concave plate (C - white region) than for a worn flat plate (E - green region).**

### 3.5.4 Damage initiation and CoF

The observed trends for the assessed lubricants were evident both visually and from dynamic CoF data. CoF values generated during this study were similar to previous studies for a cartilage-on-cartilage contact (Northwood and Fisher, 2007) (Russell, 2010) (Bowland et al., 2018). During the current study, changes in CoF appeared to be linked to the initiation of wear, damage and deformation on cartilage surfaces. Upon inspection at each 24-hour interval, alterations in sample surfaces were nearly always observed if the CoF behaviour had changed anytime during the preceding 24-hour period. In addition, the only experiment which experienced no obvious change of CoF (25% NBCS in PBS 1), showed minimal changes to the articulating surfaces after 96-hours. Changes in CoF could not predict the extent or presentation of wear, damage or deformation during the current study. It has previously been demonstrated that changes in CoF signal can be used to detect cartilage damage (described as surface cracking and internal cracking) to a high degree of accuracy (Whitney et al., 2015) and hysteresis plots of tangential friction force vs tangential displacement can be used to predict the onset of cartilage delamination (Durney et al., 2020).

It has been shown experimentally that to achieve low CoF, interstitial fluid support must be maintained (Forster and Fisher, 1996) (Krishnan et al., 2004) (Caligaris and Ateshian, 2008). Tribological rehydration has been suggested as the main mechanism via which interstitial fluid load support and hence low CoF are maintained (Moore and Burris, 2017). It has been demonstrated that surface cartilage damage due to impact injury does not negatively affect tribological rehydration (Farnham et al., 2020) and presence of osteoarthritis does not increase CoF (Caligaris et al., 2009). Results from the current study agree with these findings as all experimental groups maintained low CoF even after considerable surface damage had been observed. Previous work has also shown that a low CoF could be maintained and reduced after removal of the articular cartilage superficial zone (Krishnan et al., 2004). It was suggested that a combination of sliding induced tribological rehydration, migrating contact area and free osmotic swelling successfully maintained the interstitial fluid pressurisation. It has been shown fissures or defects penetrating to subchondral bone do negatively affect tribological rehydration (Farnham et al., 2020), findings from the current study seem to disagree with this idea. During the current research, CoF was maintained and, in some cases, reduced when Ringer's solution was used as a lubricant even though samples were worn to the subchondral bone. This level of damage would be expected to interfere with tribological rehydration and compromise fluid load support leading to an increase in CoF. Calibration of the friction rig ensured it was sensitive enough to measure friction over a range of applied loads, however, variation in rig set up could potentially have a had greater influence on CoF than the lubricant and could have contributed to this finding. A reduction in CoF has previously been observed when creating defects which penetrate to subchondral bone (Bowland et al., 2018). Bowland et al. attributed this to a reduced contact area and increased fluid load support due to additional volume of fluid within the defect. This may provide an explanation for how a low CoF was maintained whilst significant wear was observed in the current study. Another potential explanation is that reduction in hyaluronic acid trapped in the cartilage network and an increase in free hyaluronic acid at the site of articulation has been shown to reduce CoF whilst failing to improve wear resistance at higher loads over longer durations (Greene et al., 2011). After an extended period had elapsed the collagen network began to break apart due to failure of the lubrication mechanisms, this released trapped hyaluronic acid from the collagen network further compromising the wear resistance. However, this free hyaluronic acid then entered the contact and potentially reduced or maintained the low CoF.

### 3.5.5 Limitations

Several factors may have influenced the CoF and wear, damage and deformation observed during this study. A small sample size (n=3/4) was used during the current study, more samples would have been beneficial for identifying trends, particularly for the serum-based lubricants and Traumatic Physiological Lubricant as there was significant variability in ICRS grades within these groups.

This variability may have been introduced either by the equipment or samples. As previously described in Chapter 2, prior to experiments, both pin-on-plate rigs were calibrated and polyethylene pins were articulated against cobalt-chrome plates to check the coefficient of friction produced was similar to previous experiments using the same equipment. Due to the incorporation of these processes, the majority of the variation seen during experiments was likely explained by differences between individual tissue samples due to the inherent geometric variation between animals and not issues with the equipment.

Non-living osteochondral tissue was used during the current study, whilst this was consistent between groups, this may have accelerated tissue degradation compared to using viable cartilage. Development of a bioreactor system capable of maintaining tissue viability could enable more clinically meaningful results to be generated.

Pin and plate osteochondral samples were cut to fit within fixtures, during experiments, fluid could be squeezed from the cartilage matrix via the cut edges and compromised the interstitial fluid load support. There may have been variability in contact pressure for each experiment due to variable congruence between different pin and plate samples. Collagen fibres within the superficial layer are orientated to withstand loading in a specific direction (Northwood, 2007), plates were orientated in the direction of sliding however pin orientation was not controlled during experiments. Pins could rotate within the plane bearing and likely settled into the position of greatest conformity between the samples during testing. Cut edges and high-pressure contacts with suboptimal pin orientation may have left surfaces more susceptible to the initiation of wear, damage and deformation and accelerated their progression compared to a whole knee joint which would have an optimal alignment. Future studies could control pin orientation or assess lubricant performance in whole joints.

Hyaluronic acid was added to the physiological lubricants used during the current study to produce a viscosity more similar to synovial fluid. The viscosity of these lubricants was not assessed during the current study and hence may have differed from the intended value, this may have influenced tribological behavior during these experiments. In future rheology could be used to measure viscosity of lubricants prior to experiments.

Non-sterile conditions were used during experiments potentially resulting in microbial growth or biofilm formation on sample surfaces; these factors may have influenced the tribological behavior of the contact region and provided a protective effect. Sterile dissection and lubricant preparation techniques could be employed in future studies to eliminate this issue. The serum and albumin used during this study were both of bovine origin and hence may behave differently to the human equivalent.

During this study, the International Cartilage Regeneration and Joint Preservation Society (ICRS) ICRS grading system was used to evaluate wear damage and deformation of cartilage surfaces. This was a subjective scoring system and hence had the potential to introduce observer bias when recording results, especially as grading was performed by a single observer (the author). It was difficult assigning appropriate grades for borderline samples; for example, a bad Grade 2 (lesion ≤50% of cartilage depth) and a mild Grade 3 (lesion >50% of cartilage depth) looked very similar. Ideally multiple independent assessors would have scored samples and mean values could have been calculated to minimise potential bias. The single observer approach was adopted as extended experimental durations and potential degradation of the tissue left minimal time to perform observations at each designated timepoint. Additionally, due to unforeseen circumstances, lab access/space was limited, therefore it was not possible to coordinate multiple assessors under these circumstances. To reduce the potential for incorrect classification and improve the intra-rater reliability, the author retrospectively analysed images and silicone replica surfaces to compare borderline samples and better categorise them into specific grades. Overall, during the current study, the ICRS grading system provided a simple, quick and effective method for assessing wear, damage and deformation of cartilage surfaces in a limited timeframe.

## 3.6 Conclusions

This study assessed the suitability of five different lubricants for use during *in vitro* tribological investigations of natural tissue. The hypothesis stated, *"Protein containing lubricants will result in less wear, damage and deformation of cartilage surfaces compared to non-protein containing lubricants during extended duration (96 hour) pin-on-plate experiments."* The results of the current study agree with this hypothesis. Osteochondral pin and plate samples assessed in protein containing lubricants completed the 96-hour experimental duration exhibiting varying degrees of wear damage and deformation. Osteochondral sample assessed in the non-protein containing lubricant (Ringer's Solution) suffered extensive damage and experiments were terminated after 72-hours.

The aim of this work was to inform development of an enhanced experimental model for natural knee simulation, below are the conclusions drawn in this context:

- When using natural tissue, the influence of lubricants needs to be evaluated over an extended duration to determine their ability to mitigate degradation of cartilage surfaces. Choosing a suitable lubricant will minimise the potential for degradation artefacts to influence measurement of wear, damage and deformation during tribological investigations. The suitability of a lubricant will depend on the experimental duration.

    - Ringer's Solution appears an unsuitable lubricant for *in vitro* testing of natural joints over an extended duration due to consistent loss of structural integrity of cartilage surfaces after 72 hours.

    - Serum-based lubricants appear promising for use during longer-term *in vitro* studies; both lubricants demonstrated the ability to limit, wear damage and deformation of cartilage surfaces for up to 96 hours.

    - Both physiological lubricants experienced global damage to plate surfaces as opposed to the localised damage in the serum-based groups. This was more severe in the Healthy Physiological Lubricant group which showed similar wear to the Ringer's Solution group but at later time points. One Traumatic Physiological Lubricant experiment demonstrated minimal damage; therefore further optimisation of these lubricants could potentially make this approach a viable option. The method on which the current approach was based (Bortel et al., 2015) developed the lubricant using materials to make it affordable once scaled up.

- The pin-on-plate methodology has limitations likely to result in accelerated damage to natural tissues. Evaluating a whole knee joint would eliminate several of these by increasing congruence of the contact area, periodically unloading articulating surfaces and removing edge effects. This may extend the duration over which lubricants are effective.

- Maintenance of a low dynamic coefficient of friction did not indicate absence of wear, damage and deformation; hence, low CoF is an unsuitable outcome

measure to infer cartilage health when performing experiments with natural tissue.

- Damage to articulating surfaces was difficult to quantify using the Alicona methodology due to the extent of damaged caused, complex and variable geometry and lack of a suitable reference surface to measure from. Incorporating a reference surface into AccuTrans replicas would be beneficial in the future.

# Chapter 4

# Experimental Knee Simulation for an Extended Duration

## 4.1 Introduction

The pin-on-plate lubricant study (Chapter 3) demonstrated the potential for porcine/bovine osteochondral samples to be articulated for up to 96 hours with minimal damage to the cartilage surfaces when using isotonic serum-based lubricants. However, the cut edges of the osteochondral samples allowing fluid to escape which reduced interstitial fluid pressurisation and suboptimal congruence and pin alignment may have influenced the contact pressure potentially leading to accelerated wear, damage and deformation of the cartilage surfaces. Therefore the clinical relevance of the pin-on-plate approach was limited.

To generate more clinically relevant results it would be beneficial to assess early-stage knee interventions for an extended duration under conditions which more closely mimic the *in vivo* scenario. A porcine knee joint experimental simulation model was developed at the University of Leeds to enable the assessment of early-stage knee interventions under dynamic loads and motions to provide a more clinically relevant setting (Liu et al., 2015). This experimental model has previously been used to assess osteochondral grafts during walking gait simulations (Bowland et al., 2018) and the model has undergone subsequent optimisation to improve the physiological relevance of the spring constraint mechanism which aims to replicate ligament function (Liu et al., 2019). Whilst still limited in clinical relevance, porcine knees are cheap, easy to source, provide consistent tissue quality and their use does not require ethical approval. This makes them a valuable tool for method development and prevents wastage of donated human cadaveric tissue which is expensive and in limited supply.

Thus far, tibiofemoral studies conducted with the porcine knee joint experimental simulation model have been short term (≤ hours or 3600 cycles), therefore, the behaviour of the system over an extended duration remained unknown. To assess the systems suitability to investigate interventions over an extended duration, its ability to maintain

physiological kinetic and kinematic inputs/outputs and the extent to which the articulating surfaces degraded needed to be determined, which is the focus of the following chapter.

## 4.2 Aim and Objectives

### 4.2.1 Aim:

- The aim of this study was to determine if a non-living porcine knee joint was a suitable environment to assess early-stage knee interventions during extended duration walking gait simulations using a 25% NBCS in Ringer's Solution lubricant. The isotonic serum-based lubricants from Chapter 3 showed similar performance, the Ringer's Solution version was selected as the optimal choice due to having a more similar ion concentration to synovial fluid than PBS.

### 4.2.2 Objectives:

- Assess the extent of tissue degradation to articulating surfaces (articular cartilage and meniscus) after extended duration simulations in an isotonic serum-based lubricant

    - Visually inspect cartilage and meniscal surfaces to identify the presence of any surface wear, damage or deformation and score based on the ICRS grading criteria

    - Conduct histological analysis of cartilage and meniscal sections to assess the presence of any structural changes, particularly sub-surface delamination of the superficial tangential layer of the articular cartilage

- To determine if extended duration simulations negatively influence the ability of porcine knees to follow simulator inputs (i.e. kinematics remains physiological, absence of fracture or dislocation)

- To conduct histological analysis of medial femoral condyle to assess the presence of any microbial growth and/or biofilm formation on the articulating surfaces which may influence the tribology within the system

- Assess the extent of microbial growth within the system by filtering and plating lubricant samples and culturing them in nutrient broths

## 4.3 Extended Duration Simulator Studies

### 4.3.1 Introduction

This study was split into two sections. A preliminary study was conducted to assess the potential for porcine knees to run in the simulator for an extended duration using walking gait simulations. The information learned from the preliminary study was then used to develop the methodology for a second study which aimed to provide additional kinetic and kinematic data as well as more comprehensive analysis of the influence of the extended duration on the wear, damage and deformation of articulating surfaces and microbial growth within the simulation system. All simulations were conducted at room temperature, this was to reduce the rate of microbial growth. In addition, due to the limited time available, it was not practical to heat the simulation environment as this would have limited the number of samples which could be simulated. A summary of experimental conditions and subsequent analyses experienced by each knee joint have been highlighted in Table 1.

### 4.3.2 Sample preparation

All porcine knee joints (n=11) were prepared as previously described (Chapter 2), these were dissected, cemented into the correct alignment and frozen within 48-hours of delivery. Knee joints were defrosted overnight prior to experiments, with each knee experiencing only a single freeze-thaw cycle. The knees used during the Preliminary study (n=3) had been frozen for an extended period of time (Table 4.1) whereas the knees used during the enhanced analysis study (n=8) completed the experimental process within 2 weeks of the dissection date.

**Table 4.1: Experimental conditions used for each knee during extended duration study.**

| | Experiment duration (hours) | Simulated activity | Microbial growth mitigation | Lubricant | Duration frozen | Visual Inspection | Histological Staining | Culture Broths | Lubricant Filtering |
|---|---|---|---|---|---|---|---|---|---|
| **Preliminary Study Knees** | | | | | | | | | |
| **Prelim 1** | 72 | Walking gait | Gaiter sprayed with 70% ethanol | 25% new-born calf serum in PBS | ~11 months | Yes | No | No | No |
| **Prelim 2** | 46 | Walking gait | Gaiter sprayed with 70% ethanol | 25% new-born calf serum in Ringer's Solution + 0.03% sodium azide | ~ 26 months | Yes | Yes | Yes | No |
| **Prelim 3** | 48 | Walking gait | Gaiter sprayed with 70% ethanol | 25% new-born calf serum in Ringer's Solution + 0.03% sodium azide | ~14 months | Yes | Yes | Yes | Yes |
| **Experimental Study Knees** | | | | | | | | | |
| **Simulated 1** | 48 | Walking gait | Fixtures and gator autoclaved and sprayed with 70% ethanol | 25% new-born calf serum in Ringer's Solution + 0.03% sodium azide | ~2 weeks | Yes | Yes | Yes | Yes |
| **Simulated 2** | 48 | Walking gait | Fixtures and gator autoclaved and sprayed with 70% ethanol | 25% new-born calf serum in Ringer's Solution + 0.03% sodium azide | ~1 week | Yes | Yes | Yes | Yes |
| **Simulated 3** | 48 | Walking gait | Fixtures and gator autoclaved and sprayed with 70% ethanol | 25% new-born calf serum in Ringer's Solution + 0.03% sodium azide | ~1 week | Yes | Yes | Yes | Yes |
| **Simulated 4** | 48 | Walking gait | Fixtures and gator autoclaved and sprayed with 70% ethanol | 25% new-born calf serum in Ringer's Solution + 0.03% sodium azide | ~1 week | Yes | Yes | Yes | Yes |
| **Experimental Study Control Knees** | | | | | | | | | |
| **Non-Simulated 1** | 48 | N/A | Fixtures and gator autoclaved and sprayed with 70% ethanol | 25% new-born calf serum in Ringer's Solution + 0.03% sodium azide | ~1 week | Yes | Yes | Yes | Yes |
| **Non-Simulated 2** | 48 | N/A | Fixtures and gator autoclaved and sprayed with 70% ethanol | 25% new-born calf serum in Ringer's Solution + 0.03% sodium azide | ~1.5 weeks | Yes | Yes | Yes | Yes |
| **Non-Simulated 3** | 48 | N/A | Fixtures and gator autoclaved and sprayed with 70% ethanol | 25% new-born calf serum in Ringer's Solution + 0.03% sodium azide | ~2 weeks | Yes | Yes | Yes | Yes |
| **Non-Simulated 4** | 48 | N/A | Fixtures and gator autoclaved and sprayed with 70% ethanol | 25% new-born calf serum in Ringer's Solution + 0.03% sodium azide | ~2 weeks | Yes | Yes | Yes | Yes |

## 4.4 Preliminary Study

### 4.4.1 Experimental Design

#### 4.4.1.1 Delivery of kinetic/kinematic inputs

The preliminary knees (n=3) were subjected to walking gait simulation in the single station knee simulator (SSKS3). The input profiles used (Table 4.2) (Figure 4.1) were chosen to be consistent with previous literature (Liu et al., 2019). The axial force was run using force control, the flexion-extension and internal-external (tibial) rotation were run using displacement control delivered through the tibia. The abduction-adduction axis was left free to swing freely and the anterior-posterior motion of the tibia was not controlled but incorporated a spring constraint mechanism to replicate ligament function. A spring stiffness of 20N/m$^2$ and free length of 5mm were used based on previous literature (Liu et al., 2019). All simulations were run at a frequency of 1.0Hz with samples submerged in an isotonic 25% new-born calf serum lubricant throughout.

**Table 4.2: Minimum and maximum simulator input values for walking gait profile.**

**Walking Gait Inputs**

| | **min** | **max** |
|---|---|---|
| **Axial Force (N)** | 63.6 | 984.7 |
| **Flexion-Extension Rotation (°)** | 0 | 21.7 |
| **Abduction-Adduction Rotation (°)** | 0 | 0 |
| **Internal-External Rotation (°)** | -1.6 | 1.6 |
| **Anterior-Posterior Displacement (mm)** | spring controlled | |

#### 4.4.1.2 Data Logging and Analysis of Simulator Data

Three simulation cycles were logged every 600 cycles (10 minutes) for the duration of the simulation. Kinetic and kinematic data presented were the mean of 3 cycles at each of the stated time points.

#### 4.4.1.3 Condition of Knee Joint and Simulation Environment

Visual assessment of cartilage and meniscal surfaces was conducted at t=0 hours, t=24 hours, t=48 hours and t=72 hours (Prelim 1 only) to determine if any changes had occurred. AccuTrans silicone replicas of articulating surfaces were created to assist in highlighting any changes which may have been missed during the initial visual inspection. A general assessment of how the knee joint, lubricant and components looked was conducted to determine if tissue degradation and microbial growth were occurring and determine how much of an issue these factors may be for an extended duration simulation.

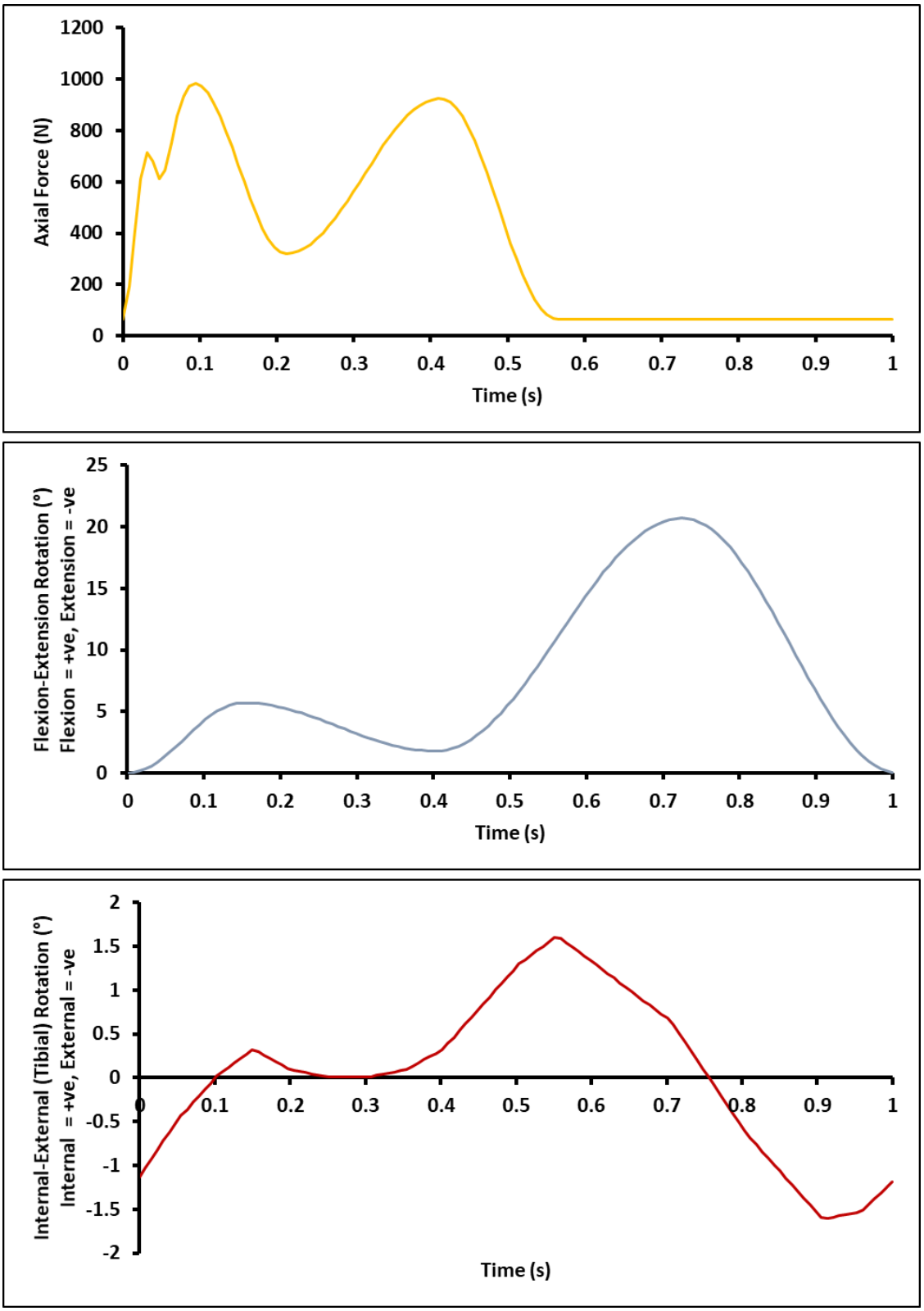


**Figure 4.1: Axial force (N), flexion-extension (°) and internal-external (tibial) rotation (°) demand waveforms for preliminary knees during extended duration walking gait simulations.**

## 4.4.2 Results of Preliminary Study

### 4.4.2.1 Condition of Knee Joint and Simulation Environment

Minimal changes were Virtually no change was observed after 48 hours for two knees. A small scratch was observed on the medial tibial plateau for Prelim 3 at t=24 hours; this remained at t=48 hours but appeared unchanged (this was potentially present pre-test but not identified). Prelim 1 experienced extensive damage after 72 hours (Table 4.3). With regards to the general degeneration of the tissue and lubricant, particles/debris were found floating in the lubricant and stuck to the inside of the gaiter for Prelim 1 at 72 hours and in the lubricant and on the surfaces of the joint of Prelim 2 at 48 hours. The femur of Prelim 3 had a reddened appearance after 48 hours.

**Table 4.3: Condition of preliminary knees at each time point.**

| Time (hours) | Prelim 1 | Prelim 2 | Prelim 3 |
|---|---|---|---|
| **0** | Swelling/dehydration of posterior femoral condyles | Femoral and meniscal surface have reddish colour | Femoral and meniscal surface have reddish colour |
| **24** | Swelling/dehydration gone, no other change to surfaces (ICRS Grade 0) | Reddish appearance gone, no change to surfaces (ICRS Grade 0) | Reddish appearance gone, small scratch on medial tibial plateau (ICRS grade 1) |
| **48** | Cartilage lesions (Grade 1/2) on femoral condyle and tibial plateau in medial and lateral compartment | No change | No change |
| **72** | Progression of cartilage lesions on femoral condyles (Grade 2/3), and tibial plateau (Grade 3/4), damage and deformation to medial meniscus (ICRS Grade 2) | N/A | N/A |

#### 4.4.2.2 Kinetics and Kinematics

All knees followed the demand waveforms within ±5% of the maximum value for the majority of the walking gait cycle (Figure 4.2). All knees had an increased axial force compared to the demand between 0.025s - 0.05s and there were small deviations in the internal-external (tibial) rotation around 0.4s and 0.8s. Axial force outputs were slightly out of phase with the demand between 0s and 0.2s of the gait cycle for Prelim 1 during the first 24 hours; PID tuning was performed after the visual inspection and this corrected the issue. For axial force, the majority of discrepancies between knees occurred during swing phase (0.6s to 1.0s).

The shape and magnitude of anterior-posterior displacements (-2mm to -6mm) were similar for two knees at all time points (Figure 4.3). Prelim 1 initially had a similar shape and magnitude as the other two knees (-1mm to -6mm) however there was a posterior shift of the waveform during stance phase (0s to 0.6s) as the simulation progressed resulting in a much larger magnitude of displacement at 72 hours (3mm to -5.5mm). The anterior-posterior displacement value at 0 seconds of the gait cycle (initiation position) influenced anterior displacement during swing phase. A posterior initiation position increased anterior displacement as there was a larger distance for the tibial slider to travel before it contacted the anterior spring. However, initiation position did not influence the maximum anterior displacement (~5-6mm for all samples) due to the 5mm spring gap used.

The shape and magnitude of anterior-posterior shear force was similar for all knees throughout most of the gait cycle (Figure 4.3). During heel strike at later time points, Prelims 1 & 3 had noticeably increased shear force (-40N) compared to the other knee (-5N). There was increased shear force between 0.6 and 0.8 seconds of the gait cycle for all knees at 24 hours.

For all knees, the adduction-abduction initially oscillated from its value at 0 seconds of the gait cycle (initiation position) to a more adducted position, then adopted a fixed position as the simulations progressed (Figure 4.3). Prelim 1 adopted a valgus orientation (-1° to -2.5°) whereas the other knees adopted varus orientations (0.4° to 1.5°).

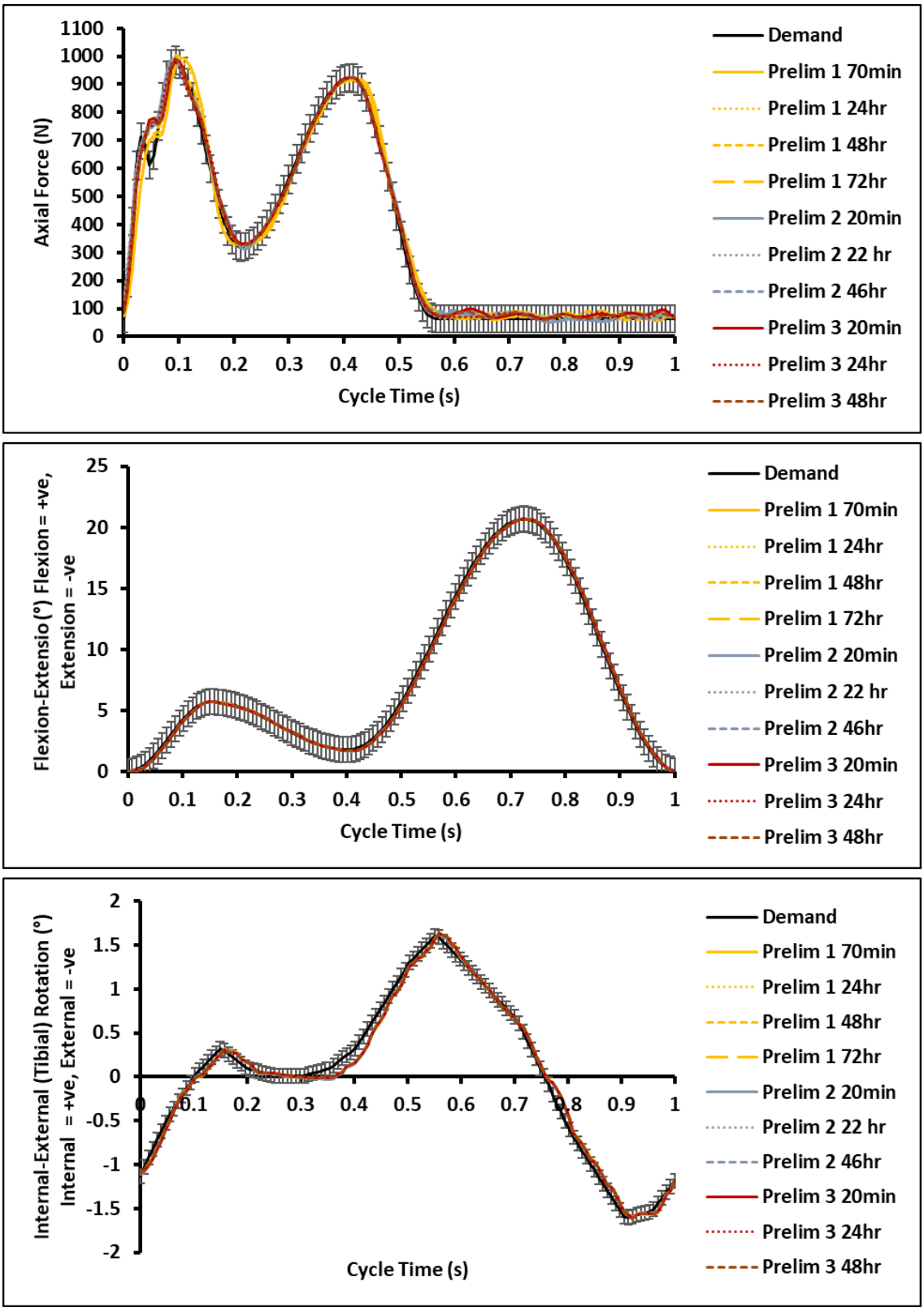


**Figure 4.2: Axial force (N), flexion-extension (°) and internal-external (tibial) rotation (°) demand following for preliminary knees during walking gait simulations (error bars = ±5% of maximum value for each axis).**

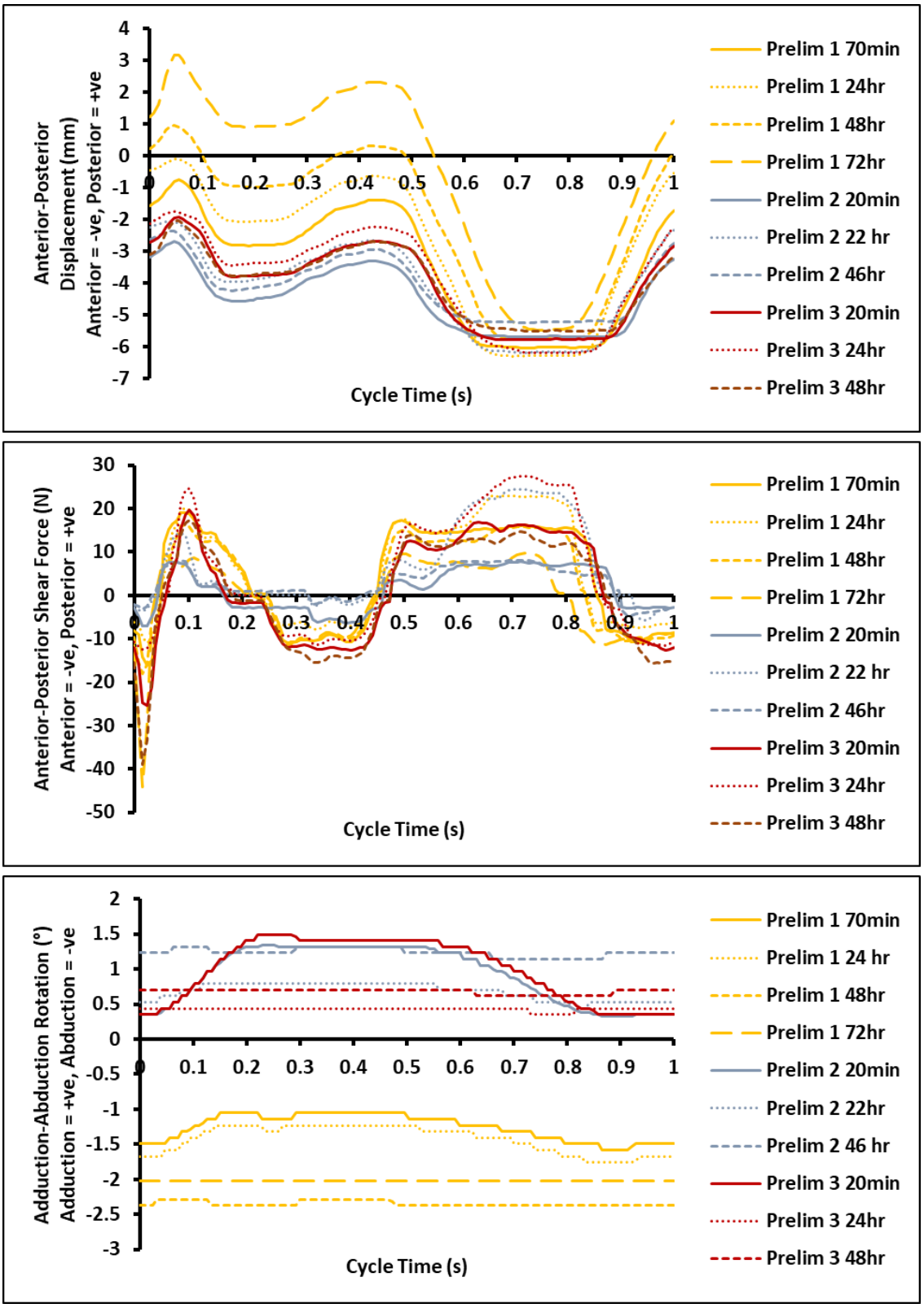


**Figure 4.3: Anterior-posterior displacement (mm), anterior-posterior shear force (N) and adduction-abduction rotation (°) for preliminary knees during walking gait simulations.**

#### 4.4.2.3 Summary of Preliminary Observations

Prelim 1 demonstrated it was possible to simulate a porcine knee joint and follow kinetic and kinematic demand waveforms without catastrophic failure (fracture/dislocation) during a 72-hour (259,200 cycle) walking gait simulation. However, there was extensive damage to femoral, tibial and meniscal surfaces. The pre-test assumption was improved congruency and maintenance of interstitial fluid pressurisation due to lack of cut edges would enable whole knee joints to be simulated for as-long-as or longer than the pin-on-plate samples in Chapter 3. Previous pin-on-plate experiments have shown multidirectional motion results in more damage/higher CoF than uniaxial sliding (Northwood and Fisher, 2007) (Cilingir, 2015). The driven tibial rotation and abduction-adduction rotation generated during the simulation may have caused greater damage to articulating surfaces despite the improved congruence of the contact. Small particles/debris were found stuck to the inside of the gaiter after the 72-hour simulation of Prelim 1. These were likely damaged pieces of tissue which detached from the joint during simulation or potentially microbial growth.

Whilst simulation inputs alone could have been responsible for the observed damage and debris/particles, there were several confounding factors which likely influenced these outcomes. Due to unforeseen circumstances, Prelim 1 was submerged in lubricant for 24 hours before simulation, and hence, whilst the knee experienced a 72-hour simulation, degradation actually occurred over 96-hours. This advanced state of degradation prior to simulation may have initiated premature damage during the simulation. When visually inspected pre-test, the posterior femoral condyles had an unusual appearance not observed during dissection; after 24 hours this had disappeared and was presumed to be dehydration/swelling of the tissue which occurred during the freezing process. However, these changes may have compromised mechanical properties of the tissue and contributed to the observed damage. Prelim 1 was frozen for ~11 months whereas pin-on-plate samples were frozen for ~3 months, therefore the duration between dissection and simulation may have been a contributing factor.

Wear, damage and deformation and microbial growth may limit simulation durations. Articulating surfaces damaged to the extent observed would not provide a representative environment in which to assess an early-stage knee intervention. Due to these issues, some alterations to the experimental design were made for Prelim 2 & 3 as follows:

1. Simulation duration was reduced from 72 hours to 48 hours. This was done for two reasons; firstly, to reduce the potential for tissue degradation and microbial growth to compromise the tribological functional evaluation, and secondly, to ensure there would be sufficient time to generate a minimum of n=3 samples during this and future experimental studies.

2. Sodium azide was added to the lubricant to retard microbial growth. This approach is commonly employed during *in vitro* investigation of total joint replacements, as recommended by ISO standards (BS ISO, 14243-1:2009+A1:2020) (BS ISO, 2014).

3. The PBS used in the lubricant for Prelim 1 was replaced with Ringer's Solution. Serum based lubricants containing PBS and Ringer's Solution can maintain cartilage surfaces for an extended duration (Chapter 3); Ringer's Solution was chosen as it was considered more physiologically relevant than PBS.

#### 4.4.2.4 Comparison of Prelim Knees 1-3

Prelim 2 and 3 followed demands and experienced no fracture or dislocation. In contrast to Prelim 1, there was very little evidence of any negative changes to the articulating surfaces of Prelim 2 and 3. Duration between freezing and simulating (~11months) was suggested as a possible contributing factor for the extent of wear, damage and deformation to Prelim 1; however, Prelim 2 (~26 months) and Prelim 3 (~14 months) were frozen longer and showed minimal damage in comparison. Prelim 2 and 3 adopted a varus orientation during simulations, whereas Prelim 1 was valgus, this could have been the natural position for Prelim 1; however, this was potentially due to suboptimal alignment of the joint during preparation and the valgus position may partly explain the observed disparity in damage (Orsi et al., 2016). The anterior-posterior displacement waveform for Prelim 1 drifted posteriorly as the simulation progressed, this could have been linked to the valgus orientation. Or alternatively, degradation of the tissue occurred due to the extended simulation duration (72 hours vs 48 hours) and extended time spent in lubricant (96 hours vs 48 hours), this may have compromised articulation and influenced the kinematics.

For Prelim 1 debris/particles were observed in the lubricant, this could have been due to removal of damaged tissue from the articulating surfaces; however, particles/debris were also found in the lubricant of Prelim 2 and 3 which experienced little damage. The debris could have been loose pieces of tissue from elsewhere on the joint which detached during the simulation or microbial growth. Loose tissue or microbial growth within the joint space could affect the tribology and/or disrupt kinematics resulting in damage to articulating surfaces. Sodium azide was added for Prelim 2 and 3, this appeared to reduce the level of particles/debris compared to Prelim 1 suggesting addition of sodium azide may have prevented some microbial growth. Alternatively there may have been more loose tissue for Prelim 1 due to more advanced degradation of the tissue.

## 4.5 Forty Eight Hour Walking Gait Simulation Study

### 4.5.1 Experimental Design

The Preliminary Study demonstrated the potential for porcine knees to complete 48-hour walking gait simulations. The focus of the following study was to assess the repeatability of the method, provide an enhanced analysis of the tissue degradation and assess the extent of microbial contamination, whilst also providing additional kinetic and kinematic data. The points listed below detail the additional experiment processes included for this study:

1. Previous pin-on-plate literature suggested sub-surface delamination of the superficial tangential layer of articular cartilage from the layers below due to fatigue failure was the predominant failure method for articular cartilage (Durney et al., 2020). The work also demonstrated sub-surface delamination could occur even if the surface appeared intact. Subsurface damage with absence of surface damage has also been observed during fatigue testing of articular cartilage (Mccormack and Mansour, 1998). Therefore, post-simulation histological analysis was included in the current study to assess if any structural changes had occurred due to the simulation, particularly the presence of sub-surface delamination.

2. In the current study, pre and post-test lubricant samples were filtered and cultured on agar plates for colony counting to assess the extent of microbial contamination within the lubricant. Post-test cartilage samples were placed into nutrient broths and cultured to determine which microbial species (aerobic/anaerobic) were present. Histological sections were viewed under a microscope to assess the presence of microbial growth or biofilm formation on the articulating surfaces.

3. During the Preliminary Study, the post-test condition of samples varied considerably. Therefore, the duration knee joints spent frozen between dissection and experimental use was minimised and kept consistent to try and ensure changes were due to simulation conditions and not variation in sample quality. All samples used during the enhanced analysis study experienced the experimental process within two weeks of dissection.

4. Sodium azide was added to lubricants for Prelim 2 and 3, however there was still evidence of potential microbial growth, to further mitigate microbial growth, fixtures in contact with the knee or lubricant were sterilised prior to simulation.

#### 4.5.1.1 Experimental Groups

Eight porcine knees were allocated into one of two experimental groups, a simulated group (n=4) and a non-simulated group (n=4). The simulated group were subjected to the same walking gait profile as the knees in the Preliminary Study. Non-simulated control knees (n=4) were positioned within the cementing jig and submerged in the lubricant; these were then placed into the back of the single station knee simulator and left there whilst the simulated knee was run. This enabled both simulated and non-simulated knees to experience similar environmental conditions to minimise differences between the experimental groups.

#### 4.5.1.2 Additional measures to minimise microbial growth

All fixtures in contact with the knee joints and lubricant during experiments were cleaned. The femoral and tibial pots, gaiters, anti-rotation screws and lubricant sample pots were all autoclaved at 121.5°C for 15 minutes then sprayed with ethanol prior to use. Gloves were worn throughout and hands sprayed with ethanol before touching any components.

#### 4.5.1.3 Preparation of samples for histological analysis

Osteochondral sections of the post-experiment medial femoral condyle and medial tibial plateau were removed from the contact regions of knee joints with a hacksaw and trimmed with a scalpel. For meniscal samples the medial meniscus was cut at the roots and a section of the contact region removed using a scalpel. A total of n=10 samples of each tissue were included as part of the analysis (n=4 non-simulated control knees, n=4 simulated knees and n=2 from the preliminary study). All samples were dissected from knee joints post-simulation except for those from Prelim 2, this knee was frozen post-simulation then defrosted at a later date to remove the samples, which were then re-frozen. Prior to sample removal, knees were left to recover for 90 minutes whilst still submerged in the lubricant. All samples were wrapped in PBS-soaked paper towels, sealed in plastic bags and stored frozen at -20°C. The medial compartment of the tibiofemoral joint was chosen for analysis as it experiences a larger proportion of the load travelling through the joint, hence wear damage and deformation may be more likely to occur in this compartment.

#### 4.5.1.4 Histological analysis of samples

To enable microscopic visualisation of tissue structures, samples were defrosted and subjected to histological processing. These were fixed in 10% neutral buffered formalin (NBF) for 48 hours then dehydrated and cleared using a tissue processor (Leica Biosystems TP1020) (Table 4.4). Upon completion, samples were removed from the tissue processor, embedded in paraffin wax and left to set on a cold plate. The wax blocks were then sectioned to a thickness of 6 μm using a microtome (Leica), placed onto glass slides (SuperFrost plus, Fisher) and stained with Haematoxylin & Eosin (H&E) to observe general tissue structure, Safranin-O + 0.01% Fast Green to assess GAG content and 0.1% Picrosirius Red to assess collagen fibre size and orientation using polarised light microscopy (Durney et al., 2020) (supplementary material). H&E-stained sections were also used to detect the formation of microbial growth articulating surfaces. Slides were imaged at x2.5 magnification using a light microscope (Zeiss), images were captured and assessed using microscopy imaging software (Zeiss Zen lite).

**Table 4.4: Tissue processor protocol used for dehydrating and clearing porcine osteochondral tissue samples.**

| Station Number | Contents | Time (hours & minutes) |
|---|---|---|
| **1** | 70% alcohol (ethanol) | 1 h |
| **2** | 90% alcohol (ethanol) | 1 h |
| **3** | 100% alcohol (ethanol) | 1 h 10 m |
| **4** | 100% alcohol (ethanol) | 1 h 10 m |
| **5** | 100% alcohol (ethanol) | 3 h 20 m |
| **6** | 100% alcohol (ethanol) | 4 h 20 m |
| **7** | Xylene | 1 h |
| **8** | Xylene | 1 h 30 m |
| **9** | Xylene | 2 h |
| **10** | Molten wax | 2 h 30 m |
| **11** | Molten wax | 2 h |
| | | Total 21 hours |

#### 4.5.1.5 Assessment of tissue microbial contamination

Post-experiment, articular cartilage samples were removed from the lateral femoral condyles of experimental knees (n=10, as explained above). These were wrapped in PBS-soaked paper towels, sealed in plastic bags and stored frozen at -20°C. To assess the presence of microbial species in the simulation environment the articular cartilage samples were cultured in nutrient broths. Samples were defrosted and bisected with a scalpel then one half was placed into a tryptone soya broth to assess the presence of aerobic bacteria and the other half was placed into a thioglcollate broth to assess the presence of anaerobic bacteria. Staphylococcus aureus and bacillus fragilis were placed into the tryptone soya and thiogylcollate broths respectively to act as positive controls for microbial growth. Negative controls consisted of a sample of each broth with nothing added. Broths were placed into an incubator at 37°C and left to culture for 14 days. The broths were photographed and checked via visual inspection after 2, 7 and 14 days to assess microbial growth.

#### 4.5.1.6 Assessment of lubricant microbial contamination

Pre (n=6) and post-experiment (n=2) lubricant samples (100ml) were taken, placed in sterile plastic containers and stored frozen at -20°C. Samples from Prelim 3 were included as part of the analysis. These were defrosted overnight in a cold room and vacuum filtered through filter paper (2 µm) using a Millipore valve system*. A fresh lubricant sample which had not been through the experimental process was spiked with staphylococcus aureus to act as a positive control with the pre-experiment samples acting as the negative controls. Filter papers were placed onto fresh blood agar plates and cultured in an incubator at 37°C. Filtration and plating was performed in a class II safety cabinet using aseptic technique to prevent environmental contamination. To assess the presence of microbial growth, agar plates were photographed and visually inspected every 24 hours for 10 days.

*All pre-experiment samples were successfully filtered; however it was not possible to filter any post-experiment samples, as the liquid could not be drawn through the filter. Filter papers which had been in contact with post-experiment samples on which filtering was attempted (Non-simulated Control Knee 1 and Prelim 3) were plated and included as part of the lubricant filtering analysis. For logistical reasons lubricants were made in batches, therefore in some cases, a single pre-experiment negative control sample represented the pre-experiment condition for two experimental samples; a breakdown of analysed samples can be seen in (Table 4.5).

**Table 4.5: Samples assessed during lubricant filtering.**

| **Pre-experiment Negative Controls** | **Associated Samples** |
|---|---|
| 1 | Simulated Knee 1 + Non-simulated Control Knee 1 |
| 2 | Non-simulated Control Knee 2 |
| 3 | Simulated Knee 2 + Non-simulated Control Knee 3 |
| 4 | Non-simulated Control Knee 4 |
| 5 | Simulated Knee 3 + Simulated Knee 4 |
| 6 | Prelim 3 |
| **Post-experiment Samples** | **Associated Samples** |
| 1 | Prelim 3 |
| 2 | Non-simulated Control Knee 1 |
| **Positive Control** | **Associated Samples** |
| 1 | Staphylococcus Aureus Spiked Lubricant |

## 4.5.2 Results of 48-hour knee simulation study

### *4.5.2.1* Visual inspection of the cartilage surfaces

Of the experimental samples used in the current study, three simulated knees and all non-simulated controls showed no obvious changes in the condition of the articulating surfaces at any time point (ICRS Grade 0). One sample (Simulated Knee 1) (Figure 4.4) had noticeable damage to the anterior aspect of the lateral femoral condyle at t=24 hours; this presented as a small deep lesion penetrating close to the subchondral bone (ICRS grade 3). When assessed at t=48 hours the lesion appeared similar in area but penetrated deeper into the femoral cartilage, exposing the subchondral bone (ICRS grade 4). Reciprocal damage was also observed on the anterior lateral tibial plateau; this presented as a shallow but obvious depression in cartilage surface (ICRS Grade 1).

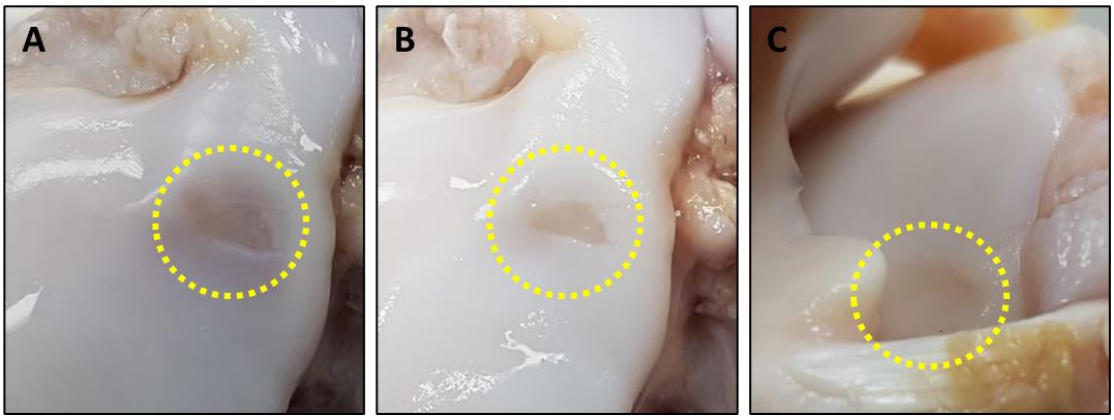


**Figure 4.4: Lesions observed in the anterior lateral femoral condyle of Simulated Knee 1 at t=24 hours (A) and t=48 hours (B). Depression observed in the anterior lateral tibial plateau of Simulated Knee 1 at t=48 hours (C).**

The same reddish appearance of the femoral and meniscal surfaces observed in the Preliminary Study was also observed at t=0 hours for half the knees in the current study; this was not present at later time points. For Non-simulated Control Knee 1 & 2 reddening of the condyles and trochlea grove was not observed at t=0 hours but was observed at t=24 hours; this had disappeared by t=48 hours. When removing the histological samples, it was noticed the subchondral bone of the non-simulated samples was red whilst the subchondral bone of the simulated samples was yellow.

#### 4.5.2.2 Histological Inspection of osteochondral samples for wear damage and deformation

Damage was observed histologically for both the simulated and non-simulated samples despite no evidence of changes when visually inspecting the articulating surfaces (Figure 4.5). There was significant variation in the extent and type of damage, delamination of the entire superficial tangential layer, small tears in the superficial tangential layer, large tears within the middle and deep layers, tears extending from the calcified cartilage to the surface and fracturing of cartilage fragments from the bulk material were all observed (Figure 4.6).

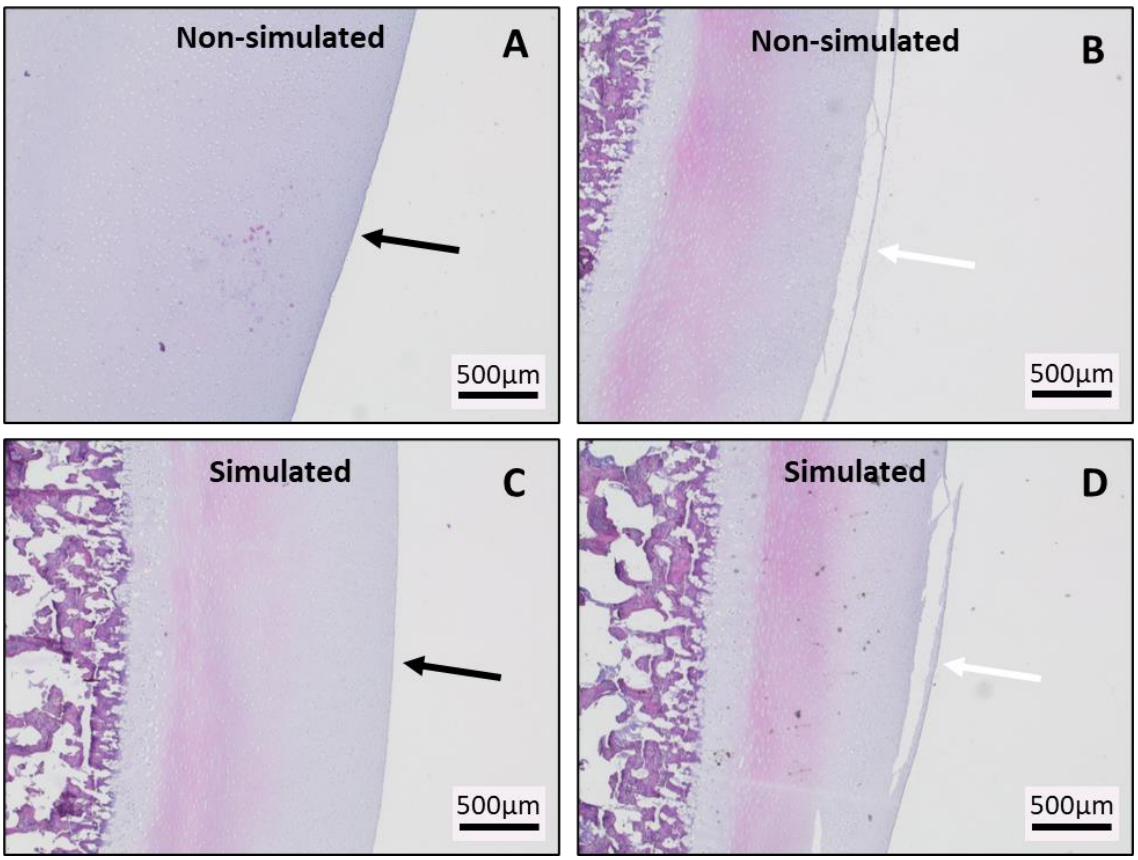


**Figure 4.5: Inconsistencies in the appearance of histological sections of medial femoral condyle for non-simulated (A and B) and simulated (C and D) knees stained with Haematoxylin & Eosin. Intact surfaces (black arrows) vs delamination of the superficial tangential zone (white arrows). Scale bar = 500µm.**

For individual samples, there was very little consistency in the condition of histological sections between the Haematoxylin & Eosin, Safranin-O and Picrosirius-Red stains despite all sections being cut from the same embedded sample block (Figure 6). Four out of ten knees showed an intact medial femoral condyle for all three stains, one showed an intact medial tibial plateau and four showed damage to both. No data were available for one knee (Simulated Knee 5) as it was not possible to section the sample.

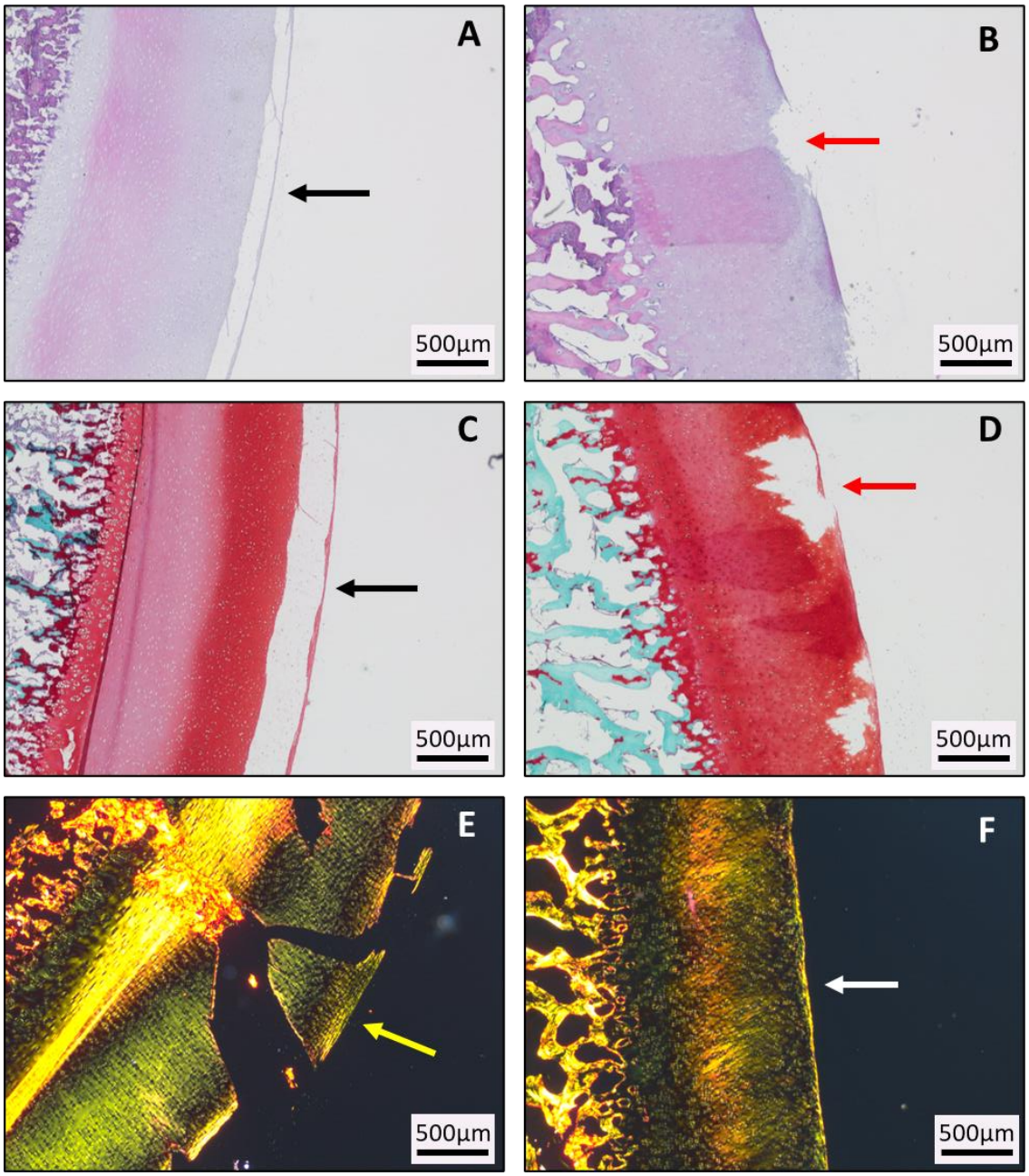


**Figure 4.6: Inconsistencies in the appearance of histological sections of medial femoral condyle (A, C, E) and tibial plateau (B, D, F) cut from the same sample. Delamination of superficial tangential layer (black arrows), potential wear (red arrows), fracture of cartilage from bulk material (yellow arrow) and intact surface (white arrow). Stained with Haematoxylin & Eosin (A & B), Safranin-O (C & D) and Picrosirius-Red (E & F). Picrosirius-Red sections imaged using polarised light filter. Scale bars = 500µm.**

#### 4.5.2.3 Kinetics and Kinematics

The 48-hour simulation knees experienced no dislocations or fracture whilst demonstrating the demand following within ±5% of maximum value (Figure 4.7).

Three knees produced similar shaped anterior-posterior displacement waveforms; the value at 0 seconds of the gait cycle (initiation position) varied between samples (-3mm to 1.5mm) (Figure 4.8). The anterior-posterior displacement waveform for Simulated Knee 1 had an unusual shape at 20 minutes and was initiating from a more anterior position (-5.25mm) than other knees. At later time points the waveform maintained an anterior initiation position (4.5mm) but reverted to the typical shape during stance phase; anterior translation during swing phase remained considerably reduced compared to other knees due to the 5mm spring gap used. There was a trend for the initiation position to move posteriorly at later time points when compared to 20 minutes.

The shape and magnitude of anterior-posterior shear force was similar for all knees at all time points (-25N to 40N), except for Simulated Knee 1 at 20 minutes which had an unusual shape and elevated shear force for the majority of the gait cycle (Figure 4.8). There was a trend for knees positioned anteriorly to have higher shear force than those positioned posteriorly.

For the adduction-abduction motion, all knees adopted slightly varus orientations (0° to 3.5°) these were either fixed or oscillating slightly (0.5° to 1.5°) from the initiation position to a more adducted position at different time points (Figure 4.8). The only exception was Simulated Knee 1 at 20 minutes, where large oscillations were observed (-3° to 5°).

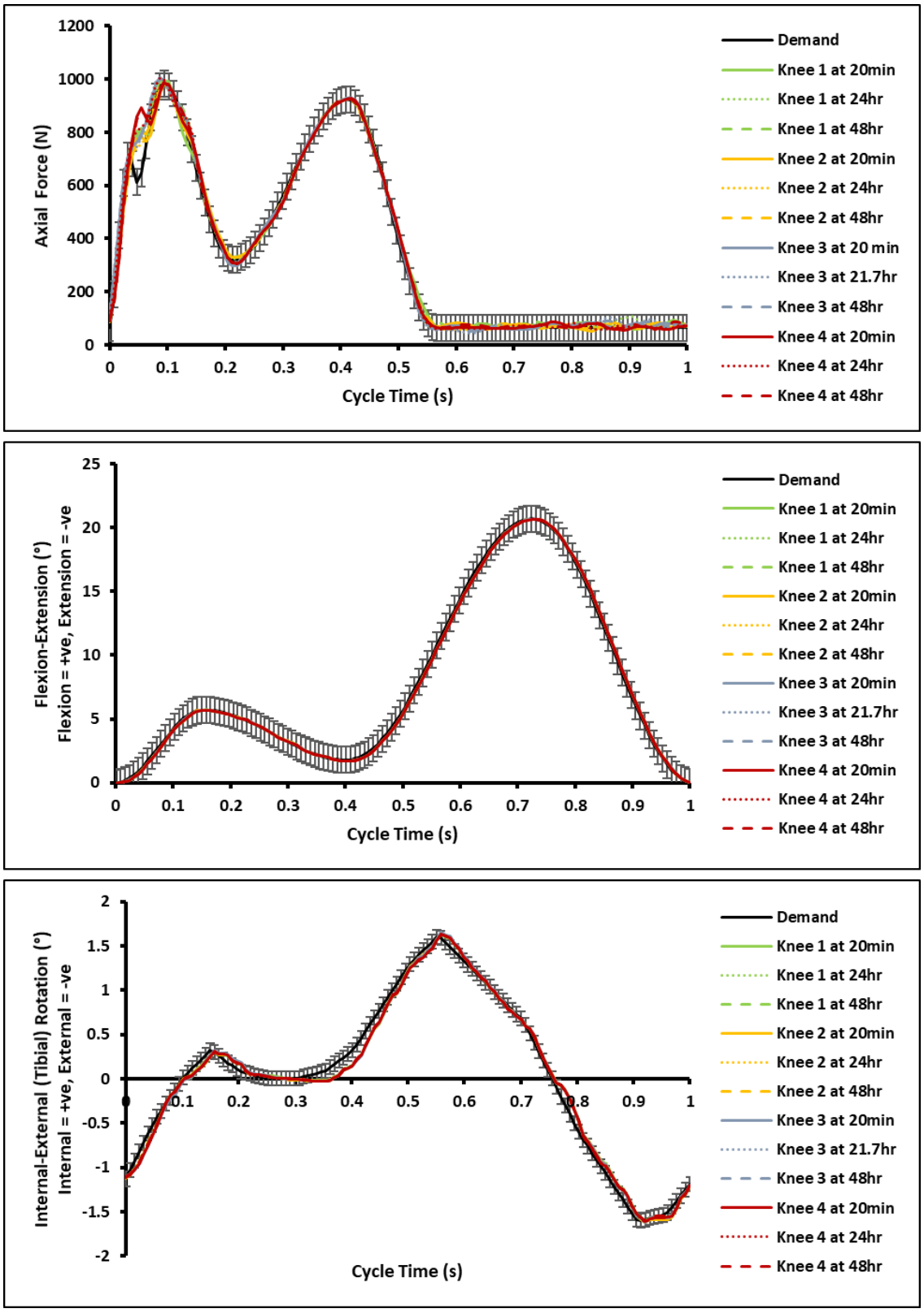


**Figure 4.7: Axial force (N), flexion-extension (°) and internal-external (tibial) rotation (°) demand following for preliminary knees during walking gait simulations (error bars = ±5% of maximum value for each axis).**

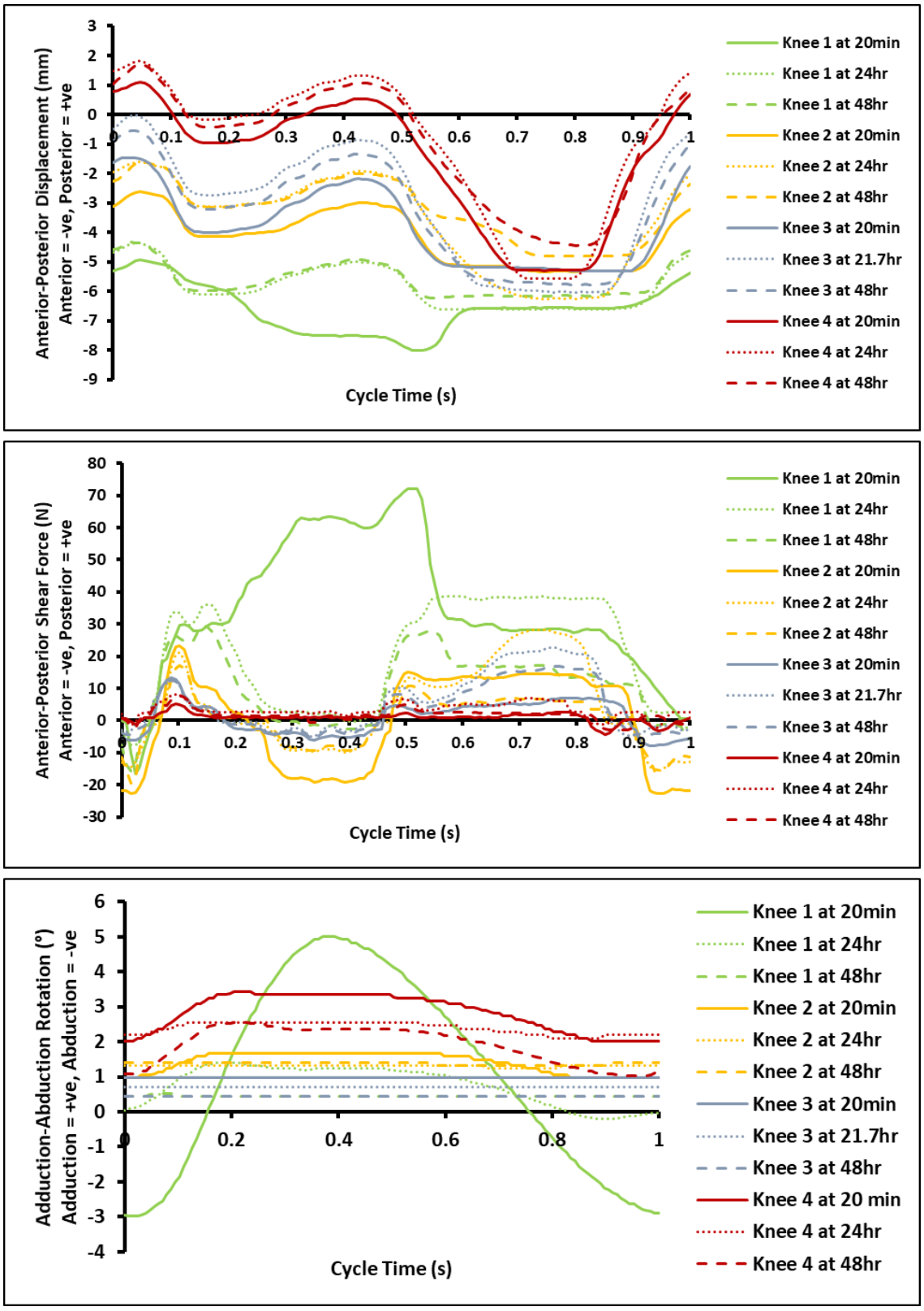


**Figure 4.8: Anterior-posterior displacement (mm), anterior-posterior shear force (N) and adduction-abduction rotation (°) for preliminary knees during walking gait simulations.**

#### 4.5.2.4 Histological inspection of cartilage surface to assess microbial/biofilm growth

No obvious microbial growth was observed on any of the histological sections.

#### 4.5.2.5 Analysis of lubricant

Pre-test lubricants were straw-coloured and translucent, post-test non-simulated control lubricants were orange-coloured and had become less translucent and post-test simulated lubricants were deep purple and opaque. After 24 hours in the incubator no microbial growth was observed for any of the pre-test control samples whereas microbial growth had occurred on both post-test samples and the positive control (Table 4.6). The extent of microbial growth varied for the post-test samples and the positive control (Figure 4.9).

**Table 4.6: Microbial growth for filtered lubricant samples, no microbial growth (green tick), microbial growth (red cross).**

| **Pre-test negative controls** | **24 hours** | **48 hours** | **72 hours** | **6 days** | **7 days** | **8 days** | **9 days** | **10 days** |
|---|---|---|---|---|---|---|---|---|
| Simulated Knee 1 + Non-simulated Control Knee 1 | ✓ | ✓ | ✗ | ✗ | ✗ | ✗ | ✗ | ✗ |
| Non-simulated Control Knee 2 | ✓ | ✓ | ✗ | ✗ | ✗ | ✗ | ✗ | ✗ |
| Simulated Knee 2 + Non-simulated Control Knee 3 | ✓ | ✓ | ✓ | ✓ | ✓ | ✓ | ✓ | ✓ |
| Non-simulated Control Knee 4 | ✓ | ✓ | ✓ | ✓ | ✓ | ✓ | ✓ | ✓ |
| Simulated Knee 3 + Simulated Knee 4 | ✓ | ✓ | ✓ | ✓ | ✓ | ✓ | ✓ | ✓ |
| Prelim 3 | ✓ | ✓ | ✓ | ✓ | ✓ | ✓ | ✓ | ✓ |
| **Post-test** | **24 hours** | **48 hours** | **72 hours** | **6 days** | **7 days** | **8 days** | **9 days** | **10 days** |
| Prelim 3 | ✗ | ✗ | ✗ | ✗ | ✗ | ✗ | ✗ | ✗ |
| Non-simulated Control Knee 1 | ✗ | ✗ | ✗ | ✗ | ✗ | ✗ | ✗ | ✗ |
| **Positive Control** | **24 hours** | **48 hours** | **72 hours** | **6 days** | **7 days** | **8 days** | **9 days** | **10 days** |
| Staphylococcus Aureus Spiked Positive Control | ✗ | ✗ | ✗ | ✗ | ✗ | ✗ | ✗ | ✗ |


**Figure 4.9: Agar-plated filter papers displaying evidence of microbial growth after 24 hours in the incubator for the two post-test samples and positive control.**

The extent of microbial growth observed for pre-test lubricants was much less than for post-test lubricants after 10 days (Figure 4.10).

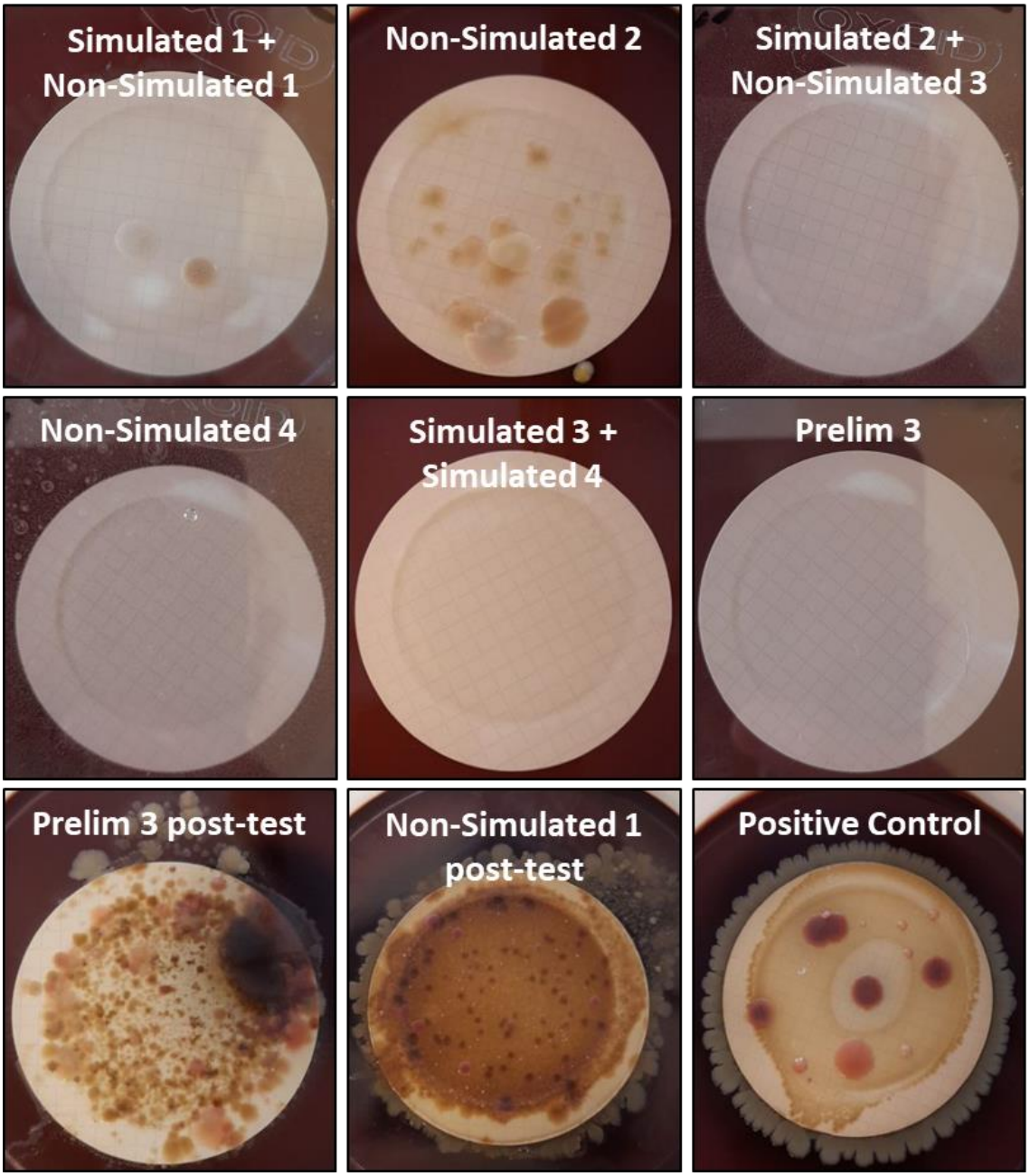


**Figure 4.10: Microbial growth of lubricant filters cultured on fresh blood agar following incubation for 10 days.**

### 4.5.2.6 Analysis of bacterial growth in broth cultures of tissue samples

After 48 hours in tryptone soya, 11 out of 12 broths were cloudy (Table 4.7), indicating growth of aerobic bacteria; the negative control remained clear after 14 days. After 7 days in thioglycollate, there was a white substance in 11 out of 13 broths, indicating

growth of anaerobic bacteria; the negative control and one other sample remained clear after 14 days.

**Table 4.7: Bacterial growth in nutrient broths, no bacterial growth (green tick), bacterial growth (red cross).**

| Sample | Tryptone Soya Broth | | | Thioglycollate Broth | | |
|---|---|---|---|---|---|---|
| | Day 2 | Day 7 | Day 14 | Day 2 | Day 7 | Day 14 |
| Non-simulated Control 1 | ✘ | ✘ | ✘ | ✘ | ✘ | ✘ |
| Non-simulated Control 2 | ✘ | ✘ | ✘ | ✘ | ✘ | ✘ |
| Non-simulated Control 3 | ✘ | ✘ | ✘ | ✘ | ✘ | ✘ |
| Non-simulated Control 4 | ✘ | ✘ | ✘ | ✓ | ✘ | ✘ |
| Simulated 1 | ✘ | ✘ | ✘ | ✓ | ✘ | ✘ |
| Simulated 2 | ✘ | ✘ | ✘ | ✘ | ✘ | ✘ |
| Simulated 3 | ✘ | ✘ | ✘ | ✓ | ✓ | ✓ |
| Simulated 4 | ✘ | ✘ | ✘ | ✘ | ✘ | ✘ |
| Prelim 2 | ✘ | ✘ | ✘ | ✓ | ✘ | ✘ |
| Prelim 3 | ✘ | ✘ | ✘ | ✓ | ✘ | ✘ |
| Positive Control | ✘ | ✘ | ✘ | ✘ | ✘ | ✘ |
| Negative Control | ✓ | ✓ | ✓ | ✓ | ✓ | ✓ |

## 4.6 Discussion

### 4.6.1 Kinetics and Kinematics

Results from the current study provide further evidence that porcine knee joints can follow demands and produce physiological outputs during 48-hour walking gait simulations without adverse effects. For most knees anterior-posterior displacement and anterior-posterior shear force outputs were similar to those observed previously in the University of Leeds porcine knee joint model (Bowland et al., 2018) (Liu et al., 2019); although Bowland *et al* used a different spring constraint. The initiation position of the anterior-posterior displacement and adduction-abduction waveforms varied between samples; this was most likely due to natural geometric variation or differences in the

accuracy of sample alignment. Only one knee experienced damage. For this knee, the shape of anterior-posterior displacement, adduction-abduction rotation and anterior-posterior shear force waveforms were different all having increased magnitudes compared to the other knees. When the simulation began the tibial slider on the simulator moved anteriorly, closing the 5mm spring gap, it then remained in this position for ~13,000 cycles. This more constrained position may have resulted in more sliding between articulating surfaces rather than the combined rolling and sliding motion of the natural knee (Masouros et al., 2010), which the simulation was intended to generate. This sliding motion, in combination with the suboptimal kinematics may have resulted in elevated shear force and created the chondral lesions observed on this sample; evidence in the literature suggests suboptimal kinematics are associated with cartilage injury (Andriacchi and Mündermann, 2006) (Chaudhari et al., 2008). Outputs typical of the other knee joints were observed after ~13,000 cycles, although the knee remained in an anterior position. This was potentially due to damaged regions wearing away until they no longer contacted enabling a more natural articulation. The most likely explanation for the anterior positioning was suboptimal alignment either due to natural variation of the tissue or experimental error during sample preparation.

### 4.6.2 Extended Simulation Duration

During normal daily activities there will be periods of motion and loading, and periods of rest during which tissues recover. The continuous motion of the knee simulation has limited physiological relevance. Whilst the migrating contact within the knee joint should maintain interstitial fluid pressurisation (Caligaris and Ateshian, 2008), running continuously may have impeded tissue recovery leading to a loss of fluid load support. The transfer of load to the solid cartilage phase, combined with the natural degradation of the tissue and extended simulation duration may have compromised the ability of articular cartilage to generate the desired rolling motion of the femur on the tibia and instead produced a higher friction sliding motion, resulting in wear, damage and deformation.

### 4.6.3 Histological Analysis

The histological analysis in this study was largely inconclusive. Delamination of the articular cartilage surfaces was observed for several samples despite a lack of damage being observed during visual inspection. Whilst subsurface cartilage damage has been observed in previous research where there appeared to be no surface damage

(Mccormack and Mansour, 1998) (Durney et al., 2020), this did not appear to be the case during the current study. Three stains were used for histological analysis, each stain was applied to two sections from the same osteochondral sample, giving a total of six sections per sample. There was no consistency between the damaged observed for the six sections from the same sample, some appeared healthy and intact whilst others showed extensive and varied damage. In addition, damage was observed for both simulated and non-simulated samples. There are several potential explanations for why this may have occurred. The extended duration of the simulation or length of time in the lubricant may have led to degeneration of the tissue. The AccuTrans silicone may have damaged the surfaces as the replicas were peeled off. The method of histological processing may not have been suitable for these tissues, leading to artefacts. Indeed, some embedded tissue blocks were difficult to get clean sections from whilst other blocks could not produce sections at all. All these factors need to be assessed to determine the cause of the damage observed.

### 4.6.4 Microbial growth within the simulation environment

Some pre-test lubricant samples showed evidence of microbial growth and others did not; this demonstrated cleaning techniques employed to minimise bacterial contamination when preparing lubricant samples were not 100% effective. Whilst it was not possible to properly filter post-test lubricant samples, this analysis did provide some insight. Both post-test samples, one simulated and one non-simulated, experienced a similar level of microbial growth, therefore additional measures to minimise microbial growth were not effective. Microbial growth may result in biofilm formation, which has been shown to reduce friction of articulating surfaces (Souza et al., 2010) (Taylor, 2012). This may have provided a protective effect to the cartilage surfaces, although no evidence of biofilm formation was observed on surfaces of imaged histological sections. Previous research has demonstrated biofilm presence in tissue fluid (Stoodley et al., 2008) (Dastgheyb et al., 2015) and therefore their presence within the lubricant and potential to influence tribology could not be ruled out.

Dissection and lubricant mixing processes were not carried out in a sterile environment; therefore it is unsurprising microbial growth occurred during the experiment. In addition, sodium azide is only capable of inhibiting the growth of gram-negative bacteria, hence there was still the potential for gram-positive bacteria to grow. These issues may be preventable if sterile dissection and antibiotics were incorporated into the lubricant. Previous research has demonstrated the potential for this approach when using a porcine acetabulum in a hemiarthroplasty study (Taylor, 2012). Antibiotics were not

included during the current study due to the large volume required and associated cost and also concerns surrounding antibiotic resistance. The influence of sodium azide on natural tissue also needs to be assessed as it has been shown to cause degenerative changes in porcine cartilage (Schiller et al., 1995). Whilst microbial contamination was present in the simulations, the lack of biofilm on cartilage surface indicates minimal influence of microbial growth on simulation outputs and tissue behaviour. Therefore, the current lubricant composition and clean simulator set-up procedure was appropriate when conducting 48-hour simulations of natural porcine knees.

### 4.6.5 Issues with blood in the lubricant

Several samples had reddening of menisci or femoral condyles at t=0 hours, this is most likely explained by blood leaking into the joint space. The femoral condyles of two non-simulated controls became reddened at t=24 hours despite this not being present at t=0 hours. However, as with samples with a reddened appearance at t=0 hours, the reddened appearance disappeared at t=48 hours, and hence, was also likely due to leakage of blood into the joint space. Once lubricants were removed to enable visual inspection of surfaces at t=24 hours the blood in the joint compartment may have escaped and the residual blood on the surface was washed out when the lubricant was returned post visual inspection.

It was not possible to filter post-test lubricant samples for any knees (although the filter paper which had been in contact with the Prelim 3 post-test ample was included). When fixing joint alignment during sample preparation, holes were drilled to attach braces to the sides of the knee. Once cemented in the desired alignment, braces were removed leaving screw holes exposed. During simulations serum changed from straw-coloured pre-test to a deep purplish colour post-test, it would appear blood was squeezed from the holes and into the lubricant during simulation. The fact lubricants from non-simulated controls were orange and could be partially filtered, indicated blood was probably the cause. In addition, the subchondral bone of histological samples was red for non-simulated controls but yellow for simulated knees, providing further evidence blood had been squeezed from the samples. The presence of blood within the lubricant may have influenced the tribology within the system.

#### 4.6.5.1 Limitations of Porcine Joint Model

There are several issues which limit the clinical relevance of the porcine joint approach. Kinetic and kinematic simulation inputs need to be scaled down to prevent joint damage. The immature porcine tissue used during the current study may have inherent differences in mechanical properties compared to human tissue which could influence outcomes. Differences in range of motion between pigs and humans limits the potential activities which can be simulated.

## 4.7 Conclusions

- It was possible to run porcine knee joints for 48-hour walking gait simulations without any major adverse events (fracture, dislocation) whilst maintaining physiological kinetic and kinematic outputs (anterior-posterior displacement, anterior-posterior shear force, adduction-abduction rotation). Demand waveforms were followed within ±5% of the maximum value for each axis for the majority of the gait cycle with only minor deviations.

- Minimal wear, damage and deformation were observed to the articulating surfaces of most porcine knees after 48-hour walking-gait simulations. The damage observed to one knee was likely due to a slight misalignment during the dissection and cementing process.

- It was not possible to draw a definitive conclusion regarding the influence of the extended duration walking gait simulations on subsurface damage (delamination of superficial tangential zone). This was due to considerable variation in changes observed between different histological sections from the same sample and between the simulated and non-simulated control groups.

- Several sources were identified which may explain the variation in damage observed (AccuTrans silicone replica making process, 25% new-born calf serum in Ringer's Solution lubricant, extended duration of the simulation, histological processing); these will be investigated in the following chapter to determine their influence on the articulating surfaces.

- Analysis of articular cartilage samples and pre- and post-experiment lubricant samples revealed there was microbial growth present within simulation environment, this may interfere with the tribology within the knee joint.

- No obvious microbial/biofilm growth was observed on the surface of any histological samples during histological analysis. Therefore this issue is unlikely to influence the tribological behaviour of the articulating cartilage surfaces during 48-hour simulations.

# Chapter 5

# The influence of Lubricant and AccuTrans silicone replica technique on the structural integrity of porcine cartilage surfaces

## 5.1 Introduction

Light microscopy of histological sections from the 48-hour study (Chapter 4) showed damage to the articular cartilage of both simulated porcine knee joints and non-simulated control joints for some samples. Different types of damage were observed, including delamination of the superficial tangential layer from the surface (Figure 5.1) and fractures which penetrated deep into the cartilage (Figure 5.2). Other samples, which experienced the same experimental conditions, appeared undamaged with smooth intact surfaces (Figure 5.3). Damage in the simulated group could be attributed to forces and motions experienced during extended duration simulations, however, this did not explain damage to non-simulated controls.

Three potential sources for the unexpected damage were identified:

- Leaving the non-living cartilage in a lubricant for an extended duration
- The method used to create replica moulds of the articulating surfaces
- Post-test histological processing

The knees were submerged in a 25% NBCS in Ringer's Solution + 0.03% sodium azide lubricant for 48 hours; over this extended duration natural degradation of the tissue, or interaction of the lubricant with the tissue may have caused degradation to occur. AccuTrans silicone was applied to the samples, left to set, then peeled off to create a replica moulds of the articulating surfaces. This method has been used previously during tribological studies of porcine meniscus (Bowland et al., 2018) and porcine articular cartilage (Cowie et al., 2021) and has shown to be highly accurate at replicating surfaces. However, these were short-term studies (≤3 hours) compared to the 48-hour study; the effects of the AccuTrans replica making process on cartilage which may have experienced degradation over a longer time-period remain unknown. There is the

potential the uppermost layers of the articular surface may have been removed from the cartilage layers beneath as the replicas were peeled off, thus compromising the efficacy of the method. Finally, there was the potential for artefacts to have occurred at various stages during histological processing of the samples; the images produced may therefore not have been representative of the post-test condition.

The three factors mentioned may have acted individually, or in combination, to produce the damage observed. To ensure differences between simulated and non-simulated samples were due to the experimental simulation process, and AccuTrans remained a valid method for replicating articular surfaces over a 48-hour duration, the influence of these potential confounding factors had to be determined.

As previously highlighted in Chapter 4, microbial growth/biofilm formation on cartilage surfaces has the ability to influence their tribological behaviour. This could potentially have affected how the AccuTrans silicone interacted with the cartilage surfaces. Therefore, the presence of microbial growth/biofilm formation on cartilage surfaces also needed to be assessed.

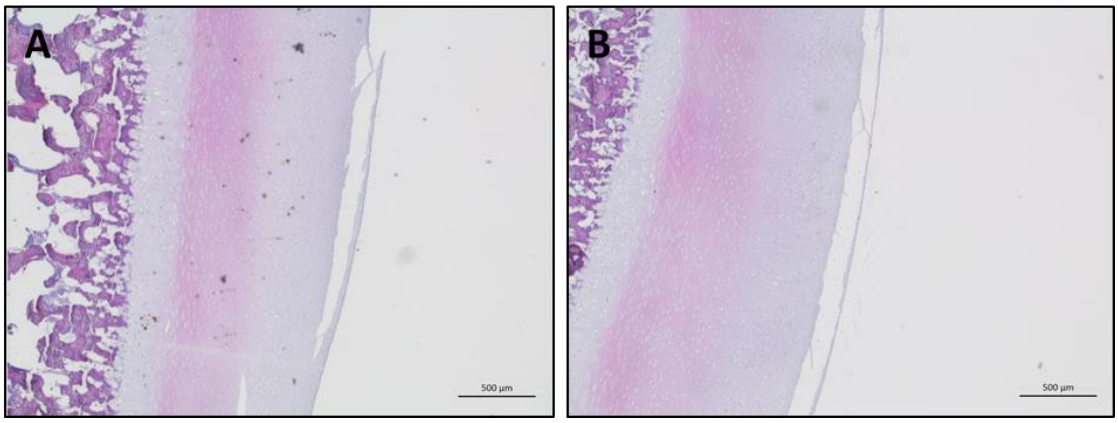


**Figure 5.1: Delamination of the superficial tangential layer of H&E-stained sections of articular hyaline cartilage from the medial femoral condyle of a knee joint which experienced a 48-hour walking gait cycle in the single station knee simulator (A), and a non-simulated control knee joint (B). Scale bar = 500μm.**

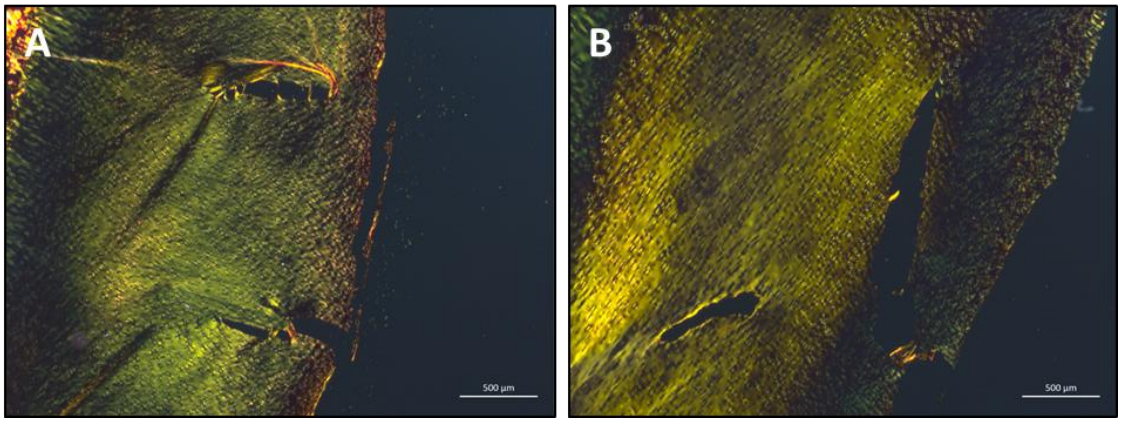


**Figure 5.2: Fractures penetrating deep into the cartilage of Sirius Red-stained sections of articular hyaline cartilage from the medial femoral condyle of a knee joint which experienced a 48-hour walking gait cycle in the single station knee simulator (A), and a non-simulated control knee joint (B). Scale bar = 500μm. During Chapter 4 samples were stained with three different stains, the Sirius Red images above were chosen instead of H&E as the damage was not observed in the H&E-stained sections for these samples.**

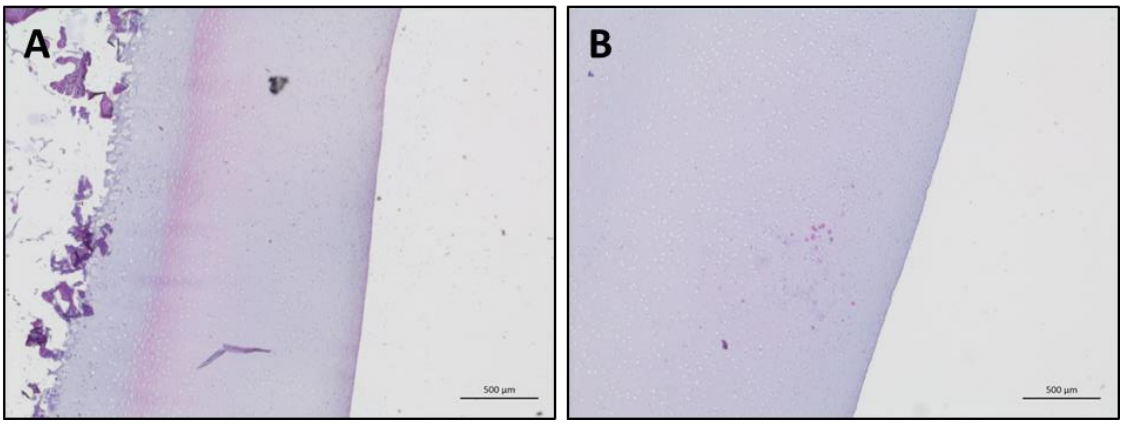


**Figure 5.3: Smooth intact surfaces of H&E-stained sections of articular hyaline cartilage from the medial femoral condyle of a knee joint which experienced a 48-hour walking gait cycle in the single station knee simulator (A), and a non-simulated control knee joint (B). Scale bar = 500μm.**

## 5.2 Aim and Objectives

### 5.2.1 Aim:

- To assess if aspects of the experimental design were responsible for the damage observed to cartilage surfaces during the 48-hour extended duration knee simulations

### 5.2.2 Objectives:

- Use histology to visualise porcine osteochondral samples and assess if there were changes in the articular cartilage surfaces due to:
    - The histological processing
    - Removal of the surface during the AccuTrans replica making process
    - Degradation of the surfaces due to being submerged in lubricant for 48 hours
    - A combination of the AccuTrans and lubricant

- Use histology to visualise porcine osteochondral samples and assess if there was microbial growth on the surfaces which could influence the tribological behaviour of the cartilage during simulations

## 5.3 Experimental Design

### 5.3.1 Preparation of experimental samples

The distal ends of porcine femurs were dissected from porcine legs and all the soft tissue removed. The femurs were clamped into a table mounted vice (Figure 5.4) and the femoral condyles removed using a hacksaw; each condyle was then cut into four using the hack saw to create n=12 femoral condyle samples. Each sample was visually inspected to ensure there was no obvious wear, damage or deformation present. A sample from each of the three femurs was then allocated into one of four experimental groups (Table 5.1) to ensure differences observed were due to experimental conditions and not variation between the porcine tissue from different pigs.

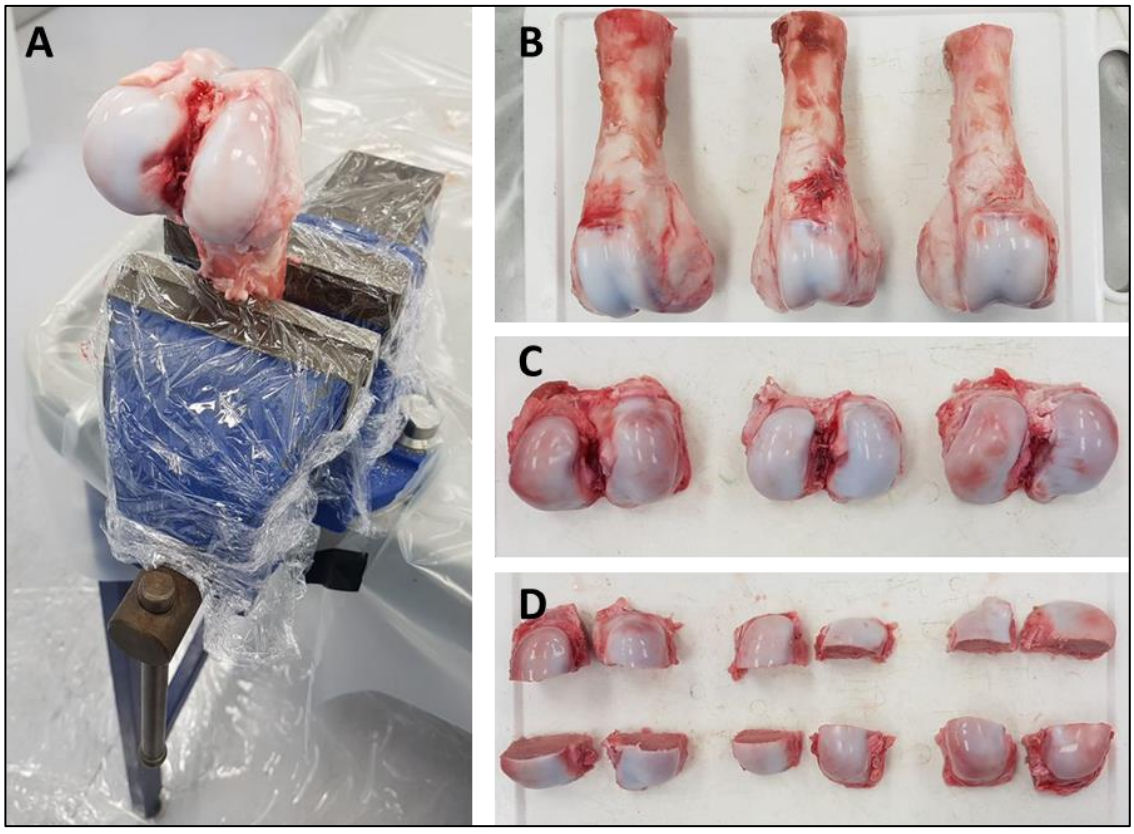


**Figure 5.4: Stages of sample preparation process. Distal femur clamped into table mounted vice (A), distal femurs (B), femoral condyles removed from distal femur (C), femoral condyles divided into experimental samples (D).**

**Table 5.1: Experimental groups.**

| Experimental group | Sample number | Time of sample harvest |
|---|---|---|
| Native | n=3 | t=0 hours |
| Native + AccuTrans | n=3 | t=0 hours |
| Native + Lubricant (25% NBCS in Ringer's Solution + 0.03% sodium azide) | n=3 | t=48 hours |
| Native + Lubricant (25% NBCS in Ringer's Solution + 0.03% sodium azide) + AccuTrans | n=3 | t=48 hours |

### 5.3.2 Experimental Conditions

The Native group experienced no experimental conditions and acted as a negative control to determine the initial condition of porcine knee joints post-dissection. The Native + AccuTrans group had replicas of the articular surfaces made at t=0 hours, these were used to determine the influence of the AccuTrans silicone. The Native + Lubricant group were fully submerged in 100ml of 25% NBCS in Ringer's Solution + 0.03% sodium azide lubricant for 48 hours, these were used to determine the influence of the lubricant. The Native + Lubricant + Accutrans group were submerged in 100ml of 25% NBCS in Ringer's Solution + 0.03% sodium azide lubricant for 48 hours; replicas were made at t=0 hours (prior to being placed in the lubricant), t=24 hours and t=48 hours. This group was used to determine the combined influence of the lubricant and the AccuTrans, as experienced by the knee joints during the 48-hour knee simulator study. Both lubricant groups were left in the back of the single station knee simulator to experience the same environmental conditions as the non-simulated control knee joints during the 48-hour knee simulator study. All lubricant samples were visually assessed for any changes to the cartilage surface at t=24 hours and t=48 hours. Histological samples were harvested from each experimental group at the appropriate time point (Table 5.1) using an surgical osteochondral grafting kit.

### 5.3.3 Preparation of histological samples

To remove osteochondral histological samples an 8.5mm diameter Smith and Nephew Accufex™ Mosaicplasty surgical kit was used (Figure 5.5). The coring tool was pressed into the articular surface by hand and hit with a mallet, the handle was then placed

through the coring tool and wiggled from side-to-side to snap the graft at the level of the subchondral bone. The tamp tool was then inserted through the centre of the coring tool and pressure applied to eject the sample; a small amount of paper towel was wedged into the coring before inserting the tamp tool to protect the cartilage surface. Once removed, the subchondral bone was trimmed with a scalpel to leave as little bone as possible without damaging the cartilage. This was done to minimise the time required for the decalcification stage of the histological processing which is directly influenced by bone volume. Each sample was then bisected with a scalpel blade (Figure 5.5), wrapped in PBS-soaked paper towels and stored frozen at -20°C.

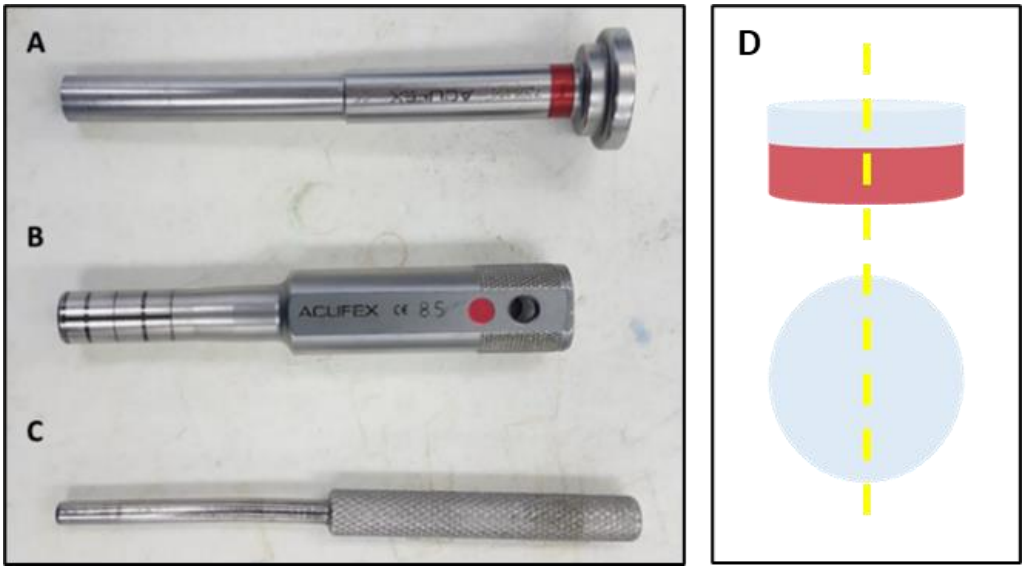


**Figure 5.5: Smith and Nephew Accufex™ Mosaicplasty surgical kit used to remove histological samples from sections of porcine femoral condyle. A) Tamp for removing grafts from coring tool (A), 8.5mm coring tool (B), handle to insert through coring tool to enable osteochondral samples to be snapped at the base (C). Bisection of osteochondral samples for histological processing (D).**

To enable imaging, samples were defrosted and subjected to histological processing. These were fixed in 10% neutral buffered formalin (NBF) for 48 hours then decalcified in 12.5 % (w/v) ethylenediaminetetraacetic acid (EDTA) for ~2 weeks. Decalcification involved submerging samples in EDTA and mechanically agitating them in an incubated shaker (150 rpm, 56°C). A ratio of 20:1, EDTA to bone volume was used and the EDTA was changed every 1-2 days to prevent the solution becoming saturated. Samples were dehydrated and cleared using a tissue processor (Leica Microsystems); the protocol used can be seen in (Table 5.2). Upon completion, samples were removed from the

tissue processor, embedded in paraffin wax and left to set on a cold plate. The wax blocks were then sectioned to a thickness of 6 μm using a microtome (Leica Microsystems), placed onto glass slides and stained with Haematoxylin & Eosin (H&E); each slide contained three sections of the same sample. Slides were imaged at x20 magnification using a slide scanner (Axioscan Z1, Zeiss) then visually assessed for microscopic changes to the cartilage tissue structure and compared using microscopy imaging software (Zeiss Zen lite).

**Table 5.2: Tissue processor protocol used for dehydrating and clearing porcine osteochondral tissue samples during current study.**

| Station Number | Contents | Time (hours & minutes) |
|---|---|---|
| **1** | 70% alcohol (ethanol) | 1 h |
| **2** | 90% alcohol (ethanol) | 1 h |
| **3** | 100% alcohol (ethanol) | 1 h 10 m |
| **4** | 100% alcohol (ethanol) | 1 h 10 m |
| **5** | 100% alcohol (ethanol) | 3 h 20 m |
| **6** | 100% alcohol (ethanol) | 4 h 20 m |
| **7** | Xylene | 1 h |
| **8** | Xylene | 1 h 30 m |
| **9** | Xylene | 2 h |
| **10** | Molten wax | 2 h 30 m |
| **11** | Molten wax | 2 h |
| | | Total 21 hours |

## 5.4 Results

No obvious change in the cartilage surface was observed for any of the experimental samples at t=0 hours or for any of the lubricant samples at t=24 hours or t=48 hours during visual inspection of the articular cartilage surfaces. There was no evidence of any obvious microbial growth on the surfaces based on the histological images.

The H&E-stained histological sections from the experimental groups (Figure 5.6) did not show any evidence of the large-scale delamination of the superficial tangential zone or

fracture penetrating deep into the cartilage which was observed during the 48-hour knee simulator study (Figure 5.1) (Figure 5.2).

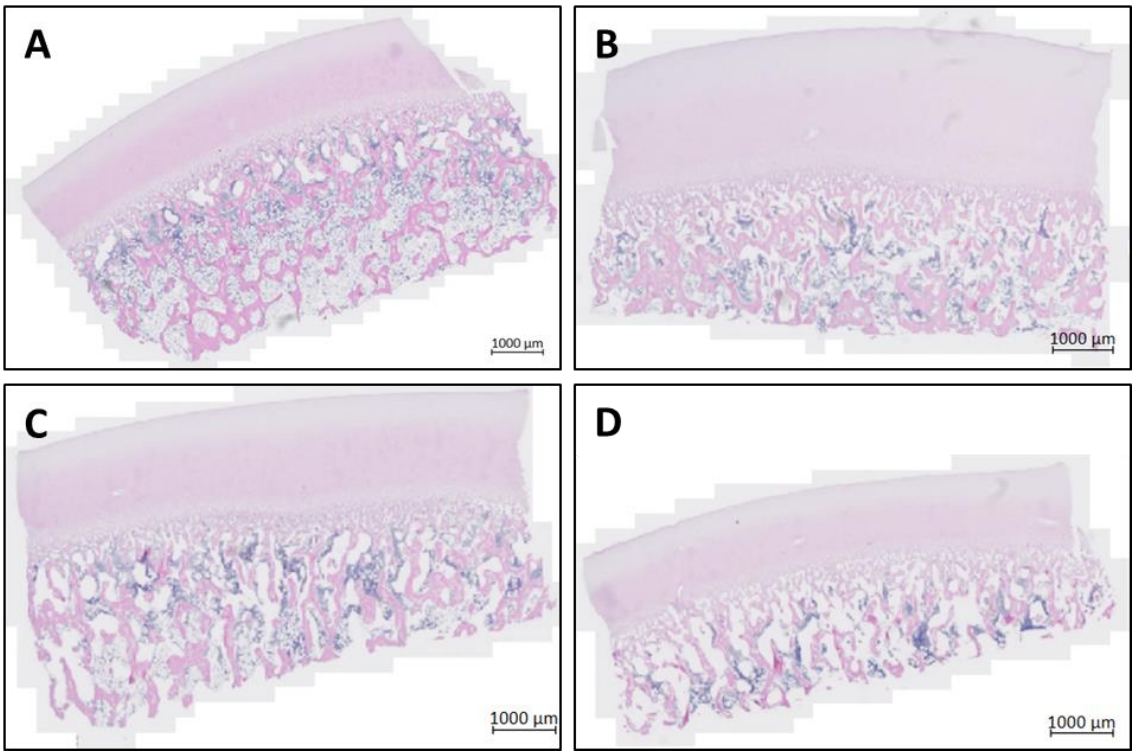


**Figure 5.6: Representative H&E-stained sections of the osteochondral samples from the four experimental groups: native (A), native + lubricant (B), native + AccuTrans (C) and native + lubricant + AccuTrans (D). No evidence of large-scale delamination of superficial tangential layer of articular hyaline cartilage was observed in any group. Scale bar = 1000µm.**

When analysing higher magnification images of the cartilage surfaces, there was no obvious damage to of any of the samples, although minimal differences in the appearance of the cartilage surfaces were observed. This variation was seen across all four groups (Figure 5.7) (Figure 5.8) (Figure 5.9) (Figure 5.10) and presented in three forms: a smooth surface, a surface with many small undulations and a surface with fewer large undulations. Small surface tears were present in two samples, one in the Native group and one in the Native + AccuTrans group.

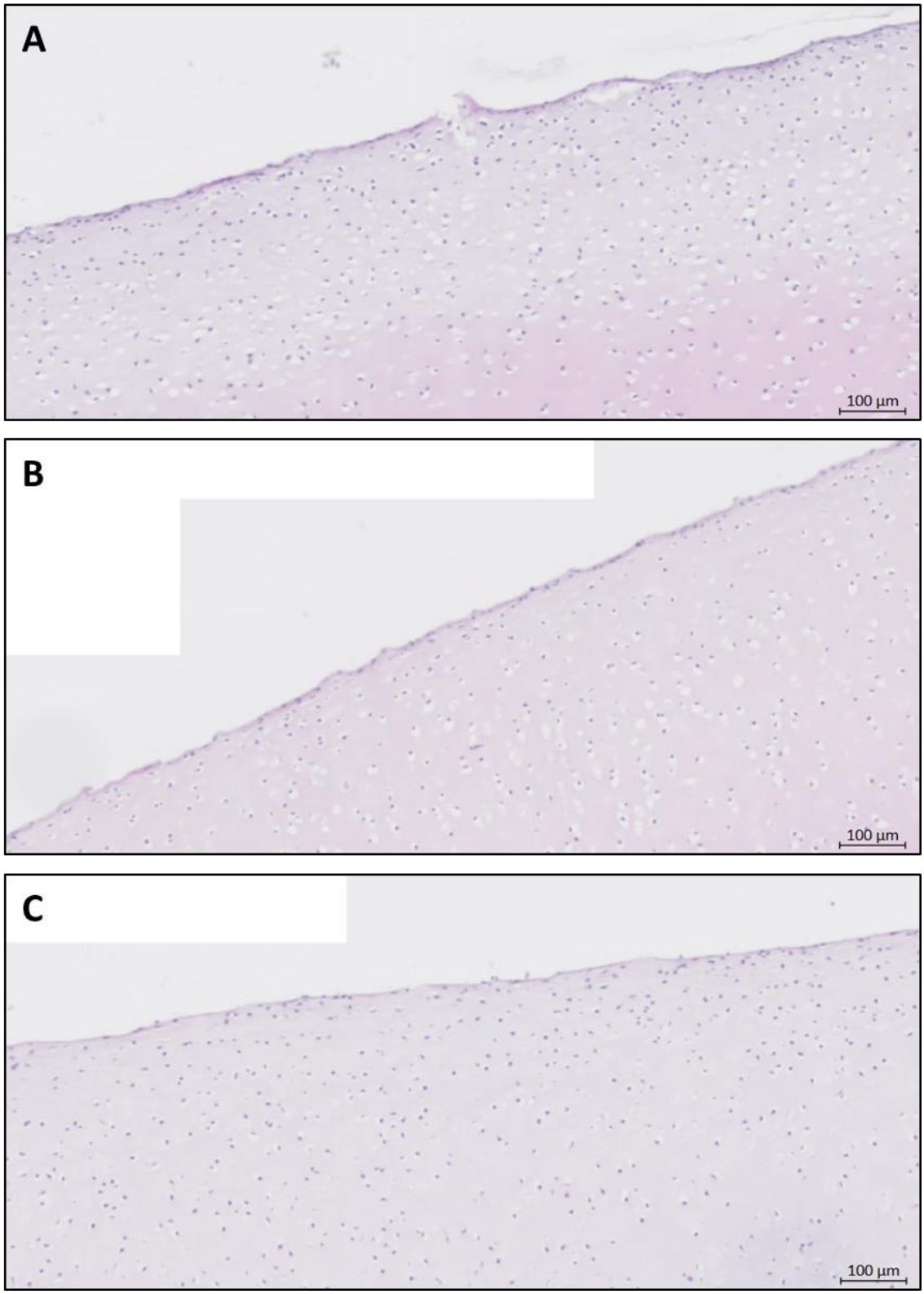


**Figure 5.7: H&E-stained sections from the Native control group: sample 1 - small tears in the surface with many small undulations (A), sample 2 - intact smooth surface (B) sample 3 - intact surface with fewer large undulations (C). Scale bar = 100µm.**

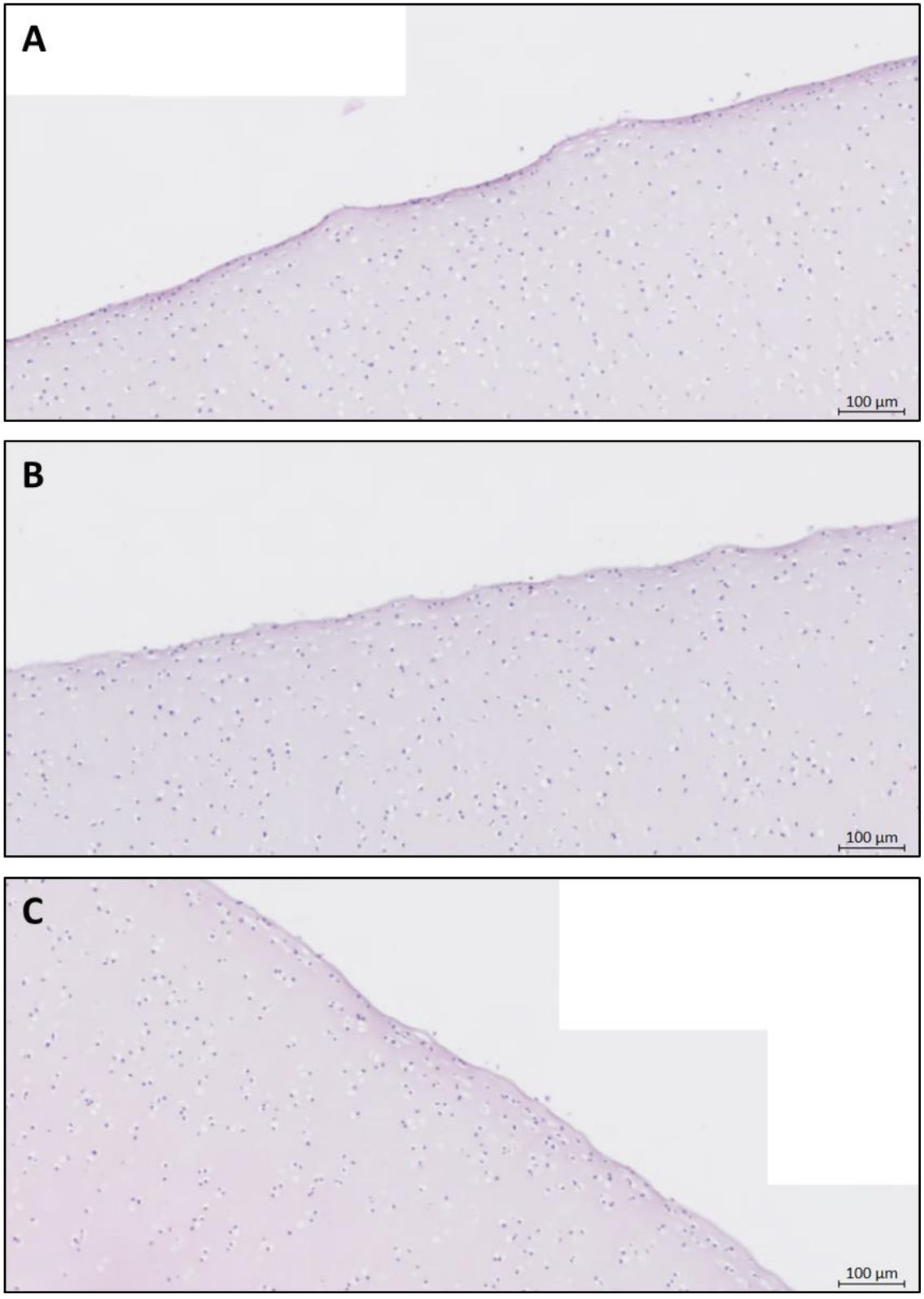


**Figure 5.8: H&E-stained sections from the Native + Lubricant group: sample 1 - intact surface with fewer large undulations (A), sample 2 - intact surface with many small undulations (B) sample 3 - intact surface with fewer larger undulations (C). Scale bar = 100µm.**

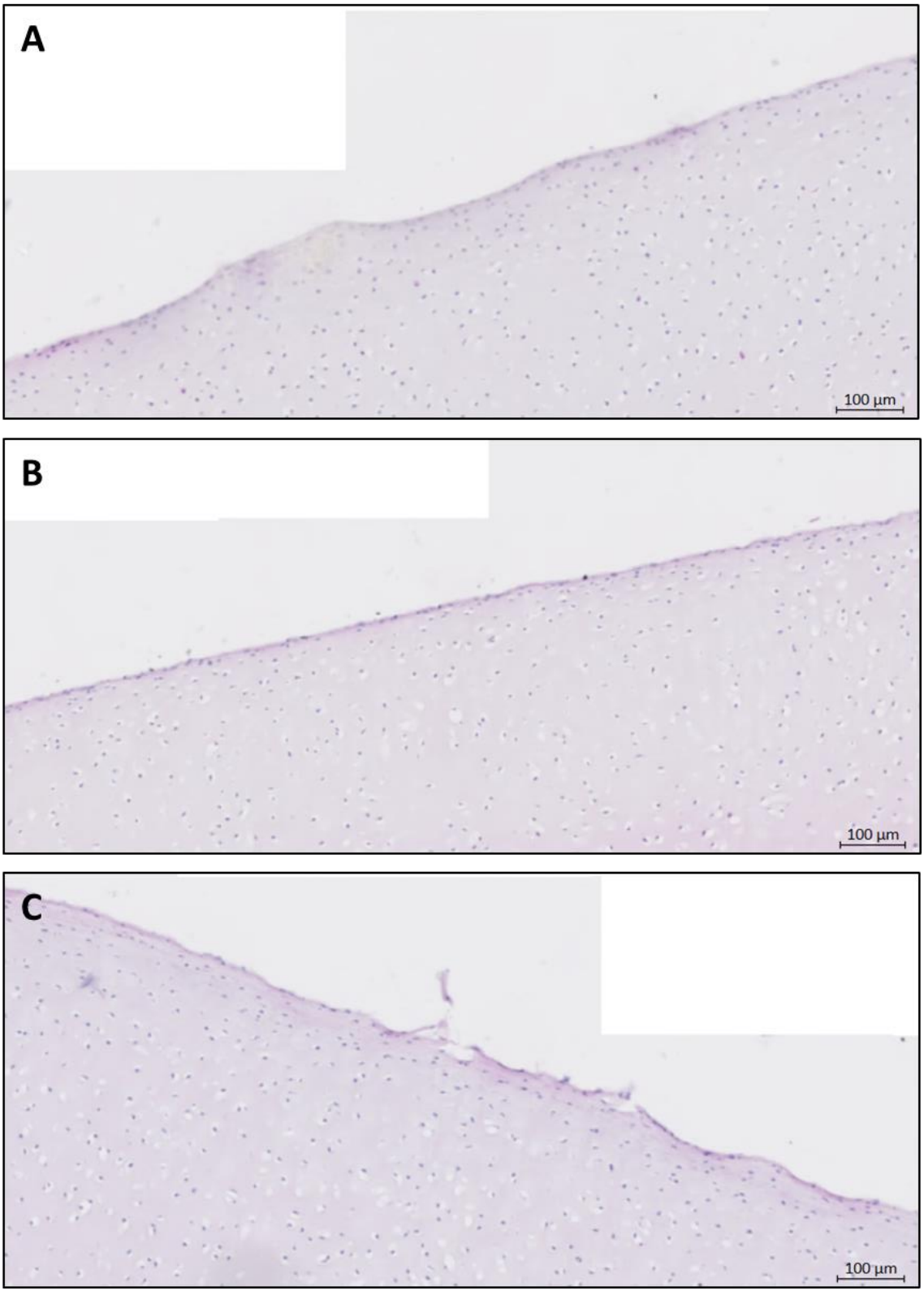


**Figure 5.9: H&E-stained sections from the Native + AccuTrans group: sample 1 – intact surface with some larger undulations (A), sample 2 - intact smooth surface (B) sample 3 – small tears in the surface with many small undulations (C). Scale bar = 100µm.**

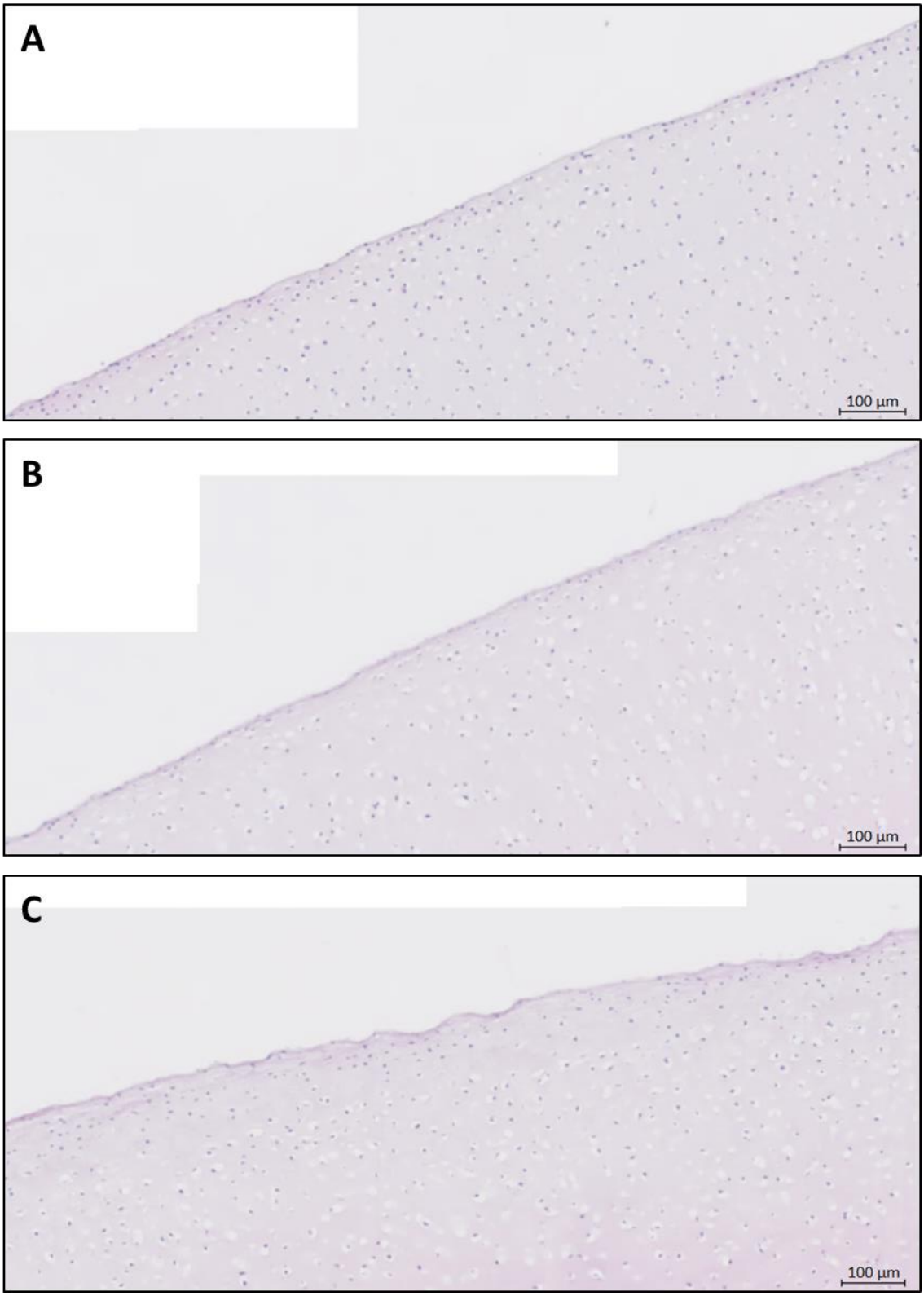


**Figure 5.10: H&E-stained sections from the Native + Lubricant + AccuTrans sample 1 - intact smooth surface (A), sample 2 - intact smooth surface (B), sample 3 - intact surface with many small undulations (C). Scale bar = 100µm. Scale bar = 100µm.**

## 5.5 Discussion

The results of this study, based on histological imaging, suggest neither submerging porcine femoral condyles in a 25% NBCS in Ringer's Solution + 0.03% sodium azide lubricant for up to 48 hours nor creating AccuTrans replicas of the surfaces at various time points, result in large-scale delamination of the superficial tangential layer of articular cartilage from the layers of cartilage beneath or penetration of fractures deep into the cartilage surfaces.

The large-scale damage observed for some samples in the 48-hour study was most likely an artefact of the histological processing. The decalcification step included in this study, designed to soften the extracellular matrix of the bone, was not included during the 48-hour study in error; this made some samples difficult to section and hence offers the most obvious explanation for the damaged observed, especially for the non-simulated controls.

Whilst no obvious large-scale change in the cartilage surface was observed, difference in the smoothness of the surfaces were observed and some samples did present with small tears in the surface. This could potentially have been as a result of the experimental conditions. The friction of porcine acetabula cartilage agitated for 4 days in a 25% serum in PBS antibiotic lubricant has been shown to increase, compared to native porcine acetabula cartilage (Taylor, 2012); it was suggested the higher friction was due to cartilage matrix degradation. Therefore, whilst no visible damage was observed in the current study, it would be reasonable to assume some degradation of the cartilage structure may potentially be occurring due to the natural breakdown of non-living tissue over several days. However, in this study, surface differences were observed within each of the experimental groups, i.e. there were samples with a smooth intact surface, a surface with small frequent undulations and a surface with larger less frequent undulations all in the same experimental group. In addition, the samples presenting with small tears were from the Native and Native + AccuTrans experimental groups, both of which had the histological samples removed at t=0 and hence, could not have been as a result of tissue degradation during the experiments.

Differences in surface condition could be explained by a number of factors. Histological artefacts may be responsible, some sections may not have been lying completely flat against the glass slide and have slight folds in surface, resulting in the undulations observed. Alternatively, samples from one knee may have been more hydrated than those of another resulting in a smoother surface. The natural geometric variation between donor animals may have been responsible. Samples were taken from both the anterior and posterior region of the medial and lateral femoral condyles of porcine knee joints, the different regions of the knee may have slightly different surface characteristics.

Natural variation between the donor animals seems a likely cause as three out of four samples from Knee 2 had smooth intact surfaces with one sample showing some small undulation and all of the samples with small tears or large undulations came from Knee 1 and Knee 3.

### 5.5.1 Limitations

The main limitation of this study is the low sample number in each experimental group (n=3), this limits the robustness when trying to explain differences between samples. It would be beneficial to determine whether the smooth intact surface or the undulating surface is the more typical condition of freshly dissected porcine cartilage so subsequent analysis of the tissue at later time points could be more certain.

## 5.6 Conclusion

Applying AccuTrans silicone to porcine femoral condyle articular cartilage surfaces which have experienced up to 48-hours submerged in a serum-based lubricant does not appear to cause damage to the surfaces, hence, AccuTrans silicone is a viable technique for replicating cartilage surfaces during extended duration tribological investigations.

# Chapter 6

# Experimental Simulation of Activities of Daily Living

## 6.1 Introduction

Walking gait simulation studies of total joint replacements have been routinely conducted to assess wear performance. Whilst this approach has been pivotal for developing safer medical devices it does not replicate the *in vivo* conditions experienced by these interventions; particularly for younger active patients whose lifestyles apply more challenging loading and complex motions which may cause adverse effects and potentially limit intervention lifetimes (L.M. Jennings et al., 2012). Progression of wear simulation studies to apply activities of daily living (Schwiesau et al., 2013) (Schwiesau et al., 2013) (Abdel-Jaber et al., 2015) (Abdel-Jaber et al., 2016) (Abdelgaied et al., 2018) or more severe walking gait kinematics (Brockett et al., 2016) have demonstrated higher polyethylene wear rates compared to standard walking gait for knee replacements. The intended patient population for early-stage knee interventions are younger more active individuals. It is plausible to assume alternative motions or more severe kinetic/kinematic conditions may influence the performance of early-stage knee interventions within natural knee joints.

Recent *in vitro* cadaveric knee joint simulation studies have applied activities of daily living to assess the kinematics of the natural knee (Sarpong et al., 2020) and total knee replacement designs (Borque et al., 2015) (Shimizu et al., 2018) (Willing et al., 2019), however none of these studies looked at the influence of activities of daily living on the mechanical and tribological behaviour of articular cartilage or meniscal surfaces. There is evidence from pin-on-plate experiments showing multi-directional motion (Northwood and Fisher, 2007) or increased loading (Katta et al., 2009) increase wear, damage and deformation when applied to articular cartilage.

During an average day people experience intermittent periods of activity e.g. stand, walk, run, sit, walk upstairs, squat etc. The most clinically relevant results would be generated by a simulation protocol incorporating these activities. It is currently possible to simulate total knee replacements unattended for an extended duration and switch between

different activities without stopping the simulation. This approach is efficient as it reduces the amount of time to simulate a large number of cycles. It would also be beneficial to adopt this approach for natural knee joints. This would enable influence of different activities to be assessed and maximise the number of simulation cycles before tissue degradation compromises the efficacy of the natural joint as an assessment tool. Chapter 4 demonstrated porcine knees could be simulated for an extended duration of 48-hours using an anterior-posterior spring constraint optimised for walking gait. It remains unknown if applying alternative loads and motions or attempting to switch between motions mid-simulation is possible when using the same spring constraint setup for porcine knee joints.

## 6.2 Aims and Objectives

### 6.2.1 Aim:

- To enhance the experimental porcine knee joint simulation methods to incorporate a wider range of input demands and enable the simulation of activities of daily living

### 6.2.2 Objectives:

- Search the literature to identify appropriate activities of daily living to simulate

- Determine the feasibility of simulating these activities using the experimental porcine knee joint model

## 6.3 Determining appropriate activities of daily living

A brief literature search was performed to identify common movements which provide more challenging kinetic and kinematic conditions than walking gait which it would also be possible to apply to the porcine model in the single station knee simulator. Simulation of these motions may identify tribological behaviours within the tibiofemoral joint which could negatively influence the behaviour of early-stage knee intervention, which may not have been apparent if simulating walking gait alone. The literature search revealed the most common activities of daily living, other than level walking, were walking up and down stairs (Morlock et al., 2001) (Schwiesau et al., 2013), this data was obtained from monitoring the daily activities of hip arthroplasty patients (Morlock et al., 2001). In addition to being a common movement, stair ascent applies a higher maximum axial force over a longer duration and this occurs around the same time as the maximum flexion so could potentially influence intervention behaviour. Deep squat was also identified as a motion which could be simulated. As well as applying a higher maximum axial force over a longer duration, a deep squat motion is a high flexion movement. Tribological behaviour in the tibiofemoral joint changes as the flexion angle increases. During the first 20° of flexion a rolling motion is generated, as the flexion angle increases the motion transitions from purely rolling to a combination of rolling and sliding then pure sliding in deep flexion (Masouros et al., 2010). Sliding is a higher friction tribological behaviour than rolling, therefore higher flexion activities, such as a deep squat, may be more likely to generate cartilage damage, especially whilst concurrently applying large loads. Both stair ascent and deep squat provide more challenging kinetic and kinematic conditions than walking gait and have previously been applied during total joint simulation and cadaveric studies. Therefore, the stair ascent and deep squat motions were chosen for inclusion during the current activities of daily living study to determine if they could be applied to a porcine knee whilst subjected to physiological loads.

## 6.4 Preliminary Work - Simulating stair ascent and deep squat with walking gait spring constraint

### 6.4.1 Experimental design

A porcine knee joint (n=1) was prepared as previously described (Chapter 2) and series of short simulations were run (Table 6.1). Walking gait was applied to ensure the knee could be simulated using the existing optimised spring setup (stiffness=20N/mm, spring gap=5mm). Subsequently, stair ascent and deep squat were applied to determine if the same spring setup was sufficient to constraint these motions during simulations. The spring control approach allows joint geometry to guide movement and therefore mitigates small inaccuracies which may have occurred during the joint alignment process. The intention of the spring control approach is to generate more physiological motion, however, if spring constraints were not appropriate for the new input profiles this could lead to joint instability and simulation failure.

**Table 6.1: Rationale for experimental methods during preliminary spring control study.**

| Input profile | Anterior-posterior control mode | Rationale |
|---|---|---|
| Walking gait | Spring (20N/mm with 5mm gap) | To assess if the knee joint produces similar kinematics to previous studies (Chapter 4) (Liu et al., 2019) |
| Stair ascent | Spring (20N/mm with 5mm gap) | Ligament tension and laxity in the joint should be consistent irrespective of the input kinematics |
| Deep squat | Spring (20N/mm with 5mm gap) | Ligament tension and laxity in the joint should be consistent irrespective of the input kinematics |

The walking gait profile simulated during the 48-hour study (Chapter 4) was used; stair ascent and deep squat profiles were taken from a study assessing activities of daily living on total knee replacements (Abdelgaied et al., 2018). Minimum and maximum demand values for each axis (Table 6.2) were scaled to the dimensions of porcine tissue (Figure 6.1) using the same scaling factors as previously described (Chapter 4), values were entered into the simulator software which generated scaled input waveforms.

**Table 6.2: Minimum and maximum simulator inputs for walking gait, stair ascent and deep squat.**

| | **Walking Gait** | | **Stair Ascent** | | **Deep Squat** | |
|---|---|---|---|---|---|---|
| | **Min** | **Max** | **Min** | **Max** | **Min** | **Max** |
| **Axial Force (N)** | 63.6 | 984.7 | 151.5 | 1139.5 | 124.3 | 1090.3 |
| **Flexion-Extension (°)** | 0 | 21.7 | 0 | 21.3 | 0 | 37.8 |
| **Abduction-Adduction (°)** | 0 | 0 | 0 | 0 | 0 | 0 |
| **Internal-External (°)** | -1.6 | 1.6 | -1.8 | 1.8 | 0 | 1.8 |
| **Anterior-Posterior (mm)** | Spring | Spring | Spring | Spring | Spring | Spring |

Axial force was driven in force control and flexion-extension and internal-external (tibial) rotation were driven in displacement control. Anterior-posterior displacement was not driven, these were generated by motion of the knee interacting with the spring constraint mechanism. The abduction-adduction axis was not driven and left free to swing and the medial-lateral axis was fixed at zero. Simulations were run for 300 cycles at 1Hz. Three simulation cycles were logged every 10 cycles for the duration of the simulation. Kinetic and kinematic data presented were the mean of three cycles. The lubricant used throughout simulations was 25% new-born calf serum in Ringer's Solution + 0.03% sodium azide.

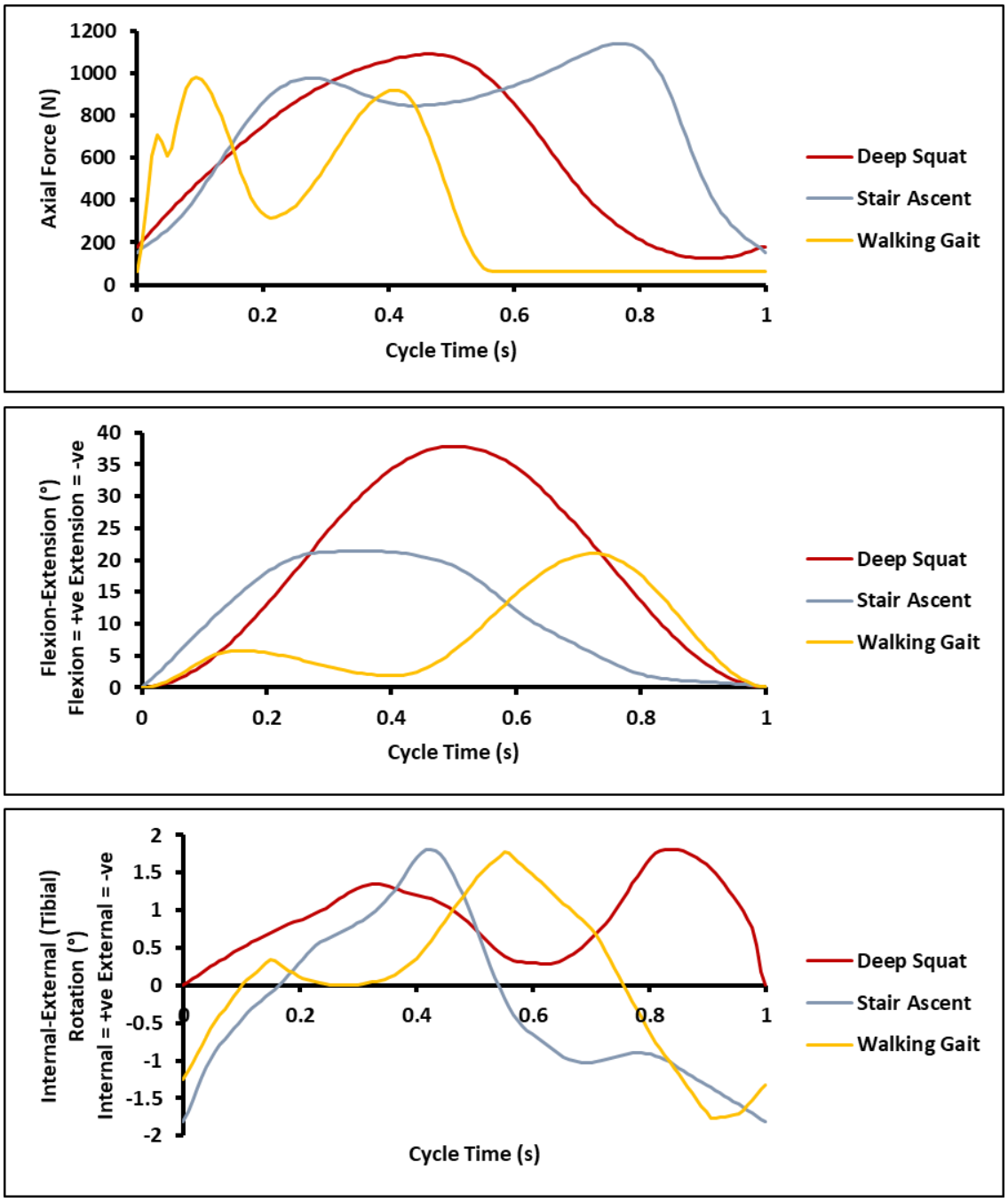


**Figure 6.1: Axial force (N), flexion-extension (°) and internal-external (tibial) rotation (°) demand waveforms for walking gait, stair ascent and deep squat.**

### 6.4.2 Results of preliminary spring control study

Demand following for walking gait and stair ascent was within or close to within ±5% of the maximum values; the only exception was the first peak of the axial force waveform for walking gait (Figure 6.2). It was not possible to apply the deep squatting profile due to repeated dislocation of the joint when attempting to run simulations.

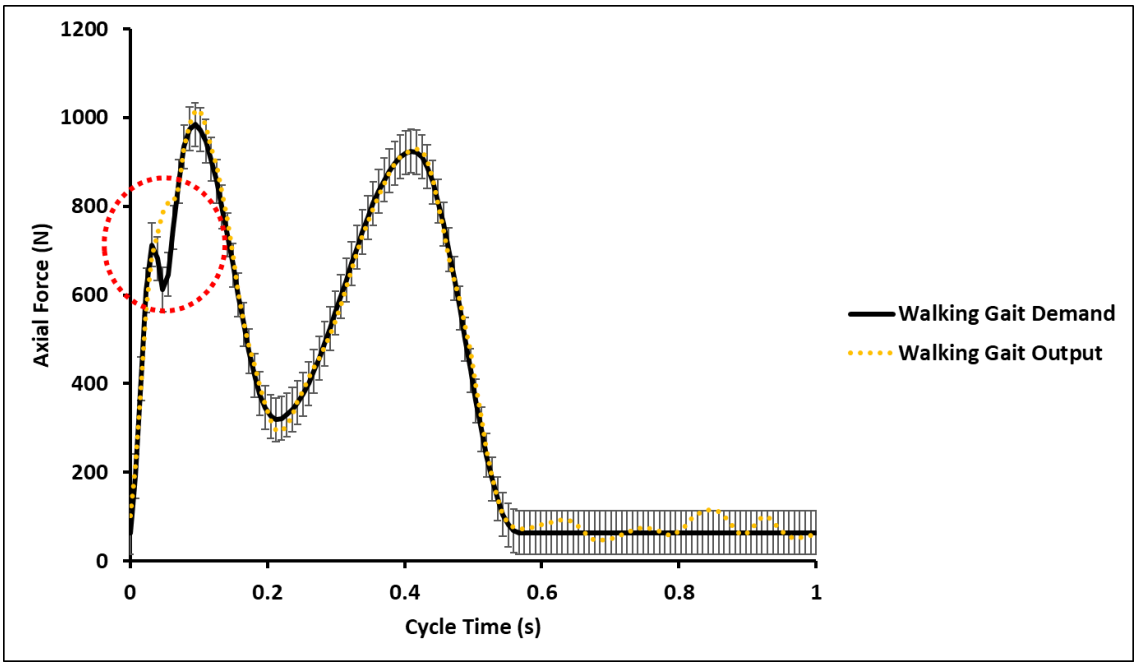


**Figure 6.2: Discrepancy between axial force demand and output during the first peak (red dotted circle) of the walking gait waveform when using spring control.**

When applying walking gait, the preliminary knee produced similar anterior-posterior displacement range (-5.3mm to 0.2mm) and anterior posterior-shear force (-18N to 9N) outputs (Figure 6.3) as knees in the 48-hour study (Chapter 4); the abduction-adduction axis oscillated between 0.5° and 2.6°. When applying stair ascent the motion of the abduction-adduction axis initiated from a more adducted position as the simulation progressed, therefore the knee was left to run for 1800 cycles (30 minutes) to determine if this behaviour continued of if an equilibrium position would be reached. The anterior-posterior displacement range (-10.8mm to -2.2mm), was about double that of walking gait and the maximum anterior-posterior shear force (-5N to 177N) was 20 times the magnitude of walking gait; the abduction-adduction axis was oscillating between 2.6° and 3.4° (Figure 6.3). Despite the position of the adduction-abduction axis being more adducted when using the stair ascent profile, the knee was stable in this position over the 30-minute duration.

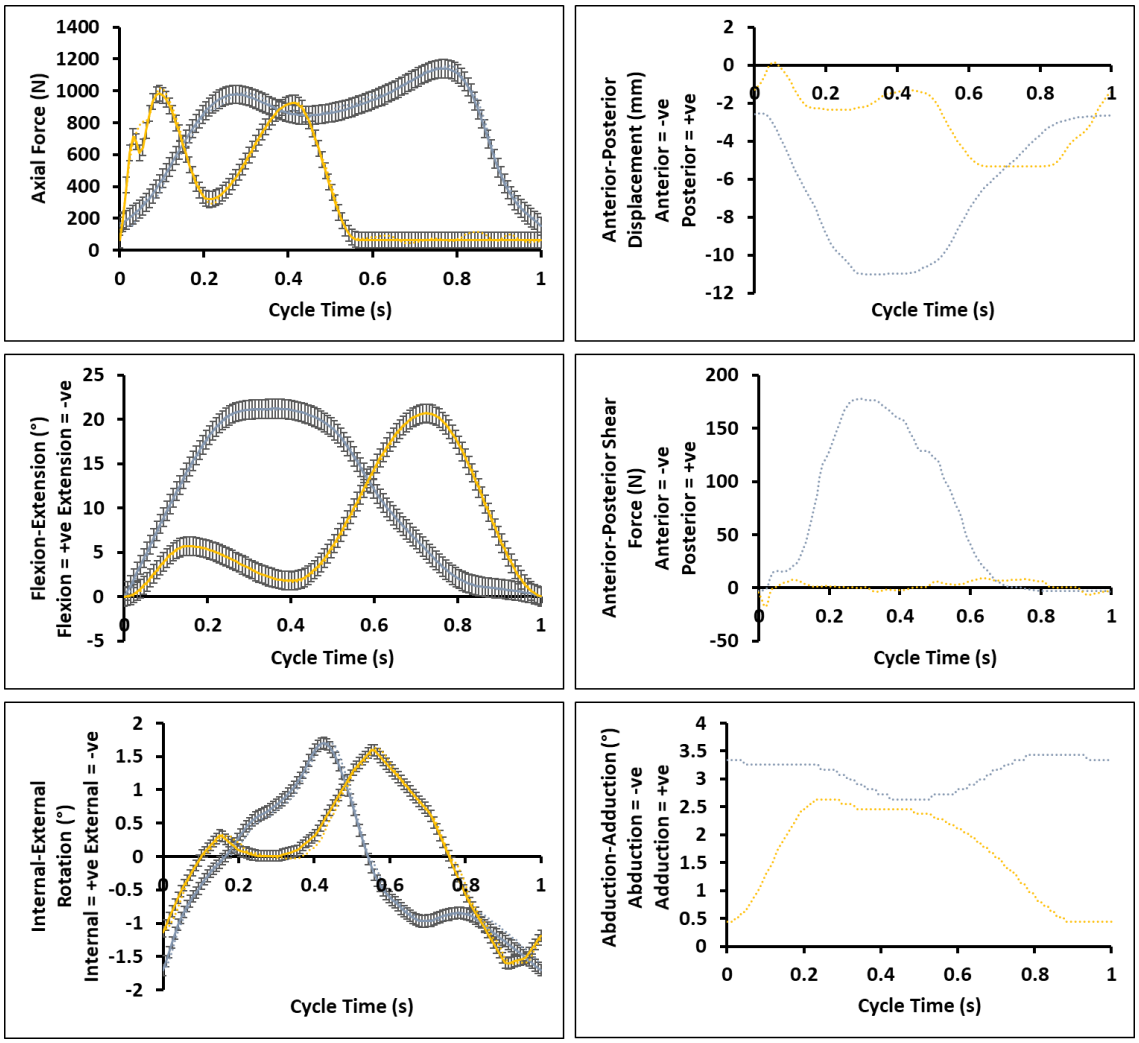


**Figure 6.3: Demanded input waveforms (solid lines) and actual output waveforms (dotted lines) with 20N/mm + 5mm gap for the preliminary knee after 240 cycles walking gait (orange) and 1800 cycles stair ascent (blue).**

## 6.5 Preliminary Work - Simulating stair ascent and deep squat with displacement control

### 6.5.1 Experimental design

Due to the larger anterior-posterior displacements observed for stair ascent and the dislocations when attempting to simulate the deep squat profile with the spring constraint, stair ascent and deep squat were simulated using displacement control. Displacement control provides joint stability by preventing excessive movement and preventing non-physiological motion. For displacement control the axial force was driven in force control and flexion-extension and internal-external (tibial) rotation and anterior-posterior displacement were driven using displacement control (Table 6.3). The anterior-posterior

input profiles were scaled as described in the previous section (Figure 6.4). All other experimental conditions remained the same as for the spring-controlled experiments and the same porcine knee was used.

**Table 6.3: Minimum and maximum simulator inputs for walking gait, stair ascent and deep squat.**

| | Stair Ascent | | Deep Squat | |
|---|---|---|---|---|
| | **Min** | **Max** | **Min** | **Max** |
| **Axial Force (N)** | 151.5 | 1139.5 | 124.3 | 1090.3 |
| **Flexion-Extension (°)** | 0 | 21.3 | 0 | 37.8 |
| **Abduction-Adduction (°)** | 0 | 0 | 0 | 0 |
| **Internal-External (°)** | -1.8 | 1.8 | 0 | 1.8 |
| **Anterior-Posterior (mm)** | -4.3 | 0 | -6.2 | 0.9 |

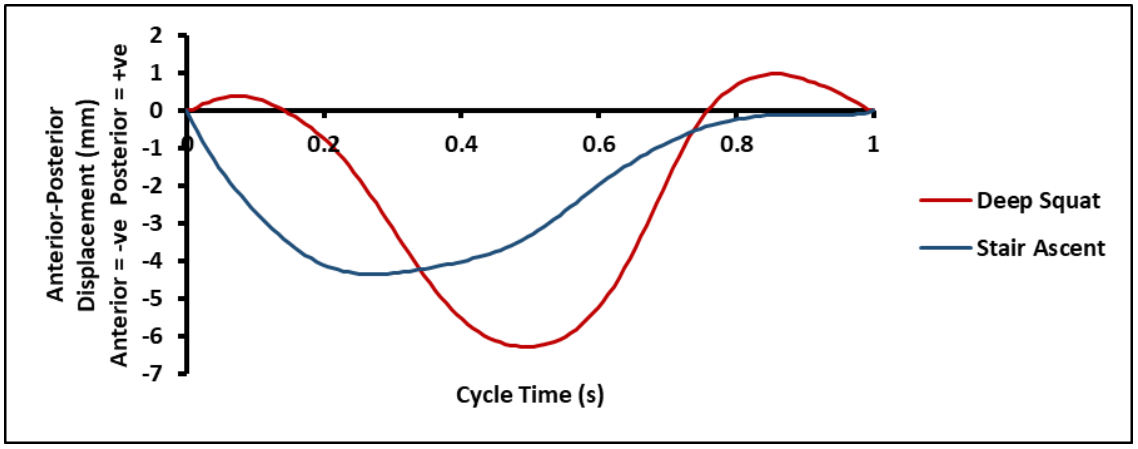


**Figure 6.4: Anterior-posterior displacement demand waveforms for stair ascent and deep squat.**

### 6.5.2 Results of simulating stair ascent and deep squat using displacement control

Demand following for stair ascent and deep squat were within, or close to within, 5% of the maximum value for each axis; except for anterior-posterior displacement outputs which were ~1mm more anterior than the demand (see discussion below). The abduction-adduction axis oscillated between -0.2° and 2° for stair ascent and -1.6° and 2° for the deep squat (Figure 6.5).

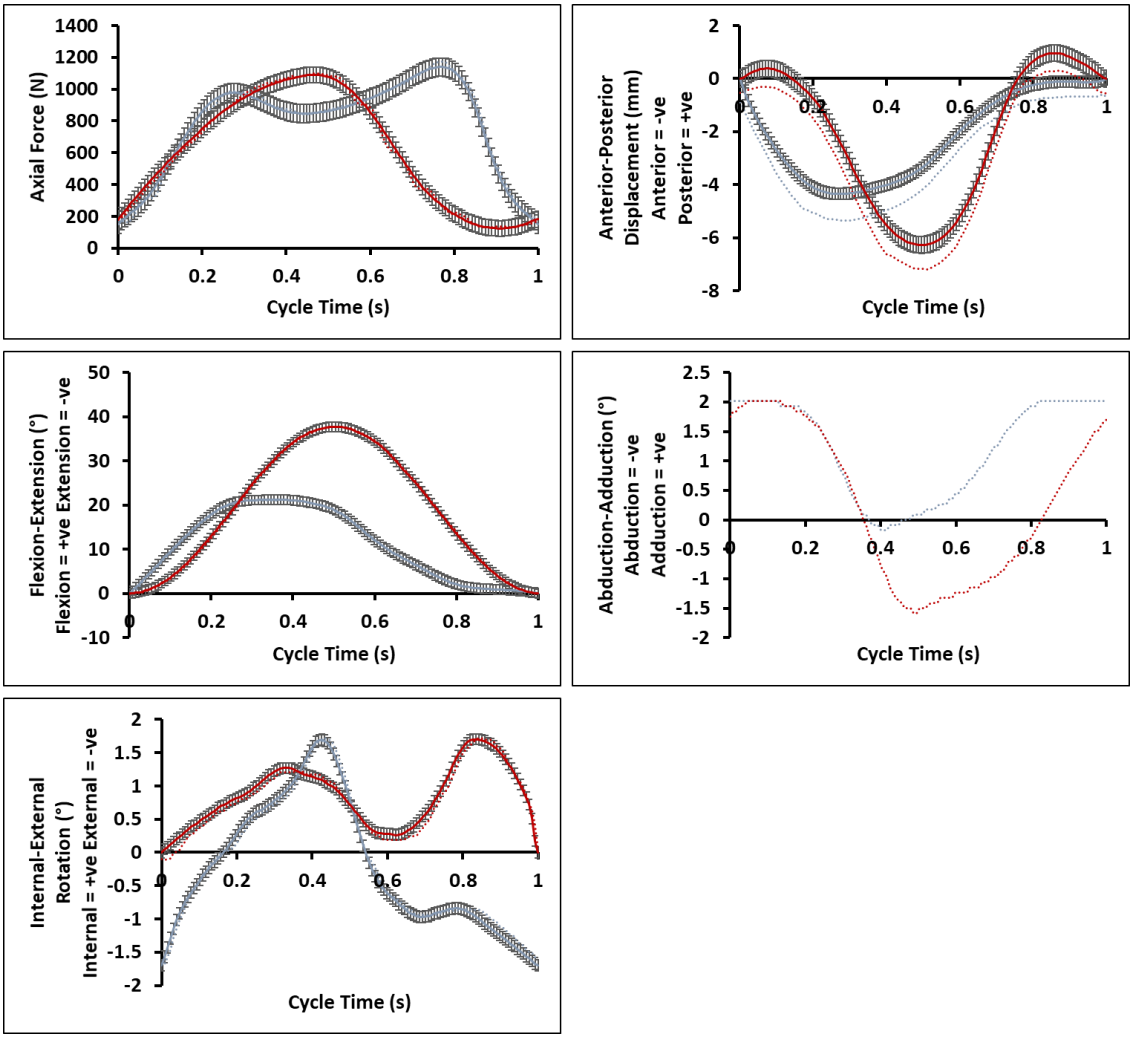


**Figure 6.5: Demanded input waveforms (solid lines) and actual output waveforms (dotted lines) with displacement control for the preliminary knee after 300 cycles stair ascent (blue) and 300 cycles deep squat (red).**

### 6.5.3 Discussion

Using the walking gait spring setup it was possible to simulate stair ascent, however anterior-posterior displacement and anterior-posterior shear force were much larger than during walking gait. Possible explanations for this are the natural anterior displacement of stair ascent may be larger than for walking gait, stair ascent was an unfamiliar motion for porcine anatomy, or the spring constraint was optimised for walking gait resulting in suboptimal kinematics and a higher shear force. It was not possible to simulate deep squat due to repeated dislocation of the samples. During deep squat it would appear the spring constraints were insufficient to restrain the anterior motion of the tibia causing the femur to fall off the posterior tibial plateau during flexion. The spring constraint mechanism is designed to replicate ligament function, at deeper flexion angles muscular forces provide more contribution to the restraint of motion; therefore the spring constraint mechanism is potentially less effective at higher flexion angles. The limited range of flexion in porcine anatomy could also potentially have contributed to the issue observed with the deep squat motion. Whilst the flexion-extension range of the deep squat motion was scaled down during the current study, this may have represented a non-physiological position for the porcine knee and caused the large anterior displacements and dislocation of the joint. Displacement control provided a stable simulation for both the stair ascent and deep squat motions with no major adverse effects (dislocations, fracture or excessive adduction-abduction motion) occurring.

When comparing anterior-posterior displacement output, magnitudes were larger for spring control than displacement control when simulating stair ascent. The displacement-controlled values for the anterior-posterior displacement used during the current study were obtained from previous total knee replacement research (Abdelgaied et al., 2018) and the original source of these values was a fluoroscopic study of total knee replacement patients (Belvedere et al., 2013). Differences between the kinematics of total knee replacement patients and healthy knees or differences between human knees and porcine knees may explain the discrepancies between anterior-posterior displacement magnitudes for the spring control and displacement control approaches. In addition, scaling of the anterior-posterior displacement inputs was potentially too severe resulting in an underestimation of physiological motion in the porcine knee joint, therefore alternative spring constraints may be required. Optimisation of spring constraints may improve simulation performance for stair ascent or enable simulation of deep squat. Applying stronger springs or adjusting spring gaps would more effectively constrain the anterior-posterior displacement and excessive motion dislocation from occurring.

The preliminary knee failed to follow the axial force demand during the first peak of walking gait (Figure 6.2), however this trend has been present for several of the

previously simulated knees (Chapter 4). An offset in the simulator motor tuning was responsible for the ~1mm anterior positioning of the anterior-posterior displacement waveforms for stair ascent and deep squat during displacement control experiments and not as a result of the sample. This was rectified by tuning motor on the anterior-posterior axis. Direct comparison of anterior-posterior shear force for the two control modes cannot made as friction within the motor may contribute to the shear force value for displacement control.

## 6.6 Preliminary Work - Alternative spring constraints on preliminary knee

### 6.6.1 Experimental Design

During the initial preliminary study, section (6.4.2), large anterior displacements were observed for the stair ascent and deep squat profiles and repeated dislocation of the knee joint occurred when applying deep squat with the 20N/mm + 5mm spring condition. The excessive anterior translation of the tibia was causing the femur to fall off the posterior tibial plateau during flexion. Therefore, during the current study, three strategies were trialled to reduce anterior displacement and prevent dislocation of the joint. The frequency of the deep squat motion was reduced to 0.5Hz to determine if slowing down the movement would increase the stability. Spring gaps were removed so the constraint force applied by the spring would start acting as soon as anterior translation occurred and spring stiffness was increased to provide a larger constraint force. Both these approaches aimed to reduce the magnitude of the anterior translation. A 41N/mm spring stiffness was selected as this provided a suitable increase in stiffness. In addition, it was available in the same material as the 20N/mm spring keeping the method consistent and it had the same internal diameter which enabled it to be easily incorporated into the existing spring constraint mechanism on the simulator. Different combinations of spring stiffness and spring gap were assessed (Table 6.4). The porcine knee used in the previous preliminary studies was used for all experiments in the current study.

**Table 6.4: Alternative spring constraint conditions.**

| Spring Stiffness (N/mm) | Spring gap (mm) | Frequency (Hz) | Aim | Rationale |
|---|---|---|---|---|
| 20 | 5 | 0.5 | Simulate deep squat without dislocation | Slower movement will be more stable |
| 20 | 0 | 1 | Simulate deep squat without dislocation | Reducing gap will reduce anterior displacement |
| 41 | 0 | 1 | Reduce anterior-posterior displacement of stair ascent and deep squat | Increasing stiffness will reduce anterior displacement |
| 41 | 5 | 1 | Reduce anterior-posterior displacement of stair ascent and deep squat | Increased stiffness + smaller gap will reduce anterior displacement |

### 6.6.2 Results

Reducing the frequency to 0.5Hz did not prevent dislocation when using the deep squat profile. As with the initial attempts to simulate deep squat, section (6.4.2), the anterior motion of the tibia caused the femur to fall off the posterior tibial plateau during flexion. Reducing the spring gap to 0mm did prevent dislocation when using the “20N/mm + 0mm condition”. When using the “41N/mm + 0mm condition”, the anterior-posterior displacements of stair ascent and deep squat were similar to the corresponding displacement control waveforms. Anterior displacement during the swing phase of walking gait was completely attenuated by application of the “41N/mm + 0mm condition”. When using the “41N/mm + 5mm condition” it was possible to simulate all three motions; anterior-posterior displacements were larger for stair ascent and deep squat but no dislocation occurred and the anterior-posterior motion for walking gait was similar to the “20N/mm + 5mm condition”.

### 6.6.3 Discussion

The “41N/mm + 5mm gap condition” could be used to simulate all three motions, this demonstrated the potential to run simulations of different motions with a single spring constraint. Whilst this shows promise, there will be inherent variability between porcine knees and the “41N/mm + 5mm condition” may not be applicable to every knee. The ability for knees to transition between profiles using both displacement control and the physical spring system needs to be determined.

## 6.7 Preliminary Work - Simulation of sequential activities of daily living using displacement control

### 6.7.1 Experimental Design

Profile loop simulations consisting of walking gait, stair ascent and deep squat were applied to a dummy knee and a porcine knee to determine the influence of transitioning between profiles on kinetic and kinematic outputs. The dummy consisted of a flat ultrahigh molecular weight polyethylene (UHMWPE) tibial component and a stainless-steel femoral component of constant 25mm radius; Vaseline was applied to dummy surfaces to lubricate the contact prior to simulations. This simplified geometry approach allowed profiles to be tuned prior to use on porcine knee to increase the chance of a successful simulation and to prevent damage to porcine knees

For all motions the axial force was driven in force control and flexion-extension, internal-external (tibial) rotation and anterior-posterior axes were driven using displacement control. For walking gait, the anterior-posterior displacement output from the previous spring control experiments was used as the input demand for anterior-posterior axis. This was done to provide more physiologically relevant motion. This approach was selected based on results from a previous study using the University of Leeds experimental porcine knee simulation model (Liu et al., 2019); it was shown an anterior-posterior spring constraint setup (stiffness=20N/mm, spring gap=5mm) effectively recreated the anterior-posterior motion of simulated porcine knees with all the ligaments still intact. Once suitable tuning had been achieved, loop profiles were then applied to a porcine knee joint; as with the previous preliminary studies the same porcine knee was used.

Two versions of each input profile were created (Figure 6.6). In loop A, profiles transitioned directly from the outgoing profile to the incoming profile. In loop B, a profile which connected the final demand value of the outgoing profile from each axis to the first demand value of the incoming profile was applied to smooth the transition between the

profiles. This was done as the final and initial waveform values for each axis were not equal for each of the different motions. All simulations were run using displacement control at a frequency of 1 Hz.

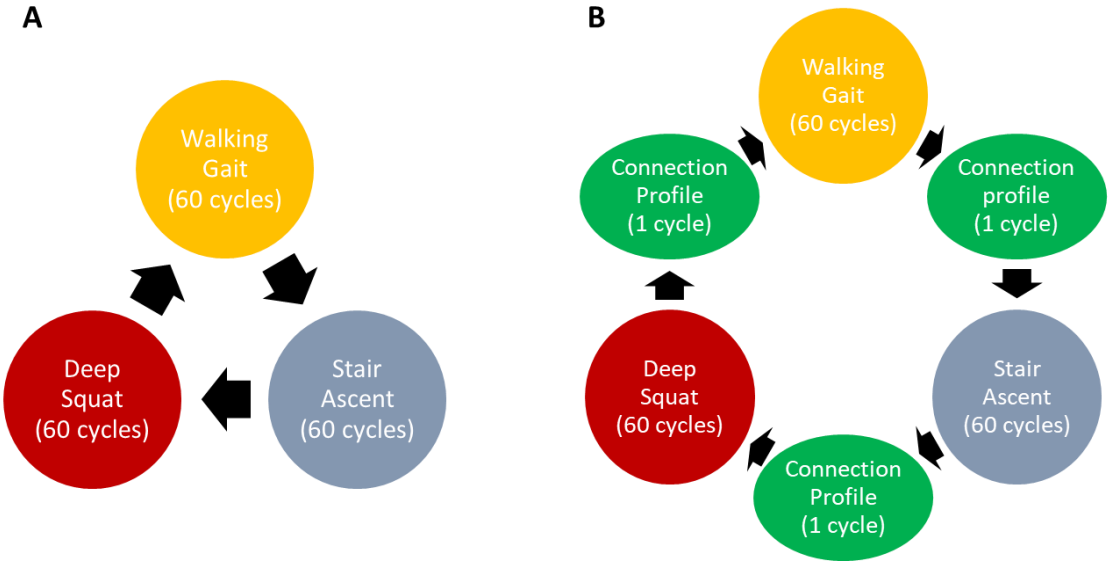


**Figure 6.6: Activities of daily living simulator profile loops without connecting profiles (A) with connecting profiles (B).**

### 6.7.2 Results

The same trends were observed for the dummy and porcine knee (Figure 6.7) (Figure 6.8). After each transition, a small change in anterior-posterior displacement occurred within the first 0.1s as did a large increase in anterior-posterior shear force; demand following was achieved 1-2 cycles after transition. This trend was observed for the loop without connection profiles and the loop with connection profiles; this occurred at both the transition from the outgoing profile to the connection profile and the transition from the connection profile to the incoming profile.

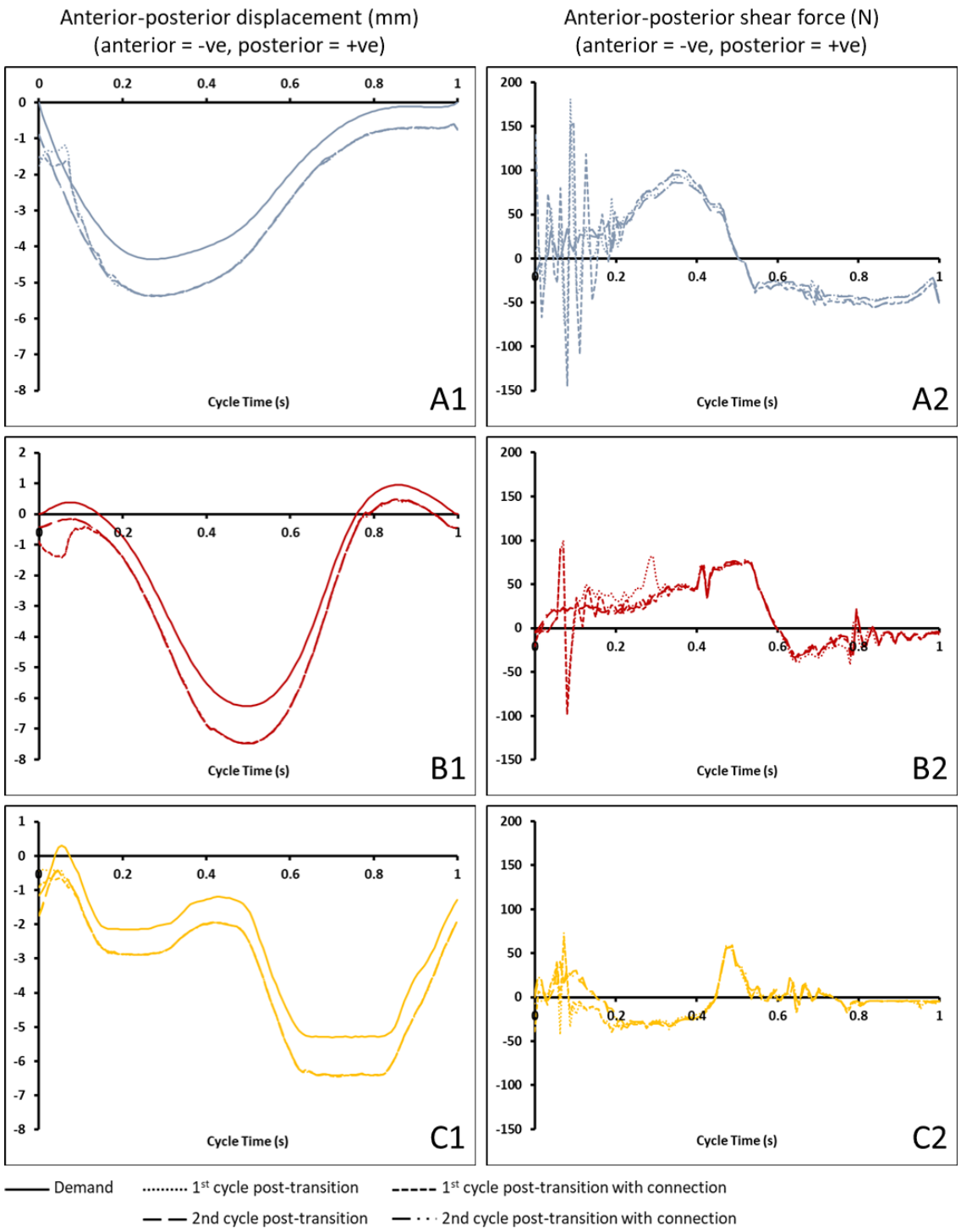


**Figure 6.7: Anterior posterior-displacement (mm) (left) and anterior-posterior shear force (N) (right) for the transitions from walking gait to stair ascent (A1 & A2), stair ascent to deep squat (B1 & B2) and deep squat to walking gait (C1 & C2) with and without connection profiles when using the dummy knee. *Anterior-posterior outputs were more anterior than the demand due to an offset in the motor tuning.**

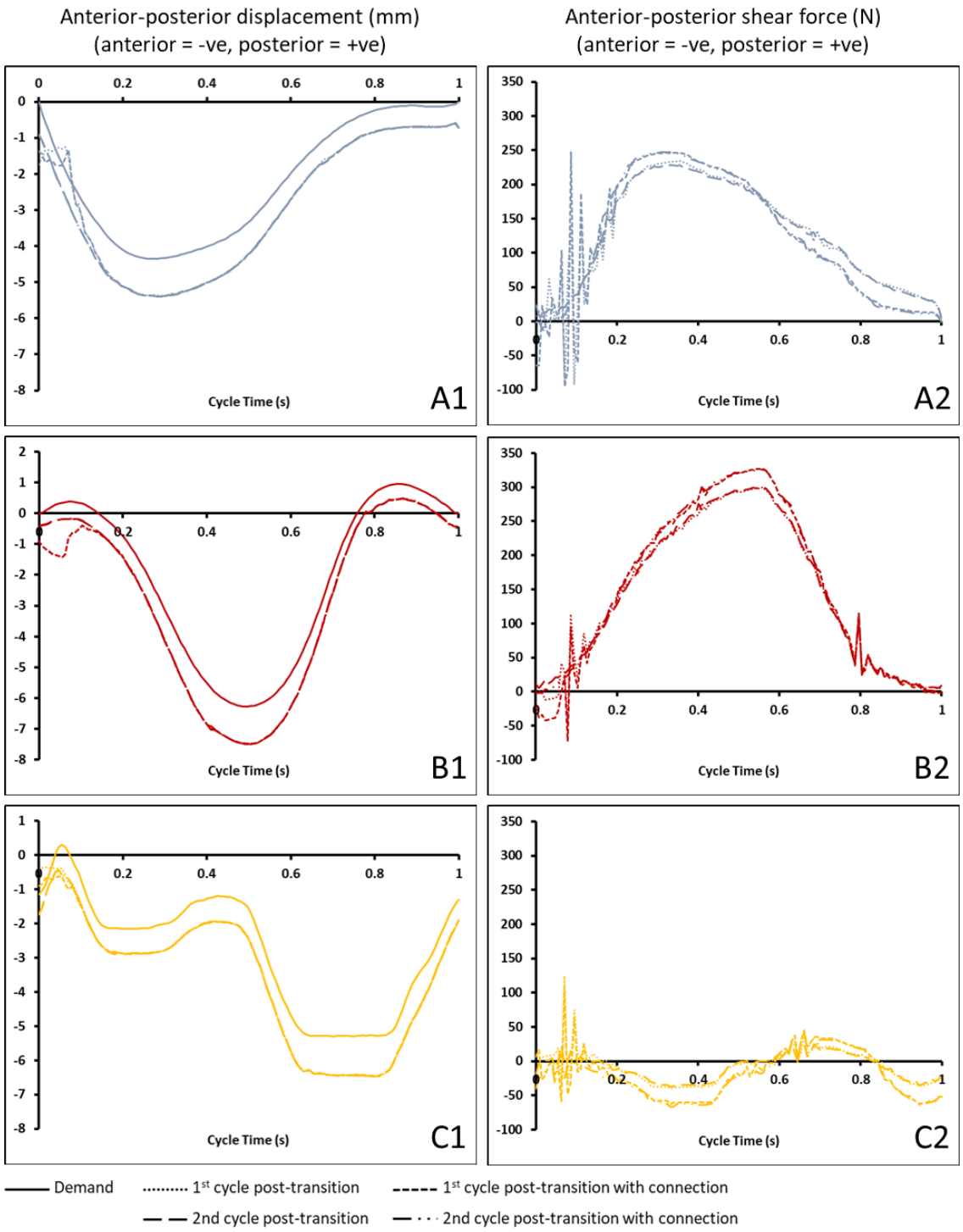


**Figure 6.8: Anterior posterior-displacement (mm) (left) and anterior-posterior shear force (N) (right) for the transitions from walking gait to stair ascent (A1 & A2), stair ascent to deep squat (B1 & B2) and deep squat to walking gait (C1 & C2) with and without connection profiles when using the porcine knee. *Anterior-posterior outputs are more anterior than the demand due to an offset in the motor tuning.**

### 6.7.3 Discussion

Brief changes in anterior-posterior displacement and anterior-posterior shear force occurred during transition from one profile to another, however demand following was achieved immediately after (within 1-2 cycles) and maintained until the subsequent transition; therefore transitioning did not compromise the stability of the simulation. Transitioning between profiles did produce a large anterior-posterior shear force; this could potentially initiate wear, damage or deformation when applied to natural joints. Profiles transitioned directly from one to the next with the maximum desired input force applied during the first cycle, this may explain the increase in anterior-posterior shear force during the first cycle of the next profile. A potential consequence of this would be the inability to differentiate between changes caused by the transition process and changes due to the new input profile; this may be a limitation of the method. If the It does not appear necessary to include a connecting profile during transition from one demand profile to another as this added no benefit to simulation performance compared to not using a connection profile. An offset in the simulator motor tuning was responsible for the ~1mm anterior positioning of the anterior-posterior displacement waveforms for star ascent and deep squat during displacement control experiments and not as a result of the sample.

## 6.8 Dummies and Experimental Knees (n=3, 4x spring control + loops and displacement control + loops)

### 6.8.1 Experimental Design

The previous section demonstrated walking gait, stair ascent and deep squat profiles could transition from one to the next using displacement control. The next step was to investigate the feasibility and repeatability of transitioning from one profile to the next when applying anterior-posterior spring constraints to the dummy components and porcine knees to create simulation loops. Porcine knees (n=3) were prepared as previously described and dummy components were greased with Vaseline. A series of simulations (Figure 6.9) were run using four different anterior-posterior spring constraint combination (Table 6.5) and displacement control.

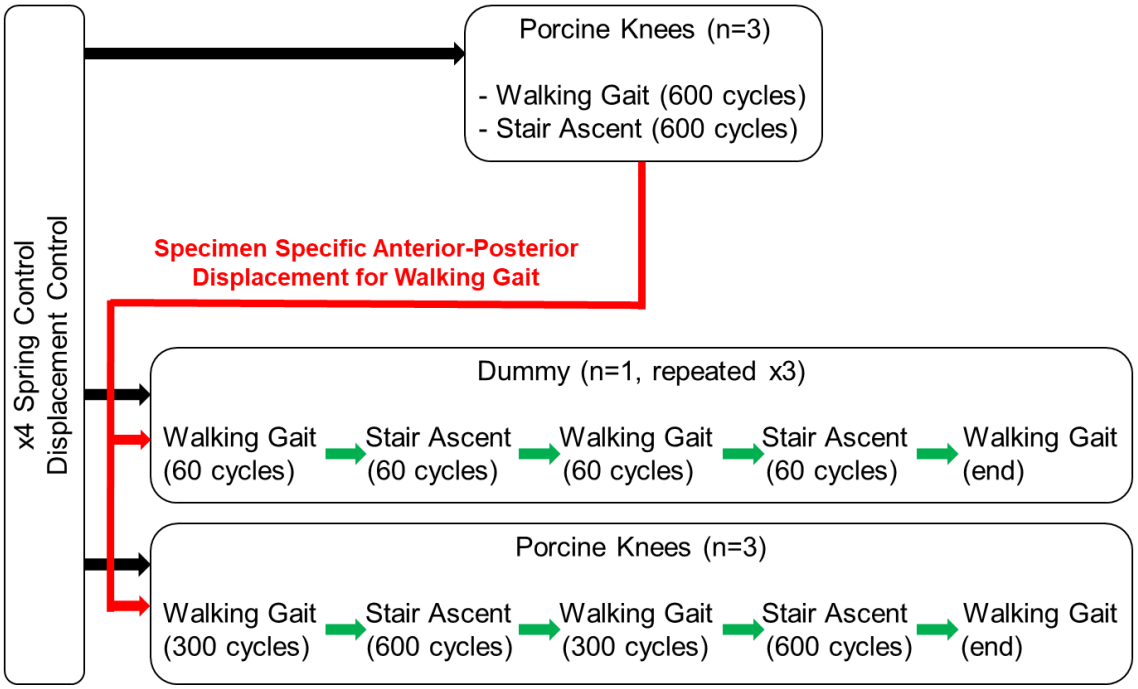


**Figure 6.9: Simulation conditions for porcine knee and dummy investigations.**

Only walking gait and stair ascent were simulated during the current study. Due to the previous difficulties with simulating deep squat using the spring control approach, sections (6.4.2) and (6.6.2), this motion was not included. There was a significant potential for simulation failure which may have damaged knee joints and compromised their ability to be assessed during subsequent experiments. In addition, the current study was designed to inform a future study assessing an intervention during activities of daily living. Due to the additional time required to acquire, process and analyse the data, it would not have been feasible to include deep squat during the future study, hence, it was not included during the current study.

**Table 6.5: Experimental groups**

| Anterior-posterior control mode | Spring Stiffness (N/mm) | Spring gap (mm) |
|---|---|---|
| Spring constraint | 20 | 0 |
| Spring constraint | 20 | 5 |
| Spring constraint | 41 | 0 |
| Spring constraint | 41 | 5 |
| Displacement control | N/A | N/A |

Some alteration of demand waveforms implemented during the current study was necessary. The first peak of the walking gait axial force waveform was removed, studies suggest this is not present for many patients (Bergmann et al., 2014) (Meireles et al., 2017). The axial force waveform for stair ascent was taken from a study assessing stair climbing in total knee replacements (Battaglia et al., 2014) and scaled to porcine tissue. The axial force waveform for stair ascent used in the preliminary work (Abdelgaied et al., 2018) had originally been scaled from the waveform used by Battaglia *et al.,* hence the axial force used in preliminary work, sections (6.4) (6.5) (6.6) (6.7), was an underestimate as it had been scaled twice. The minimum and maximum values for the altered waveforms can be seen in (Table 6.6).

For each walking gait experiment incorporating a spring constraint, anterior-posterior displacement outputs were generated by the axial force, flexion-extension and internal-external (tibial) rotation inputs. For the displacement control experiments the anterior-posterior displacement output from the 41N/mm + 5mm gap spring condition of each of the three knees was used as a specimen specific the input for anterior-posterior displacement for each knee. All other inputs remained the same as previously. All experiments were run at a frequency of 1 HZ.

**Table 6.6: Minimum and maximum simulator demand inputs for walking gait and stair ascent.**

| | **Walking Gait** | | **Stair Ascent** | |
|---|---|---|---|---|
| **Axis** | **Min** | **Max** | **Min** | **Max** |
| Axial Force (N) | 63.6 | 984.7 | 201.5 | 1515.5 |
| Flexion-Extension (°) | 0 | 21.7 | 0 | 21.3 |
| Abduction-Adduction (°) | 0 | 0 | 0 | 0 |
| Internal-External (Tibial) Rotation (°) | -1.6 | 1.6 | -1.8 | 1.8 |
| Anterior-Posterior Displacement (mm) | Specimen specific | Specimen specific | -4.3 | 0 |

### 6.8.2 Results

All dummy simulations ran successfully. For the porcine knee joints the results varied when using spring constraints (Figure 6.10). One knee could be simulated using all spring combinations, for the other two knees some simulations were stopped due to non-physiological kinematics (most often due to excessive abduction-adduction rotation) and some of loop profiles were not attempted due to failure to simulate either walking gait or stair ascent with the same spring constraint. All displacement controlled porcine knee simulations ran successfully. For 2 out of 3 knees the initiation position of the abduction-adduction output crept from the initial position to a more adducted position as the simulation progressed when applying the stair ascent profile (Figure 6.11).

| | Knee 1 | | | | | Knee 2 | | | | | Knee 3 | | | | |
|---|---|---|---|---|---|---|---|---|---|---|---|---|---|---|---|
| k<br>gap | 20,<br>0 | 20,<br>5 | 41,<br>0 | 41,<br>5 | DC | 20,<br>0 | 20,<br>5 | 41,<br>0 | 41,<br>5 | DC | 20,<br>0 | 20,<br>5 | 41,<br>0 | 41,<br>5 | DC |
| WG | | | | | | | | | | | | | | | |
| SA | | | | | | | | | | | | | | | |
| Loop | | | | | | | | | | | | | | | |

**Figure 6.10: Simulation results for each knee using different spring constraint combinations and displacement control: successful simulation (green), failed simulation due to non-physiological motion (red), not simulated due to failure of previous profiles (grey). Spring stiffness, k (N/mm), spring gap (mm), walking gait (WG), stair ascent (SA), walking gait + stair ascent profile loop (Loop), displacement control (DC).**

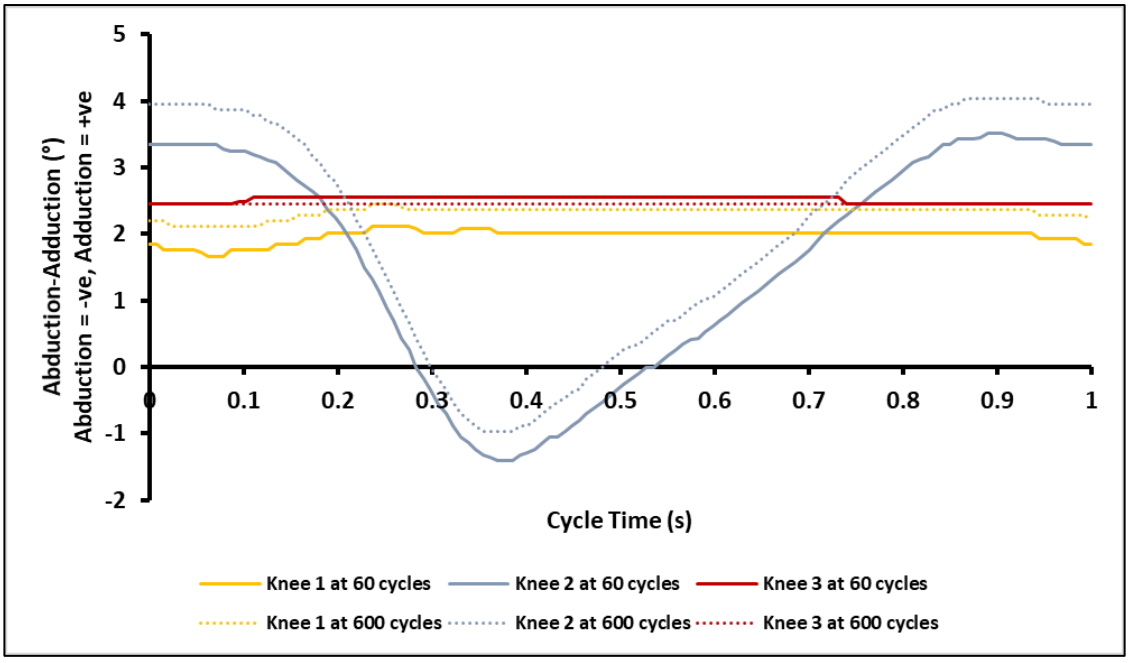


**Figure 6.11: Abduction-adduction rotation (mean of n=3 cycles) for each porcine knee at the start and end of displacement-controlled stair ascent simulations.**

## 6.9 Overall Discussion

In the natural knee ligaments provide restraining forces to prevent excessive motion during many different movements. It was therefore presumed a spring constraint optimised to restrain walking gait motion (20N/mm stiffness + 5mm gap) (Liu et al., 2019), would also be suitable to effectively constrain other activities of daily living (stair ascent and deep squat). Results of the current study corroborate the previous finding of Liu et al. as the walking gait simulation could be run for all knees when using this spring setup. However, the repeatability of this approach for applying the same spring constraints during stair ascent and deep squat simulations was limited.

The potential to simulate walking gait, stair ascent and deep squat profiles using the same spring constraint for each profile was demonstrated in section (6.6). However, this required the spring stiffness to be increased to 41N/mm as the restraint force of the 20N/mm spring was insufficient to prevent non-physiological motion. Section (6.8) assessed the repeatability of this approach; considerable variability was observed for the three experimental knees in this study (Figure 6.10). Walking gait and stair ascent were simulated with the same spring constraint, this was possible for 2 out of 3 knees using the 41N/mm + 5mm gap condition and for 1 out of 3 knees when using all spring combinations. For the remaining knee, it was not possible to simulate stair ascent using any of the spring constraints.

A combination of the inherent geometric variability between knees and accuracy of alignment during the dissection and cementing processes are likely responsible for the observed differences. Porcine knees were aligned and cemented to fix the tibiofemoral joint angle at 24° flexion to simulate heel strike in a pig. Suboptimal alignment may have compromised congruency between femoral condyles and menisci resulting in non-physiological motion during simulations.

In future, if looking to utilise physical spring constraints, an optimised anterior-posterior spring constraint may be necessary for each individual motion for each individual knee; in addition, spring constraints could also be added to the internal-external, adduction-abduction or medial lateral axes. As an alternative to the existing physical spring constraint mechanism, the simulator used during the current studies could be run in force control and virtual spring constraints applied using the simulator software. This approach may enable simulation of a wider range of activities as constraints could be applied to the anterior-posterior and internal-external (tibial) rotation axes. A study assessing the ability of virtual spring constraints to replicate soft tissue function in cadaveric knees identified specimen specific spring constrains were required for both the anterior-posterior and internal-external (tibial rotation) axes (Liu et al., 2020).

Although this would still be unsuitable for simulating loop profiles, as only one spring constraint may be applied to each axis in a single .kst file so the springs specified for the first motion would be unsuitable for the subsequent motions.

Other existing simulator systems also enable creation of virtual ligaments. One system, the Advanced Mechanical Technology (AMTI) VIVO™ simulator has been used to simulate stair ascent and deep knee bend on a cadaveric human knee joint. A virtual posterior cruciate ligament was shown to restore anterior-posterior motion of the knee to within ≥8% random mean square error of the intact condition for stair ascent (Sarpong et al., 2020); the random mean square errors for deep knee bend were less favourable at 10% and 25% with a third sample not tested. These results show a similar trend to the work in the current chapter as stair ascent was easier to replicate than deep squat (knee bend) and it was difficult to consistently replicate *in vivo* conditions for multiple movements with a single constraint. This also highlights the issues associated with the inherent variation between samples. Another work utilising the AMTI VIVO™ identified significant differences in anterior-posterior kinematics when incorporating virtual muscle forces to apply stair ascending and descending motions to two total knee replacement devices in a cadaveric human knee (Willing et al., 2019). Significant limitations for the approaches of Sarpong *et al*. and Willing *et al*. were the frequency of simulations (0.04Hz), which is very slow compared to *in vivo* movement and the low cycle numbers, three and four respectively. In addition, simulations during the Willing *et al*. study were

conducted at 75% reduced force (Willing et al., 2019). It was unclear whether either of these approaches applied the activities of daily living sequentially.

When simulating stair ascent, the value of the adduction-abduction at t=0s of each cycle crept from its initial position into a more adducted position as the simulation progressed causing knees to adopt a more varus orientation; this occurred for both the spring constraints and displacement control. The magnitude of the change was less pronounced for displacement control however this trend was also observed during the first preliminary study when running a porcine knee for 1800 cycles. This behaviour may limit potential simulation duration for stair ascent using displacement control as continuing creep would result in non-physiological motion or simulation failure. Additionally, the varus orientation may cause excessive loading in the medial compartment of the tibiofemoral joint and initiate damage. Hence, creeping of the adduction-abduction axis may limit the clinical relevance of results.

### 6.9.1 Limitations

The main limitation of the current study was the small samples size (n=3); there was significant variability between samples therefore confidence in the spring constraint method to generate repeatable results using porcine knees is limited. Variability could potentially have been introduced by the samples or the equipment. However, as previously mentioned (Chapter 2), the simulator was calibrated and verification checks with polyethylene and metal components were performed prior to experiments to confirm the simulator was functioning as expected. Therefore, the variability is more likely due to variation between the porcine knee joint samples. During the final study it would have been beneficial to also simulate the deep squat motion, however, due to the potential for simulation failure to initiate damage and compromise further investigations it was not included. Further optimisation of spring constraints may enable this motion to be simulated.

## 6.10 Conclusions

- It was possible to simulate a porcine knee using a single spring constraint for three different activities of daily living and transition between the motions whilst maintaining acceptable demand following; however this approach showed limited repeatability

    - Porcine knees may require knee specific and profile-specific spring constraints to ensure acceptable demand following can be achieved. Constraint of the anterior-posterior axis alone may be insufficient to enable simulation of more complex motions

- It was possible to consistently simulate stair ascent on porcine knee joints using displacement control, however, creep of the adduction-abduction axis during the simulation led to a change in the loading on the joint which could potentially lead to instability or initiate damage during longer testing

    - When applying the stair ascent motion to a porcine knee joint simulation duration may have to be limited due to creep of the adduction-abduction axis

- The large shear forces generated at the transition between outgoing and incoming profiles when using looped profiles may initiate wear, damage and deformation of articulating surfaces.

# Chapter 7

# Wear, damage and deformation of porcine osteochondral allografts and decellularised porcine osteochondral allografts during activities of daily living

## 7.1 Introduction

Osteochondral autografting and allografting are the gold surgical techniques used to repair focal cartilage lesions in the tibiofemoral joint and have shown good long term results in some patients (Hangody et al., 2008) (Torrie et al., 2015) (Keszég et al., 2022). The advantage of these approaches is they restore the articular hyaline cartilage surface. However, both interventions have existing issues, including quality and availability of replacement tissue, incongruence between donor graft and host cartilage, donor-site morbidity (autografting) and potential immunological or pathogen transmission complications (allografting) (Bowland et al., 2015).

Various natural and synthetic scaffolds have been investigated as replacements for osteochondral grafting. However, natural biomaterials often have insufficient mechanical properties and synthetic approaches have poor cellular interaction which limits successful tissue remodelling and graft integration (Niu et al., 2023).

Decellularised osteochondral allografts offer a potential solution to the existing issues of osteochondral grafting techniques but currently lack *in vitro* evidence to support their clinical use. To be accepted as a viable alternative to the established gold standard, decellularised grafts must demonstrate efficacy and comparable mechanical and tribological performance to osteochondral allografts/autografts. During this study the work of the previous studies was combined to simulate porcine osteochondral allografts and decellularised porcine osteochondral allografts under more physiologically relevant conditions. This involved using an optimised lubricant (Chapter 3), extending the test duration (Chapter 4) and applying kinematic conditions (Chapter 6) with more challenging loads than previously attempted. Analysis of wear, damage, deformation and graft stability was then performed incorporating a method validated for replicating cartilage surfaces after extended duration simulations (Chapter 5).

## 7.2 Aims and Objectives

### 7.2.1 Aim:

- To compare the mechanical and tribological performance of decellularised porcine osteochondral allografts to porcine osteochondral allografts during simulated activities of daily living

### 7.2.2 Objectives:

- To implant osteochondral interventions into porcine knees and run 47-hour simulations of walking gait and additional 1-hour simulations of stair ascent in a 6 DoF knee simulator using a 25% NBCS in Ringer's Solution lubricant
- To quantify the extent of wear, damage and deformation to the articulating surfaces (cartilage of femoral condyle and tibial plateau and menisci) within the tibiofemoral joint based on ICRS/Osteoarthritis Research Society International (OARSI) grading for the cartilage and meniscus
- To qualitatively assess structural changes (e.g. sub-surface cartilage delamination) and GAG content of cartilage and menisci using histological staining and optical microscopy
- To assess stability of osteochondral interventions within the recipient site by quantifying changes in graft/pin position at different stages of the simulation
- To assess kinetic and kinematic outputs to determine whether physiological motion was maintained during simulations

## 7.3 Hypotheses

The hypotheses for this study were:

- Decellularised osteochondral allografts would perform comparably to osteochondral allografts in terms of wear, damage and deformation (similar ICRS/OARSI grading and evidence of histological changes) as they were structurally similar
- Decellularised osteochondral allografts would perform comparably to osteochondral allografts in terms of stability within the recipient site (ability to resist displacement of the graft from the originally implanted position) as they were structurally similar

- Applying a stair ascent input profile to a porcine knee would result in more wear, damage and deformation (higher ICRS/OARSI grading and evidence of histological changes) than walking gait for all experimental groups due a higher maximum load, and longer duration for which an elevated load is applied

## 7.4 Experimental Design

### 7.4.1 Sample Preparation

Porcine knee joints (n=9) were prepared to be mounted into the knee simulator as previously described, including the procedure to minimise bacterial contamination (Chapter 2); these were defrosted overnight prior to simulation with each knee having undergone only a single freeze thaw cycle. Osteochondral allografts and decellularised osteochondral allografts were removed from the freezer and defrosted in a warm water bath on the day prior to simulation. All allografts and decellularised allografts experienced a single freeze-thaw cycle before testing (decellularised allografts had previously experienced an additional four freeze-cycles as part of the decellularisation process).

### 7.4.2 Experimental Groups

Knees were allocated into one of three experimental groups (Table 7.1). The two intervention groups and positive control group each had an osteochondral graft or steel pin inserted into the medial femoral condyle within the contact region. All grafts/pins were cylindrical with a diameter of 6.5mm. The lateral compartments of three knees (one from each experimental group) acted as untreated negative controls. Knees were simulated and wear, damage and deformation assessed using a method based on the ICRS/OARSI (Table 7.2) scoring criteria. Post-test knees were wrapped in PBS-soaked paper towels, sealed in plastic bags and stored frozen at -20°C. These were defrosted and graded again before histological processing.

**Table 7.1: Experimental groups for allograft and decellularised allograft comparison study.**

| Experimental group | Sample number (n) | Compartment |
|---|---|---|
| Osteochondral Allografts | 3 | Medial |
| Decellularised Osteochondral Allografts | 3 | Medial |
| Stainless Steel Pins (Positive Controls) | 3 | Medial |
| No intervention (Negative Controls) | 3 | Lateral |

**Table 7.2: Grading system form meniscal damage based on OARSI system.**

| OARSI grade | Changes observed |
|---|---|
| 0 | Faint striations, absence of tearing, deformation or discolouration |
| 1 | Dark/thick striations, no or partial tearing, deformation, discolouration |
| 2 | Complete or non-complex tearing, absence of or limited degeneration |
| 3 | Complex tearing, moderate degeneration |
| 4 | Complete structural loss |

### 7.4.3 Experimental Setup

Knees were placed into the simulator with the flexion-extension arm positioned at 0° flexion and a mark was made on the medial side of the medial femoral condyle in the centre of the contact region using a tissue marking pen. The knee was then flexed to ~21°, the maximum flexion value experienced during the simulations, and a second mark was made. These marks provided guidelines to identify the contact region when drilling osteochondral graft sites. The gaiter was filled with 25% NBCS in Ringer's Solution lubricant and knees were subjected to a 15-minute trial simulation using the 2-peak walking gait profile (Table 7.3) to ensure they were capable of running successfully in the simulator. These were then removed from the simulator and a 6.5mm x 10mm osteochondral graft site was created within the contacting region of the medial femoral condyle using the 6.5mm Accufex drill bit. Graft length (9 ± 1 mm) was measured with callipers and electrical tape was added to the drill bit just above the 10mm line to indicate drill depth, as the engraved marking were not visible when the drill rotated. The base of

the hole was flattened using a tamp tool and measured with callipers to check the graft/pin length and recipient site depth matched to ensure a bottomed graft and a congruent articular surface. If the hole was too shallow, additional drilling was performed, if the hole was too deep some of the removed subchondral bone was inserted into the hole and compacted using the tamp tool and the depth re-measured. Once a suitable recipient site had been created the grafts/pins were inserted. As in a previous knee simulation study (Bowland et al., 2018), this was done without dilation of the recipient site as previous work demonstrated dilation results in a loose interference fit between the graft and recipient site in immature porcine tissue (Bowland et al., 2020). Decellularised grafts and stainless-steel pins were inserted by manual pressure using the thumb whereas allografts were hammered into place with a mallet and the tamp tool.

### 7.4.4 Kinetic and Kinematic Input Profiles

Knees were simulated using the displacement controlled walking gait and stair ascent profiles based on findings from Chapter 6 (Table 7.3). Chapter 4 showed the initiation position of the anterior-posterior displacement varied for each knee. The anterior-posterior displacement waveform was shifted 1mm anteriorly during the current study as this most closely matched the initiation position for porcine knees with all the ligaments still attached (Liu et al., 2019). Prior to simulations a static axial force was applied to each knee joint to determine if knees displaced in a particular direction. One sample moved posteriorly when load was applied therefore the anterior-posterior displacement waveform was shifted 0.5mm posteriorly in an effort to generate more physiological motion.

**Table 7.3: Kinetic and kinematic inputs for walking gait and stair ascent.**

| Axis | Walking Gait | | Stair Ascent | |
|---|---|---|---|---|
| | **min** | **max** | **min** | **max** |
| Axial Force (N) | 63.6 | 984.7 | 201.5 | 1515.5 |
| Flexion-Extension Rotation (°) | 0 | 21.7 | 0 | 21.3 |
| Abduction-Adduction Rotation (°) | free | free | free | free |
| Internal-External Rotation (°) | -1.6 | 1.6 | -1.8 | 1.8 |
| Anterior-Posterior Displacement (mm) | -5.3* | 0.5* | -4.3 | 0 |

Simulations consisted of 47 hours walking gait followed by 1 hour of stair ascent. Previous research used an optimised anterior-posterior spring constraint to replicate ligament function during walking gait in the porcine knee joint (Liu et al., 2019). Therefore, the values used for the anterior-posterior displacement during walking gait were based on displacements generated by a porcine knee used during the 48-hour knee simulator study (Chapter 4). The 47-hour simulation length was chosen as the study in Chapter 4 demonstrated knees suffered minimal wear damage and deformation over this timeframe. Stair ascent simulation length was chosen to be representative of how much time people spend ascending stairs in 48 hours (Schwiesau, Schilling, Kaddick, et al., 2013); this was ~2 hours, however simulation length was limited to 1 hour due to concerns over the abduction-adduction axis creeping (Chapter 6).

### 7.4.5 Wear, damage and deformation (ICRS/OARSI grading)

Wear, damage and deformation to the articulating surfaces was assessed using a scoring system based on the ICRS grading criteria for the femoral and tibial cartilage and a system based on the OARSI for the meniscus. The femoral condyle and tibial plateau were divided into nine regions and the meniscus into three (Figure 7.1). For 8/9 samples the graft/pin was positioned in the centre of the grid on the medial femoral condyle. The femoral condyle of one knee was small and had a high degree of curvature, therefore one allograft graft had to be positioned in the lateral central region to provide congruent fit between the curvature of the graft and the curvature of the condyle. After visual inspection each region of the grid, including the graft was scored 0-4 based on the respective scoring criteria for the different tissues; the central region of the femoral condyle was not scored for the positive control group (stainless steel pins).

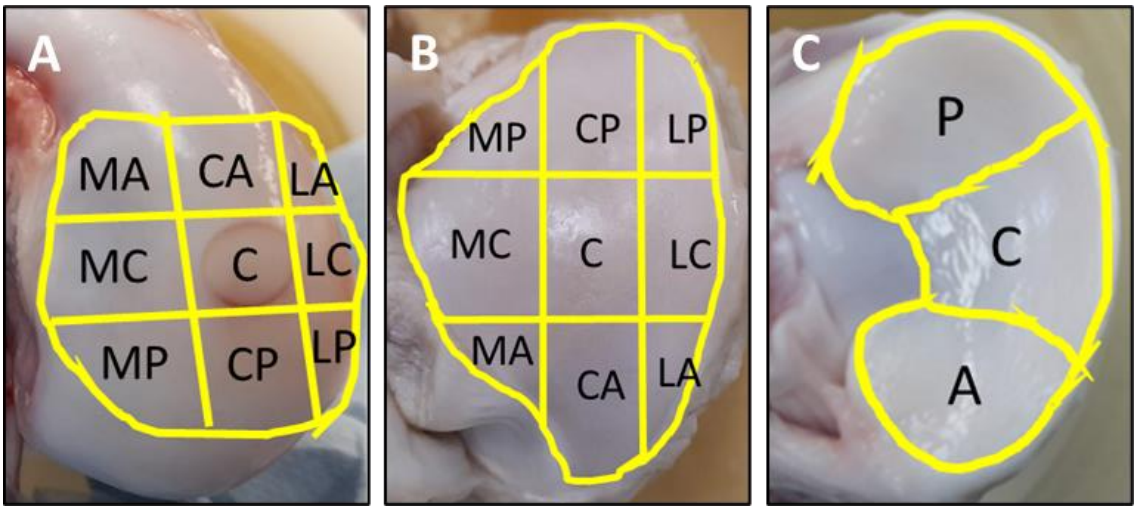


**Figure 7.1: Division of articulating surfaces into different regions to enable ICRS/OARSI grading. Femoral condyle (image A) and tibial plateau (image B) divided into nine regions: medial anterior (MA), medial central (MC), medial posterior (MP), central anterior (CA), central (C), central posterior (CP), lateral anterior (LA), lateral central (LC) and lateral posterior (LP). Meniscus (image C) divided into three regions: anterior (A), central (C) and posterior).**

During experiments cartilage/meniscus grading was conducted at three separate time points: 1) post-graft/pin insertion (t=0 hours), 2) post-walking gait (t=47 hours), 3) post-stair ascent (t=48 hours). It was not possible to score the lateral tibial plateau as the membranous attachments of the lateral meniscus prevented the meniscus from being lifted. At a later date (~6 weeks after the first simulation) all knees were defrosted and re-graded (the lateral tibial plateau was scored at this stage). Inspecting samples a second time allowed a side-by-side comparison of each knee and enabled the changes observed to be more accurately allocated the correct grade. It also enabled a qualitative assessment if changes previously observed were likely to be deformation as opposed to permanent wear or damage. Where results of the second grading contradicted initial scoring, the grade assigned at the second check was accepted as the value e.g. if a section of the meniscus was graded 2 post walking gait but graded 1 at the final check, the grade assigned would be 1. At all stages scoring was completed by two assessors who had to agree on the values assigned to each region.

When analysing ICRS/OARSI grading data two approaches were used to more fully describe what had happened. In the first approach, all the values in the grid were totalled to give a score for the whole articular surface, 0-36 for femoral condyles and tibial plateau and 0-12 for the meniscus; this provided a measure of how widespread wear, damage and deformation were. In the second approach, the highest grade was selected to

represent the condition of the particular articulating surface; this provided a measure of the severity of acute damage.

### 7.4.6 Measurement of graft/pin stability (Alicona)

Once ICRS/OARSI grading had been completed at each time point, Accutrans silicone replicas were created of the medial femoral condyles in the region of the graft/pin. These replicas were scanned using the Alicona Infinite Focus optical profiler to generate a 3D dataset which could be analysed. The position of the graft/pin within the recipient site was assessed pre-experiment (t=0 hours), post walking gait (t=47 hours) and post stair ascent (t=48 hours) to determine the stability of the interventions (i.e. ability to resist displacement). This was achieved by measuring the height difference between the graft surface in relation to the femoral condyle surface at eight locations around the circumference of the recipient site (Figure 7.2). Traces drawn across the graft surface calculated the mean of the points over the width of the trace to produce a 2D image. Crosshairs were then positioned onto the 2D image (Figure 7.3) to enable the relative height difference between the femoral condyle and graft/pin surfaces at each point to be calculated by the Alicona analysis software. The mean relative height difference of the eight points around the circumference was then calculated to describe quantitatively how graft/pin position had altered throughout the experiment (positive=proud, negative=subsided). In some instances, air bubbles in the AccuTrans replicas created voids in the 2D images (Figure 7.3), for these situations crosshairs were placed onto the nearest available surface to enable a measurement to be taken. To visualise the initially implanted orientation and subsequent changes in graft/pin position within the recipient site and changes to articulating surfaces, pseudo-colour images were generated to enable comparison of the different experimental groups.

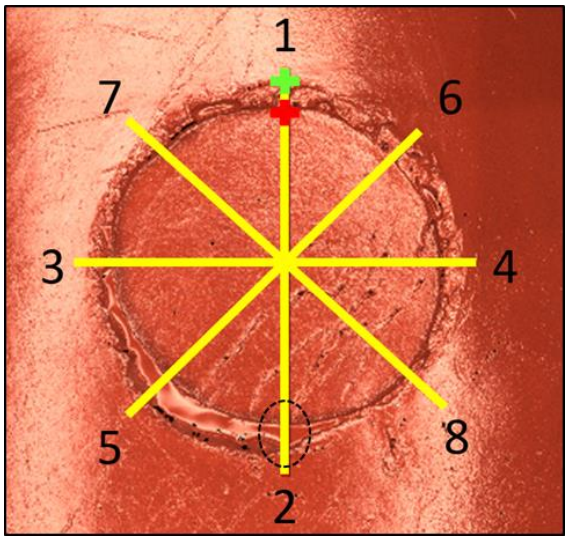


**Figure 7.2: Traces (yellow lines) drawn across the graft/pin surface to enable relative height difference between the femoral condyle and graft/pin to be measured. Eight measurement points around the circumference were selected on the femoral condyle (green cross) and graft/pin (red cross). Void in replica on femoral condyle surface (black dotted oval).**

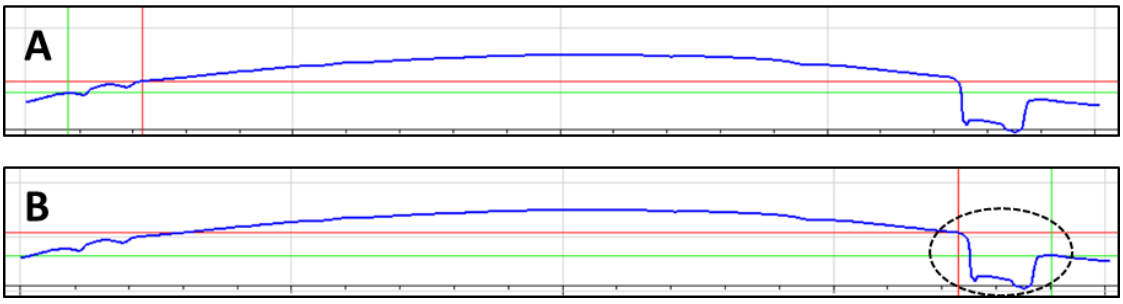


**Figure 7.3: Placement of red and green crosshairs on 2D trace corresponding to position 1 in Figure 2 (A). Placement of red and green crosshairs on 2D trace corresponding to position 2 in Figure 2 (B). Void present in femoral surface replica for position 2 due to air bubble in replica (B - black dotted oval).**

### 7.4.7 Histological Sample Preparation

Immediately after re-grading of simulated knees, femoral, tibial and meniscal tissue samples were harvested for histological processing. Osteochondral sections of the post-test femoral condyle and tibial plateau were removed from the contact regions of each knee with a hacksaw and trimmed with a scalpel (Figure 7.4). Medial femoral condyle samples were cut to ensure there was a suitable region around the pin/graft from which to visualise the graft position in relation to the surface of the condyle; these samples

were cut to sufficient depth so assessment of graft position within the base of the recipient site could be made. For the stainless-steel pin group, the pins were removed to enable histological processing, so only the condition of the recipient site could be assessed. Pins were removed from osteochondral sections by creating a hole in the base with a small diameter drill bit and pushing them out (Figure 7.4). The menisci were cut at the roots and a section of the contact region removed using a scalpel. All samples were bisected to create an 'A' sample and 'B' sample for each tissue, these were compared to support or reject the legitimacy of any wear, damage and deformation observed and identify potential artefacts. Samples were then histologically processed before staining with H&E, picrosirius red and safranin-O as previously described (Chapter 2).

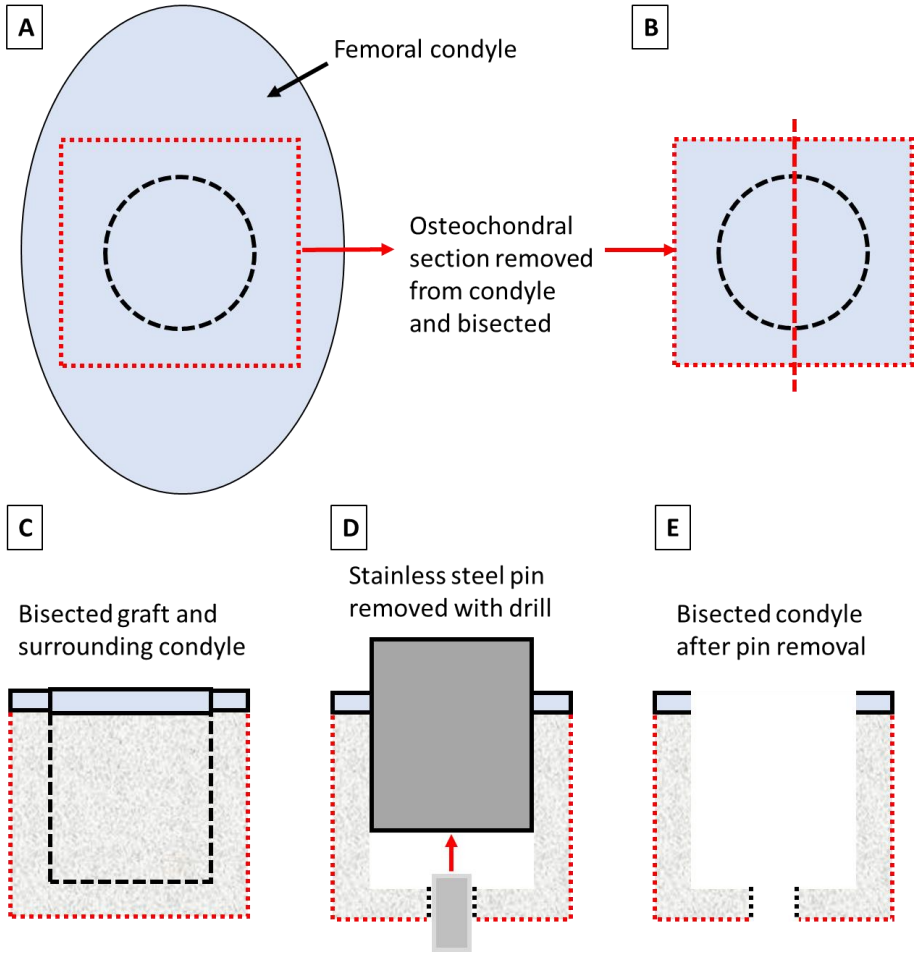


**Figure 7.4: Removal of osteochondral graft and femoral condyle histological samples from the knee joint.**

### 7.4.8 Statistical Analysis

ICRS/OARSI data were not normally distributed. A non-parametric test, a Kruskal-Wallis* test with a post-hoc Dunn's test with Bonferroni correction was performed to assess statistical significance. *Minimum sample size for Kruskal-Wallis is meant to be n=5, each experimental group in this study only had n=3/4 samples. ICRS/OARSI data are reported as the mean grade for each experimental group with standard deviation.

Relative graft height data were normally distributed. A parametric test, a one-way ANOVA with a post-hoc Tukey HSD was used to assess statistical significance. Relative graft height data are reported as the mean value for each experimental group with 95% confidence limits.

A Shapiro-Wilk test was performed to assess if data were normally distributed, α was set at 0.05 and statistical significance was set at $p<0.05$ in all cases. All data analysis was carried out using IBM SPSS Statistics 26 for Windows.

## 7.5 Results

### 7.5.1 Wear, damage and deformation post 48-hour simulation

#### 7.5.1.1 Negative Controls

Mostly superficial changes were observed for the negative controls. Small scratches (Grade 1) were present on the femoral condyles of one sample, a shallow deformation (Grade 1) had formed in the meniscus of one sample and scratching/roughening (Grade 1) had occurred on the tibial plateau of two samples. One abnormal change, a deeper wear track/indentation (Grade 2) was observed on the tibial plateau of the remaining negative control. All negative controls were assigned ICRS/OARSI Grade 0 for the three articulating surfaces post walking gait. The highest ICRS/OARSI grades assigned post stair ascent were Grade 1 for femoral condyles and meniscus, and Grade 2 for the tibial plateau (Figure 7.5).

#### 7.5.1.2 Positive Controls

Superficial scratching/roughening (Grade 1) was present on the femoral condyles for all three samples. Severely abnormal changes were observed to the meniscus and tibial plateau for two samples. In each case this presented as a small 'Bucket-handle' tear in the meniscus (Grade 4) and a cartilage lesion penetrating into the subchondral bone of the tibial plateau (Grade 4) (Figure 7.6). The remaining sample experienced abnormal

changes to the meniscus, a deeper deformation/wear track (Grade 2) had formed and superficial scratching/roughening of the tibial plateau (Grade 1) was observed. For positive controls the highest ICRS/OARSI grades assigned post walking gait were Grade 1 for femoral condyles, Grade 3 for tibial plateau and Grade 4 for meniscus. The highest ICRS/OARSI grades assigned post stair ascent were Grade 1 for femoral condyles and Grade 4 for the tibial plateau and meniscus (Figure 7.5).

#### 7.5.1.3 Allografts and Decellularised allografts

The presentation of wear, damage and deformation was largely the same for allografts and decellularised allografts. In both experimental groups superficial scratching/roughening (Grade 1) was present on the femoral condyles and tibial plateau of all samples; shallow deformations (Grade 1) had formed in the meniscus of two samples and abnormal damage, a deeper deformation/wear track (Grade 2), had formed in the remaining sample. The only visual difference was decellularised allografts appeared more deformable than allografts. They were less circular than pre simulation (this was particularly pronounced for one sample), and two samples developed a ridge along one edge of the graft (Figure 7.9). For allografts and decellularised allografts the highest ICRS/OARSI grade assigned to all articulating surfaces was Grade 1 post walking gait (Figure 7.5). The highest ICRS/OARSI grades assigned post stair ascent were Grade 1 for the femoral condyle, graft and tibial plateau and Grade 2 for meniscus (Figure 7.5).

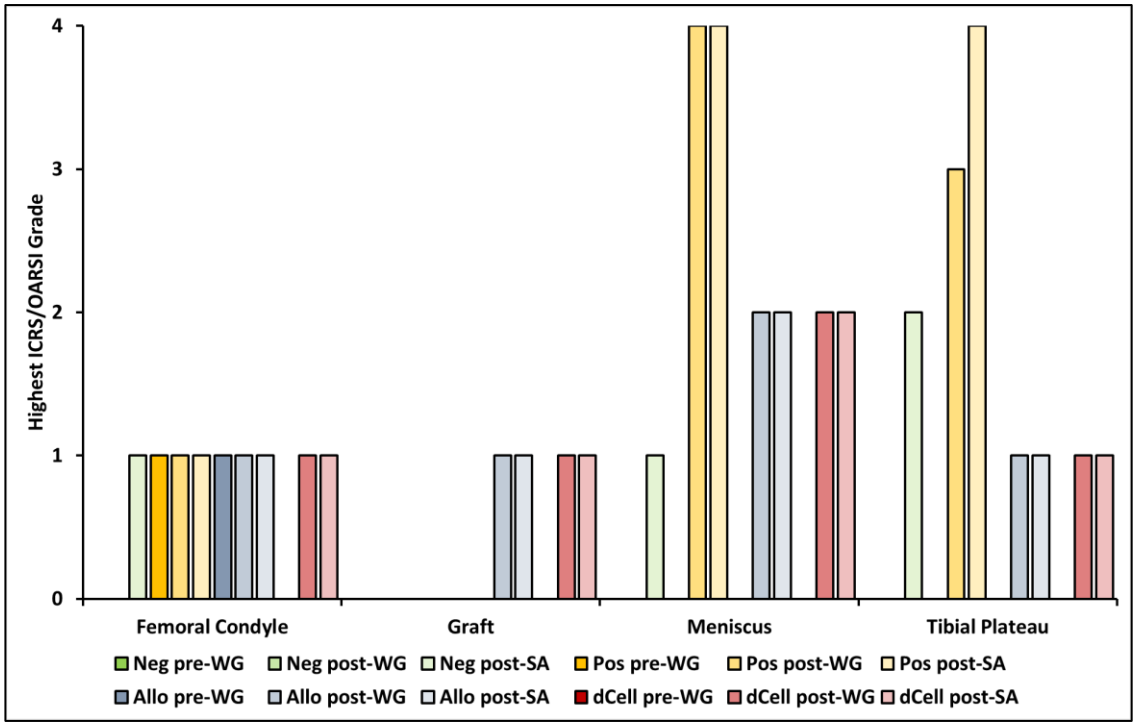


**Figure 7.5: Highest IRCS/OARSI grades assigned within experimental groups for each articulating surface pre walking gait, after 47 hours walking gait and after an additional 1-hour of stair ascent (total=48hrs). Femoral condyles, menisci, tibial plateau and graft scored 0-4. Neg = negative controls, Pos = positive controls, Allo = allografts, dCell = decellularised allografts, WG = walking gait, SA = stair ascent.**

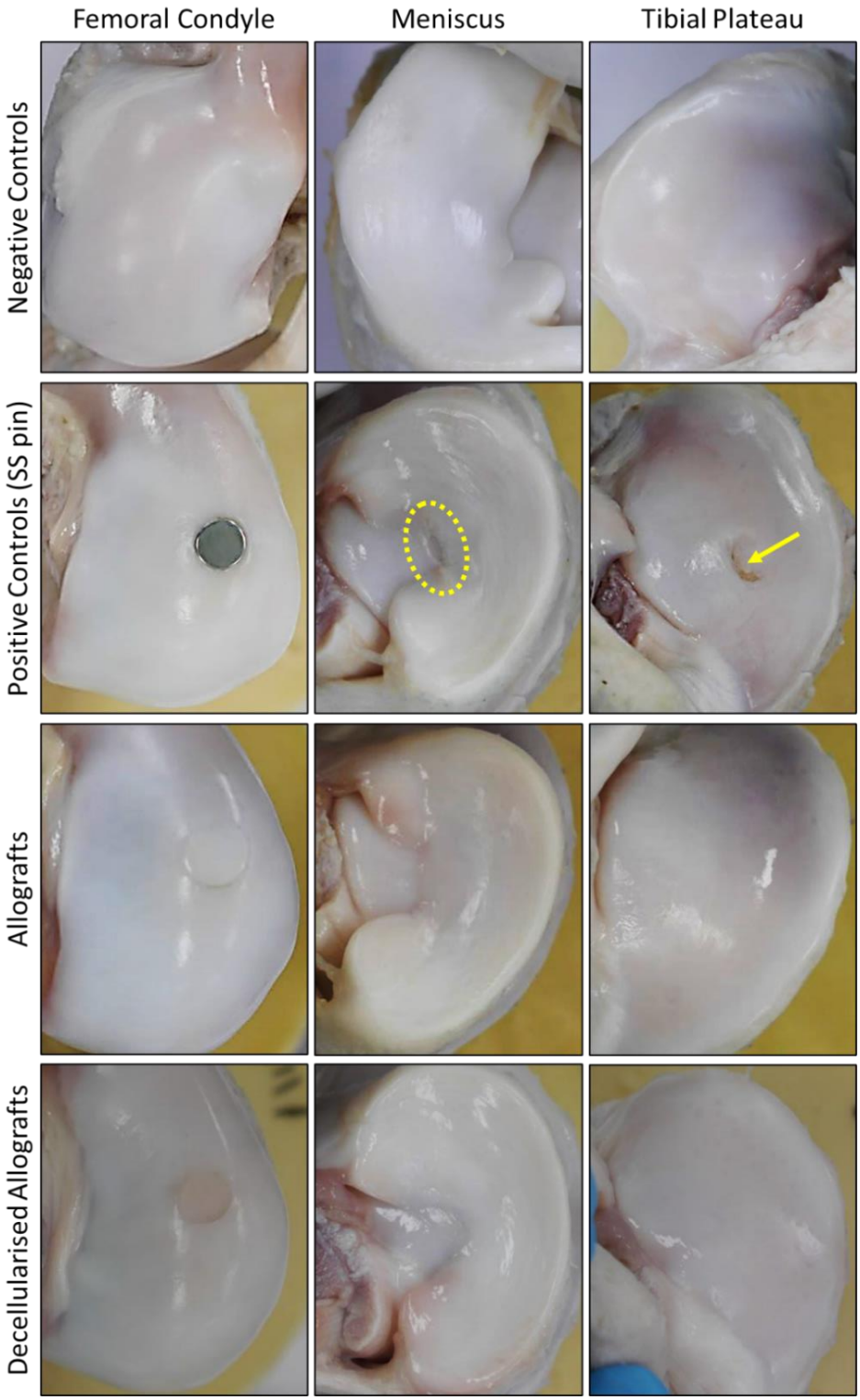


**Figure 7.6: Post-simulation representative images of each experimental group. Mostly superficial damage (ICRS/OARSI Grade 1) was observed within the allograft, decellularised allograft and negative control groups with some abnormal damage (ICRS/OARSI Grade 2). 'Bucket-handle' meniscus tears (yellow dotted circle) and chondral lesions which exposed subchondral bone in the tibial plateau (yellow arrow) (both ICRS/OARSI Grade 4) were observed within the positive control group.**

#### 7.5.1.4 Mean total ICRS/OARSI scores post walking gait

No changes in mean total ICRS/OARSI score were observed to any surface within the lateral compartment (negative controls) after 47-hours of walking gait. There was a trend of increasing mean total ICRS/OARSI score for all knees (n=9) containing grafts post walking gait (Figure 7.7). There were small increases in mean total ICRS score on femoral condyles and tibial plateaus for positive controls, allografts and decellularised allografts, but no statistically significant differences ($p>0.05$) between groups. The largest increases for femoral condyles and tibial plateaus were observed within the allograft and positive control groups respectively. For the meniscus a small increase in mean total OARSI score was observed for allografts and decellularised allografts and a large increase was observed for positive controls. When comparing mean total ICRS/OARSI scoring for the whole of each articulating surface, statistically significant differences were identified post walking gait between negative controls and allografts for the femoral condyle ($p=0.017$) and negative controls and positive controls for the meniscus ($p=0.013$).

#### 7.5.1.5 Mean total ICRS/OARSI scores post stair ascent

Application of an additional 1-hour of stair ascent increased mean total ICRS/OARSI scores for all experimental groups (Figure 7.7). There were small increases in mean total ICRS scores on the femoral condyles and tibial plateaus for all groups, but no statistically significant differences ($p>0.05$) between groups. The largest increases for femoral condyles and tbial plateaus was observed within the allograft and positive control groups respectively. For the meniscus there were small increases in mean total ICRS scores for all groups, but no statistically significant differences ($p>0.05$) between groups. Positive controls experienced no increase in mean total OARSI score after stair ascent. When comparing total ICRS/OARSI scoring for the whole of each articulating surface, statistically significant differences were identified post stair ascent between negative controls and positive controls for the meniscus ($p=0.026$).

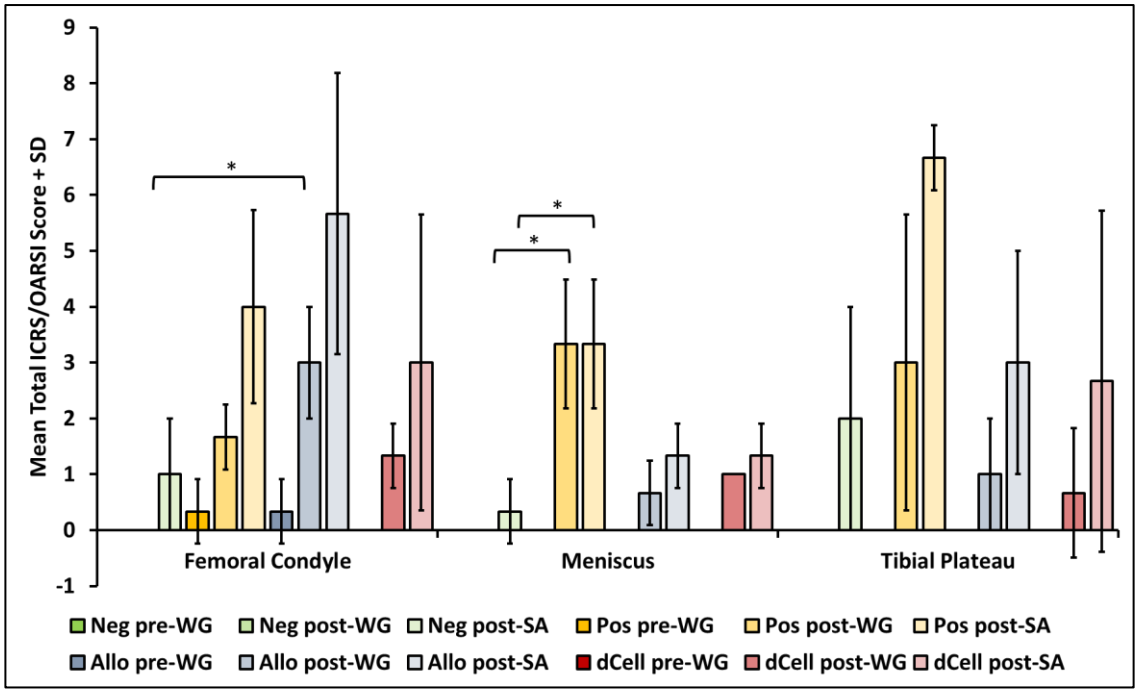


**Figure 7.7: Mean total IRCS/OARSI score assigned to each articulating surface + standard deviation pre walking gait, after 47 hours walking gait and after an additional 1 hour of stair ascent (total=48hrs). Neg = negative controls, Pos = positive controls, Allo = allografts, dCell = decellularised allografts, WG = walking gait, SA = stair ascent. Femoral condyles and tibial plateau scored 0-36, menisci scored 0-12. Statistical analysis for each articulating surface was performed using a Kruskal-Wallis test with post hoc Dunn-Bonferroni correction (* indicates statistical significance between: Neg post-WG and Allo post-WG for the femoral condyle (p=0.017), Neg post-WG and Pos post-WG for meniscus, (p=0.013), Neg post-SA and Pos post-SA for meniscus, (p=0.026)).**

### 7.5.1.6 Location of wear, damage and deformation

In the medial compartment most regions of the femoral condyle experienced some damage, whereas the negative controls were largely undamaged. For all experimental groups, meniscal damage was confined to the central region and damage to the tibial plateau was most frequently observed in the central and central anterior regions (Figure 7.8).

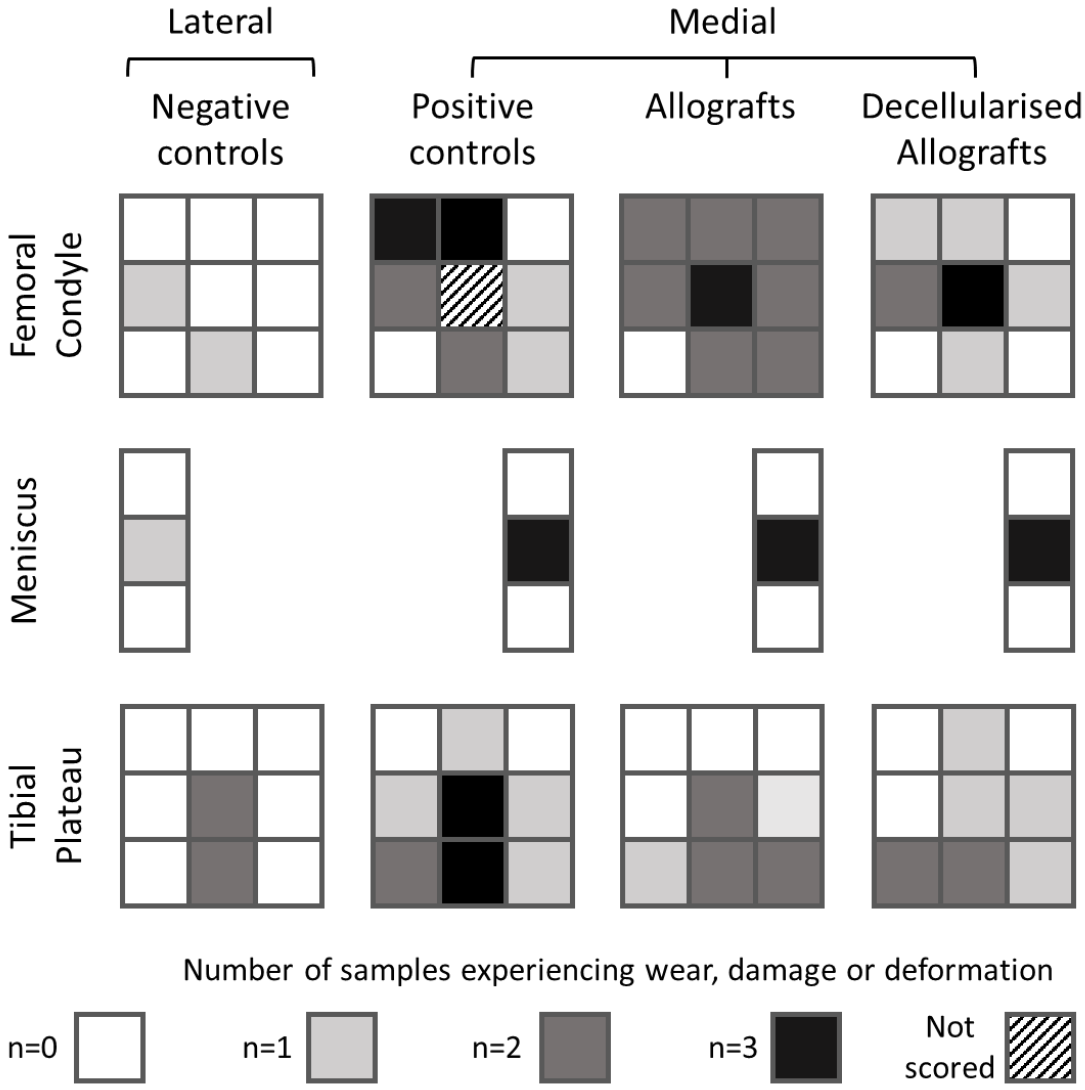


**Figure 7.8: Post-experimental condition of the articulating surfaces of each experimental group. Each grids represent the different regions of the articulating surfaces within the tibiofemoral joint scored during the ICRS/OARSI grading. The different colours represent the number of knees from each experimental group which experienced wear, damage or deformation in a particular region: n=0 (white), n=1 (light grey), n=2 (dark grey), n=3 (black). The hatched region in the centre of the femoral condyle of the positive control group represents the stainless-steel pins which were not scored during the grading.**

### 7.5.2 Graft/Pin Stability

The relative height between graft/pin cartilage and femoral condyle cartilage and the orientation of grafts/pins in relation to the femoral surfaces were visualised at the three different timepoints using pseudo-colour images generated from scanned silicone replicas (Figure 7.9). Initially positive controls (stainless steel pins) had a flat surface and allografts had a flat/domed surface. Decellularised grafts had sloped surfaces, some regions were proud of the femoral surface and others were level with, or subsided beneath, the femoral cartilage.

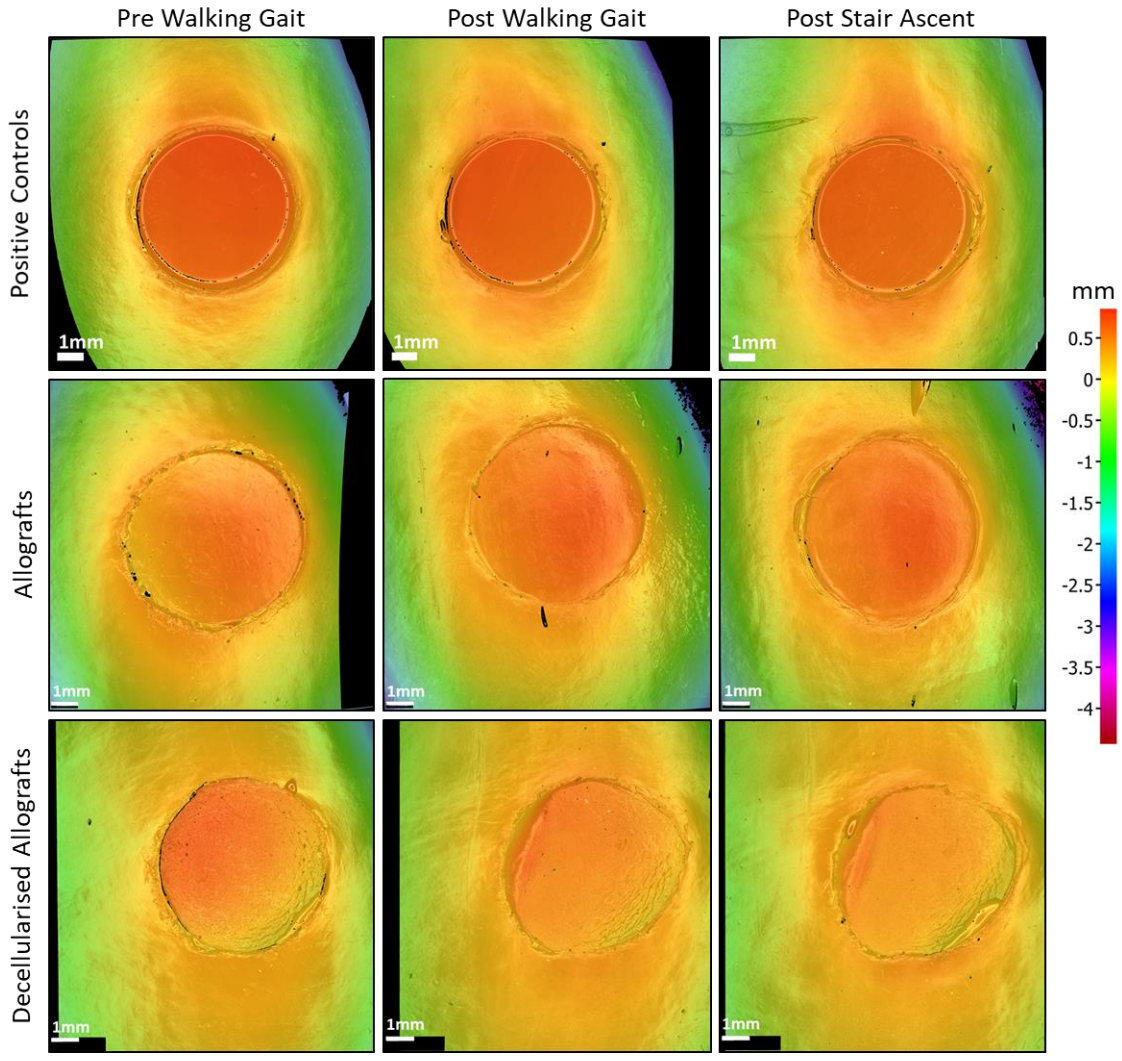


**Figure 7.9: Representative pseudo-colour images for positive control (top), allograft (middle) and decellularised allograft (bottom) experimental groups. The influence of simulations on graft position, orientation and shape can be inferred from the colour changes in the images (femoral surface, 0 = yellow/orange, proud = orange/red, subsided = yellow/green).**

Mean graft/pin height relative to the surrounding cartilage was plotted for each experimental group (Figure 7.10). Analysis of mean height data from the eight points around the recipient site showed positioning of each individual graft/pin (n=9) was initially slightly proud of the femoral condyle surface following implantation. Positive controls and allografts showed only small differences in relative height between the femoral cartilage and graft cartilage after both walking gait and stair ascent, suggesting minimal movement from the initial position. Decellularised allografts showed a change in relative height after walking gait and a further change after stair ascent; the decellularised grafts had subsided below congruence. Post walking gait there were no statistically significant differences in relative height between any of the groups. Post stair ascent there were statistically significant differences in relative height between positive controls and decellularised allografts (p=0.001) and between allografts and decellularised allografts (p=0.002).

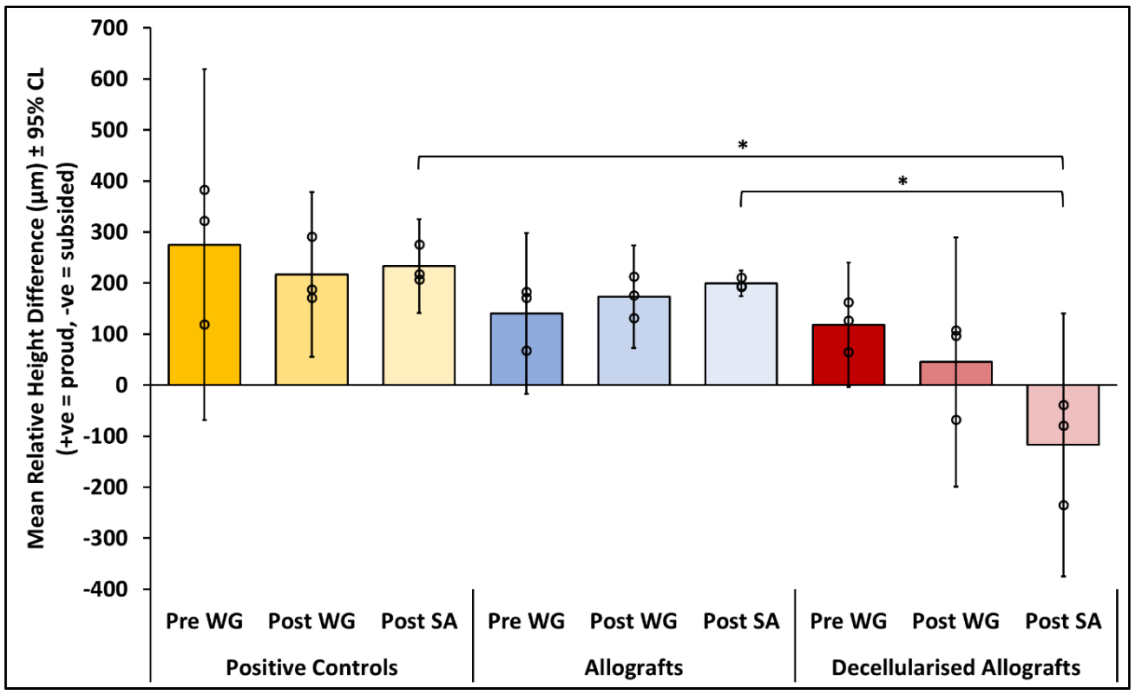


**Figure 7.10: Relative height difference between graft/pin and femoral condyle pre-walking gait (pre WG), after 47-hours of walking gait (post WG) and after 1-hour of stair ascent (post SA) for positive controls (orange), allografts (blue) and decellularised allografts (red). Bars are the mean of n=3 with 95% confidence limits; points on the bars represent the height value for the individual samples within each group. Statistical analysis was performed using a one-way ANOVA with post hoc Tukey HSD test (* indicates statistical significance, p<0.05).**

### 7.5.3 Histology

Results of histological staining for sections of femoral condyle, tibial plateau and meniscus to identify wear, damage and deformation were highly variable. Tissue samples (in most cases) had a total of six sections (three stains each with an ‘A’ sample and ‘B’ sample). Variability in both the presence and severity of damage was observed within the six sections for many samples (Figure 7.11). In all experimental groups some sections showed healthy cartilage, some showed small tears in or just below the superficial tangential layer and others showed large scale or complete delamination of the superficial tangential layer from the layers beneath.

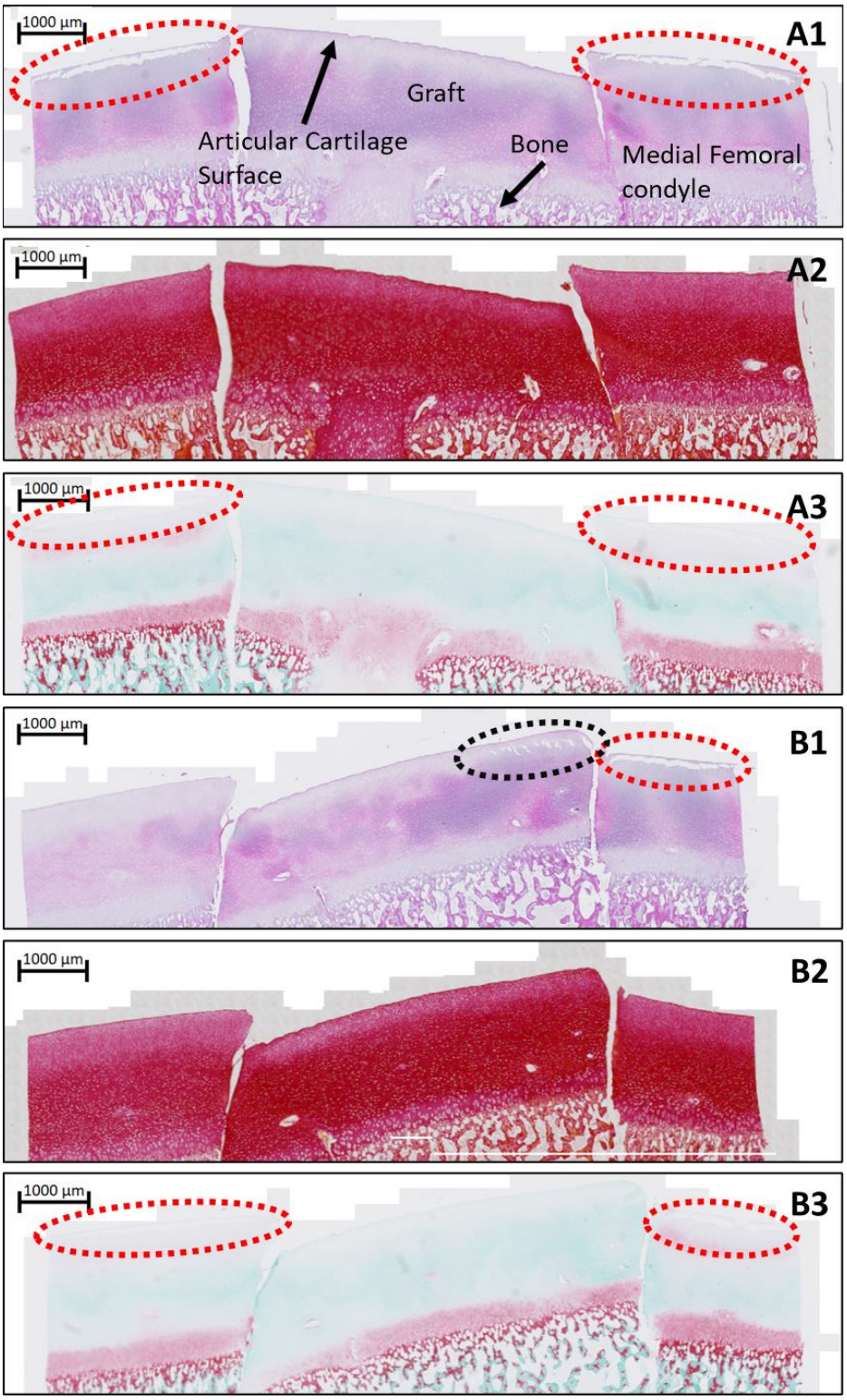


**Figure 7.11: Osteochondral graft and medial femoral condyle sections stained with Haematoxylin & Eosin (A1 and B1), Picrosirius Red (A2 and B2) and Safranin-O (A3 and B3). All sections from same sample (dCell 2) with an 'A' and 'B' section for each stain. It was not possible to confirm the cause of damage as there were inconsistencies between the severity and location of damage in different sections. Delamination or articular cartilage on femoral condyles (red dotted circles) and graft (black dotted circles).**

Based on histological staining of osteochondral samples, there were no clear qualitative differences between the severity of damage caused to allografts and decellularised allografts (Figure 7.12).

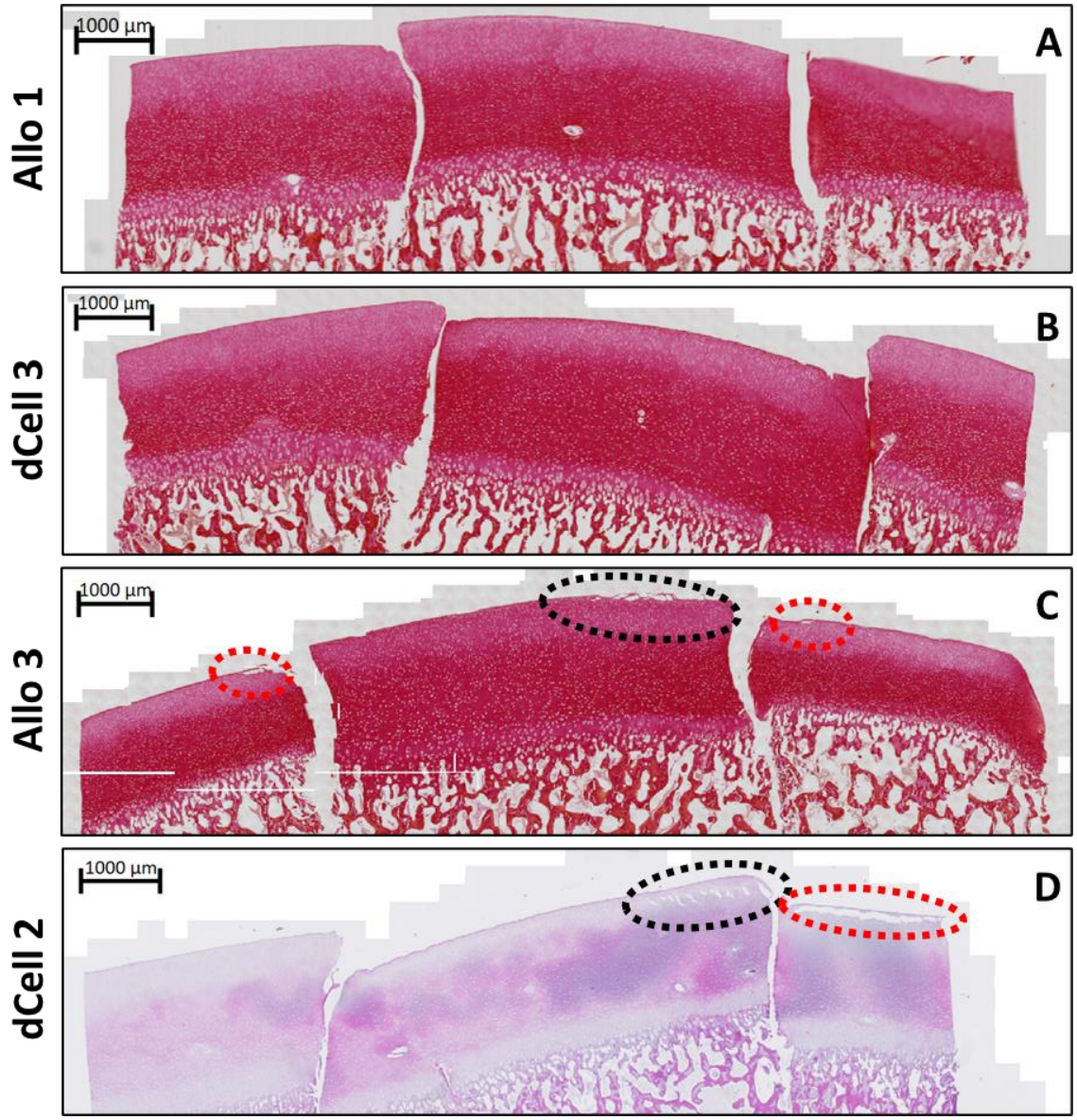


**Figure 7.12: Stained osteochondral graft and medial femoral condyle sections highlighting similarities between the allograft group and decellularised allograft group. Intact cartilage on both the graft and femoral condyle (A and B), evidence of delamination on both the graft (black dotted circles) and femoral condyles (red dotted circles).**

Representative composite histological images highlighted the typical condition of each experimental group post-simulation (Figure 7.13) (Figure 7.14) (Figure 7.15) (Figure 7.16). ‘Bucket-handle’ tears in the medial meniscus (OARSI Grade 4) and cartilage lesions which penetrated through into subchondral bone of the tibial plateau (ICRS Grade 4) were observed for two of the positive control group (Figure 7.14).

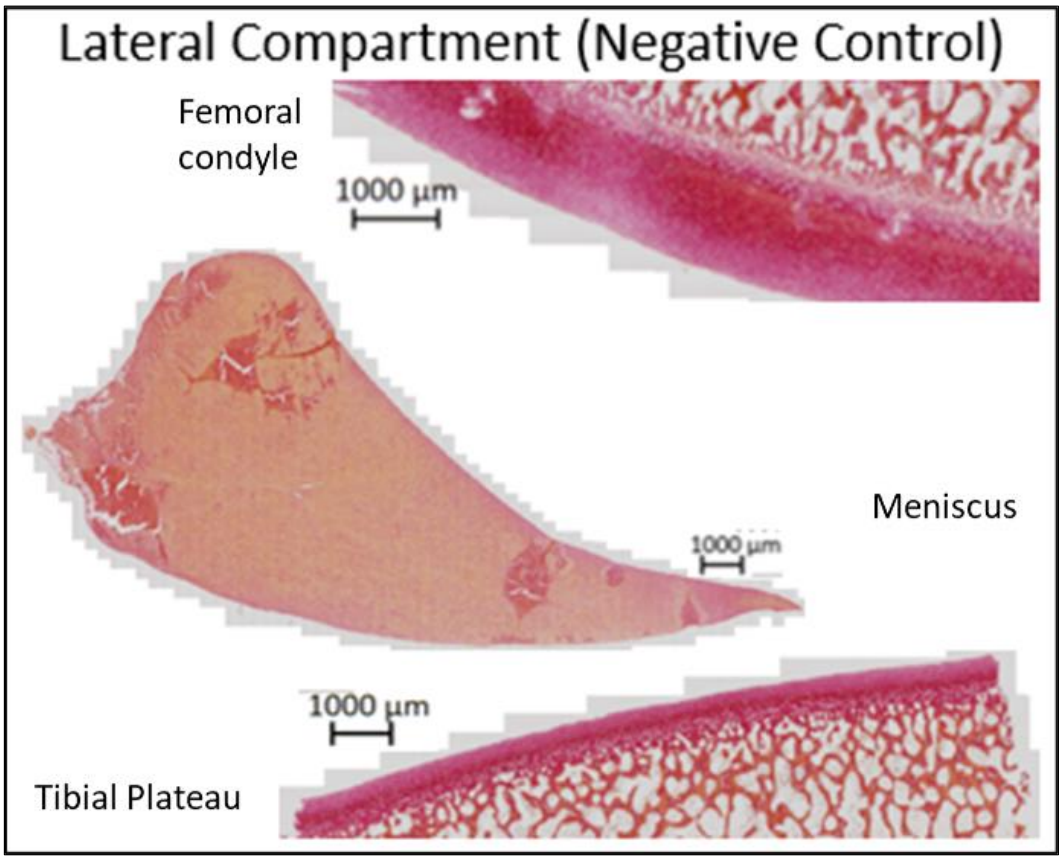


**Figure 7.13: Representative composite image of the typical condition of Negative Control group samples. Minimal damage to the femoral condyle, meniscus and tibial plateau was observed.**

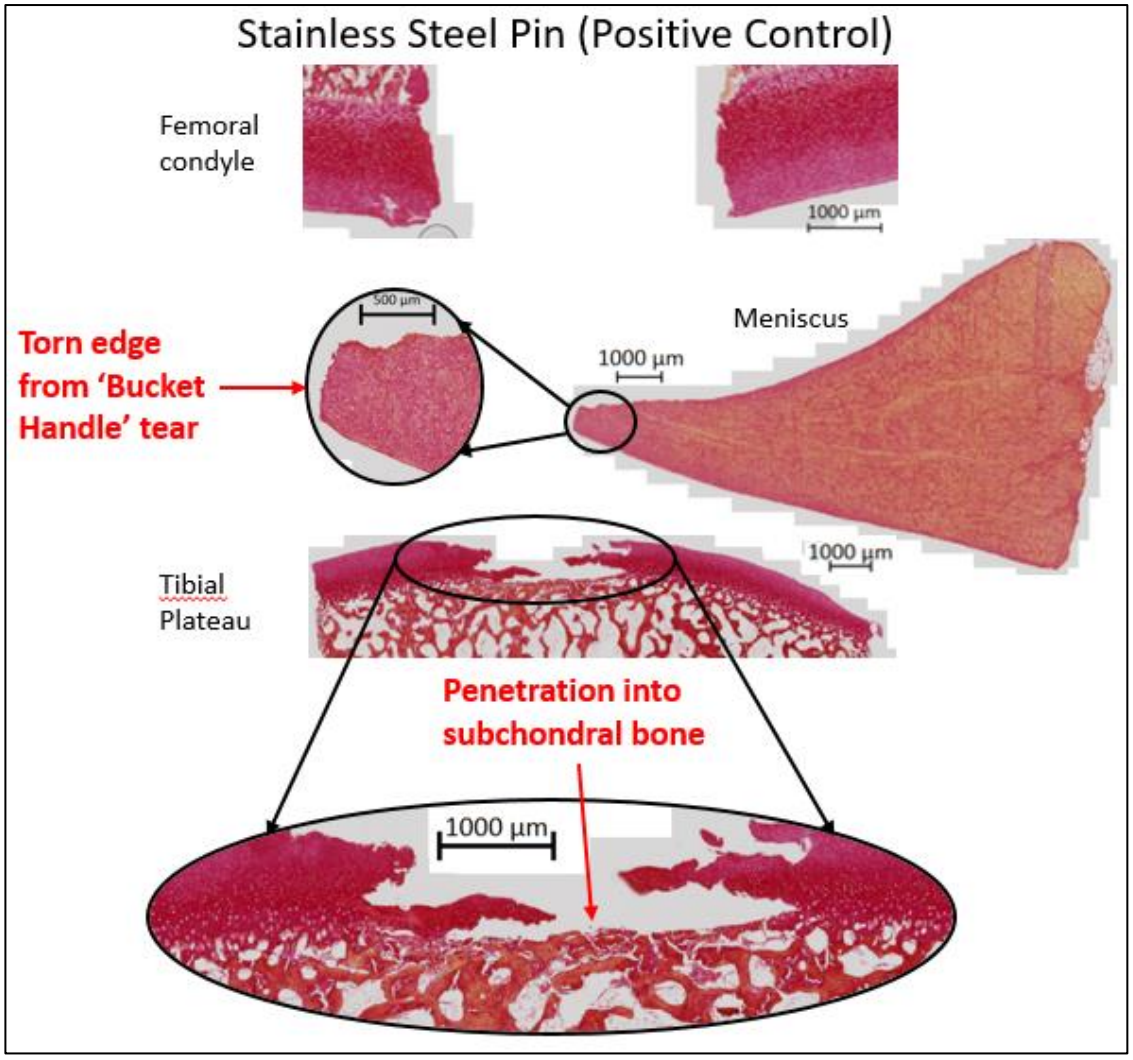


**Figure 7.14: Representative composite image of the medial compartment for positive controls. Minimal damage to the femoral condyle, 'Bucket Handle' tear of the meniscus and penetration into the subchondral bone of the tibial plateau.**

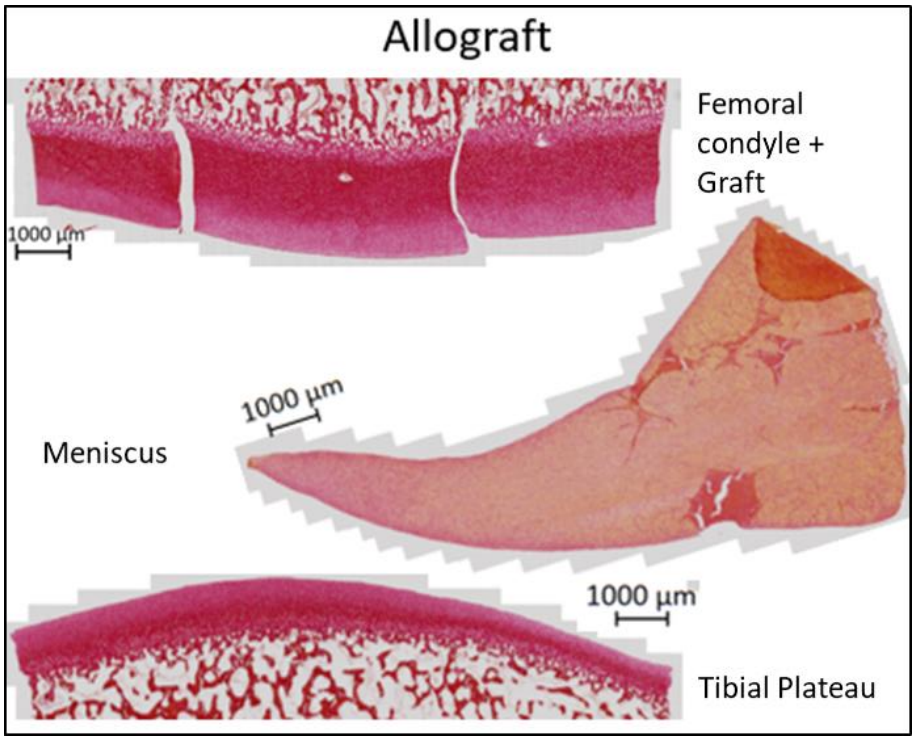


**Figure 7.15: Representative composite image of the typical condition of allografts. Minimal damage to the femoral condyle, meniscus and tibial plateau was observed.**

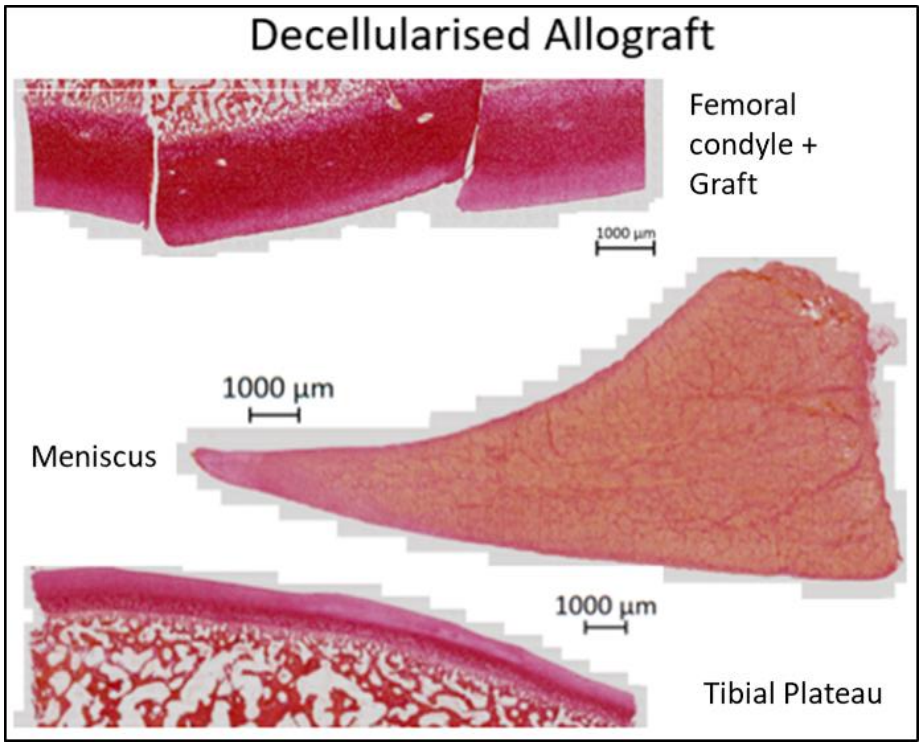


**Figure 7.16: Representative composite image of the typical condition of decellularised allografts. Minimal damage to the femoral condyle, meniscus and tibial plateau was observed.**

Safranin-O staining of post-experimental osteochondral samples indicated an absence of GAGs within the tissue for all experimental groups (Figure 7.17).

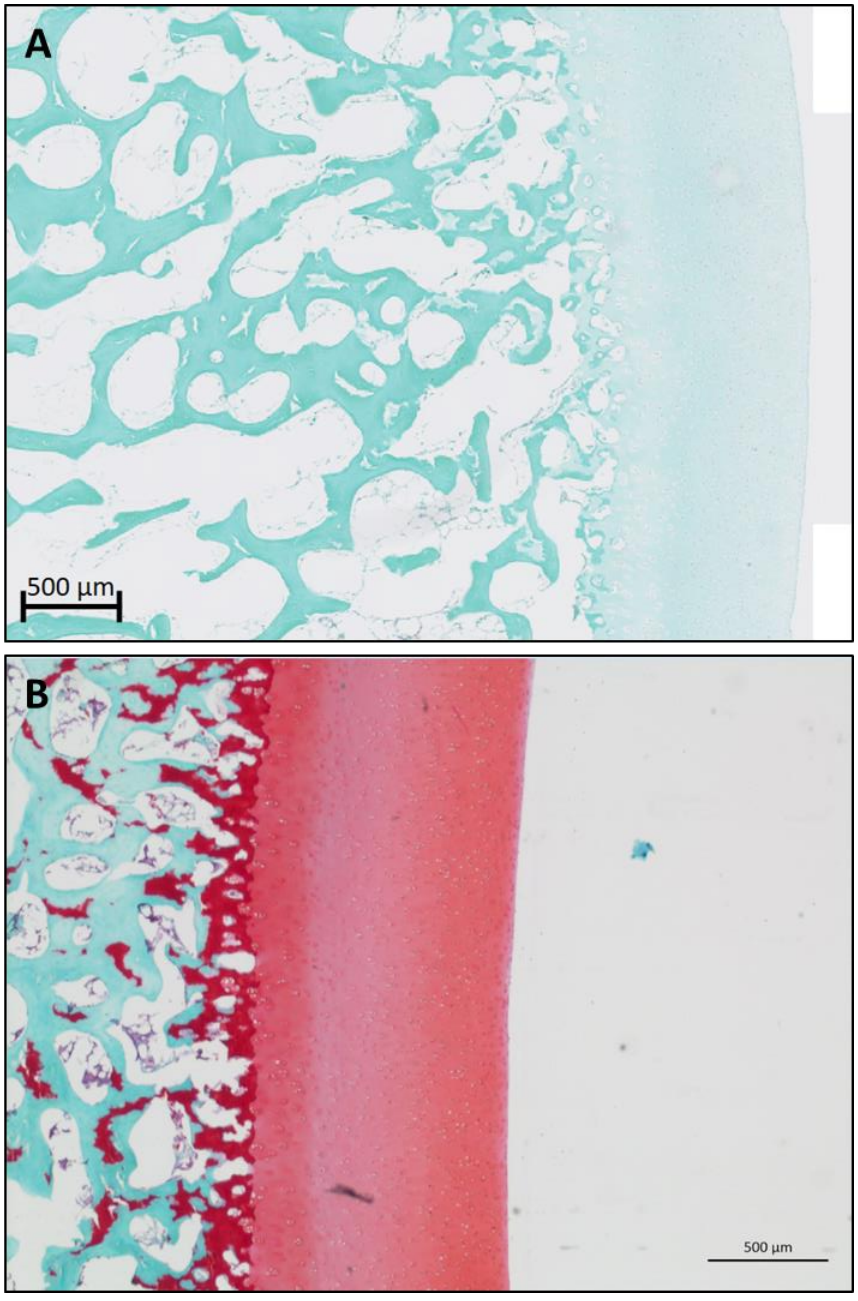


**Figure 7.17: Safranin-O staining of osteochondral sections of tibial plateau highlighting the GAG content of the tissues. A complete loss of GAGs (lack of red staining) was observed in the current study for all samples after 47-hours walking gait + 1-hour stair ascent (A). GAGs were retained within the tissue (red staining) during a previous study (Chapter 4) for all samples after 48-hours walking Gait.**

### 7.5.4 Kinetics and Kinematics

For walking gait and stair ascent, axial force and flexion-extension demand following was within the 5% tolerance throughout the cycle (5% of maximum value on each axis as recommended by ISO standards for wear assessment of knee replacements); the anterior-posterior following for stair ascent was also within the 5% tolerance throughout (Figure 7.18) (Figure 7.19). The anterior-posterior following for walking gait was within the 5% tolerance for the majority of the cycle for demand 1 (dCell 1 and dCell 2) and demand 2 (dCell 3) (Figure 7.18) (Figure 7.19). Internal-external (tibial) rotation demand following was within the 5% tolerance during some points of the cycle but outside the tolerance at other points for both motions (Figure 7.18) (Figure 7.19).

The abduction-adduction motions generated during simulations varied between samples for both motions. For walking gait, five knees adopted a fixed adducted position and four knees oscillated between an initially adducted position and a more adducted position. There was a trend for knees which oscillated to move into a more adducted position as the simulation progressed (Figure 7.20). This occurred for three out of four knees; there was no data at the later time point for the fourth oscillating knee. For stair ascent, four knees adopted a fixed adducted position and five knees oscillated between an initially adducted position and a less adducted position. There was a trend for knees (n=8) to move into a more adducted position as the simulation progressed (Figure 7.21). The observed adduction movement was greater in magnitude for walking gait but occurred over a much longer timeframe than for stair ascent (≤1mm in 46 hours compared to ≤0.5mm in less than 1 hour).

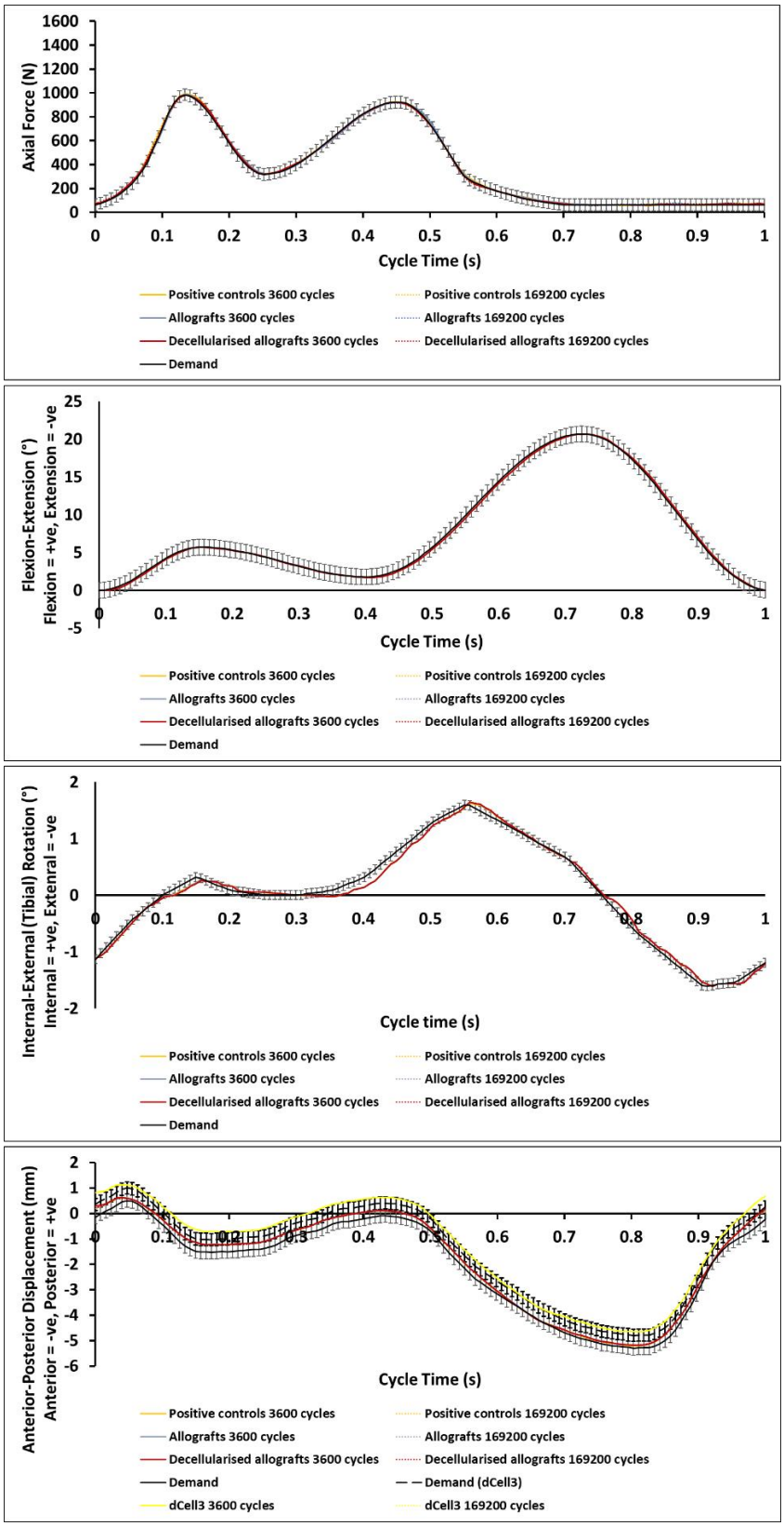


**Figure 7.18: Waveforms for each experimental group (mean of n=3*^) at 3600 cycles and 169200 cycles compared to the demand for walking gait. Error bars represent 5% of maximum value for each demand waveform. * n=2 at 3600 and n=1 at 169200 for decellularised allograft group. ^ Decellularised allograft 3 (n=1) waveform shifted 5mm posteriorly.**

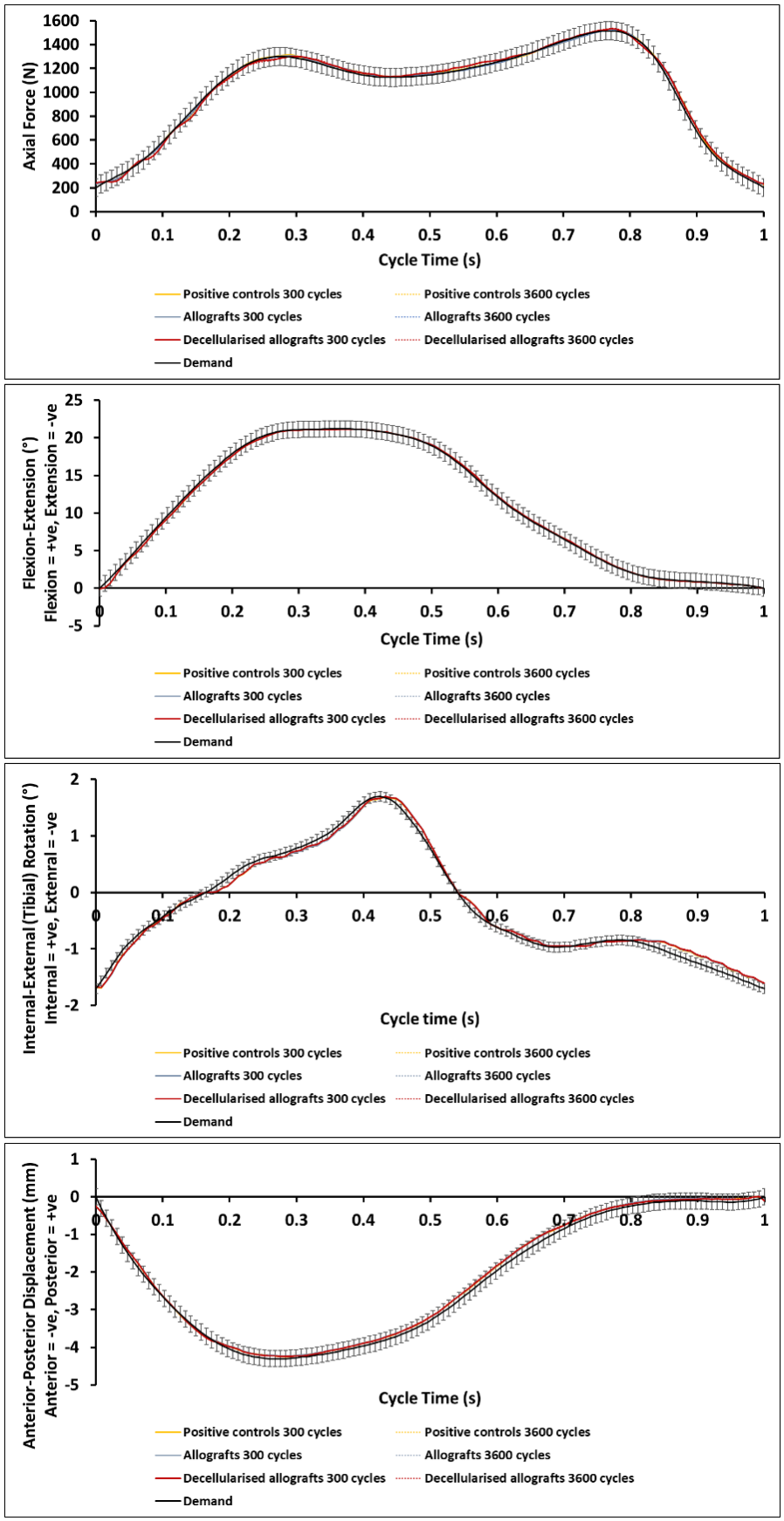


**Figure 7.19: Waveforms for each experimental group (mean of n=3) at 300 cycles and 3600 cycles compared to the demand for stair ascent. Error bars represent 5% of maximum value for each demand waveform.**

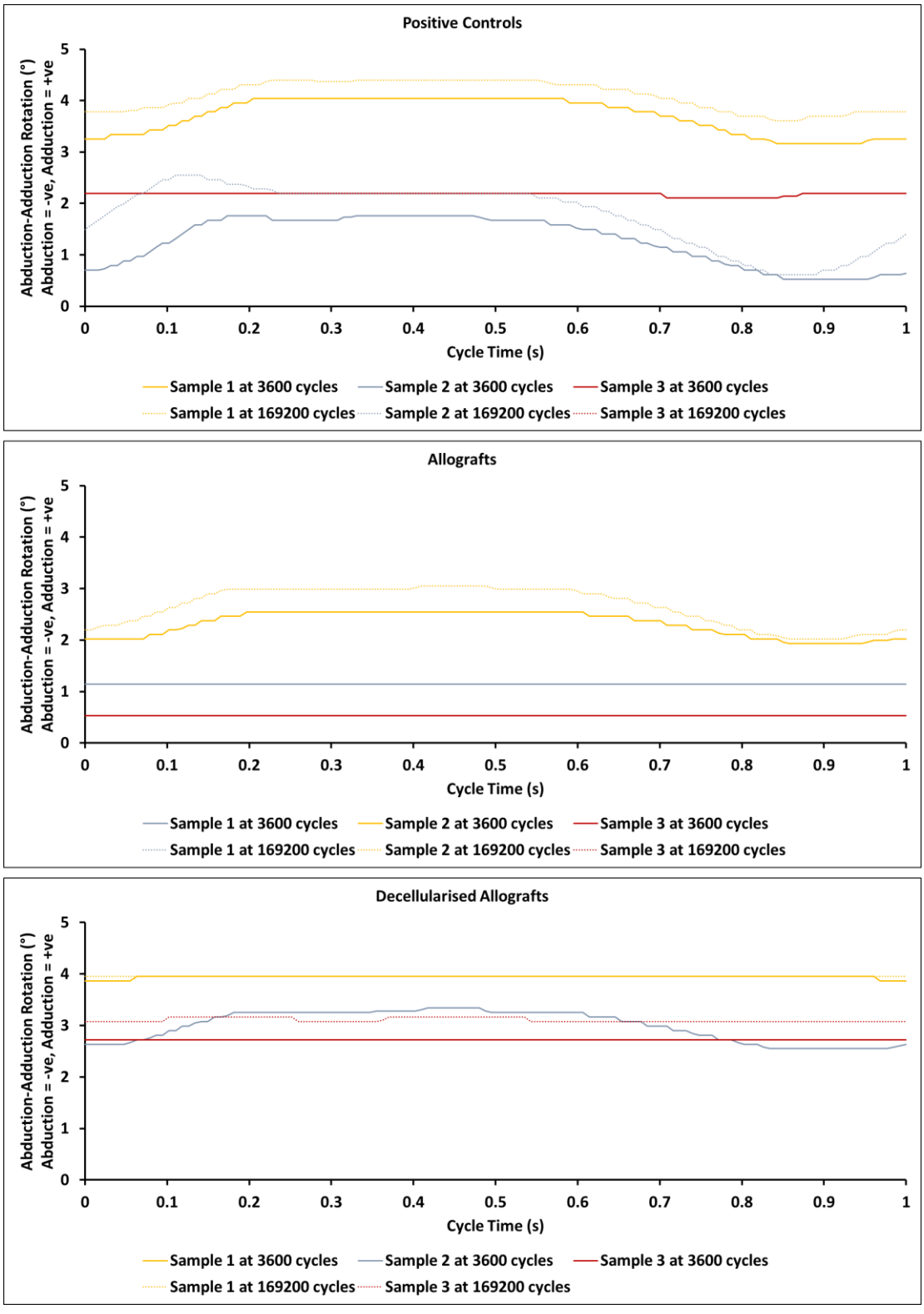


**Figure 7.20: Abduction-adduction rotation for samples in each experimental group at 300 cycles and 3600 cycles when applying walking gait. No data for dCell 2 at 169200 cycles.**

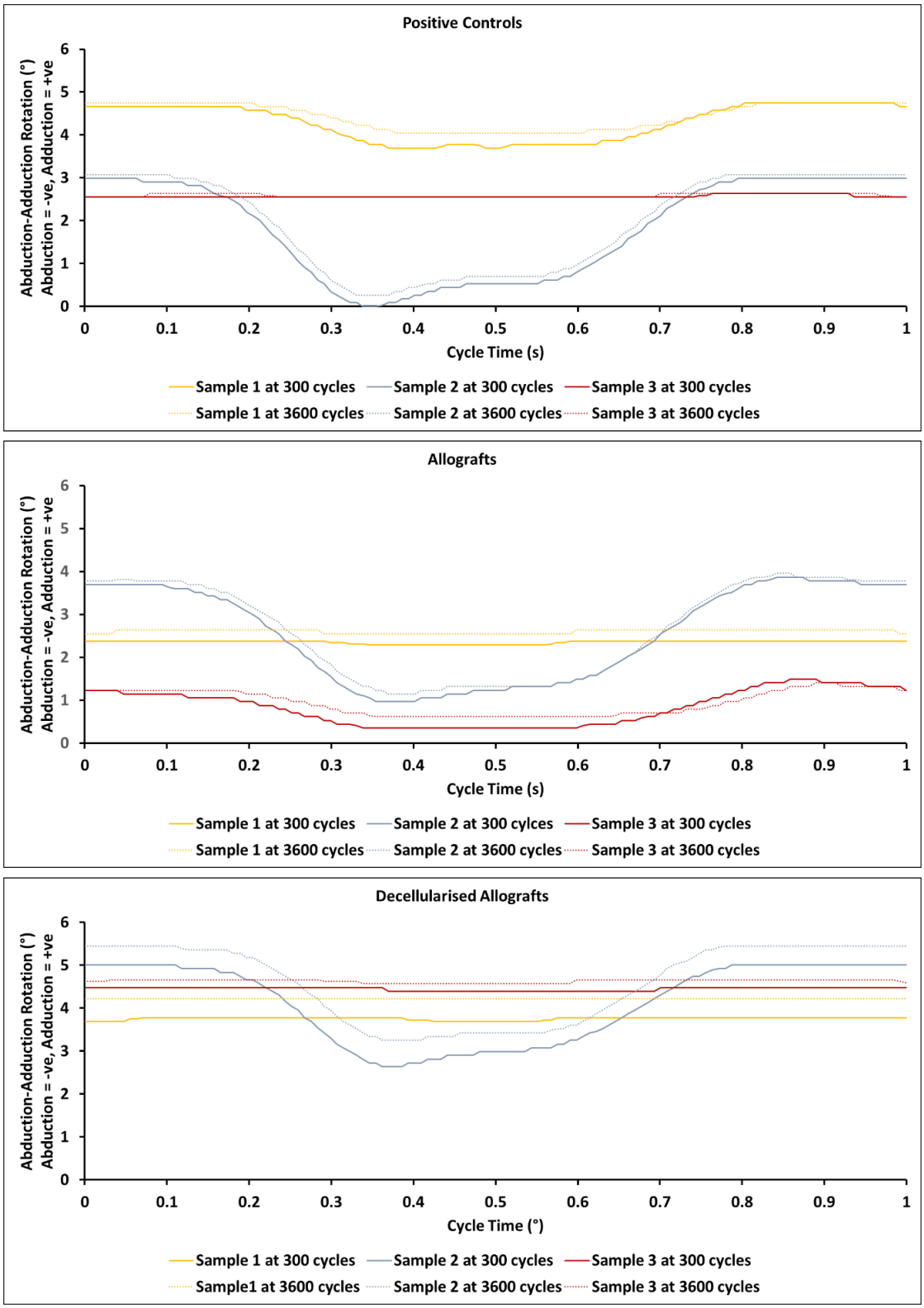


**Figure 7.21: Abduction-adduction rotation for samples in each experimental group at 300 cycles and 3600 cycles when applying stair ascent.**

## 7.6 Discussion

### 7.6.1 Summary

For the first time, the mechanical and tribological performance of novel decellularised porcine osteochondral allografts were compared to porcine osteochondral allografts, positive controls (stainless steel pins) and untreated negative controls during 48-hour simulations designed to replicate activities of daily living. There were no statistically significant differences between allografts, decellularised allografts and positive controls based on ICRS/OARSI grading. However, positive controls caused considerably more damage compared to the other two groups. Application of a stair ascent profile increased ICRS scores and there was a statistically significant ($p<0.05$) difference in relative height difference between decellularised allografts and the other two experimental groups after stair ascent.

### 7.6.2 Wear damage and deformation

Previous porcine knee simulation studies have assessed the influence of allografts and stainless-steel pins on opposing surfaces in the medial tibiofemoral joint (Bowland et al., 2018) and patellofemoral joint (Cowie et al., 2021).

Bowland et al observed anterior-posterior scratches in the central region of the medial meniscus when assessing allografts; during the current study shallow deformations/indentations were observed in meniscal surfaces. This was potentially due to differences in anterior-posterior axis control mode (spring constrained vs displacement control) but most likely due to the extended duration (48 hours vs 2 hours) and/or addition of the stair ascent motion. This applied a higher maximum load (1515N) and a higher load over a longer duration (>1200N for 0.6s) compared to walking gait. As with the Bowland *et al*. study, all meniscal damage in the current study was located within the central region of the medial meniscus. The Bowland *et al.* study did not report results for the condition of the femoral condyles or tibial plateau.

In the Cowie et al study, scratching was observed on the trochlear grove of negative control samples after three hours; during the current study damage was not observed on negative controls until post-simulation. This is most likely due to differences in the joints being assessed. Cowie et al observed grade 1 trochlea groove lesions for flush allografts, during the current study similar damage was observed on the femoral condyles and tibial plateau for allografts and decellularised allografts. Damaged caused by flush allografts and decellularised allografts in the current study was largely superficial, despite the extended simulation duration compared to the previous studies (48 hours vs 2-3 hours).

This suggests whilst some minor damage may occur, progression of the damage may be limited as long as graft positioning is accurate. All three studies demonstrated elevated levels of wear, damage and deformation when using stainless steel pins as positive controls.

Previous histological evidence has demonstrated subsurface delamination of the superficial tangential layer of articular cartilage can occur during cartilage-on-cartilage experiments; even in the absence of obvious surface changes (Durney et al., 2020). Histological evidence in the current study agrees with this finding, as delamination of the superficial tangential layer (Figure 7.11) was observed, despite most cartilage surfaces appearing to show minimal changes in ICRS grade. However, due to inconsistencies between sections taken from the same sample, it was difficult to confirm damage as a genuine result and not a false positive, as both damage and absence of damage were observed. Alternatively, these could be genuine changes which occurred over a very localised area and hence not present within each section. Delamination of the bulk articular cartilage from the subchondral bone has previously been observed clinically for a decellularised osteochondral intervention (Farr et al., 2016); there was no evidence of bulk delamination for the novel decellularised osteochondral allografts used during the current study.

Decellularised allografts deformed from a circular shape to a more oval shape, however the magnitude of change may have been exaggerated due to femoral cartilage obscuring the outline of subsided regions of the grafts. Decellularised allograft surfaces also showed evidence of deformation on the surface as a ridge had formed along the edge of two samples. Decellularised allografts were sloped, leading to proud positioning of one edge above the femoral cartilage and the other below. Incongruent graft positing has been shown to result in elevated contact pressures (Koh et al., 2004), therefore suboptimal orientation may have exacerbated the observed deformation in the current study.

### 7.6.3 Graft stability

The main predictors of success for osteochondral grafting are restoring the congruency of the articulating surface and ensuring the graft is supported from beneath by the underlying bone (Bowland et al., 2015). Decellularised allografts in the current study showed a trend to subside into the recipient site during simulations (statistically significant compared to the other experimental groups for stair ascent, $p<0.05$), whereas the allograft and positive control groups showed little movement. Results from animal models (Huang et al., 2004) (Nosewicz et al., 2014) and clinical observations (Nakagawa

et al., 2007) have shown excessive subsidence (>1mm) results in fibrocartilage overgrowth; this has suboptimal biomechanical properties compared to articular hyaline cartilage and may lead to degenerative changes. However, autografts experiencing minimal subsidence (up to 1mm) have shown a capacity for cartilage thickening and remodelling (Huang et al., 2004). In the current study, mean subsidence in the decellularised group was less than 0.24mm and individual sample subsided further than 0.4mm. The current study investigated primary graft stability prior to tissue integration. Clinically, postoperative rehabilitation recommends two weeks non weight-bearing to prevent graft subsidence and a subsequent 2-3 weeks reduced weight bearing for autografts (Hangody et al., 2008) and up to 8 weeks non-weight bearing for larger allograft repairs (Haber et al., 2019); this period allows ingrowth of host tissue into the graft. In vivo, tissue ingrowth may prevent or reduce subsidence.

Allografts and steel pins did not subside. Previous work has demonstrated subsidence of steel pins and allografts during porcine patellofemoral simulations (Cowie et al., 2021), differences between this study and the current study are most likely due to difference between the patellofemoral and tibiofemoral joints and the experimental conditions. In the current study, decellularised allografts and steel pins were inserted via manual thumb pressure, this suggests subsidence of decellularised grafts was due to changes in the graft and not the recipient site, as the steel pins were easy to insert but did not move. Allografts required hammering into recipient sites indicating a tighter fit than the other two groups. Decellularised allografts were more deformable than native allografts, they could be compressed by applying force with the thumb and finger. Both grafts were extracted from similar tissue using the same diameter chisel, therefore decellularisation appears to be responsible for the differences between grafts. Previous research has shown decellularisation can reduce mechanical properties of osteochondral tissues (Kheir et al., 2011) (Fermor et al., 2015). Subsidence likely occurred due to large loads deforming the less stiff decellularised grafts during simulations. In addition, loss of graft material removed as part of the decellularisation process made grafts more porous reducing the contact area between the graft and the recipient site. This reduced the force between the graft and recipient site walls lowering the push-in force require to displace the graft and further compounded the subsidence due to deformation.

Primary graft stability in the postoperative period is reliant on the interference fit of the graft-host interface (Bowland et al., 2015). Porcine tissue in the current study was from 4–6-month-old pigs, these were not skeletally mature; previous studies have identified immature tissue provides inferior stability results compared to mature tissue. Use of dilation for osteochondral grafting in immature porcine tissue was contraindicated due to a loose interference fit between graft and recipient site (Bowland et al., 2018) (Bowland

et al., 2020) and lower graft push-out forces were observed when using immature porcine tissue as either the graft or host (Bowland et al., 2020). Greater graft subsidence was observed for steel pins and allografts in immature porcine tissue compared to mature porcine tissue during a patellofemoral joint study (Cowie et al., 2021). If tissue ingrowth is insufficient to overcome subsidence when using decellularised immature porcine tissue clinically then an alternative more mature donor tissue may be necessary. Recent evidence has shown no differences in mechanical properties between native and decellularised human bone taken from the same location (Norbertczak et al., 2022), therefore this may also be the case for osteochondral tissue.

### 7.6.4 Absence of GAG's for SAF-O Staining

During the current study Safranin-O-stained osteochondral sections showed a complete loss of GAGs from the tissue; this was in direct contradiction to the previous simulator study (Chapter 4), where GAGs were retained post simulation. There were several differences between the studies (Table 7.4).

**Table 7.4: Differences between Chapter 4 and Chapter 7 simulation studies.**

| Chapter 4 | Chapter 7 (current study) |
|---|---|
| 48-hours walking gait<br>(maximum axial force = 985N) | 47-hours walking gait + 1-hour stair ascent<br>(maximum axial force = 1516N) |
| Spring-constrained anterior-posterior axis | Displacement controlled anterior-posterior axis |
| 3 freeze-thaws before histology | 4 freeze-thaws before histology |
| No decalcification before histology | Decalcification before histology |

The higher load of the stair ascent motion or over-constraint of natural motion by the displacement control may have squeezed GAGs from the cartilage during simulations. Complete GAG loss would be expected to compromise interstitial fluid load support and lead to tissue degeneration; however, little difference was observed between studies with respect to wear, damage and deformation of articulating surfaces. Decellularisation reduces GAG content (Kheir et al., 2011) (Fermor et al., 2015), so reduced staining would be expected for the decellularised osteochondral grafts; however, complete GAG loss from the grafts and condyle occurred for samples in every experimental group.

Therefore, post simulation handling of samples seems a more likely explanation. The decalcification protocol (time, temperature, rpm) in the current study may have been too harsh or other experimental variables such as the time elapsed between sectioning and staining may also be responsible for the observed GAG loss.

### 7.6.5 Limitations

Low sample size (n=3) was a significant limitation. Variation in results emphasises the need for larger sample sizes to confirm/deny potential trends during natural tissue work. Ideally more samples would have been used however, due to the extended duration of experiments (48 hours) this was not practical within the time available. Despite the limited sample size it was still possible to identify some trends. In addition, the minimum sample size for a Kruskal-Wallis test is meant to be n>5 as there were only n=3 samples in each experimental group. However results generated using this statistical approach supported the observed trends in the experiments as steel pins caused more damage than the other groups.

The lateral compartment of three experimental knees were used as negative controls and therefore did not represent an ideal negative control as the presence of grafts in the medial compartment may have influenced the wear damage and deformation in the lateral compartment. This approach was selected due to time constraints. It was not possible to view the lateral tibial plateau until post-simulation as the membranous attachments of the lateral meniscus prevented it from being lifted, therefore damage observed at this stage was potentially pre-existing.

There was a trend for the abduction-adduction waveform to initiate from an adducted position (varus alignment) and move into a more adducted position as simulations progressed. This alignment may have transferred a larger proportion of the load through the medial tibiofemoral compartment and a reduced load through the lateral compartment. This may have influenced results in two ways. Firstly, knees with decellularised grafts were more adducted than the other experimental groups for walking gait and stair ascent; a larger load or larger angle may have contributed to the graft subsidence observed for this group. Secondly, the reduced load in the lateral compartment may have reduced wear, damage and deformation; in future, it would be beneficial to have an independent negative control group and assess the medial compartment. Potential causes of the adducted alignment include suboptimal alignment of knees during cementing, over-constraint of physiological motion due to use of displacement control, natural variation between samples or inherent differences between porcine and human motion. Walking gait and stair ascent profiles were applied

sequentially, therefore there was the potential for changes observed during walking gait to have exacerbated any negative changes observed during stair ascent. As an alternative to displacement control, future work could look at further optimisation of spring constraints (physical or virtual) to enable improved kinematics for stair ascent or other input profiles

All grafts were initially slightly proud of femoral surfaces and decellularised allografts were sloped so some regions were proud and others subsided. Incongruence has been shown to negatively influence mechanical and tribological conditions, so whilst minimal in magnitude these issues may have contributed to wear, damage and deformation during the current study. The preparation process for decellularised allografts needs to be optimised to ensure grafts restore congruence once implanted (Figure 7.22) also see section (8.2.3).

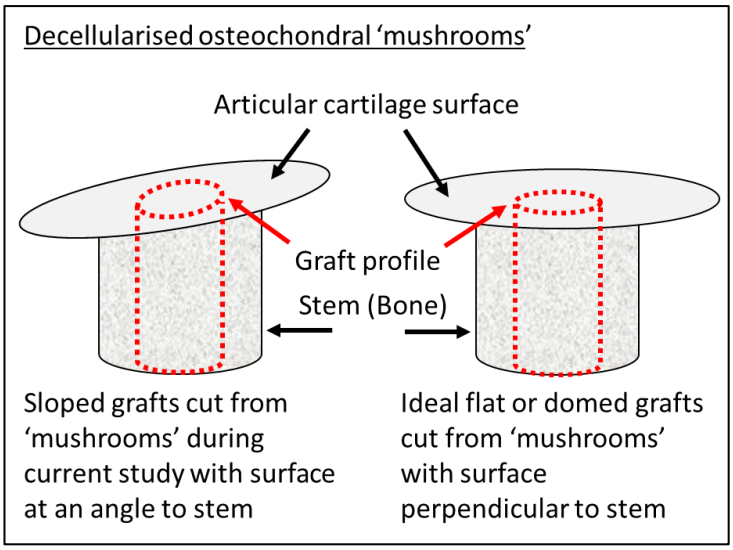


**Figure 7.22: Sloped grafts used during the current compared to the ideal scenario.**

When calculating relative height difference, crosshairs were positioned on scanned replicas using the Alicona software. Changes occurring during simulations meant replica surfaces had differences at each time point, therefore the measurement position selected on each replica may have varied slightly for each time point. This was a limiting factor on the accuracy of the approach. Suboptimal crosshair placement due to air bubble formation in AccuTrans replicas was also an issue. In addition, it was not possible to definitively infer if graft/pin position within the recipient site had changed as wear, damage or deformation of grafts or femoral condyles may have contributed to the changes in relative height between the graft/pin and femoral condyle.

Grading systems based on the International Cartilage Regeneration and Joint Preservation Society (ICRS) and Osteoarthritis Research Society International (OARSI) clinical classification systems were used to quantify wear, damage and deformation of cartilage and meniscal surfaces. As previously mentioned in Chapter 3, these are subjective scoring systems and could bias results. Therefore during the current study the approach to grading was made more robust by including a second observer to assess sample surfaces. Both observers inspected samples then discussed the outcome before jointly agreeing on an appropriate grade. This process could have been improved by blinding the two observers results from one another to increase the inter-rater reliability; however, the logistics/timing required to enable knee joints to be removed from and re-mounted into the knee simulator during extended duration experiments made this unfeasible. To make the process more robust and improve the intra-rater reliability, samples were regraded post-experiment (after defrosting) by both observers to confirm the validity of the originally allocated scores, identify temporary deformation as opposed to permanent damage and allocate new scores as appropriate.

In future, to improve the ICRS/OARSI grading approach, comparison of pre-experimental and post-experimental CT or MRI scans of knee joints could be used to quantify the extent of cartilage wear, damage and deformation in knee joints. This approach would enable more accurate measurement and reduce the potential for subjective observer bias to influence results. These imaging modalities could also measure graft position relative to the graft site to provide information about graft stability and could therefore be used either as an alternative to the histology or silicone replica methods or as an additional layer of analysis. The disadvantages of these approaches are they would be more expensive and require additional training.

## 7.7 Summary

- Negative controls experienced minimal damage (Grade 1) throughout simulations
- Implantation of stainless-steel pins (positive controls) lead to extensive (ICRS Grade 4) wear, damage and deformation of the opposing meniscus and tibial plateau
- Allografts and decellularised allografts had comparable performance in terms of wear damage with mainly superficial (ICRS Grade 1) changes observed on the opposing meniscal and tibial surfaces
- Decellularised porcine allografts subsided, most likely due to forces generated during simulations deforming the grafts. The combination of immature porcine

tissue and decellularisation potentially creates a graft with insufficient mechanical properties to prevent subsidence from occurring.

    - Decellularised grafts need to be assessed in a cadaveric human knee joint or animal model to determine if the stiffer human bone or tissue ingrowth will prevent subsidence. Ideally this should be done with a larger sample size.

- The preparation of decellularised osteochondral allografts should be optimised to ensure a flat/domed articular surface and straight stem to provide a good interference fit and congruence between graft and recipient site. This will minimise the potential for unfavourable outcomes
- Application of a stair ascent activity increased ICRS/OARSI grades for samples in all experimental groups and produced a statistically significant difference between the decellularised allografts and other experimental groups with regards to stability of grafts/pins within the recipient site
    - In future it is recommended to simulate as many activities as possible to identify the worst-case scenarios and reduce risk before animal trials or clinical application.
- With regards to delamination of articular cartilage, histological evidence was inconsistent, however some osteochondral sections in each experimental group had intact cartilage after the 48-hour simulation.
- The complete absence of GAGs in the Safranin-O sections in this study compared to the study in Chapter 4 indicated there was an artefact in the histological processing

# Chapter 8

# Discussion & Conclusions

## 8.1 Introduction

### 8.1.1 Aims of project

The first aim of the research in this thesis was to advance an experimental porcine knee joint simulation model used to study the wear of early knee interventions, by investigating suitable lubricants, activities of daily living and the maximum study duration. The second aim was to assess the tribological performance of a novel decellularised porcine osteochondral allograft under these enhanced simulation conditions for the first time.

### 8.1.2 Clinical need for *in vitro* experimental assessment of early stage knee interventions

Early-stage knee interventions, such as osteochondral grafting, have been developed to try and delay or prevent progression of cartilage deterioration to end-stage osteoarthritis and subsequent knee replacement. However, thus far, clinical success has been limited. There is a lack of *in vitro* experimental evidence demonstrating the mechanical and tribological function of early-stage knee interventions under physiologically relevant conditions before clinical use (Bowland et al., 2015) (Patel et al., 2019). The intended patient population of early-stage knee interventions are younger or active people. These individuals are likely to undertake more functionally demanding tasks which subject interventions to larger loads and more complex motions. Evidence from joint simulation wear studies and *in vitro* tribological investigations of cartilage demonstrate more demanding simulation conditions may negatively influence articulating surfaces. Therefore, similar issues may arise when introducing early-stage knee interventions into the joint.

Osteochondral allografting and autografting are existing surgical techniques which aim to restore the articular cartilage surface. Whilst effective in certain instances (Hangody

et al., 2008) (Hangody et al., 2010) (Torrie et al., 2015) (Filardo et al., 2015) (Keszég et al., 2022), these approaches have several inherent limitations which mean they remain suboptimal solutions. Decellularised osteochondral grafts have been developed as an alternative method which aims to eliminate the shortcomings of the existing approaches. Thus far, clinical use of decellularised interventions has been limited, with the first available product generating inconsistent outcomes with a large number of failures observed in certain cases (Long et al., 2016) (Degen et al., 2016) (Johnson et al., 2017) (Farr et al., 2016). The literature shows decellularisation of osteochondral tissues can reduce mechanical properties (Kheir et al., 2011) (Fermor et al., 2015) making them more deformable than native tissue. These issues may have been present within the clinically used decellularised osteochondral interventions and potentially compromised the *in vivo* performance leading to the observed clinical failures.

*In vitro* experimental analysis could identify potential issues early, improve the safety and efficacy of these interventions and prevent costly failures and unnecessary suffering during animal trials and clinical use. This approach would hopefully provide more reliable interventions, resulting in better outcomes and improve the patient experience.

### 8.1.3 Previous development of the University of Leeds porcine knee experimental simulation model

The porcine knee experimental simulation model used during three studies within the current project (Chapter 4) (Chapter 6) (Chapter 7) was developed at the University of Leeds. This model has gone through several stages of development. Initial work validated the ability of a 6-DoF freedom knee simulator to differentiate between tribological behaviours within a porcine knee joint (Liu et al., 2015). Differences in anterior-posterior shear force were measured within the tibiofemoral compartment when applying three different degrees of constraint to the anterior-posterior displacement axis during five-minute (300 cycle) simplified kinematic and complex kinematic (walking gait) simulations. This work demonstrated the ability to identify changes within the joint and therefore the potential to assess the influence of early-stage interventions.

The porcine knee model was subsequently utilised to assess the effect of an existing surgical intervention, osteochondral graft implantation, on the tribology within the joint for the first time (Bowland et al., 2018). The ability of osteochondral allografting to restore tribological performance within the medial tibiofemoral compartment was assessed during two-hour (7,200 cycle) walking gait simulations. The intervention was compared with the native joint, a defect injury model and stainless-steel pins; variations in surgical precision (proud positioning of grafts/steel pins) was also investigated. Performance was

determined based on the wear, deformation and damage caused to opposing articular surfaces during simulations. Positioning the graft flush with the surface resulted in the lowest levels of wear, deformation and damage; proud positioning of grafts or steel pins increased wear, deformation and damage.

In the next stage of development, the anterior-posterior spring constraint mechanism was optimised to improve the physiological relevance of the porcine knee model (Liu et al., 2019). The porcine knee model approach removes all soft tissue to enable interventions to be easily implanted into the joint. The anterior-posterior constraint mechanism was designed to replicate the restraining forces applied by the resected soft tissues (ligaments). Walking gait simulations of intact porcine knees (all soft tissue removed but ligaments still attached) were used to obtain anterior-posterior displacement and anterior-posterior shear force outputs. Springs of different stiffness and a range of spring gaps (to represent ligament laxity) were then investigated to determine which combinations most accurately recreated the outputs of the intact ligament condition.

### 8.1.4 Extending simulation duration for natural knee joints

The aim of early-stage knee interventions is to delay or prevent progression of cartilage deterioration, if these interventions perform as intended, they should last for years. Searching literature identified only two tribological studies assessing osteochondral interventions in whole-joint models during physiologically relevant simulations; these were both short-term investigations at 7,200 cycles (2 hours) (Bowland et al., 2018) and 10,800 cycles (3 hours) (Cowie et al., 2021) respectively. Therefore, one of the main objectives of this thesis was to extend the simulation duration. Evidence from the literature has shown live and dead cartilage-on-cartilage contacts experience similar wear over the short-term (Trevino et al., 2017). Natural tissue degrades over time, therefore it needed to be determined how long samples could be articulated under load before the cartilage surfaces were compromised. Mechanical and tribological cartilage studies in the literature (Weightman, 1976) (Weightman et al., 1978) (Mccormack and Mansour, 1998) (Taylor, 2012) (Durney et al., 2020) suggested the potential to extend simulation duration from several hours to several days. Extending simulation duration was investigated in three stages.

In the first stage (Chapter 3), 96-hour tribological experiments assessed the influence of five lubricants on the wear, damage and deformation response of cartilage using a simple geometry pin-on-plate set-up. This aimed to identify the lubricant which maintained cartilage surfaces for the longest possible duration. Isotonic bovine serum lubricants

were most effective whereas Ringer's Solution resulted in catastrophic failure of samples; custom lubricant performance was more effective than Ringer's Solution but worse than serum-based lubricants. This was mostly likely explained by the absence of boundary molecules in the Ringer's Solution which is in agreement with previous literature (Forster and Fisher, 1996) (Caligaris and Ateshian, 2008).

The second stage determined the effects of extended simulation duration on a whole porcine knee joint (Chapter 4). The validity of the optimised spring constraint mechanism to maintain kinematics and an assessment of microbial growth and its influence on tribology were determined during 48-hours simulations. Results suggested the porcine knee joint remained a suitable model for the assessment of osteochondral interventions during 48-hour simulations as physiological kinematics were maintained and wear, damage and deformation were minimal; although microbial growth was identified within the lubricants.

Assessment of microbial growth in the current work was limited to determining if growth had occurred. In future, quantifying microbial growth may be beneficial. This could make it possible to identify a microbial growth threshold below which there is negligible influence on the tribology within the joint. This information could be used to determine an appropriate simulation duration for which microbial growth would be minimised and physiological relevance could be maintained. Three methods commonly used for quantification of microbial growth are: counting colony forming units, optical density via spectrophotometry and flow cytometry. Colony counting is considered to have good reliability and specificity but is time consuming and usually provides an underestimate as only certain microbes can be cultured. Measurement of optical density is simple and quick but may overestimate growth as both live and dead cells are counted and does not provide an exact count. Flow cytometry enables identification of all cell types but is an expensive process and results are potentially difficult to interpret (Pan et al., 2014).

Although not observed on histological sections, due to the non-sterile conditions used during the current work, the microbial growth which occurred may have resulted in biofilm formation within lubricants or on cartilage surfaces. Whilst biofilm formation in this particular setting was undesirable, and in general due to issues relating to antibiotic resistant infection (e.g. MRSA), biofilms have demonstrated the ability to reduce friction on both organic (Taylor 2012) and inorganic (Souza et al., 2010) materials. If the molecules responsible for reducing friction could be identified and isolated from the harmful aspects of the biofilm, they could potentially enable the development of effective lubricants for a variety of applications. Glycoprotein, lipid and polysaccharide molecules have been suggested as being responsible for the reduced friction properties of biofilms (Souza et al., 2010) (Taylor 2012).

Ideally, it would be beneficial to develop a sterile setup, for the dissection, cementing and lubricant making process to eliminate the issue of microbial growth. A potentially viable approach has previously been investigated (Taylor, 2012), although issues surrounding antibiotic resistance may limit the appropriateness of this approach.

Whilst the current approach increased simulation duration from 2/3 hours to 48 hours, this is still a very limited duration in comparison to the intended lifetime of the intervention. Incorporating the simulation capabilities of the current approach with a bioreactor approach (see section 8.2.4) may enable longer simulation durations to be attempted.

The third stage of extending simulation duration (Chapter 5) focused on ensuring a method previously developed to enable analysis of wear, damage and deformation of cartilage surfaces in the porcine knee joint during a 2-hour study (Bowland et al., 2018) remained valid over a longer duration. Results validated the use of AccuTrans silicone for replicating surfaces which had been submerged in lubricant for up to 48 hours.

For the first time, minimal degradation of a non-living porcine knee joint using a bovine serum in Ringer's Solution lubricant was demonstrated during 48-hour walking gait simulations. Hence, the porcine knee represented a suitable model of a 'healthy' knee joint in which to assess osteochondral interventions during 48-hour simulations. In addition, previous methods utilised during 2-hour walking gait simulations (the ability of spring constraints to control kinematics and use of AccuTrans to create replicas articulating surfaces) remained valid over a 48-hour timeframe.

### 8.1.5 Improving physiological relevance of natural knee simulation

Improving the physiological relevance of *in vitro* simulations will improve the clinical translation of results. Therefore, during the current project, investigation of strategies to improve physiological relevance were assessed. This aim was achieved via two separate studies. The pin-on-plate study in Chapter 3 included two custom physiological lubricants designed to more closely mimic synovial fluid and Chapter 6 focussed on the feasibility of applying activities of daily living (stair ascent and squatting) to a porcine knee joint.

One criticism of existing lubricants was inability to effectively replicate synovial fluid (Galandáková et al., 2017). By adapting a previous method (Bortel et al., 2015), two lubricants were developed to represent healthy synovial fluid (the ideal scenario in a healthy knee) and traumatic synovial fluid (the typical synovial fluid of the early-stage knee intervention patient population). Custom lubricants were less effective than isotonic serum-based lubricants but more effective than Ringer's Solution at minimising wear,

damage and deformation of cartilage surfaces. The traumatic version was more effective than the healthy version; potential explanations were discussed in detail in Chapter 3.

Within the knee, soft tissues (ligaments) act to restrain motion during a variety of different movements. It was assumed the anterior-posterior spring constraint optimised to replicate soft tissue function for walking gait in the porcine model (Liu et al., 2019), was appliable to other activities of daily living (stair ascent and deep squat). The existing spring constraint was not sufficient to constrain all three motions leading to simulation failure. Increasing spring stiffness enabled simulation of all three activities, but this approach had limited repeatability. In future, driving simulations in force control and applying specimen specific spring constraints (Liu et al., 2020) could solve this problem; although difficulty with simulating the same three motions have been encountered previously when attempting to apply virtual ligament constraint to human knees (Sarpong et al., 2020). This may be an inherent limitation of the cadaveric joint approach and requires further investigation.

The ability to transition directly from walking gait to stair ascent and back to create a simulation loop using physical spring constraints was also demonstrated. However, due to limited repeatability, and a large anterior-posterior shear force generated at the transition potentially confounding wear, damage and deformation analysis, displacement control was selected for simulating walking gait and stair ascent in Chapter 7. Whilst less physiological, this ensured simulations could complete the 48 hour duration to enable graft performance to be assessed.

### 8.1.6 Assessment of novel decellularised osteochondral grafts during simulation of activities of daily living

During the final stage of the project (Chapter 7), learning from previous chapters was combined to compare the tribological performance of a novel decellularised porcine osteochondral allograft to the gold standard porcine osteochondral allograft, native knees (negative controls) and stainless-steel pins (positive controls) under enhanced simulation conditions. Simulations were run for 48 hours (Chapter 4), using an optimised lubricant (Chapter 3), whilst applying a walking gait (47 hours) + stair ascent (1 hour) activities of daily living profile (Chapter 6), and wear, damage, deformation and graft stability were analysed using scans generated from AccuTrans silicone replicas of articulating surfaces (Chapter 5) and histological analysis.

To the best of the authors knowledge, this study represents the longest tribological investigation of a porcine osteochondral allograft and the first investigation of a

decellularised osteochondral allograft under physiologically relevant loading in a whole natural knee joint. This study demonstrated allografts and decellularised allografts had similar wear/damage performance but enhanced simulation conditions influenced deformation and stability of the decellularised grafts. Evidence from this study adds to previous data from joint simulation studies and pin-on-plate cartilage studies supporting the idea walking gait alone is insufficient to represent the *in vivo* environment experienced by knee interventions. This work also demonstrates the potential consequence of reducing the mechanical properties of osteochondral tissue during the decellularisation process. These results suggest early-stage knee interventions should be subjected to as wide a range of kinetic and kinematic conditions as possible during robust *in vitro* assessment to identify worst case scenarios prior to animal trials or clinical use.

### 8.1.7 Overall Limitations

#### 8.1.7.1 Low sample numbers

A common limitation throughout all the studies in the current project was the low sample numbers used during experiments. Whilst trends were observed for some experimental groups it would have been beneficial to include additional samples to gain a deeper understanding in experimental groups which showed more variable results.

#### 8.1.7.2 Physiological relevance of lubricants

Another common limitation was the use of an isotonic bovine serum lubricant during experiments. This lubricant differs from synovial fluid, particularly the absence of hyaluronic acid, and therefore *in vivo* intervention performance may differ. The custom lubricants highlighted the potential to minimise cartilage damage and with more development, could potentially prove to be a more effective solution. However, until a suitable alternative is available, 25% new-born calf serum in Ringer's Solution is an effective lubricant for tribological investigations.

#### 8.1.7.3 Mechanical properties of immature porcine tissue

Whilst useful for method development, porcine tissue is still limited in clinical relevance. The non-living immature porcine tissue used throughout this project may have different mechanical properties to that of the intended patient population (young human adults). This may have contributed to the deformation of the decellularised osteochondral grafts and hence more mature tissue or an alternative animal or human tissue source may be

necessary. Translation of osteochondral graft assessment into a human cadaveric model is necessary to provide more clinically meaningful results.

#### 8.1.7.4 Physiological relevance of spring constraint mechanism

The linear physical compression springs used during two of the knee simulator studies (Chapter 4) (Chapter 6) do not function like the nonlinear soft tissues they are meant to represent. This limits the physiological relevance of this approach. Future simulator studies incorporating natural joints could be driven in force control and incorporate virtual springs to apply soft tissue constraints to solve this issue (Liu et al., 2020).

#### 8.1.7.5 Lack of contact pressure measurement during simulation studies

During the simulation studies incorporating whole porcine knee joints (Chapter 4, 6 and 7), measurement of contact pressure within the tibiofemoral joint was not included as part of the experimental protocol. Due to extended simulation durations and other experimental processes necessary to enable analysis of wear, damage and deformation, there was insufficient time to incorporate contact pressure measurements.

Differences in contact pressure due to the natural geometric variation between animals, the different kinetic/kinematic input profiles used (walking gait and stair ascent) or variation of implanted graft/pin height relative to the femoral condyle surfaces may have influenced the results. Incongruence can lead to elevated contact pressures (Koh et al., 2004) which can be detrimental to cartilage health (Lizhang et al., 2011) therefore some samples may have been more susceptible to wear, damage and deformation than others. In future whole joint experiments, it would be beneficial to quantify the contribution of contact pressure toward wear, damage and deformation when analysing results.

Existing literature highlights methods for measurement of contact pressure and contact area within both human and animal knee joints. Most recent approaches have involved inserting either a pressure sensitive film (Fujifilm) or pressure sensitive film sensor (Tekscan) between the menisci and tibial plateau (Walker et al., 2015) (Sezaki et al., 2021). Many studies applied static loading at intervals between 0° and 90° of flexion, although some have made dynamic measurements during walking gait and stair ascent simulations (Gilbert et al., 2014) (Bedi et al., 2010). This approach could be applied to future extended duration knee simulation studies but would be limited to pre-test and post-test analysis as the gaiter (and lubricant) would have to be removed to take measurements.

### 8.1.8 Current state of *in vitro* assessment of early stage knee interventions

It was stated in a previous PhD thesis that there was a limited number of *in vitro* experimental knee joint models (Bowland, 2016); with only three (Lane et al., 2009) (Walter et al., 2013) (Bobrowitsch et al., 2014) investigating osteochondral repair. Since that time there have been an additional three (one from the Bowland PhD thesis) *in vitro* experimental joint studies focusing on osteochondral repair. Approaches investigated the effect of surgical positioning on wear, damage and deformation of opposing surfaces (P. Bowland et al., 2018) (Cowie et al., 2021) or friction (dissipated energy) (Walter et al., 2020) in porcine tibiofemoral, porcine patellofemoral and ovine tibiofemoral models respectively. A similar trend was observed for all studies, with flush graft positioning showing minimal difference from the native condition and proud graft positioning resulting in increased wear, damage, deformation or friction. In addition, the patellofemoral model approach showed grafts subsided into the patella during testing (Cowie et al., 2021).

Other investigations of *in vitro* knee joint models have been undertaken. Several approaches have investigated the influence of injury or surgical repair techniques on knee joint kinematics. These have included ACL injury in a caprine model (van de Bunt et al., 2017), ACL repair (Boguszewski et al., 2014) (Lorenz et al., 2015) and posterolateral complex repair (Panzica et al., 2015) in human models. Four approaches have assessed kinematics during soft tissue constraint development. Optimised physical springs constraints were developed for a porcine model (Liu et al., 2019), specimen specific virtual spring (Liu et al., 2020) and virtual ligament (Sarpong et al., 2020) constraints were developed for human models and a virtual ligament model was applied during assessment of a TKR (Willing et al., 2019). Other human models have investigated TKR devices (Shimizu et al., 2018) (Borque et al., 2015), patella stability (Lorenz et al., 2015) and a polyurethane meniscal scaffold (Maher et al., 2011).

### 8.1.9 Regulation of medical devices

In several countries throughout world national joint registries have been set up to monitor the performance of total joint replacements throughout the lifetime of the devices (Lübbeke et al., 2017). This post-market surveillance enables comparison of devices and helps guide clinical practice by identifying trends and highlighting outliers and serious adverse outcomes. Due to major issues previously observed with some medical devices, such as metal-on-metal hips, there is an increasing trend toward stricter regulations and enhanced post-market surveillance. The new European Union Medical Device Regulations (EU MDR) have expanded the necessary requirements which medical

devices must meet, and continue to meet, to gain and maintain approval for clinical use. The level of clinical information required to ensure the continued safety, efficacy and performance of medical devices has become more comprehensive.

The clinical use of early-stage knee interventions is increasing and registries for other orthopaedic activities are now starting to be set up to monitor their performance. The American Academy of Orthopaedic Surgeons (AAOS) has introduced a registry program covering Fracture and Trauma, Musculoskeletal Tumours, the Shoulder and Elbow and the Spine (AAOS, 2022) and the International Cartilage Regeneration & Joint Preservation Society has introduced a registry for cartilage repair strategies (Tawy and McNicholas, 2022).

The clinical failures of existing decellularised osteochondral interventions are concerning, work from the current thesis demonstrated a significant difference between a decellularised osteochondral graft and the existing gold standard allografting technique in term of subsidence after stair ascent. Whilst the current approach is still limited in its ability to represent the clinical scenario, due to lack of host tissue integration reducing graft stability, this result highlights the value of *in vitro* experimental assessment of these interventions before clinical use as subsidence results in poor clinical outcomes. It would be beneficial to include the preclinical experimental evaluation of early-stage knee interventions in regulatory requirements to mitigate issues from occurring clinically.

### 8.1.10 Summary of Novelty

To the best of the authors knowledge the studies in this thesis represent:

- The longest (48 hours) tribological investigation of wear, damage and deformation within a whole knee joint model during physiological walking gait simulations
- The longest (48 hours) tribological investigation of wear, damage and deformation for an osteochondral allograft within a whole knee joint model during physiological walking gait simulations
- The only tribological investigation of wear, damage and deformation for an osteochondral allograft and decellularised osteochondral allograft within a whole joint model during physiological 47 hour walking gait and 1 stair ascent simulations
- The only investigation of osteochondral allograft and decellularised osteochondral allograft stability within the tibiofemoral joint during physiological 47 hour walking gait and 1 stair ascent simulations in a whole joint model

- The longest (96 hours) tribological investigation of wear, damage and deformation for a sliding cartilage-on-cartilage contact using various lubricants (Ringer's Solution, Isotonic serum-based lubricants, custom lubricants design to mimic healthy and traumatic synovial fluid)
- The validation of AccuTrans silicone for replicating non-living porcine cartilage surfaces which have spent a prolonged duration (48 hours) in lubricant

## 8.2 Future Work

### 8.2.1 Making results more clinically translatable

Whilst effective for method development, the immature porcine tissue used during this thesis has different mechanical properties from adult human tissue and may have contributed to the subsidence of the decellularised osteochondral grafts. To provide more clinically translatable results, grafts need to assessed within human knee joints and then, if successful, implanted into a living large animal model to determine how tissue ingrowth affects the stability. If unsuccessful, other decellularised osteochondral tissue sources (e.g. mature porcine tissue or human tissue) could be investigated as potential alternatives.

### 8.2.2 Optimised springs for different motions

During simulations in the graft study (Chapter 7), at heel strike all knees initially adopted an adducted alignment, and for the majority of knees this became more adducted as simulations progressed. Simulations were run using displacement control to minimise the chance of dislocation during the short-term experiments. However, this produced suboptimal abduction-adduction kinematics and would likely cause issues if attempting to run longer simulations using the stair ascent profile. It would be beneficial to identify more optimised spring constraints (different stiffness's/gaps) for motions other than walking gait. In addition, adding springs to the internal-external, abduction-adduction or medial-lateral axes to further constrain the motion may improve simulations. This could be done when applying force control by using a virtual spring setup incorporated within the simulator software.

### 8.2.3 Optimising decellularised osteochondral graft preparation

The process for preparing decellularised osteochondral mushrooms needs to be optimised to ensure both a flat-bottomed graft and a flat/domed articular cartilage surface to match the curvature of the condyle can be achieved. Decellularised osteochondral allografts were chiselled from pre-prepared 'mushroom shaped' regions of decellularised porcine femoral condyles. The mushroom shape is utilised to reduce bone volume, enabling sufficient penetration of solutions into the tissue to ensure removal of cellular material below the 50 $ng \cdot mg^{-1}$ threshold (Crapo et al., 2011); there is also a central canal drilled into the stalk to aid this process. Mushroom stalks were inserted into a jig to hold them in place whilst grafts were removed. Due to the manual preparation of the mushrooms, stalks were not always perpendicular to the articular cartilage surface, therefore it was not possible to obtain a flat or domed cartilage surface as the jig fixed the angle of the chisel in-line with the stalk. This issue resulted in sloped grafts, where one edge of the graft was above the level of the surrounding femoral cartilage and the other was below. This is of particular concern as even small incongruencies have been shown to result in elevated contact pressure withing the knee (Koh et al., 2004) and could potentially lead to damage. In addition, the jig did not allow sufficient penetration of the chisel to cut through the full depth of the mushroom stalk and graft edges had to be trimmed with a scalpel blade. In future, the orientation of the graft surface in relation to the stem should be optimised for the desired insertion location as geometry of different surfaces (femoral condyle, tibial plateau, patella, trochlea groove) will vary. An alternative jig for chiselling the decellularised grafts would also be beneficial to enable full penetration of the chisel through the decellularised mushroom.

### 8.2.4 Developing a reference frame for Alicona measurements of natural tissue

Due to the issues observed during the current project with regards to measuring changes between individual cartilage samples at different timepoints it would be beneficial to include reference points within AccuTrans replicas. These would enable more accurate values to be obtained. This would also enable use of the 'Difference' method (an analysis module within the Alicona Software). This enables the difference in position of points on an initial scan to be compared to the same points on a subsequent scan. This is beneficial for identifying any changes which may have occurred from the original condition to the current condition e.g. wear, damage and deformation of cartilage surfaces; this method allows both quantification and visualisation of changes. To obtain accurate results the before and after scans have to be matched using the software. Inclusion of reference

points within the replica would improve the accuracy of scan matching. It is recommended that reference frames be included at a similar level to the surface being measured as increasing the ‘z’ dimension of the replica will increase scanning time (potentially several hours). This should be easily achievable for pin-on-plate replicas however may be more challenging with curved geometries such as the femoral condyle. Be careful to identify ‘rogue’ pixels generated during the scanning process and crop them out of the scans. These will interfere with the values generated by the software (especially the maximum difference between scans) if a pixel is present in one scan but not the other.

### 8.2.5 Further extending the duration of *in vitro* experiments

Bioreactor systems which aim to maintain tissue viability whilst applying forces and motions have been developed for cardiovascular (Amrollahi and Tayebi, 2016) (Devillard and Marquette, 2021), tendon and ligament (Wang et al., 2013) (Dyment et al., 2020) (Delakowski et al., 2022) and cartilage (Tekari et al., 2020) (Fu et al., 2021) (Yuh et al., 2021) (Hallas et al., 2022) interventions. Currently no such approach exists for the assessment of early-stage knee interventions in a whole natural knee joint, however, this is an active area of research (Fox et al., 2018) (Lin et al., 2018). An approach which combines the viability of the bioreactor approach, with the geometrical relevance of a natural knee joint and relevant physiological loading, whilst maintaining aseptic conditions, would be a promising step forward for the assessment of early-stage knee interventions.

## 8.3 Conclusions

- The lubricant can have a significant effect on the wear, damage and deformation of articular cartilage during longer-term tribological investigations. Isotonic serum-based lubricants showed the potential to maintain cartilage surfaces for up to 96 hours during pin-on-plate experiments, whereas when using Ringer’s Solution as a lubricant, catastrophic damage to articulating surfaces had occurred after 72 hours

- Porcine knee joints can be simulated for up to 48 hours with minimal wear, damage and deformation to the articulating surfaces and no serious adverse effects (fracture, dislocation or excessive adduction-abduction motion) and

therefore provide a suitable environment in which to assess the influence of early-stage knee interventions over the same duration

- It was possible to run a stair ascent input profile during simulations when using a physical spring constraint mechanism to replicate soft tissue function, but not possible to run a deep squatting profile. Porcine knees require movement specific and potentially specimen specific spring constraints to enable simulation of a wider range of activities, this approach should be applied during future simulation studies

- The process for creating AccuTrans silicone replicas of articular cartilage does not cause damage to the articulating surfaces of samples which have been submerged in an isotonic serum-based lubricant for up to 48 hours and hence is a suitable approach for replicating articular cartilage surfaces after 48-hour simulations

- Applying a stair ascent input profile during activities of daily living simulations resulted in increased wear, damage and deformation and was responsible for a statistically significant subsidence of the decellularised allografts compared to allografts. Interventions should be assessed by simulating a wide range of kinetic and kinematic inputs *in vitro* to ensure worse case scenarios are accounted for in order to mitigate the potential for clinical failure

- Decellularised porcine osteochondral allografts showed similar wear and damage and deformation of the articulating surfaces as porcine allografts during 48-hour simulations; therefore they are potentially a viable alternative to the existing gold standard allografting technique

- Decellularised porcine osteochondral allografts grafts were less stable than porcine osteochondral allografts as they subsided into the recipient site during simulations. This is of concern in a clinical setting as subsidence of osteochondral grafts has shown to result in poor clinical outcomes. Whilst tissue ingrowth will provide additional stability *in vivo* and potentially reduce/eliminate this issue, further investigation is necessary to determine the cause of the subsidence

# References

AAOS 2022. About the AAOS Registry Program.

Abdelgaied, A., Fisher, J. and Jennings, L.M. 2017. A comparison between electromechanical and pneumatic-controlled knee simulators for the investigation of wear of total knee replacements. *Proceedings of the Institution of Mechanical Engineers, Part H: Journal of Engineering in Medicine*. **231**(7), pp.643–651.

Abdelgaied, A., Fisher, J. and Jennings, L.M. 2018. A comprehensive combined experimental and computational framework for pre-clinical wear simulation of total knee replacements. *Journal of the Mechanical Behavior of Biomedical Materials*. **78**, pp.282–291.

Abdelgaied, A., Fisher, J. and Jennings, L.M. 2022a. Understanding the differences in wear testing method standards for total knee replacement. *Journal of the Mechanical Behavior of Biomedical Materials*. **132**, p.105258.

Abdelgaied, A., Fisher, J. and Jennings, L.M. 2022b. Understanding the differences in wear testing method standards for total knee replacement. *Journal of the Mechanical Behavior of Biomedical Materials*. **132**.

Abdel-Jaber, S., Belvedere, C., Leardini, A. and Affatato, S. 2015. Wear simulation of total knee prostheses using load and kinematics waveforms from stair climbing. *Journal of Biomechanics*. **48**(14), pp.3830–3836.

Abdel-Jaber, S., Belvedere, C., Mattia, J.S. de, Leardini, A. and Affatato, S. 2016. A new protocol for wear testing of total knee prostheses from real joint kinematic data: Towards a scenario of realistic simulations of daily living activities. *Journal of Biomechanics*. **49**(13), pp.2925–2931.

Agha, M. and Agha, R. 2017. The rising prevalence of obesity: part A: impact on public health. *International Journal of Surgery: Oncology*. **2**(7), p.17.

Altman, R., Asch, E., Bloch, D., Bole, G., Borenstein, D., Brandt, K., Christy, W., Cooke, T.D., Greenwald, R., Hochberg, M., Howell, D., Kaplan, D., Koopman, W., Longley, S., Mankin, H., McShane, D.J., Medsger, T., Meenan, R., Mikkelsen, W., Moskowitz, R., Murphy, W., Rothschild, B., Segal, M., Sokoloff, L. and Wolfe, F. 1986. Development of criteria for the classification and reporting of osteoarthritis: Classification of osteoarthritis of the knee. *Arthritis & Rheumatism*. **29**(8), pp.1039–1049.

Altman, R.D. and Gold, G.E. 2007. Atlas of individual radiographic features in osteoarthritis, revised. *Osteoarthritis and Cartilage*. **15**, pp.A1–A56.

Amrollahi, P. and Tayebi, L. 2016. Bioreactors for heart valve tissue engineering: A review. *Journal of Chemical Technology and Biotechnology*. **91**(4), pp.847–856.

Andrade, R., Vasta, S., Pereira, R., Pereira, H., Papalia, R., Karahan, M., Oliveira, J.M., Reis, R.L. and Espregueira-Mendes, J. 2016. Knee donor-site morbidity after mosaicplasty – a systematic review. *Journal of Experimental Orthopaedics*. **3**(1).

Andriacchi, T.P. and Mü Ndermann, A. 2006. *The role of ambulatory mechanics in the initiation and progression of knee osteoarthritis*. Lippincott Williams & Wilkins.

ASTM n.d. ASTM F3141-17a Standard Guide for Total Knee Replacement Loading Profiles.

Ateshian, G.A. 2009. The role of interstitial fluid pressurization in articular cartilage lubrication. *Journal of Biomechanics*. **42**(9), pp.1163–1176.

Ateshian, G.A., Soltz, M.A., Mauck, R.L., Basalo, I.M., Hung, C.T. and Lai, W.M. 2003. *The Role of Osmotic Pressure and Tension-Compression Nonlinearity in the Frictional Response of Articular Cartilage*.

Bates, N.A., McPherson, A.L., Nesbitt, R.J., Shearn, J.T., Myer, G.D. and Hewett, T.E. 2017. Robotic simulation of identical athletic-task kinematics on cadaveric limbs exhibits a lack of differences in knee mechanics between contralateral pairs. *Journal of Biomechanics*. **53**, pp.36–44.

Bates, N.A., Nesbitt, R.J., Shearn, J.T., Myer, G.D. and Hewett, T.E. 2015. A Novel Methodology for the Simulation of Athletic Tasks on Cadaveric Knee Joints with Respect to In Vivo Kinematics. *Annals of Biomedical Engineering*. **43**(10), pp.2456–2466.

Battaglia, S., Belvedere, C., Jaber, S.A., Affatato, S., D'Angeli, V. and Leardini, A. 2014. A new protocol from real joint motion data for wear simulation in total knee arthroplasty: Stair climbing. *Medical Engineering and Physics*. **36**(12), pp.1605–1610.

Bedi, A., Kelly, N.H., Baad, M., Fox, A.J.S., Brophy, R.H., Warren, R.F. and Maher, S.A. 2010. Dynamic contact mechanics of the medial meniscus as a function of radial tear, repair, and partial meniscectomy. *Journal of Bone and Joint Surgery*. **92**(6), pp.1398–1408.

Bell, C.J., Ingham, E. and Fisher, J. 2006. Influence of hyaluronic acid on the time-dependent friction response of articular cartilage under different conditions. *Proceedings of the Institution of Mechanical Engineers, Part H: Journal of Engineering in Medicine*. **220**(1).

Belvedere, C., Tamarri, S., Notarangelo, D.P., Ensini, A., Feliciangeli, A. and Leardini, A. 2013. Three-dimensional motion analysis of the human knee joint: Comparison

between intra- and post-operative measurements. *Knee Surgery, Sports Traumatology, Arthroscopy*. **21**(10), pp.2375–2383.

Benders, K.E.M., Weeren, P.R. van, Badylak, S.F., Saris, D.B.F., Dhert, W.J.A. and Malda, J. 2013. Extracellular matrix scaffolds for cartilage and bone regeneration. *Trends in Biotechnology*. **31**(3), pp.169–176.

Bentley, G., Biant, L.C., Vijayan, S., Macmull, S., Skinner, J.A. and Carrington, R.W.J. 2012. Minimum ten-year results of a prospective randomised study of autologous chondrocyte implantation versus mosaicplasty for symptomatic articular cartilage lesions of the knee. *THE JOURNAL OF BONE AND JOINT SURGERY*. **94-B**(4), pp.504–509.

Bergmann, G., Bender, A., Graichen, F., Dymke, J., Rohlmann, A., Trepczynski, A., Heller, M.O. and Kutzner, I. 2014. Standardized loads acting in knee implants. *PLoS ONE*. **9**(1).

Binette, J.P. and Schmid, K. 1965. The proteins of synovial fluid: A study of the α1/α2 globulin ratio. *Arthritis & Rheumatism*. **8**(1), pp.14–28.

Bobrowitsch, E., Lorenz, A., Jörg, J., Leichtle, U.G., Wülker, N. and Walter, C. 2014. Changes in dissipated energy and contact pressure after osteochondral graft transplantation. *Medical Engineering and Physics*. **36**(9), pp.1156–1161.

Bobrowitsch, E., Lorenz, A., Wülker, N. and Walter, C. 2014. Simulation of in vivo dynamics during robot assisted joint movement. *BioMedical Engineering Online*. **13**(1).

Boguszewski, D. v., Joshi, N.B., Wang, D., Markolf, K.L., Petrigliano, F.A. and McAllister, D.R. 2014. Effect of different preconditioning protocols on anterior knee laxity after ACL reconstruction with four commonly used grafts. *Journal of Bone and Joint Surgery - American Volume*. **97**(13), pp.1059–1066.

Bonnevie, E.D., Galesso, D., Secchieri, C., Cohen, I. and Bonassar, L.J. 2015. Elastoviscous transitions of articular cartilage reveal a mechanism of synergy between lubricin and hyaluronic acid. *PLoS ONE*. **10**(11).

van den Borne, M.P.J., Raijmakers, N.J.H., Vanlauwe, J., Victor, J., de Jong, S.N., Bellemans, J. and Saris, D.B.F. 2007. International Cartilage Repair Society (ICRS) and Oswestry macroscopic cartilage evaluation scores validated for use in Autologous Chondrocyte Implantation (ACI) and microfracture. *Osteoarthritis and Cartilage*. **15**(12), pp.1397–1402.

Borque, K.A., Gold, J.E., Incavo, S.J., Patel, R.M., Ismaily, S.E. and Noble, P.C. 2015. Anteroposterior Knee Stability During Stair Descent. *Journal of Arthroplasty*. **30**(6), pp.1068–1072.

Bortel, E.L., Charbonnier, B. and Heuberger, R. 2015. Development of a synthetic synovial fluid for tribological testing. *Lubricants*. **3**(4), pp.664–686.

Bowland, P. 2016. *Biotribology of Osteochondral Grafts in the Knee*.[Online] University of Leeds. Available from: http://etheses.whiterose.ac.uk/id/eprint/17556.

Bowland, P., Cowie, R.M., Ingham, E., Fisher, J. and Jennings, L.M. 2020. Biomechanical assessment of the stability of osteochondral grafts implanted in porcine and bovine femoral condyles. *Proceedings of the Institution of Mechanical Engineers, Part H: Journal of Engineering in Medicine*. **234**(2), pp.163–170.

Bowland, P., Ingham, E., Fisher, J. and Jennings, L.M. 2018. Development of a preclinical natural porcine knee simulation model for the tribological assessment of osteochondral grafts in vitro. *Journal of Biomechanics*. **77**.

Bowland, Philippa, Ingham, E., Fisher, J. and Jennings, L.M. 2018. Simple geometry tribological study of osteochondral graft implantation in the knee. *Proceedings of the Institution of Mechanical Engineers, Part H: Journal of Engineering in Medicine*. **232**(3).

Bowland, P., Ingham, E., Jennings, L. and Fisher, J. 2015. Review of the biomechanics and biotribology of osteochondral grafts used for surgical interventions in the knee. *Proceedings of the Institution of Mechanical Engineers, Part H: Journal of Engineering in Medicine*. **229**(12).

Braun, H.J. and Gold, G.E. 2012. Diagnosis of osteoarthritis: Imaging. *Bone*. **51**(2), pp.278–288.

BRITISHHEARTFOUNDATION 2015. *Physical Activity Statistics 2015*.

Brittberg, M. 2018. Clinical articular cartilage repair—an up to date review. *Annals of Joint*. **3**, pp.94–94.

Brittberg, M., Lindahl, A., Nilsson, A., Ohlsson, C., Isaksson, O. and Peterson, L. 1994. Treatment of deep cartilage defects in the knee with autologous chondrocyte transplantation. *New England Journal of Medicine*. **331**(14), pp.889–895.

Brittberg, M. and Winalski, C.S. 2003. *Evaluation of Cartilage Injuries and Repair* [Online]. Available from: www.cartilage.org.

Brockett, C.L., Abdelgaied, A., Haythornthwaite, T., Hardaker, C., Fisher, J. and Jennings, L.M. 2016. The influence of simulator input conditions on the wear of total knee replacements: An experimental and computational study. *Proceedings of the Institution of Mechanical Engineers, Part H: Journal of Engineering in Medicine*. **230**(5), pp.429–439.

BS ISO 2009. Implants for surgery — Wear of total knee-joint prostheses — Part 1: Loading and displacement parameters for wear-testing machines with load control and corresponding environmental conditions for test.

BS ISO 2014. Implants for surgery — Wear of total knee-joint prostheses — Part 3: Loading and displacement parameters for wear-testing machines with displacement control and corresponding environmental conditions for test.

Buckwalter, J.A. 1998. Articular cartilage: injuries and potential for healing. *J Orthop Sports Phys Ther*. **28**(4), pp.192–202.

Bulstra, S., Kuijer, R., Eerdmans, P. and van der Linden, A. 1994. The effect in vitro of irrigating solutions on intact rat articular cartilage. *J Bone Joint Surg Br*. **76**(3), pp.468–470.

van de Bunt, F., Emanuel, K.S., Wijffels, T., Kooren, P.N., Kingma, I. and Smit, T.H. 2017. A novel physiological testing device to study knee biomechanics in vitro. *Knee*. **24**(4), pp.718–725.

Caligaris, M. and Ateshian, G.A. 2008. Effects of sustained interstitial fluid pressurization under migrating contact area, and boundary lubrication by synovial fluid, on cartilage friction. *Osteoarthritis and Cartilage*. **16**(10).

Caligaris, M., Canal, C.E., Ahmad, C.S., Gardner, T.R. and Ateshian, G.A. 2009. Investigation of the frictional response of osteoarthritic human tibiofemoral joints and the potential beneficial tribological effect of healthy synovial fluid. *Osteoarthritis and Cartilage*. **17**(10).

Campos, G.E.R., Luecke, T.J., Wendeln, H.K., Toma, K., Hagerman, F.C., Murray, T.F., Ragg, K.E., Ratamess, N.A., Kraemer, W.J. and Staron, R.S. 2002. Muscular adaptations in response to three different resistance-training regimens: Specificity of repetition maximum training zones. *European Journal of Applied Physiology*. **88**(1–2), pp.50–60.

Carr FMedSci, A.J., Price FRCS, A.J., Arden FRCP, N.K., Judge, A, Beard, D J, Carr, A.J., Robertsson, O., Graves, S., Price, A.J., Arden, N.K., Judge, Andrew and Beard, David J 2012. Knee replacement. *www.thelancet.com*. **379**.

Charnley, J. 1960. *THE LUBRICATION OF ANIMAL JOINTS IN RELATION TO SURGICAL RECONSTRUCTION BY ARTHROPLASTY**.

Chaudhari, A.M.W., Briant, P.L., Bevill, S.L., Koo, S. and Andriacchi, T.P. 2008. Knee kinematics, cartilage morphology, and osteoarthritis after ACL injury. *Medicine and Science in Sports and Exercise*. **40**(2), pp.215–222.

Choi, Y.J. and Ra, H.J. 2016. Patient satisfaction after total knee arthroplasty. *Knee Surgery and Related Research*. **28**(1), pp.1–15.

Cilingir, A.C. 2015. Effect of Rotational and Sliding Motions on Friction and Degeneration of Articular Cartilage under Dry and Wet Friction. *Journal of Bionic Engineering*. **12**(3), pp.464–472.

Cook, J.L., Kuroki, K., Visco, D., Pelletier, J.P., Schulz, L. and Lafeber, F.P.J.G. 2010. The OARSI histopathology initiative - recommendations for histological assessments of osteoarthritis in the dog. *Osteoarthritis and Cartilage*. **18**(SUPPL. 3).

Cooke, A.F., Dowson, D. and Wright, V. 1978. The Rheology of Synovial Fluid and Some Potential Synthetic Lubricants for Degenerate Synovial Joints. *Engineering in Medicine*. **7**(2), pp.66–72.

Cowie, R.M., Bowland, P., Baji, D., Fermor, H.L., Ingham, E., Fisher, J. and Jennings, L.M. 2021. An experimental simulation model to assess wear of the porcine patellofemoral joint. *PLoS ONE*. **16**(4 April).

Crapo, P.M., Gilbert, T.W. and Badylak, S.F. 2011. An overview of tissue and whole organ decellularization processes. *Biomaterials*. **32**(12), pp.3233–3243.

Creamer, P. and Hochberg, M.C. 1997a. Osteoarthritis. *The Lancet*. **350**(9076), pp.503–509.

Creamer, P. and Hochberg, M.C. 1997b. Why does osteoarthritis of the knee hurt--sometimes? *Rheumatology*. **36**(7), pp.726–728.

Curl, W.W., Krome, J., Gordon, E.S., Rushing, J., Smith, B.P. and Poehling, G.G. 1997. Cartilage injuries: A review of 31,516 knee arthroscopies. *Arthroscopy: The Journal of Arthroscopic & Related Surgery*. **13**(4), pp.456–460.

Danzl, R., Helmli, F. and Scherer, S. 2011. Focus variation - A robust technology for high resolution optical 3D surface metrology. *Strojniski Vestnik/Journal of Mechanical Engineering*. **57**(3), pp.245–256.

Das, S., Banquy, X., Zappone, B., Greene, G.W., Jay, G.D. and Israelachvili, J.N. 2013. Synergistic interactions between grafted hyaluronic acid and lubricin provide enhanced wear protection and lubrication. *Biomacromolecules*. **14**(5), pp.1669–1677.

Dastgheyb, S.S., Hammoud, S., Ketonis, C., Liu, A.Y., Fitzgerald, K., Parvizi, J., Purtill, J., Ciccotti, M., Shapiro, I.M., Otto, M. and Hickok, N.J. 2015. Staphylococcal persistence due to biofilm formation in synovial fluid containing prophylactic cefazolin. *Antimicrobial Agents and Chemotherapy*. **59**(4), pp.2122–2128.

Davies, D.V. 1966. Paper 7: Properties of Synovial Fluid. *Proceedings of the Institution of Mechanical Engineers, Conference Proceedings*. **181**(10), pp.25–29.

Davis, S., Roldo, M., Blunn, G., Tozzi, G. and Roncada, T. 2021. Influence of the Mechanical Environment on the Regeneration of Osteochondral Defects. *Frontiers in Bioengineering and Biotechnology*. **9**.

Decker, B., McKenzie, B.F., McGuckin, W.F. and Slocumb, C.H. 1959. Comparative distribution of proteins and glycoproteins of serum and synovial fluid. *Arthritis & Rheumatism*. **2**(2), pp.162–177.

Degen, R.M., Tetreault, D., Mahony, G.T. and Williams, R.J. 2016. Acute Delamination of Commercially Available Decellularized Osteochondral Allograft Plugs: A Report of Two Cases. *Cartilage*. **7**(4), pp.316–321.

Delakowski, A.J., Posselt, J.D. and Wagner, C.T. 2022. Modular Bioreactor Design for Directed Tendon/Ligament Tissue Engineering. *Bioengineering*. **9**(3).

Devillard, C.D. and Marquette, C.A. 2021. Vascular Tissue Engineering: Challenges and Requirements for an Ideal Large Scale Blood Vessel. *Frontiers in Bioengineering and Biotechnology*. **9**.

Devitt, B.M., Bell, S.W., Webster, K.E., Feller, J.A. and Whitehead, T.S. 2017. Surgical treatments of cartilage defects of the knee: Systematic review of randomised controlled trials. *Knee*. **24**(3), pp.508–517.

D'Lima, D.D., Steklov, N., Fregly, B.J., Banks, S.A. and Colwell, C.W. 2008. In vivo contact stresses during activities of daily living after knee arthroplasty. *Journal of Orthopaedic Research*. **26**(12), pp.1549–1555.

Dowson, D. 1966. Paper 12: Modes of Lubrication in Human Joints. *Proceedings of the Institution of Mechanical Engineers, Conference Proceedings*. **181**(10), pp.45–54.

Drummond, J., Tran, P. and Fary, C. 2015. Metal-on-Metal Hip Arthroplasty: A Review of Adverse Reactions and Patient Management. *Journal of Functional Biomaterials*. **6**(3), pp.486–499.

Durney, K.M., Shaeffer, C.A., Zimmerman, B.K., Nims, R.J., Oungoulian, S., Jones, B.K., Boorman-Padgett, J.F., Suh, J.T., Shah, R.P., Hung, C.T. and Ateshian, G.A. 2020. Immature bovine cartilage wear by fatigue failure and delamination. *Journal of Biomechanics*. **107**.

Dwyer, T., Martin, C.R., Kendra, R., Sermer, C., Chahal, J., Ogilvie-Harris, D., Whelan, D., Murnaghan, L., Nauth, A. and Theodoropoulos, J. 2017. Reliability and Validity of the Arthroscopic International Cartilage Repair Society Classification System: Correlation With Histological Assessment of Depth. *Arthroscopy - Journal of Arthroscopic and Related Surgery*. **33**(6), pp.1219–1224.

Dyment, N.A., Barrett, J.G., Awad, H.A., Bautista, C.A., Banes, A.J. and Butler, D.L. 2020. A brief history of tendon and ligament bioreactors: Impact and future prospects. *Journal of Orthopaedic Research*. **38**(11), pp.2318–2330.

Eckstein, F., Hudelmaier, M. and Putz, R. 2006. The effects of exercise on human articular cartilage. *Journal of Anatomy*. **208**(4), pp.491–512.

Edwards, J.H., Ingham, E. and Herbert, A. 2019. Decellularisation affects the strain rate dependent and dynamic mechanical properties of a xenogeneic tendon intended for anterior cruciate ligament replacement. *Journal of the Mechanical Behavior of Biomedical Materials*. **91**, pp.18–23.

Elvidge, J., Bullement, A. and Hatswell, A.J. 2016. Cost Effectiveness of Characterised Chondrocyte Implantation for Treatment of Cartilage Defects of the Knee in the UK. *PharmacoEconomics*. **34**(11), pp.1145–1159.

Farnham, M.S., Larson, R.E., Burris, D.L. and Price, C. 2020. Effects of mechanical injury on the tribological rehydration and lubrication of articular cartilage. *Journal of the Mechanical Behavior of Biomedical Materials*. **101**.

Farr, J., Gracitelli, G.C., Shah, N., Chang, E.Y. and Gomoll, A.H. 2016. High Failure Rate of a Decellularized Osteochondral Allograft for the Treatment of Cartilage Lesions. *American Journal of Sports Medicine*. **44**(8), pp.2015–2022.

Fermor, H.L., Russell, S.L., Williams, S., Fisher, J. and Ingham, E. 2015. Development and characterisation of a decellularised bovine osteochondral biomaterial for cartilage repair. *Journal of Materials Science: Materials in Medicine*. **26**(5).

Filardo, G., Kon, E., Perdisa, F., Tetta, C., di Martino, A. and Marcacci, M. 2015. Arthroscopic mosaicplasty: Long-term outcome and joint degeneration progression. *Knee*. **22**(1), pp.36–40.

Flandry, F. and Hommel, G. 2011. *Normal Anatomy and Biomechanics of the Knee* [Online]. Available from: www.sportsmedarthro.com.

Flanigan, D.C., Harris, J.D., Trinh, T.Q., Siston, R.A. and Brophy, R.H. 2010. Prevalence of chondral defects in Athletes' Knees: A systematic review. *Medicine and Science in Sports and Exercise*. **42**(10), pp.1795–1801.

Forsey, R.W., Fisher, J., Thompson, J., Stone, M.H., Bell, C. and Ingham, E. 2006. The effect of hyaluronic acid and phospholipid based lubricants on friction within a human cartilage damage model. *Biomaterials*. **27**(26), pp.4581–4590.

Forster, H. and Fisher, J. 1996. The influence of loading time and lubricant on the friction of articular cartilage. *Proceedings of the Institution of Mechanical Engineers, Part H: Journal of Engineering in Medicine*. **210**(2).

Fox, A.J.S., Bedi, A. and Rodeo, S.A. 2012. The Basic Science of Human Knee Menisci: Structure, Composition, and Function. *Sports Health*. **4**(4), pp.340–351.

Fox, N., Stanley, M., Thomas, D., Fisher, J. and Ingham, E. 2018. EX VIVO ORGAN CULTURE OF THE PORCINE FEMORAL-TIBIAL JOINT. *Orthopaedic Proceedings*. **99-B**(9).

Frank, C.B. 2004. Ligament structure, physiology and function. *J Musculoskelet Neuronal Interact*. **4**(2), pp.199–201.

Frank, R.M., Mccormick, F., Rosas, S., Amoo-Achampong, K., Erickson, B., Bach, B.R. and Cole, B.J. 2018. *Reoperation Rates After Cartilage Restoration Procedures in the Knee: Analysis of a Large US Commercial Database Take-Home Points* [Online]. Available from: www.amjorthopedics.com.

Fu, L., Li, P., Li, H., Gao, C., Yang, Z., Zhao, T., Chen, W., Liao, Z., Peng, Y., Cao, F., Sui, X., Liu, S. and Guo, Q. 2021. The Application of Bioreactors for Cartilage Tissue Engineering: Advances, Limitations, and Future Perspectives. *Stem Cells International*. **2021**.

Fukubayashi, T., Torzilli, P., Sherman, M. and Warren, R. 1982. An in vitro biomechanical evaluation of anterior-posterior motion of the knee. Tibial displacement, rotation, and torque. *J Bone Joint Surg Am*. **64**(2), pp.258–264.

Furmann, D., Nečas, D., Rebenda, D., Čípek, P., Vrbka, M., Křupka, I. and Hartl, M. 2020. The effect of synovial fluid composition, speed and load on frictional behaviour of articular cartilage. *Materials*. **13**(6).

Galandáková, A., Ulrichová, J., Langová, K., Hanáková, A., Vrbka, M., Hartl, M. and Gallo, J. 2017. Characteristics of synovial fluid required for optimization of lubrication fluid for biotribological experiments. *Journal of Biomedical Materials Research - Part B Applied Biomaterials*. **105**(6), pp.1422–1431.

Gallo, J., Goodman, S.B., Konttinen, Y.T. and Raska, M. 2013. Particle disease: Biologic mechanisms of periprosthetic osteolysis in total hip arthroplasty. *Innate Immunity*. **19**(2), pp.213–224.

Gilbert, S., Chen, T., Hutchinson, I.D., Choi, D., Voigt, C., Warren, R.F. and Maher, S.A. 2014. Dynamic contact mechanics on the tibial plateau of the human knee during activities of daily living. *Journal of Biomechanics*. **47**(9).

Goldring, S. and Goldring, M. 2017. Biology of the Normal Joint *In*: *Structure and Function of bone, Joints and Connective Tissue*.

Goldring, S.R. 2012. Alterations in periarticular bone and cross talk between subchondral bone and articular cartilage in osteoarthritis. *Therapeutic Advances in Musculoskeletal Disease*. **4**(4), pp.249–258.

Gomoll, A.H. 2013. Osteochondral allograft transplantation using the chondrofix implant. *Operative Techniques in Sports Medicine*. **21**(2), pp.90–94.

GOVUK 2019. Musculoskeletal health: applying All Our Health.

Gracitelli, G.C., Moraes, V.Y., Franciozi, C.E.S., Luzo, M. v. and Belloti, J.C. 2016. Surgical interventions (microfracture, drilling, mosaicplasty, and allograft transplantation) for treating isolated cartilage defects of the knee in adults. *Cochrane Database of Systematic Reviews*. **2016**(9).

Graham, B.T., Moore, A.C., Burris, D.L. and Price, C. 2017. Sliding enhances fluid and solute transport into buried articular cartilage contacts. *Osteoarthritis and Cartilage*. **25**(12), pp.2100–2107.

Greaves, N.S., Benatar, B., Baguneid, M. and Bayat, A. 2013. Single-stage application of a novel decellularized dermis for treatment-resistant lower limb ulcers: Positive outcomes assessed by SIAscopy, laser perfusion, and 3D imaging, with sequential timed histological analysis *In*: *Wound Repair and Regeneration*., pp.813–822.

Greene, G.W., Banquy, X., Woog Lee, D., Lowrey, D.D., Yu, J. and Israelachvili, J.N. 2011. Adaptive mechanically controlled lubrication mechanism found in articular joints. *Proceedings of the National Academy of Sciences of the United States of America*. **108**(13), pp.5255–5259.

Gudas, R., Gudaite, A., Pocius, A., Gudiene, A., Čekanauskas, E., Monastyreckiene, E. and Basevičius, A. 2012. Ten-year follow-up of a prospective, randomized clinical study of mosaic osteochondral autologous transplantation versus microfracture for the treatment of osteochondral defects in the knee joint of athletes. *American Journal of Sports Medicine*. **40**(11), pp.2499–2508.

Haber, D.B., Logan, C.A., Murphy, C.P., Sanchez, A., LaPrade, R.F. and Provencher, M.T. 2019. OSTEOCHONDRAL ALLOGRAFT TRANSPLANTATION for the KNEE: POST-OPERATIVE REHABILITATION. *International Journal of Sports Physical Therapy*. **14**(3), pp.487–499.

HAIDER, H. and WALKER, P. 2002. Analysis and recommendations for the optimum spring configurations for soft tissue restraint in force-control knee simulator testing. *TRANSACTIONS OF THE ANNUAL MEETING-ORTHOPAEDIC RESEARCH SOCIETY*., pp.912–912.

Hallas, J., Janvier, A.J., Hoettges, K.F. and Henstock, J.R. 2022. Pneumatic piston hydrostatic bioreactor for cartilage tissue engineering. *Instrumentation Science and Technology*.

Hambly, K., Silvers, H.J. and Steinwachs, M. 2012. Rehabilitation after Articular Cartilage Repair of the Knee in the Football (Soccer) Player. *Cartilage*. **3**(1 SUPPL.).

HAMROCK, B., SCHMID, S. and JACOBSON, B. 2004. *Fundamentals of Fluid Film Lubrication*. Taylor and Francis.

Hangody, L., Dobos, J., Balo, E., Panics, G., Rudolf Hangody, L. and Berkes, I. 2010. Clinical experiences with autologous osteochondral mosaicplasty in an athletic population: A 17-year prospective multicenter study. *American Journal of Sports Medicine*. **38**(6), pp.1125–1133.

Hangody, L. and Fules, P. 2003. Autologous osteochondral mosaicplasty for the treatment of full-thickness defects of weight-bearing joints: ten years of experimental and clinical experience. *J Bone Joint Surg Am*. **85-A**(Suppl 2), pp.25–32.

Hangody, L., Vásárhelyi, G., Hangody, L.R., Sükösd, Z., Tibay, G., Bartha, L. and Bodó, G. 2008. Autologous osteochondral grafting-Technique and long-term results. *Injury*. **39**(1 SUPPL.), pp.32–39.

Harris, J.D., Brophy, R.H., Siston, R.A. and Flanigan, D.C. 2010. Treatment of Chondral Defects in the Athlete's Knee. *Arthroscopy: The Journal of Arthroscopic & Related Surgery*. **26**(6), pp.841–852.

Harsha, A.P. and Joyce, T.J. 2011. Challenges associated with using bovine serum in wear testing orthopaedic biopolymers. *Proceedings of the Institution of Mechanical Engineers, Part H: Journal of Engineering in Medicine*. **225**(10), pp.948–958.

Hashemi, J., Chandrashekar, N., Jang, T., Karpat, F., Oseto, M. and Ekwaro-Osire, S. 2007. An alternative mechanism of non-contact anterior cruciate ligament injury during jump-landing: In-vitro simulation. *Experimental Mechanics*. **47**(3), pp.347–354.

Herbert, A., Jones, G.L., Ingham, E. and Fisher, J. 2015. A biomechanical characterisation of acellular porcine super flexor tendons for use in anterior cruciate ligament replacement: Investigation into the effects of fat reduction and bioburden reduction bioprocesses. *Journal of Biomechanics*. **48**(1), pp.22–29.

Heuberger, R., Bortel, E.L., Sague, J., Escuder, P. and Nohava, J. 2020. Shear resistance and composition of polyethylene protuberances from hip-simulating pin-on-disc wear tests. *Biotribology*. **23**.

Hinterwimmer, S., Krammer, M., Krötz, M., Glaser, C., Baumgart, R., Reiser, M. and Eckstein, F. 2004. Cartilage atrophy in the knees of patients after seven weeks of partial load bearing. *Arthritis and Rheumatism*. **50**(8), pp.2516–2520.

van Houtem, M., Clough, R., Khan, A., Harrison, M. and Blunn, G.W. 2006. Validation of the soft tissue restraints in a force-controlled knee simulator. *Proceedings of the Institution of Mechanical Engineers, Part H: Journal of Engineering in Medicine*. **220**(3), pp.449–456.

Huang, F.S., Simonian, P.T., Norman, A.G. and Clark, J.M. 2004. Effects of small incongruities in a sheep model of osteochondral autografting. *American Journal of Sports Medicine*. **32**(8), pp.1842–1848.

Huiskes, R., Ruimerman, R., van Lenthe, G. and Janssen, J. 2000. Effects of mechanical forces on maintenance and adaptation of form in trabecular bone. *Nature*. **405**(6787), pp.704–706.

Iijima, H., Aoyama, T., Ito, A., Tajino, J., Nagai, M., Zhang, X., Yamaguchi, S., Akiyama, H. and Kuroki, H. 2014. Immature articular cartilage and subchondral bone covered by menisci are potentially susceptive to mechanical load. *BMC Musculoskeletal Disorders*. **15**(1).

ISO 2014. BS ISO 14243-3:2014+A1:2020 Implants for surgery — Wear of total knee-joint prostheses Part 3: Loading and displacement parameters for wear-testing machines with displacement control and corresponding environmental conditions for test.

ISO 2018. ISO 10993-1:2018 Biological evaluation of medical devices — Part 1: Evaluation and testing within a risk management process.

Jennings, L., Al-Hajjar, M., Brockett, C., Williams, S., Tipper, J., Ingham, E. and Fisher, J. 2012. (iv) Enhancing the safety and reliability of joint replacement implants. *Orthopaedics and trauma*. **26**(4), pp.246–252.

Jennings, L.M., Al-Hajjar, M., Brockett, C.L., Williams, S., Tipper, J.L., Ingham, E. and Fisher, J. 2012. *(iv) Enhancing the safety and reliability of joint replacement implants*.

Jody Northwood MEng, E. 2007. *Cartilage Wear simulation models for Surface and Spacer Hemiarthroplasty and Tissue Engineering*.

Johnson, C.C., Johnson, D.J., Garcia, G.H., Wang, D., Pais, M., Degen, R.M., Burge, A.J. and Williams, R.J. 2017. High Short-Term Failure Rate Associated With Decellularized Osteochondral Allograft for Treatment of Knee Cartilage Lesions. *Arthroscopy - Journal of Arthroscopic and Related Surgery*. **33**(12), pp.2219–2227.

Johnston, H., Abdelgaied, A., Pandit, H., Fisher, J. and Jennings, L.M. 2018. Representing the effect of variation in soft tissue constraints in experimental

simulation of total knee replacements. *Journal of the Mechanical Behavior of Biomedical Materials*. **87**, pp.87–94.

Kahlenberg, C.A., Nwachukwu, B.U., McLawhorn, A.S., Cross, M.B., Cornell, C.N. and Padgett, D.E. 2018. Patient Satisfaction After Total Knee Replacement: A Systematic Review. *HSS Journal*. **14**(2), pp.192–201.

Kaplan, J.T., Neu, C.P., Drissi, H., Emery, N.C. and Pierce, D.M. 2017. Cyclic loading of human articular cartilage: The transition from compaction to fatigue. *Journal of the Mechanical Behavior of Biomedical Materials*. **65**, pp.734–742.

Katta, J., Jin, Z., Ingham, E. and Fisher, J. 2009. Effect of nominal stress on the long term friction, deformation and wear of native and glycosaminoglycan deficient articular cartilage. *Osteoarthritis and Cartilage*. **17**(5), pp.662–668.

Kellgren, J.H. and Lawrence, J.S. 1957. *RADIOLOGICAL ASSESSMENT OF OSTEO-ARTHROSIS*.

Keszég, M., Hangody, L., Egyed, Z., Tóth, G. and Pánics, G. 2022. Long-term (10-25 years) outcomes of knee osteochondral autologous transplantation in soccer players. *Journal of Cartilage & Joint Preservation*. **2**(2), p.100062.

Kheir, E., Stapleton, T., Shaw, D., Jin, Z., Fisher, J. and Ingham, E. 2011. Development and characterization of an acellular porcine cartilage bone matrix for use in tissue engineering. *Journal of Biomedical Materials Research - Part A*. **99 A**(2), pp.283–294.

Kimmel, H. and Gittleman, H. 2017. Retrospective observational analysis of the use of an architecturally unique dermal regeneration template (Derma Pure®) for the treatment of hard-to-heal wounds. *International Wound Journal*. **14**(4), pp.666–672.

Kirkley, A., Birmingham, T.B., Litchfield, R.B., Giffin, J.R., Willits, K.R., Wong, C.J., Feagan, B.G., Donner, A., Griffin, S.H., D'Ascanio, L.M., Pope, J.E. and Fowler, P.J. 2008. A Randomized Trial of Arthroscopic Surgery for Osteoarthritis of the Knee. *New England Journal of Medicine*. **359**(11), pp.1097–1107.

Kocher, M.S., Tucker, R., Ganley, T.J. and Flynn, J.M. 2006. Management of osteochondritis dissecans of the knee: Current concepts review. *American Journal of Sports Medicine*. **34**(7), pp.1181–1191.

Koh, J.L., Wirsing, K., Lautenschlager, E. and Zhang, L.O. 2004. The Effect of Graft Height Mismatch on Contact Pressure Following Osteochondral Grafting: A Biomechanical Study. *American Journal of Sports Medicine*. **32**(2), pp.317–320.

Kreuz, P.C., Steinwachs, M.R., Erggelet, C., Krause, S.J., Konrad, G., Uhl, M. and Südkamp, N. 2006. Results after microfracture of full-thickness chondral defects in

different compartments in the knee. *Osteoarthritis and Cartilage*. **14**(11), pp.1119–1125.

Krishnan, R., Caligaris, M., Mauck, R.L., Hung, C.T., Costa, K.D. and Ateshian, G.A. 2004. Removal of the superficial zone of bovine articular cartilage does not increase its frictional coefficient. *Osteoarthritis and Cartilage*. **12**(12), pp.947–955.

Krishnan, Ramaswamy, Kopacz, M. and Ateshian, G.A. 2004. Experimental verification of the role of interstitial fluid pressurization in cartilage lubrication. *Journal of Orthopaedic Research*. **22**(3).

Krishnan, R., Mariner, E.N. and Ateshian, G.A. 2005. Effect of dynamic loading on the frictional response of bovine articular cartilage. *Journal of Biomechanics*. **38**(8), pp.1665–1673.

Lafortune, M.A., Cavanagh, P.R., Sommer, H.J. and Kalenak~i, A. 1992. *THREE-DIMENSIONAL KINEMATICS OF THE HUMAN KNEE DURING WALKING**.

Lane, J., Healey, R. and Amiel, D. 2009. Changes in Condylar Coefficient of Friction After Osteochondral Graft Transplantation and Modulation With Hyaluronan. *Arthroscopy - Journal of Arthroscopic and Related Surgery*. **25**(12), pp.1401–1407.

Lewis, P.R. and McCutchen, C.W. 1959. Experimental evidence for weeping lubrication in mammalian joints. *Nature*. **184**, p.1285.

Lim, H.C., Bae, J.H., Song, S.H., Park, Y.E. and Kim, S.J. 2012. Current treatments of isolated articular cartilage lesions of the knee achieve similar outcomes knee. *Clinical Orthopaedics and Related Research*. **470**(8), pp.2261–2267.

lin, Y., Hall, A.C., R W Simpson, A.H. and orthopaedic Surgeon, C. 2018. A novel organ culture model of a joint for the evaluation of static and dynamic load on articular cartilage Objectives. *Bone Joint Res*. **7**(3), pp.205–212.

Link, J.M., Salinas, E.Y., Hu, J.C. and Athanasiou, K.A. 2020. The tribology of cartilage: Mechanisms, experimental techniques, and relevance to translational tissue engineering. *Clinical Biomechanics*. **79**.

Liu, A., Ingham, E., Fisher, J. and Jennings, L.M. 2019. Development of a pre-clinical experimental simulation model of the natural porcine knee with appropriate ligamentous constraints. *PLoS ONE*. **14**(5).

Liu, A., Jennings, L.M., Ingham, E. and Fisher, J. 2015. Tribology studies of the natural knee using an animal model in a new whole joint natural knee simulator. *Journal of Biomechanics*. **48**(12).

Liu, A., Sanderson, W.J., Ingham, E., Fisher, J. and Jennings, L.M. 2020. Development of a specimen-specific in vitro pre-clinical simulation model of the human

cadaveric knee with appropriate soft tissue constraints. *PLoS ONE*. **15**(10 October).

Lizhang, J., Fisher, J., Jin, Z., Burton, A. and Williams, S. 2011. The effect of contact stress on cartilage friction, deformation and wear *In*: *Proceedings of the Institution of Mechanical Engineers, Part H: Journal of Engineering in Medicine*., pp.461–475.

Loeser, R.F. 2006. Molecular mechanisms of cartilage destruction: Mechanics, inflammatory mediators, and aging collide. *Arthritis and Rheumatism*. **54**(5), pp.1357–1360.

Loeser, R.F., Goldring, S.R., Scanzello, C.R. and Goldring, M.B. 2012. Osteoarthritis: A disease of the joint as an organ. *Arthritis and Rheumatism*. **64**(6), pp.1697–1707.

Long, W.J., Greene, J.W. and Cushner, F.D. 2016. Early Clinical Outcomes Associated with a Novel Osteochondral Allograft Transplantation System in the Knee. *Advances in Orthopedic Surgery*. **2016**, pp.1–6.

Lorenz, A., Bobrowitsch, E., Wünschel, M., Walter, C., Wülker, N. and Leichtle, U.G. 2015. Robot-aided in vitro measurement of patellar stability with consideration to the influence of muscle loading. *BioMedical Engineering Online*. **14**(1).

Lorenz, A., Rothstock, S., Bobrowitsch, E., Beck, A., Gruhler, G., Ipach, I., Leichtle, U.G., Wülker, N. and Walter, C. 2013. Cartilage surface characterization by frictional dissipated energy during axially loaded knee flexion-An in vitro sheep model. *Journal of Biomechanics*. **46**(8), pp.1427–1432.

Lorenz, A., Röttgerkamp, H., Bobrowitsch, E., Leichtle, C.I. and Leichtle, U.G. 2016. Tibial rotation influences anterior knee stability - A robot-aided in-vitro study. *Clinical Biomechanics*. **32**, pp.131–137.

Lübbeke, A., Silman, A.J., Prieto-Alhambra, D., Adler, A.I., Barea, C. and Carr, A.J. 2017. The role of national registries in improving patient safety for hip and knee replacements. *BMC Musculoskeletal Disorders*. **18**(1).

Maag, C., Metcalfe, A., Cracaoanu, I., Wise, C. and Auger, D.D. 2021. The development of simulator testing for total knee replacements. *Biosurface and Biotribology*. **7**(2), pp.70–82.

Maglio, M., Brogini, S., Pagani, S., Giavaresi, G. and Tschon, M. 2019. Current Trends in the Evaluation of Osteochondral Lesion Treatments: Histology, Histomorphometry, and Biomechanics in Preclinical Models. *BioMed Research International*. **2019**.

Maher, S.A., Rodeo, S.A., Potter, H.G., Bonassar, L.J., Wright, T.M. and Warren, R.F. 2011. A Pre-Clinical Test Platform for the Functional Evaluation of Scaffolds for Musculoskeletal Defects: The Meniscus. *HSS Journal*. **7**(2), pp.157–163.

Marchiori, G., Berni, M., Boi, M., Bianchi, M. and Filardo, G. 2019. Cartilage mechanical tests: Evolution of current standards for cartilage repair and tissue engineering. A literature review. *Clinical Biomechanics*. **68**, pp.58–72.

Masouros, S.D. and Bull, A.M.J. 2010. *(i) Biomechanics of the knee joint*.

Matharu, G.S., Judge, A., Pandit, H.G. and Murray, D.W. 2018. Follow-up for patients with metal-on-metal hip replacements: Are the new MHRA recommendations justified? *BMJ (Online)*. **360**.

Mazzucco, D., Scott, R. and Spector, M. 2004. Composition of joint fluid in patients undergoing total knee replacement and revision arthroplasty: Correlation with flow properties. *Biomaterials*. **25**(18), pp.4433–4445.

McAdams, T.R., Mithoefer, K., Scopp, J.M. and Mandelbaum, B.R. 2010. Articular cartilage injury in athletes. *Cartilage*. **1**(3), pp.165–179.

McCann, L., Ingham, E., Jin, Z. and Fisher, J. 2009. Influence of the meniscus on friction and degradation of cartilage in the natural knee joint. *Osteoarthritis and Cartilage*. **17**(8), pp.995–1000.

McCann, L., Udofia, I., Graindorge, S., Ingham, E., Jin, Z. and Fisher, J. 2008. Tribological testing of articular cartilage of the medial compartment of the knee using a friction simulator. *Tribology International*. **41**(11), pp.1126–1133.

Mccormack, T. and Mansour, J.M. 1998. *Reduction in tensile strength of cartilage precedes surface damage under repeated compressive loading in vitro*.

McCormick, F., Harris, J.D., Abrams, G.D., Frank, R., Gupta, A., Hussey, K., Wilson, H., Bach, B. and Cole, B. 2014. Trends in the surgical treatment of articular cartilage lesions in the United States: An analysis of a large private-payer database over a period of 8 years. *Arthroscopy - Journal of Arthroscopic and Related Surgery*. **30**(2), pp.222–226.

McCutchen, C.W. 1962. The frictional properties of animal joints. *Wear*. **5**(1), pp.1–17.

McEwen, H.M.J., Barnett, P.I., Bell, C.J., Farrar, R., Auger, D.D., Stone, M.H. and Fisher, J. 2005. The influence of design, materials and kinematics on the in vitro wear of total knee replacements. *Journal of Biomechanics*. **38**(2), pp.357–365.

Meireles, S., Wesseling, M., Smith, C.R., Thelen, D.G., Verschueren, S. and Jonkers, I. 2017. Medial knee loading is altered in subjects with early osteoarthritis during gait but not during step-up-and-over task. *PLoS ONE*. **12**(11).

Meng, X., Ziadlou, R., Grad, S., Alini, M., Wen, C., Lai, Y., Qin, L., Zhao, Y. and Wang, X. 2020. Animal Models of Osteochondral Defect for Testing Biomaterials. *Biochemistry Research International*. **2020**.

MHRA 2018. Animal use in medicines and medical devices regulation. *www.gov.uk*. [Online]. [Accessed 14 May 2023]. Available from: https://www.gov.uk/government/publications/animal-use-in-medicines-and-medical-devices-regulation.

Mistry, H., Metcalfe, A., Smith, N., Loveman, E., Colquitt, J., Royle, P. and Waugh, N. 2019. The cost-effectiveness of osteochondral allograft transplantation in the knee. *Knee Surgery, Sports Traumatology, Arthroscopy*. **27**(6), pp.1739–1753.

Mithoefer, K., Hambly, K., Villa, S. della, Silvers, H. and Mandelbaum, B.R. 2009. Return to Sports Participation after Articular Cartilage Repair in the Knee: Scientific Evidence. *American Journal of Sports Medicine*. **37**(1_suppl), pp.167S-176S.

Mithoefer, K., Mcadams, T., Williams, R.J., Kreuz, P.C. and Mandelbaum, B.R. 2009. Clinical efficacy of the microfracture technique for articular cartilage repair in the knee: An evidence-based systematic analysis. *American Journal of Sports Medicine*. **37**(10), pp.2053–2063.

Moore, A.C. and Burris, D.L. 2017. Tribological rehydration of cartilage and its potential role in preserving joint health. *Osteoarthritis and Cartilage*. **25**(1), pp.99–107.

Moore, M.A., Samsell, B., Wallis, G., Triplett, S., Chen, S., Jones, A.L. and Qin, X. 2015. Decellularization of human dermis using non-denaturing anionic detergent and endonuclease: a review. *Cell and Tissue Banking*. **16**(2), pp.249–259.

Morlock, M., Schneider, E., Bluhm, A., Vollmer, M., Bergmann, G., Uller D, V.M. and Honl, M. 2001. *Duration and frequency of every day activities in total hip patients* [Online]. Available from: http://www.tu-harburg.de/bim.

Mow, V.C., Kuei, S.C., Lai, W.M. and Armstrong, C.G. 1980. Biphasic creep and stress relaxation of articular cartilage in compression: Theory and experiments. *Journal of Biomechanical Engineering*. **102**(1), pp.73–84.

Mündermann, A., Dyrby, C.O., D'Lima, D.D., Colwell, C.W. and Andriacchi, T.P. 2008. In vivo knee loading characteristics during activities of daily living as measured by an instrumented total knee replacement. *Journal of Orthopaedic Research*. **26**(9), pp.1167–1172.

Murakami, T., Yarimitsu, S., Nakashima, K., Sawae, Y. and Sakai, N. 2013. Influence of synovia constituents on tribological behaviors of articular cartilage. *Friction*. **1**(2), pp.150–162.

Nakagawa, Y., Suzuki, T., Kuroki, H., Kobayashi, M., Okamoto, Y. and Nakamura, T. 2007. The effect of surface incongruity of grafted plugs in osteochondral grafting: A report of five cases. *Knee Surgery, Sports Traumatology, Arthroscopy*. **15**(5), pp.591–596.

Newman, A.P. 1998. *Current Concepts Articular Cartilage Repair*.

NICE 2017. Autologous chondrocyte implantation for treating symptomatic articular cartilage defects of the knee Technology appraisal guidance [TA477]. *National Institute for Health Care Excellence*.

Nielsen, E.S., McCauley, J.C., Pulido, P.A. and Bugbee, W.D. 2017. Return to Sport and Recreational Activity after Osteochondral Allograft Transplantation in the Knee. *American Journal of Sports Medicine*. **45**(7), pp.1608–1614.

Niu, X., Li, N., Du, Z. and Li, X. 2023. Integrated gradient tissue-engineered osteochondral scaffolds: Challenges, current efforts and future perspectives. *Bioactive Materials*. **20**, pp.574–597.

NJR 2022. *National Joint Registry 19th Annual Report*.

Nooeaid, P., Salih, V., Beier, J.P. and Boccaccini, A.R. 2012. Osteochondral tissue engineering: Scaffolds, stem cells and applications. *Journal of Cellular and Molecular Medicine*. **16**(10), pp.2247–2270.

Norbertczak, H.T., Fermor, H.L., Edwards, J.H., Rooney, P., Ingham, E. and Herbert, A. 2022. Decellularised human bone allograft from different anatomical sites as a basis for functionally stratified repair material for bone defects. *Journal of the Mechanical Behavior of Biomedical Materials*. **125**.

Northwood, E. and Fisher, J. 2007. A multi-directional in vitro investigation into friction, damage and wear of innovative chondroplasty materials against articular cartilage. *Clinical Biomechanics*. **22**(7), pp.834–842.

Nosewicz, T.L., Reilingh, M.L., Wolny, M., van Dijk, C.N., Duda, G.N. and Schell, H. 2014. Influence of basal support and early loading on bone cartilage healing in press-fitted osteochondral autografts. *Knee Surgery, Sports Traumatology, Arthroscopy*. **22**(6), pp.1445–1451.

Novakofski, K.D., Pownder, S.L., Koff, M.F., Williams, R.M., Potter, H.G. and Fortier, L.A. 2016. High-Resolution Methods for Diagnosing Cartilage Damage In Vivo. *Cartilage*. **7**(1), pp.39–51.

OFFICEFORNATIONALSTATISTICS 2018. *Overview of the UK population: November 2018*.

Oláh, T., Cai, X., Michaelis, J.C. and Madry, H. 2021. Comparative anatomy and morphology of the knee in translational models for articular cartilage disorders. Part I: Large animals. *Annals of Anatomy*. **235**.

Orsi, A.D., Chakravarthy, S., Canavan, P.K., Peña, E., Goebel, R., Vaziri, A. and Nayeb-Hashemi, H. 2016. The effects of knee joint kinematics on anterior cruciate ligament injury and articular cartilage damage. *Computer Methods in Biomechanics and Biomedical Engineering*. **19**(5), pp.493–506.

Oungoulian, S.R., Durney, K.M., Jones, B.K., Ahmad, C.S., Hung, C.T. and Ateshian, G.A. 2015. Wear and damage of articular cartilage with friction against orthopedic implant materials. *Journal of Biomechanics*. **48**(10).

Outerbridge, R.E. 1961. The etiology of chondromalacia patellae. *J Bone Joint Surg Br*. **43-b**, pp.752–757.

Pan, H., Zhang, Y., He, G.X., Katagori, N. and Chen, H. 2014. A comparison of conventional methods for the quantification of bacterial cells after exposure to metal oxide nanoparticles. *BMC Microbiology*. **14**(1).

Pandit, H., Glyn-Jones, S., Mclardy-Smith, P., Gundle, R., Whitwell, D., Gibbons, C.L.M., Ostlere, S., Athanasou, N., Gill, H.S. and Murray, D.W. 2008. Pseudotumours associated with metal-on-metal hip resurfacings. . **90**(7).

Panzica, M., Janzik, J., Bobrowitsch, E., Krettek, C., Hawi, N., Hurschler, C. and Jagodzinski, M. 2015. Biomechanical comparison of two surgical techniques for press-fit reconstruction of the posterolateral complex of the knee. *Archives of Orthopaedic and Trauma Surgery*. **135**(11), pp.1579–1588.

Park, S., Nicoll, S.B., Mauck, R.L. and Ateshian, G.A. 2008. Cartilage mechanical response under dynamic compression at physiological stress levels following collagenase digestion. *Annals of Biomedical Engineering*. **36**(3), pp.425–434.

Patel, J.M., Wise, B.C., Bonnevie, E.D. and Mauck, R.L. 2019. A Systematic Review and Guide to Mechanical Testing for Articular Cartilage Tissue Engineering. *Tissue Engineering - Part C: Methods*. **25**(10), pp.593–608.

Randsborg, P.H., Brinchmann, J., Løken, S., Hanvold, H.A., Aae, T.F. and Årøen, A. 2016. Focal cartilage defects in the knee -a randomized controlled trial comparing autologous chondrocyte implantation with arthroscopic debridement. *BMC Musculoskeletal Disorders*. **17**(1).

Rebenda, D., Vrbka, M., Ćípek, P., Toropitsyn, E., Nečas, D., Pravda, M. and Hartl, M. 2020. On the dependence of rheology of hyaluronic acid solutions and frictional behavior of articular cartilage. *Materials*. **13**(11).

Reynolds, K.L. and Bishai, S.K. 2014. In situ evaluation of chondrofix® osteochondral allograft 25 months following implantation: A case report. *Osteoarthritis and Cartilage*. **22**, pp.S155–S156.

Robinson, E., Mulliken, B., Bourne, R., Rorabeck, C. and Alvarez, C. 1995. Catastrophic osteolysis in total knee replacement. *Clinical Orthopaedics and Related Research*. (321), pp.98–105.

Ronga, M., Stissi, P., Barbera, G., Valoroso, M., Angeretti, G., Genovese, E. and Cherubino, P. 2016. Treatment of unstable osteochondritis dissecans in adults with autogenous osteochondral grafts (Mosaicplasty): long-term results. *Joints*. **3**(4), pp.173–178.

Roos, E.M. and Dahlberg, L. 2005. Positive effects of moderate exercise on glycosaminoglycan content in knee cartilage: A four-month, randomized, controlled trial in patients at risk of osteoarthritis. *Arthritis and Rheumatism*. **52**(11), pp.3507–3514.

Rosa, N., Simoes, R., Magalhães, F.D. and Marques, A.T. 2015. From mechanical stimulus to bone formation: A review. *Medical Engineering & Physics*. **37**(8), pp.719–728.

Rowe, P.J., Myles, C.M., Walker, C. and Nutton, R. 2000. *Knee joint kinematics in gait and other functional activities measured using flexible electrogoniometry: how much knee motion is sufficient for normal daily life?* [Online]. Available from: www.elsevier.com/locate/gaitpos.

Rumian, A.P., Wallace, A.L. and Birch, H.L. 2007. Tendons and ligaments are anatomically distinct but overlap in molecular and morphological features - A comparative study in an ovine model. *Journal of Orthopaedic Research*. **25**(4), pp.458–464.

Russell, S. 2010. *Friction, wear, wear debris and functional biocompatibility of cartilage substitution biomaterials*.[Online] University of Leeds. Available from: http://etheses.whiterose.ac.uk/id/eprint/12742.

Saari, H., Konttinen, Y.T., Friman, C. and Sorsa, T. 1993. *DIFFERENTIAL EFFECTS OF REACTIVE OXYGEN SPECIES ON NATIVE SYNOVIAL FLUID AND PURIFIED HUMAN UMBILICAL CORD HYALURONATE*.

Sanctuary, C.S., Wiskott, H.W.A., Justiz, J., Botsis, J. and Belser, U.C. 2005. In vitro time-dependent response of periodontal ligament to mechanical loading.

Sarpong, N.O., Sonnenfeld, J.J., LiArno, S., Rajaravivarma, R., Donde, S., Sneddon, E., Kaverina, T., Cooper, H.J., Shah, R.P. and Geller, J.A. 2020. Virtual

reconstruction of the posterior cruciate ligament for mechanical testing of total knee arthroplasty implants. *Knee*. **27**(1), pp.151–156.

Schiller, J., Arnhold, J., Grunder, W., Wagner, M., Werner, A. and Arnold, K. 1995. Comparison of the Bactericidal Efficacy of Sodium Azide and Methiolate - An NMR Study. *Biomed.Technik*. **40**, pp.250–254.

Schmidt, T.A., Gastelum, N.S., Nguyen, Q.T., Schumacher, B.L. and Sah, R.L. 2007. Boundary lubrication of articular cartilage: Role of synovial fluid constituents. *Arthritis and Rheumatism*. **56**(3).

Schmidt, T.A. and Sah, R.L. 2007. Effect of synovial fluid on boundary lubrication of articular cartilage. *Osteoarthritis and Cartilage*. **15**(1), pp.35–47.

Schwiesau, J., Schilling, C., Kaddick, C., Utzschneider, S., Jansson, V., Fritz, B., Blömer, W. and Grupp, T.M. 2013. Definition and evaluation of testing scenarios for knee wear simulation under conditions of highly demanding daily activities. *Medical Engineering and Physics*. **35**(5), pp.591–600.

Schwiesau, J., Schilling, C., Utzschneider, S., Jansson, V., Fritz, B., Blömer, W. and Grupp, T.M. 2013. Knee wear simulation under conditions of highly demanding daily activities - Influence on an unicompartmental fixed bearing knee design. *Medical Engineering and Physics*. **35**(8), pp.1204–1211.

Screen, H.R.C., Bader, D.L., Lee, D.A. and Shelton, J.C. 2004. Local strain measurement within tendon. *Strain*. **40**(4), pp.157–163.

Seedhom, B.B. 1979. Transmission of the Load in the Knee Joint with Special Reference to the Role of the Menisci:Part I: Anatomy, Analysis and Apparatus. *Engineering in Medicine*. **8**(4), pp.207–219.

Sezaki, S., Otsuki, S., Ikeda, K., Okuno, N., Okamoto, Y., Wakama, H., Okayoshi, T. and Neo, M. 2021. Development of a Pressure-Sensitive Conductive Rubber Sensor for Analyzing Meniscal Injury in Porcine Models. *Applied Bionics and Biomechanics*. **2021**.

Shepherd, D.E.T. and Seedhom, B.B. 1999. *Thickness of human articular cartilage in joints of the lower limb*.

Shi, L., Sikavitsas, V.I. and Striolo, A. 2011. Experimental friction coefficients for bovine cartilage measured with a pin-on-disk tribometer: Testing configuration and lubricant effects. *Annals of Biomedical Engineering*. **39**(1), pp.132–146.

Shimizu, N., Tomita, T., Patil, S., Yamazaki, T., Iwamoto, K., Kurita, M., Fujii, M., D'Lima, D. and Sugamoto, K. 2018. The Differences of TKA Kinematics in Cruciate Retaining Insert and Condylar Stabilised Insert. *Orthopaedic Proceedings*. **95-B**(15).

Solheim, E., Hegna, J. and Inderhaug, E. 2018. Early determinants of long-term clinical outcome after cartilage repair surgery in the knee. *Journal of Orthopaedics*. **15**(1), pp.222–225.

Solheim, E., Hegna, J., Inderhaug, E., Øyen, J., Harlem, T. and Strand, T. 2016. Results at 10–14 years after microfracture treatment of articular cartilage defects in the knee. *Knee Surgery, Sports Traumatology, Arthroscopy*. **24**(5), pp.1587–1593.

Solheim, E., Hegna, J., Strand, T., Harlem, T. and Inderhaug, E. 2018. Randomized Study of Long-term (15-17 Years) Outcome After Microfracture Versus Mosaicplasty in Knee Articular Cartilage Defects. *American Journal of Sports Medicine*. **46**(4), pp.826–831.

Sophia Fox, A.J., Bedi, A. and Rodeo, S.A. 2009. The basic science of articular cartilage: Structure, composition, and function. *Sports Health*. **1**(6), pp.461–468.

Souza, J.C.M., Henriques, M., Oliveira, R., Teughels, W., Celis, J.P. and Rocha, L.A. 2010. Biofilms inducing ultra-low friction on titanium. *Journal of Dental Research*. **89**(12), pp.1470–1475.

STANDRING, S. 2016. Functional anatomy of the musculoskeletal system *In*: *Gray's Anatomy: The Anatomical Basis of Clinical Practice*. Elsevier, pp.81–122.

Stewart, T.D. and Hall, R.M. 2006. (iv) Basic biomechanics of human joints: Hips, knees and the spine *In*: *Current Orthopaedics*., pp.23–31.

Stoodley, P., Nistico, L., Johnson, S., Lasko, L.A., Baratz, M., Gahlot, V., Ehrlich, G.D. and Kathju, S. 2008. Direct demonstration of viable Staphylococcus aureus biofilms in an infected total joint arthroplasty: A case report. *Journal of Bone and Joint Surgery*. **90**(8), pp.1751–1758.

Stoop, R., van der Kraan, P.M., Buma, P., Hollander, A.P., Poole, A.R. and van den Berg, W.B. 1999. Denaturation of type II collagen in articular cartilage in experimental murine arthritis. Evidence for collagen degradation in both reversible and irreversible cartilage damage. *Journal of Pathology*. **188**(3), pp.329–337.

Sutton, L.G., Werner, F.W., Haider, H., Hamblin, T. and Clabeaux, J.J. 2010. In vitro response of the natural cadaver knee to the loading profiles specified in a standard for knee implant wear testing. *Journal of Biomechanics*. **43**(11), pp.2203–2207.

Tanner, R.I. 1966. An Alternative Mechanism for the Lubrication of Synovial Joints. *Physics in Medicine & Biology*. **11**(1), pp.119–127.

Tawy, G. and McNicholas, M. 2022. *ICRS PATIENT REGISTRY Annual Report 2022*.

Taylor, C. 2013. *Development and characterisation of mechanical and enzymatic models of cartilage degeneration*.[Online] University of Leeds. Available from: http://etheses.whiterose.ac.uk/id/eprint/6807.

Taylor MEng, S.D., Taylor, S., Tsiridis, E., Ingham, E., Jin, Z., Fisher, J. and Williams, S. 2012. *An In-vitro Medium Term Simulation of Hip Hemiarthroplasty*.

Tekari, A., Egli, R.J., Schmid, V., Justiz, J. and Luginbuehl, R. 2020. A Novel Bioreactor System Capable of Simulating the in Vivo Conditions of Synovial Joints. *Tissue Engineering - Part C: Methods*. **26**(12), pp.617–627.

Torrie, A.M., Kesler, W.W., Elkin, J. and Gallo, R.A. 2015. Osteochondral allograft. *Current Reviews in Musculoskeletal Medicine*. **8**(4), pp.413–422.

Trevino, R.L., Stoia, J., Laurent, M.P., Pacione, C.A., Chubinskaya, S. and Wimmer, M.A. 2017. Establishing a live cartilage-on-cartilage interface for tribological testing. *Biotribology*. **9**, pp.1–11.

Ulstein, S., Årøen, A., Røtterud, J.H., Løken, S., Engebretsen, L. and Heir, S. 2014. Microfracture technique versus osteochondral autologous transplantation mosaicplasty in patients with articular chondral lesions of the knee: A prospective randomized trial with long-term follow-up. *Knee Surgery, Sports Traumatology, Arthroscopy*. **22**(6), pp.1207–1215.

Vanwanseele, B., Eckstein, F., Knecht, H., Spaepen, A. and Stüssis, E. 2003. Longitudinal Analysis of Cartilage Atrophy in the Knees of Patients with Spinal Cord Injury. *Arthritis and Rheumatism*. **48**(12), pp.3377–3381.

Vazquez, K.J., Andreae, J.T. and Henak, C.R. 2019. Cartilage-on-cartilage cyclic loading induces mechanical and structural damage. *Journal of the Mechanical Behavior of Biomedical Materials*. **98**, pp.262–267.

VERSUSARTHRITIS 2021. *The State of Musculoskeletal Health 2021*.

Veselack, T., Aldebert, G., Trunfio-Sfarghiu, A.M., Schmid, T.M., Laurent, M.P. and Wimmer, M.A. 2018. Phospholipid vesicles in media for tribological studies against live cartilage. *Lubricants*. **6**(1).

Walker, P.S., Arno, S., Bell, C., Salvadore, G., Borukhov, I. and Oh, C. 2015. Function of the medial meniscus in force transmission and stability. *Journal of Biomechanics*. **48**(8).

Walker, P.S., Blunn, G.W., Broome, D.R., Perry, J., Watkins, A., Sathasivam, S., Dewart, M.E. and Paul$, J.P. 1997. *A KNEE SIMULATING MACHINE FOR PERFORMANCE EVALUATION OF TOTAL KNEE REPLACEMENTS*.

Walker, P.S., Dowson, D., Longfield, M.D. and Wright4, V. 1968. *'BOOSTED LUBRICATION' IN SYNOVIAL JOINTS BY FLUID ENTRAPMENT AND ENRICHMENT*.

Walter, C., Leichtle, U., Lorenz, A., Mittag, F., Wülker, N., Müller, O., Bobrowitsch, E. and Rothstock, S. 2013. Dissipated energy as a method to characterize the cartilage damage in large animal joints: An in vitro testing model. *Medical Engineering and Physics*. **35**(9), pp.1251–1255.

Walter, C., Trappe, D., Beck, A., Jacob, C. and Hofmann, U.K. 2020. Effect of graft positioning on dissipated energy in knee osteochondral autologous transplantation—A biomechanical study. *Journal of Orthopaedic Research*. **38**(8), pp.1727–1734.

Wang, J.H.C. 2006. Mechanobiology of tendon. *Journal of Biomechanics*. **39**(9), pp.1563–1582.

Wang, T., Gardiner, B.S., Lin, Z., Rubenson, J., Kirk, T.B., Wang, A., Xu, J., Smith, D.W., Lloyd, D.G. and Zheng, M.H. 2013. Bioreactor design for tendon/ligament engineering. *Tissue Engineering - Part B: Reviews*. **19**(2), pp.133–146.

Wang, Y., Chen, Y. and Wei, Y. 2022. Osteoarthritis animal models for biomaterial-assisted osteochondral regeneration. *Biomaterials translational*. **3**(4).

Weightman, B. 1973. Fatigue of articular cartilage. *Nature*. **244**(5414), pp.303–304.

Weightman, B. 1976. Tensile fatigue of human articular cartilage. *J Biomech*. **9**(4), pp.193–200.

Weightman, B., Chappell, D.J. and Jenkins, E.A. 1978. A second study of tensile fatigue properties of human articular cartilage. *Annals of the Rheumatic Diseases*. **37**(1), pp.58–63.

Whitney, G.A., Mansour, J.M. and Dennis, J.E. 2015. Coefficient of Friction Patterns Can Identify Damage in Native and Engineered Cartilage Subjected to Frictional-Shear Stress. *Annals of Biomedical Engineering*. **43**(9), pp.2056–2068.

Widuchowski, W., Widuchowski, J. and Trzaska, T. 2007. Articular cartilage defects: Study of 25,124 knee arthroscopies. *Knee*. **14**(3).

Willing, R., Moslemian, A., Yamomo, G., Wood, T., Howard, J. and Lanting, B. 2019. Condylar-Stabilized TKR May Not Fully Compensate for PCL-Deficiency: An In Vitro Cadaver Study. *Journal of Orthopaedic Research*. **37**(10), pp.2172–2181.

Wu, J.Z., Herzog, W. and Hasler, E.M. 2002. *Inadequate placement of osteochondral plugs may induce abnormal stress-strain distributions in articular cartilage-finite element simulations 1* [Online]. Available from: www.elsevier.com/locate/medengphy.

Yuh, C., Laurent, M.P., Espinosa-Marzal, R.M., Chubinskaya, S. and Wimmer, M.A. 2021. Transient stiffening of cartilage during joint articulation: A microindentation study. *Journal of the Mechanical Behavior of Biomedical Materials*. **113**.

Zhang, Z., Barman, S. and Christopher, G.F. 2014. The role of protein content on the steady and oscillatory shear rheology of model synovial fluids. *Soft Matter*. **10**(32), pp.5965–5973.